General Disclaimer

One or more of the Following Statements may affect this Document

- This document has been reproduced from the best copy furnished by the organizational source. It is being released in the interest of making available as much information as possible.

- This document may contain data, which exceeds the sheet parameters. It was furnished in this condition by the organizational source and is the best copy available.

- This document may contain tone-on-tone or color graphs, charts and/or pictures, which have been reproduced in black and white.

- This document is paginated as submitted by the original source.

- Portions of this document are not fully legible due to the historical nature of some of the material. However, it is the best reproduction available from the original submission.

Produced by the NASA Center for Aerospace Information (CASI)

SPACE DIVISION

NASA CR-144853

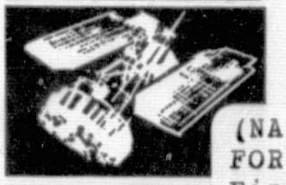

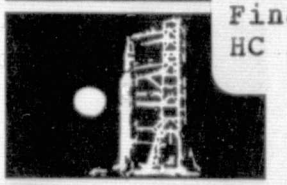

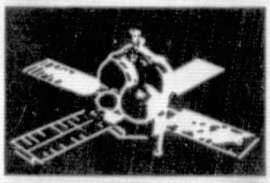

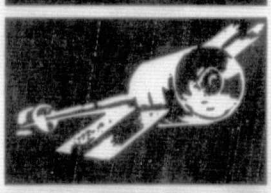

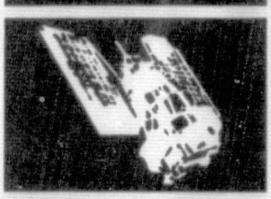

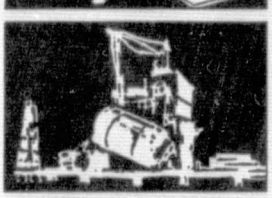

(NASA-CR-144853) SCANNING MECHANISM STUDY FOR MULTI-FREQUENCY MICROWAVE RADIOMETERS Final Report (General Electric Co.) 175 p HC A08/MF A01 CSCL 14B

N77-15369

Unclas
G3/35 12305

SCANNING MECHANISM STUDY

FOR

MULTI-FREQUENCY MICROWAVE RADIOMETERS

IHSUK SHIN

GENERAL ELECTRIC COMPANY

SPACE DIVISION

VALLEY FORGE SPACE CENTER

P. O. BOX 8555 PHILADELPHIA, PA. 19101

APRIL 1976

FINAL REPORT

PREPARED FOR

GODDARD SPACE FLIGHT CENTER

GREENBELT, MD. 20771

GENERAL ELECTRIC

TECHNICAL REPORT STANDARD TITLE PAGE

1. Report No.	2. Government Accession No.	3. Recipient's Catalog No.

4. Title and Subtitle	5. Report Date
SCANNING MECHANISM STUDY FOR MULTI-FREQUENCY MICROWAVE RADIOMETER	8 July 1976
	6. Performing Organization Code
7. Author(s) Ihsuk Shin	8. Performing Organization Report No.
9. Performing Organization Name and Address General Electric Company Space Division P. O. Box 8555 Philadelphia, Pa. 19101	10. Work Unit No.
	11. Contract or Grant No. NAS 5-22490
12. Sponsoring Agency Name and Address Goddard Space Flight Center National Aeronautics & Space Administration Greenbelt, Md. 20771	13. Type of Report and Period Covered Contractor Final
	14. Sponsoring Agency Code

15. Supplementary Notes

16. Abstract

In this report scanning mode for a microwave radiometer having large aperture antenna is determined from scientific needs by engineering tradeoffs. Two configurations of the scan drive mechanism with an integral momentum compensation are formulated for 1.0M and 1.4M diameter antennas. As the formulation is based on currently available components, it is possible to design and fabricate the formulated mechanism without new hardware development.

A preliminary specification for major components of formulated drives are also included in the report.

17. Key Words (Selected by Author(s))	18. Distribution Statement
Scanning Mechanism, Microwave Radiometer, Momentum Compensation, Resonant Spring, Parabolic Reflector	

19. Security Classif. (of this report)	20. Security Classif. (of this page)	21. No. of Pages	22. Price*
Uncla-sified	Unclassified	174	

*For sale by the Clearinghouse for Federal Scientific and Technical Information, Springfield, Virginia 22151.

ORIGINAL PAGE IS
OF POOR QUALITY

JAN 1977
RECEIVED
NASA STI FACILITY
INPUT BRANCH

PREFACE

In this report scanning mode for a microwave radiometer having large aperture antenna is determined from scientific needs by engineering tradeoffs. Two configurations of the scan drive mechanism with an integral momentum compensation are formulated for 1.0M and 1.4M diameter antennas. As the formulation is based on currently available components, it is possible to design and fabricate the formulated mechanism without new hardware development.

The formulated drive mechanisms have been analyzed by use of analog simulation. The results indicate that for an antenna having 1.0M diameter aperture both configuration can provide equally satisfactory performance about the scan axis. The momentum disturbance in transverse axis due to a coupling through products of inertia is, however, greater than the residual momentum disturbance in the scan axis.

For an antenna having 1.4M aperture the configuration having a short shaft supported structure (Configuration II) has shown better performance about the scan axis than the one having long truss supported structure (Configuration I). A large distrubing momentum in transverse axis due to products of inertia appears for both configuration and requires an active compensation.

A preliminary specification for major components of formulated drives are also included in the report.

TABLE OF CONTENTS

LIST OF ILLUSTRATIONS

1.0 Introduction

This final report is submitted by the General Electric Company in accordance with Article X of NASA contract NAS 5-22490.

Recent development in microwave remote sensing is providing powerful new tools that can provide all weather measurement of many parameters related to ocean/atmospheric momentum and energy transfer. One of these parameters important to meteological and oceanographic communities is the sea surface temperature which is measured by a microwave radiometer. In order to make the temperature measurement less sensitive to surface wind speed it is preferred to use lower microwave frequencies. Then a large aperture antenna is required to provide small footprint sizes at the low frequencies. It has been shown that spacecraft microwave experiments which use two or more frequencies require a mechanically scanned antenna to provide sufficient resolution for efficient collection of the microwave experimental data. Reflectors such as offset parabolic sections with aperture diameter of one to 2.5M may be employed in these experiment.

The objectives of this study are to determine a scan mode for such large aperture antennas satisfying scientific needs by engineering tradeoffs, to define a drive mechanism with an integral momentum compensation which can accommodate reflectors with large aperture diameters and to demonstrate the adequacy of the system design. A mechanically scanned multi-frequency microwave radiometer (SMMR) being developed for Nimbus "G" satellite and also planned to be on board Seasat satellite. It has 0.8 meter diameter reflector and the scan amplitude is limited to $\pm$25 degrees about nadir due to constraints imposed by the spacecraft design. Large spacecrafts with different design configuration, for example a Space Shuttle, can accommodate a larger antenna and a larger scan amplitude.

In Section 2.0 of this report the preferred scan mode for a large aperture SMMR is determined by investigating the merits of various scan modes related to the radiometer performance characteristics such as the ground resolution and the integration time. The selected scan parameters are (1) sinusoidal scan with $\pm$45 degree amplitude (2) 2 second scan period, and (3) conical scan about nodir with 45 degrees half cone angle.

In Section 3.0 drive mechanisms in 2 different configurations are formulated. The Configuration I is very similar to the one proposed for the Nimbus "G" spacescraft - the reflector antenna is mounted by a truss support on a drive pedestal which wraps around the feed assembly. The antenna reflector in Configuration II is directly attached to a drive shaft which is located in the opposite side of reflective surface.

Components selected for the drive mechamism formulation are discussed in Section 4.0 and preliminary specifications are presented in Appendix A. All components selected are obtainable either by modifying existing hardware or by designing based on current state-of-art.

Structural properties of the formulated mechanism design are analyzed in Section 5.0 and the resulting mechanical parameters based on digital computer modeling are used in Section 6.0 for the performance analysis. Equations of motion in 3 axes derived from Lagrange equation using a generalized coordinate system are presented in Appendix B. The equations are simulated on an analog computer to assess the performance of the scan drive mechanism. The results are shown in Appendix C and discussed in Section 6.0.

2.0 DETERMINATION OF SCAN MODES

The scientific needs of a spaceborne microwave radiometer application require high spatial resolutions as well as high temperature resolutions. Since these conflicting requirements cannot be satisfied simultaneously, however, the preference is given to the spatial resolutions in selecting the scan mode for this study. The selected scan parameters are:

1) Scan pattern - sinusoidal
2) Scan period - 2 second (0.5 Hz)
3) Scan amplitude - $\pm$ 45 degrees
4) Scan cone angle - 45 degrees

The rationale for the selection of these parameters are discussed in the following paragraphs.

2.1 SCIENTIFIC NEEDS

The major application of spaceborne microwave radiometer includes global monitoring/mapping of ocean/atmospheric energy transfer process, remote sensing of soil moisture content and salinity of sea water. For these measurements, the following resolutions are needed:

(1) Temperature resolution

Relative $0.1 \sim 2^{o}K$

Absolute $0.5 \sim 2^{o}K$

(2) Spatial resolution

Sea / Ocean $5 \sim 100$ KM

Land / Coast $0.1 \sim 5$ KM

It is also desired that the SMMR scan pattern provides at least a contiguous coverage for all microwave frequencies with a swath width of 1000 KM.

Since it is recognized that both temperature and spatial resolutions cannot be satisfied at the same time, the most acceptable compromise is to provide best spatial resolution which can be afforded by antenna size constraint imposed by the spacecraft design, and then optimize temperature resolution.

2.2 SPATIAL RESOLUTION

The spatial resolution of the SMMR is determined by the size of antenna beam footprint, which is approximately given by (see Figure 2.1)

$$L = \frac{2R\theta_b}{\cos\theta_i}$$

where

L	linear size of antenna beam footprint (L_c or L_i)
R	slant range (a function of altitude and θ_i)
θ_b	beam width of the radiometer antenna (half angle)
θ_i	angle of beam incidence

Assuming that the beam width is strictly determined by the diffraction theory

$$\theta_b \cong \frac{\lambda}{D}$$

and as it is desired to have the best resolution from a given antenna,

$$L = \frac{2R}{\cos\theta_i} \cdot \frac{\lambda}{D}$$

where

λ	RF wavelength
D	antenna aperture diameter

For a given antenna size and the spacecraft altitude the resolution is dependent on the beam incident angle which depends on the physics of the desired measurement. An angle of incidence between 40° to 50° is a good compromise for the conflicting factors of the spatial resolutions and the measurement physics [1].

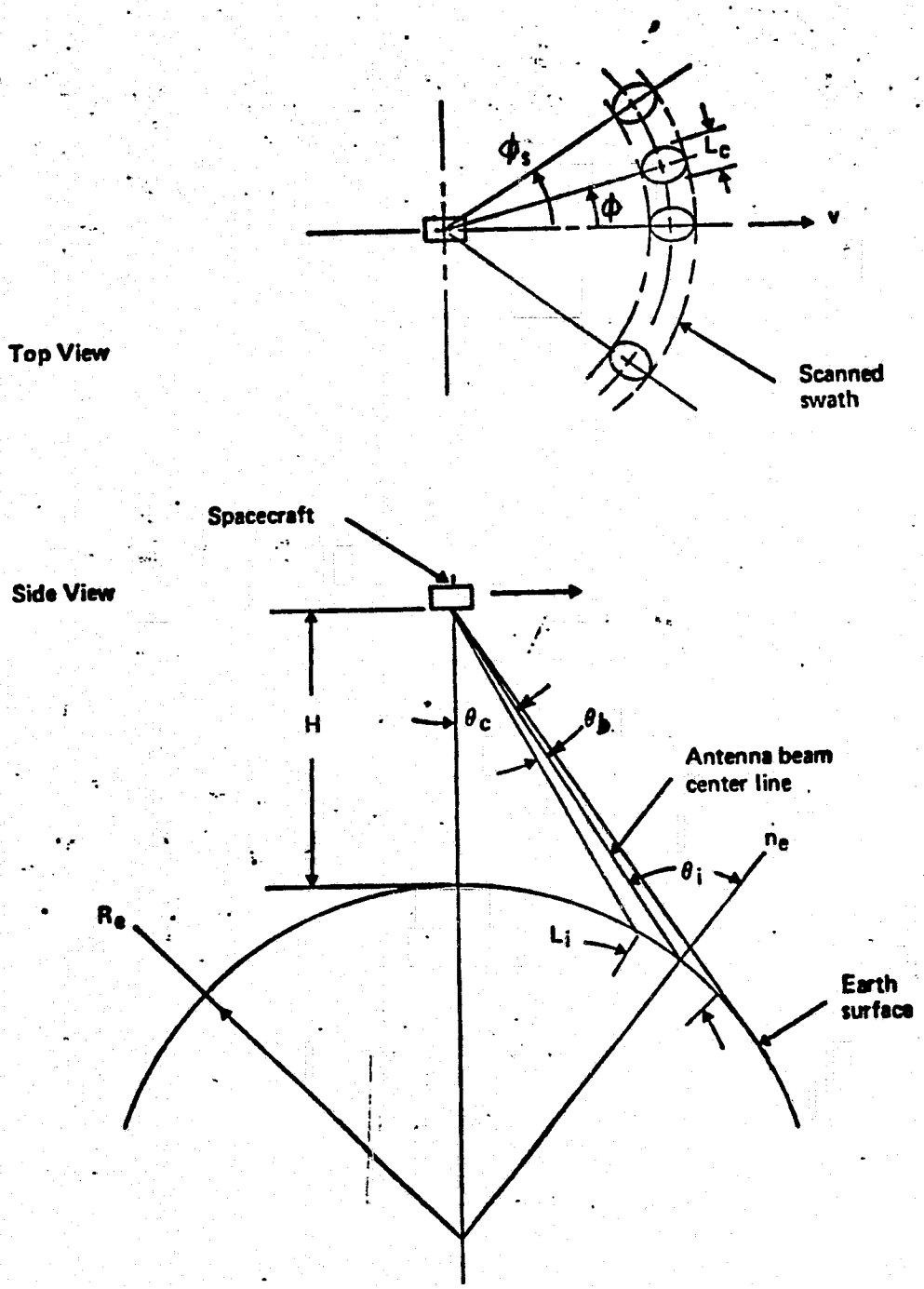

Legend:

R_e	:	earth radius
H	:	spacecraft altitude
L	:	linear size of antenna beam footprint*
n_e	:	normal vector (to earth surface)
v	:	spacecraft orbital velocity vector
θ_b	:	antenna beamwidth (3 dB)
θ_c	:	half angle of scan cone
θ_i	:	angle of incidence
ϕ_i	:	azimuthal angle of antenna beam
ϕ_s	:	total azimuthal scan angle in one side

*L_i : in-track footprint

L_c : cross-track footprint

FIGURE 2.1 SCANNING OF THE SMMR ANTENNA

In Figure 2.2 the spatial resolution as a function of the antenna diameter and the spacecraft altitude is given for 45^{o} angle of beam incidence. The spatial resolution for various beam incident angle and altitude can be obtained from Figures 2.3 and 2.4.

The relationship between the angle of beam incidence and the spacecraft altitude is given in Figure 2.3 for various scan cone angle. It shows that the scan cone angle of 45 degrees with 1000 KM altitude corresponds to beam incident angle of 55 degrees. If 50 degree incident angle is desired at 800 KM altitude, the required scan cone angle is 43 degrees. The linear beam footprint size of the antenna having 100 wavelength diameter and 45 degrees cone angle with 1000 KM altitude is shown to be 54 KM in Figure 2.4 while the same antenna at 800 KM altitude with 43 degree cone angle has a linear beam footprint size of 37 KM.

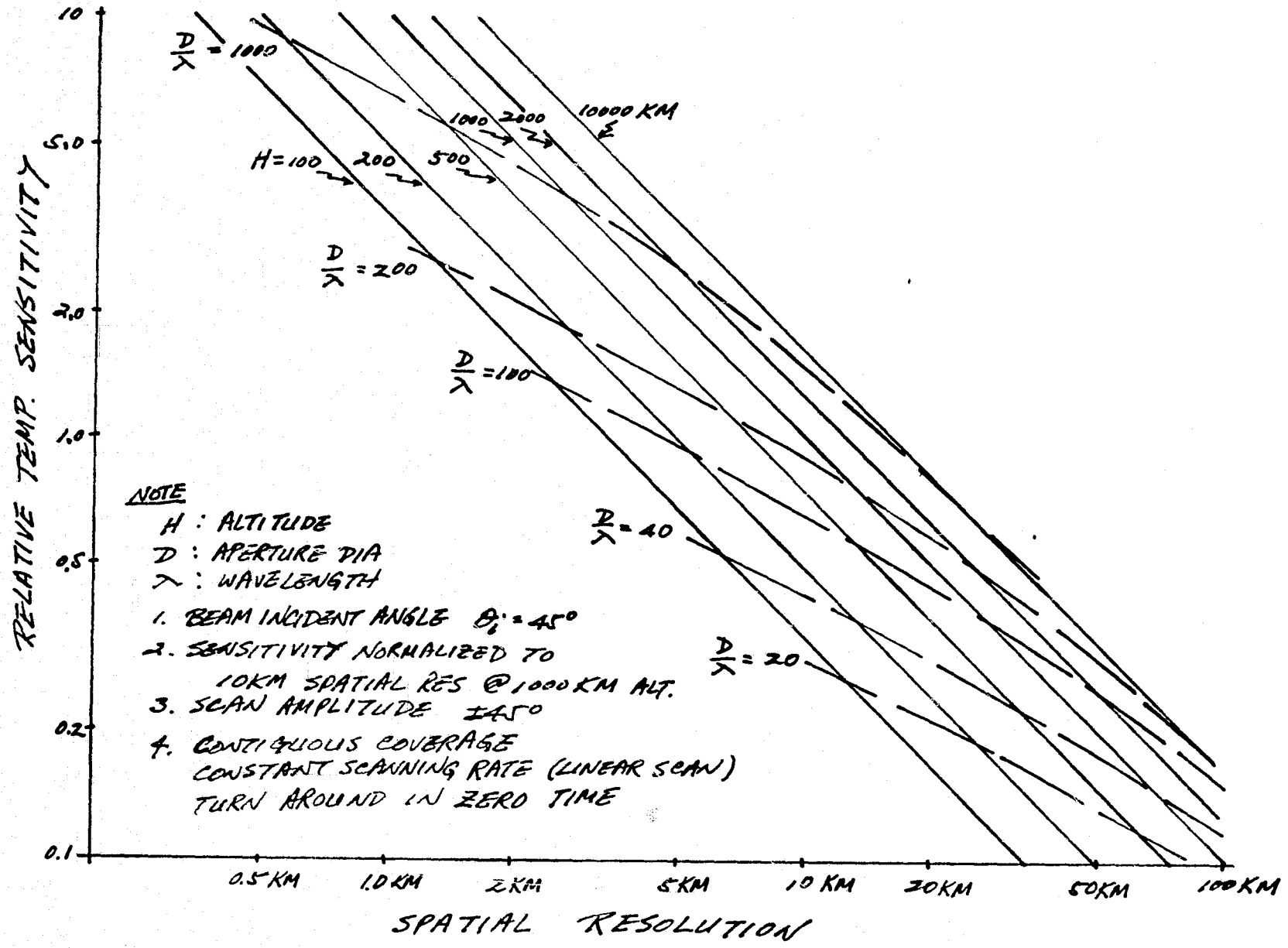

Figure 2.2 Temperature and Spatial Resolutions

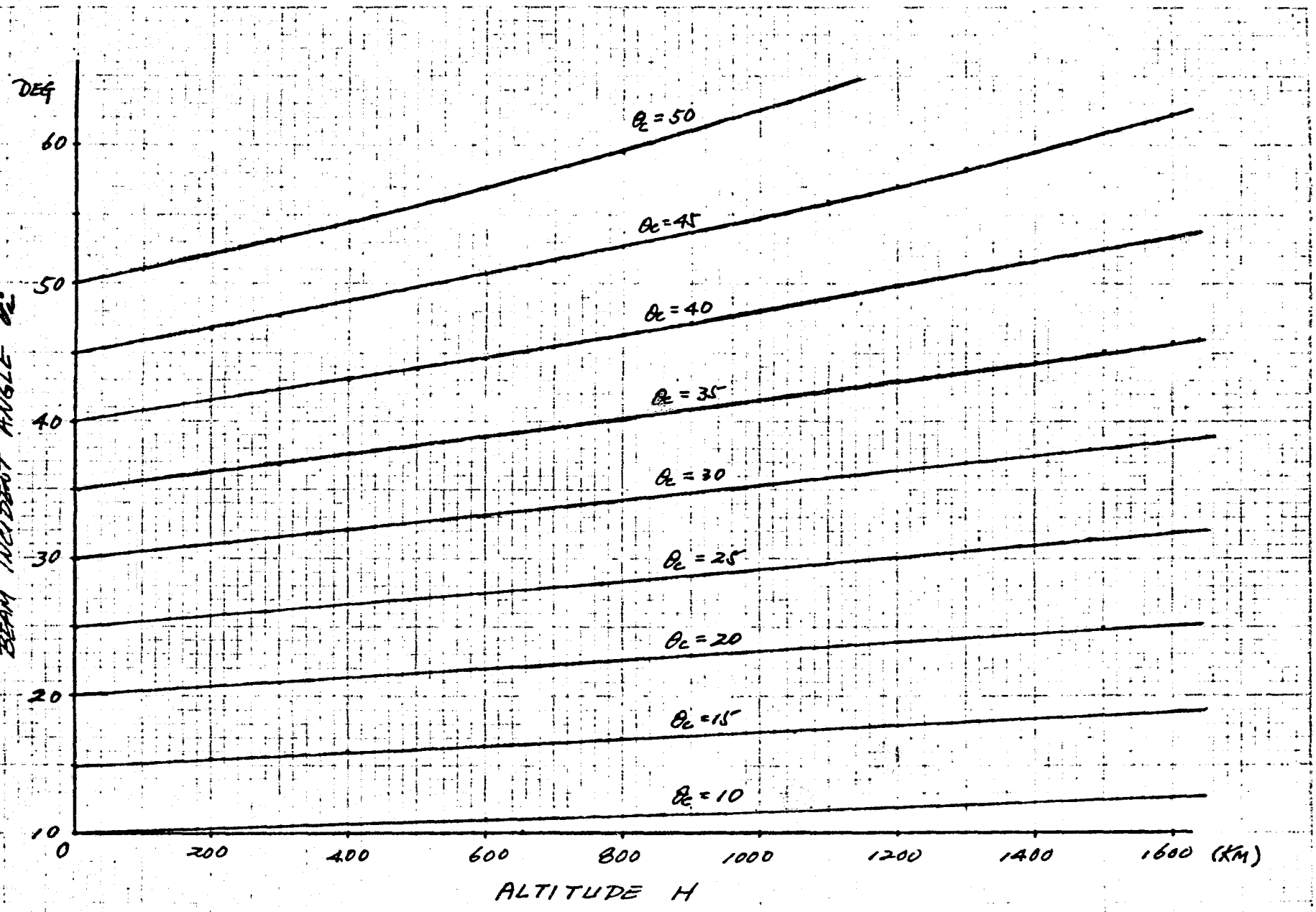

Figure 2.3 Beam Incident and Cone Angles

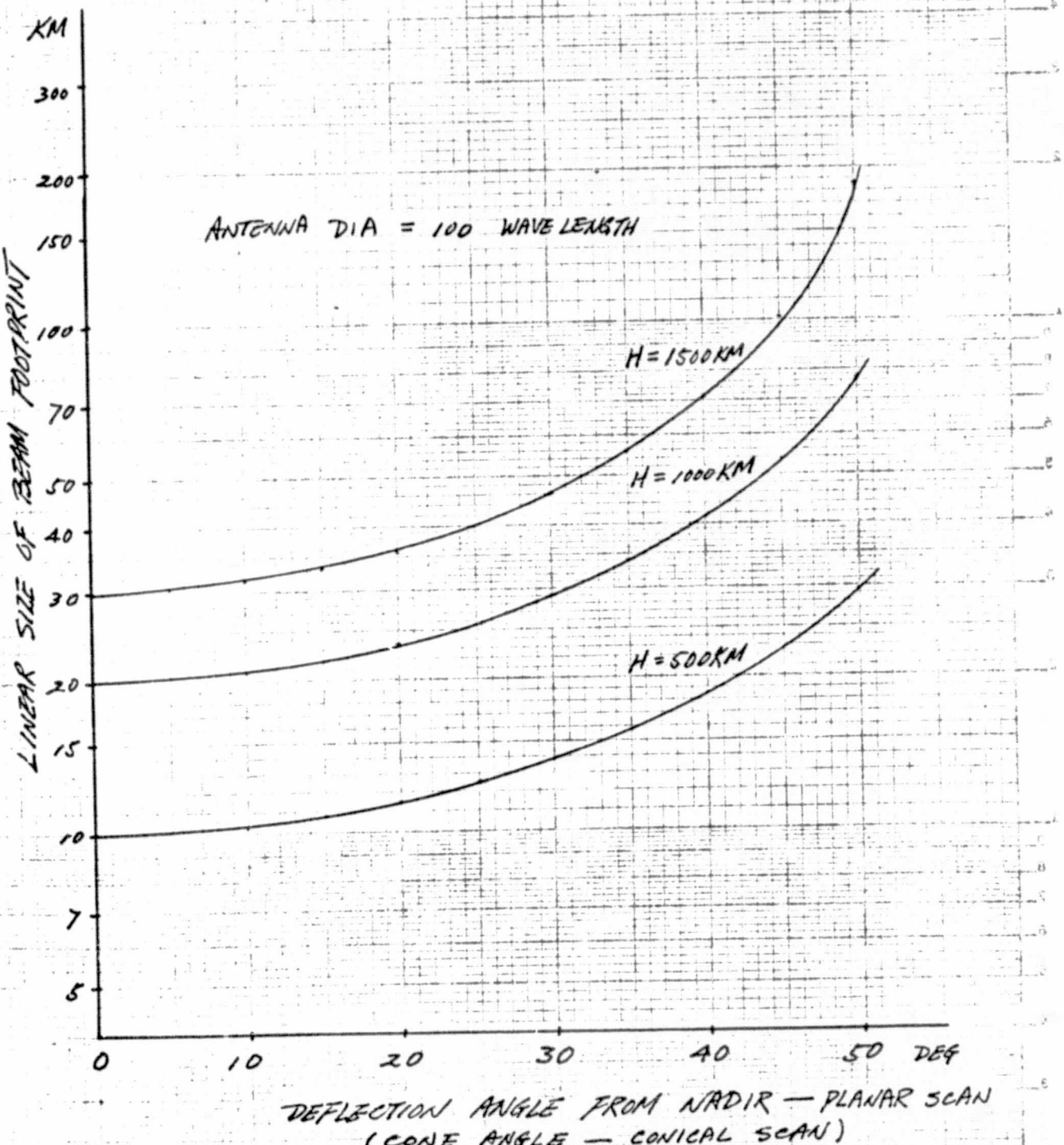

Figure 2.4 Spatial Resolution vs. Cone Angle

ORIGINAL PAGE IS
OF POOR QUALITY

2.3 TEMPERATURE RESOLUTION

The temperature resolution ΔT which is a measure of the sensitivity of a microwave radiometer is given by [2]

$$\Delta T = 2 T_N / \sqrt{B_R \tau}$$

where

T_N absolute system noise temperature

B_R RF noise bandwidth

τ post detection integration time

For a given microwave radiometer receiver T_N and B_R are fixed, and the temperature resolution is inversely proportional to the square root of the integration time. The integration time is the amount of time available to each beam position as the scanning beam moves on the surface of earth, or the dwell time of the beam for each spatial resolution cell. Hence, it can be easily obtained if it is assumed that the beam is step-scanned from one cell position to the next rather than continuously scanned.

Although the antenna beam must scan in two orthogonal axes to obtain an image of temperature brightness of earth, only one dimensional scan across the orbital track is needed for low-orbit satellite. The orbital motion of the spacecraft itself moves the beam in-track direction for this case and the scanning period is constrained by spacecraft track velocity and footprint size of the antenna beam. The scan period τ_s is given by

$$\tau_s = \frac{C_1 L_i}{V_g} = \frac{2 C_1 R \theta_b}{V_g \cos \theta_i}$$

where

V_g ground track velocity

L_i in-track footprint size

C_1 contiguity ratio

$C_1 = 1$ means contiguous, i.e. The resolution cells at swath center are just touching each other. When $C_1 > 1$, there are gaps and when $C_1 < 1$ they overlap.

Planar and conical scans are frequently used in imaging radiometers. In planar scan, the antenna beam moves in a plane perpendicular to the velocity vector of the spacecraft. For a mechanically scanned reflector-type antenna this scan offers some advantages. During each scan cycle, there is an opportunity for the reflector to view the cold space for calibration. The shortcoming is that both spatial resolution and angle of incidence vary as the beam moves away from nadir. The angle of incidence can be obtained from Figure 2.3 and the spatial resolution for 100 wavelength diameter antenna is given in Figure 2.4.

In conical scanning, the beam moves on the surface of a cone whose axis is parallel to local vertical with the antenna at the apex. Such a scan maintains constant spatial resolution and angle of incidence. For applications such as sea surface temperature or sea state measurements, where the polarized surface brightness temperature varies with incidence angle, this is particularly suitable and selected for this study.

For planar scan the angle of incidence at nadir is zero and the slant range equals the altitude. If a linear scan with zero turn around time and amplitude ϕ_s is employed, the angular scan rate is a constant $4\phi_s/T_s$.

Therefore, the limiting dwell time (integration time) is given by

$$\tau = \left(\frac{\lambda_{min}}{D}\right)^2 \frac{H}{2\phi_s V_g}$$

and the temperature sensitivity is

$$\Delta T = \frac{2T_N}{\sqrt{B_R}} \sqrt{\frac{2\phi_s V_g}{H}} \left(\frac{D}{\lambda_{min}}\right)$$

where λ_{min} is the shortest wavelength (highest frequency) of the radiometer measurement.

For the conical scan with a constant rate (linear with zero turnaround time), the azimuthal ground velocity is a constant $4R \cdot \sin\theta_c \, \phi_s / \tau_s$ and the dwell time is given by

$$\tau = \left(\frac{\lambda_{min}}{D}\right)^2 \frac{R}{2\phi_s V_g \sin\theta_c \cdot \cos\theta_i}$$

where

L_c cross track footprint size

θ_c half cone angle

$$R = (R_e + H)\cos\theta_c - R_e \cos\theta_i$$

and the temperature resolution is given by

$$\Delta T = \frac{2T_N}{\sqrt{B_R}} \cdot \sqrt{\frac{2\Phi_s \sqrt{g} \sin\theta_c \cdot \cos\theta_i}{R}} \cdot \left(\frac{D}{\lambda_{min}}\right)$$

Above two temperature equations (for planar and conical scans) indicate that as small an antenna as possible should be used for best temperature resolution. Since the antenna diameter varies inversely with the spatial resolution on the surface, the temperature sensitivity also varies inversely with the spatial resolution. This relationship is also shown in Figure 2.2. There are three prime features that can be observed:

1. For a given spatial resolution, temperature resolution is reduced as the altitude increases. For example, a radiometer receiver with 10 Km spatial resolution which could measure 1°K at 1000 Km could have only 1.25°K resolution at 2000 Km.

2. For a given antenna diameter (in terms of RF wavelength), temperature resolution improves with increasing altitude. For example, a hundred wavelength diameter antenna which could measure 1°K at 1000 Km could resolve 0.66°K at 2000 Km.

3. For a given altitude, the antenna diameter is increased, temperature resolution is reduced while spatial resolution is improved. For example, a radiometer receiver with 100 wavelength diameter antenna which could measure 1°K with 28 Km spatial resolution at 1000 Km could measure only 2.1°K with 13 Km spatial resolution at 1000 Km when the antenna diameter is increased to 200 wavelength.

2.4 SCAN AMPLITUDE

The scan amplitude of a SMMR is dependent on the swath width desired and the scan pattern. As shown in Figure 2.5, a conical scan requires smaller scan amplitude to cover the same swath width when the beam incident angle is increased. Also, it shows that for altitude between 700 Km to 1500 Km the amplitudes required for planar scan and conical scan with 55^{o} incident angle are about the same. As noted earlier, an angle of beam incidence between 40^{o} to 50^{o} is a good compromise between the spatial resolution and measurement physics. From the scan amplitude requirement which angular momentum and drive torque are directly proportional to, however, it is desired to have a larger incident angle. For 1000 Km swath width from 1000 Km altitude 55^{o} beam incident angle is selected as a good compromise. The 55^{o} incident angle results in 45^{o} half cone angle and $\pm 45^{o}$ scan amplitude.

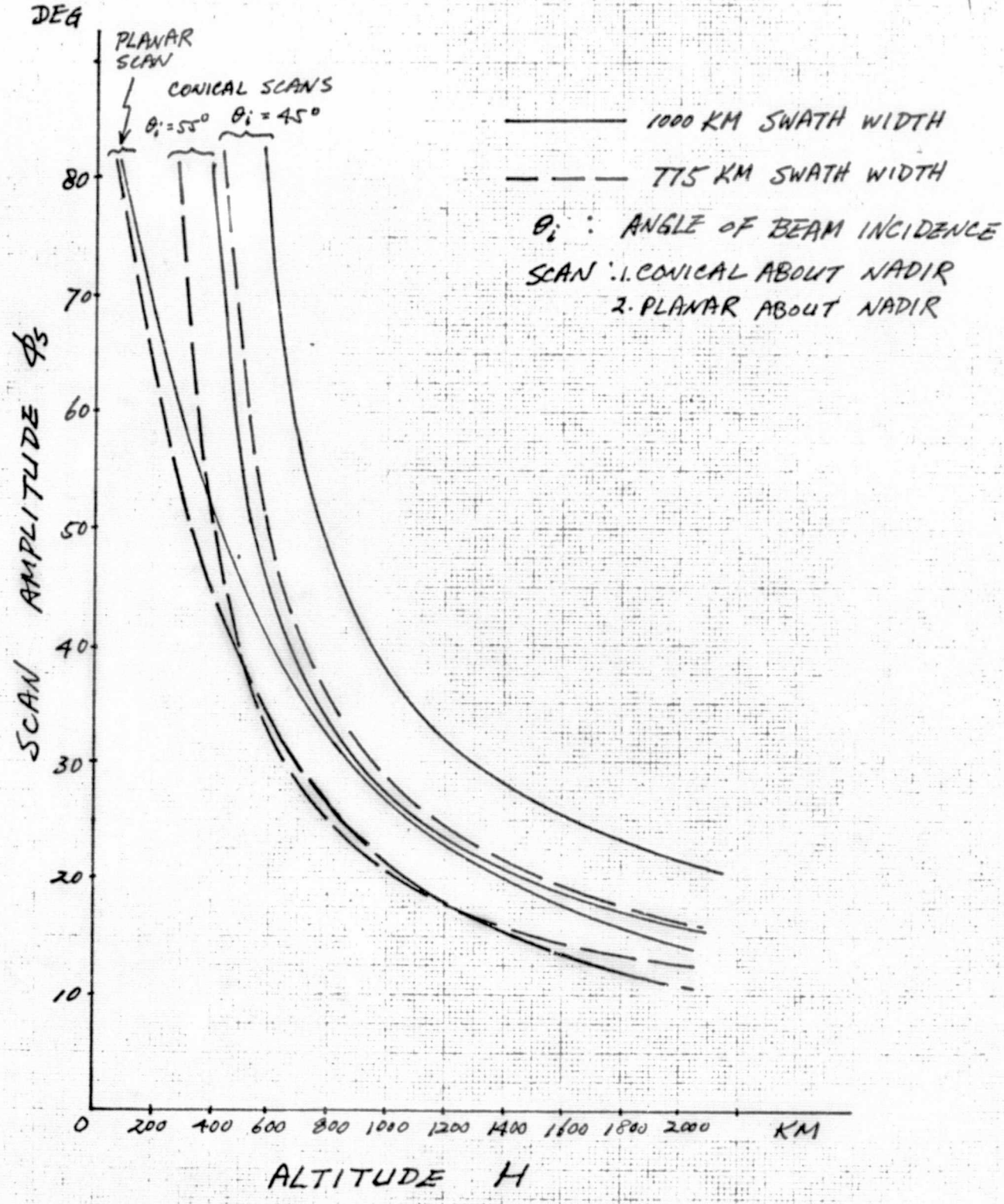

Figure 2.5 Scan Amplitude

2.5 SCAN PATTERN

Scan patterns considered in this study are (see Figure 2.6):

1. linear
2. sinusoidal
3. sine distorted
4. continuous rotation

For the linear scan, the angular rate of antenna beam is constant throughout the scan and the rate is reversed at the end of travel in zero time. Since the acceleration required is infinite, it is impossible to implement a true linear scan drive mechanism.

For the sinusoidal scan, the angular rate of antenna beam varies sinusoidally with the maximum rate occuring at the center of swath width. It requires a sinusoidally varying acceleration with the maximum acceleration occuring at each end of swath width.

For the sine distorted scan, the angular rate of antenna beam is constant for a portion of scan period, $(1-k)\tau_s$, and varies linearily during the finite turn around period. The turn around occurs with $(1/2)k\tau_s$ at the each end of swath with a finite constant acceleration.

When $k = 0$, of course, the sine distorted case degenerates into the linear scan.

For continuous rotation, the angular rate of antenna beam is constant and independent of the scan amplitude ϕ_s. Since it has a constant rate and requires no turn around, no acceleration is required for this scan pattern.

ORIGINAL PAGE IS
OF POOR QUALITY

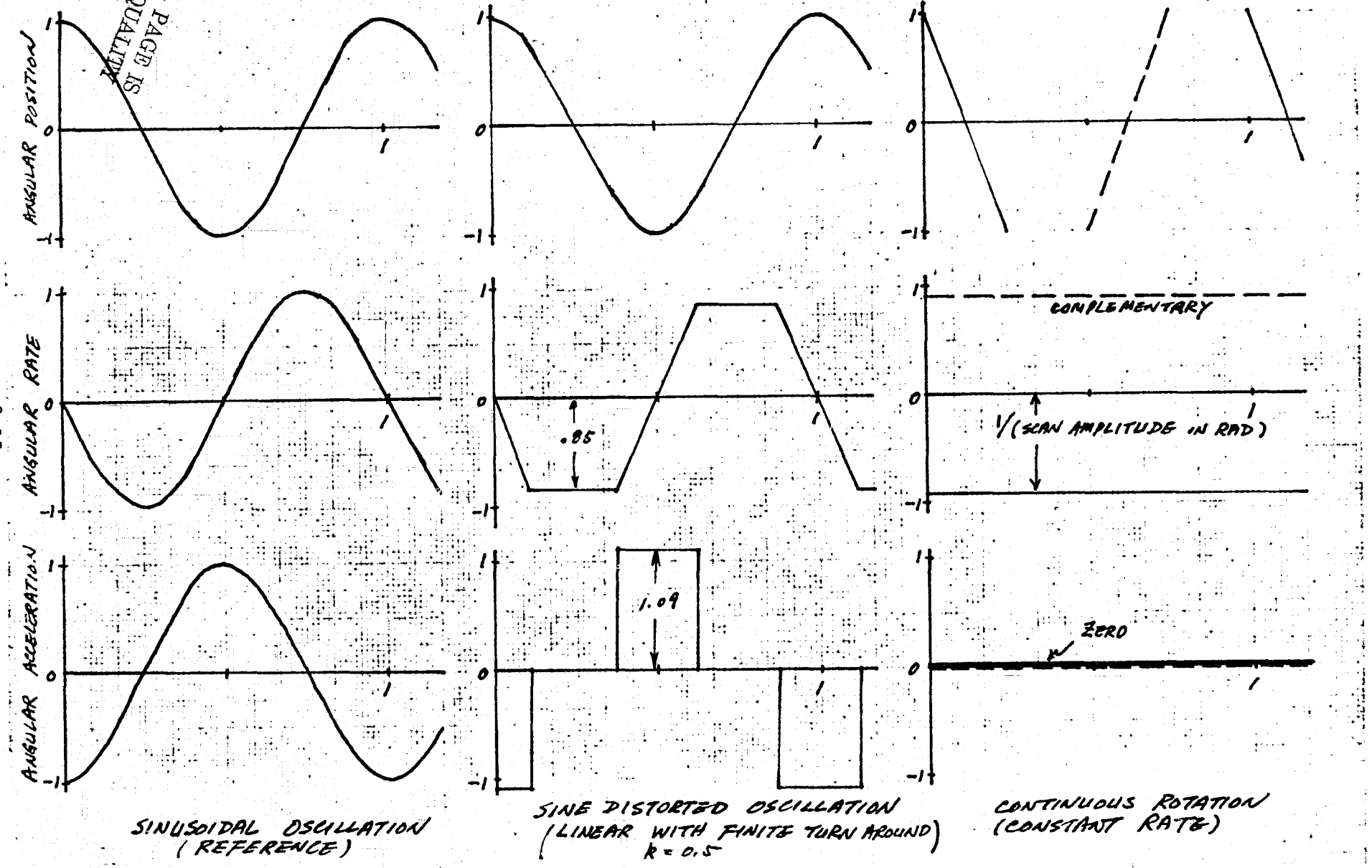

Figure 2.6 Scan Patterns

In previous study scanning mechanism with sinusoidal pattern has been investigated [3] . It was shown that better than 93% of sinusoidally varying angular momentum can be easily compensated by use of a compensation wheel even in presence of friction and backlash.

To assess the merit of sine distorted scan pattern, it is compared with the sinusoidal in Figure 2.7 for various turn around time. The acceleration required for turn around, to which the motor torque as well as the peak power input required is proportional, decreases as the turn around time increases. When the turn around time exceeds 57% of scan period, the required acceleration is less than the peak acceleration for the sinusoidal scan. The scan rate increases as the turn around time is increased and the temperature sensitivity is proportionally degraded. When the turn around time is more than 72% of the scan period, the maximum scan rate exceeds that of the sinusoidal. As the angular momentum is also proportional to the scan rate, amplitude of momentum variation will be also increased. Hence, a sine distorted scan pattern having turn around time between 57 to 72% of scan period requires less torque and generates less momentum variation than the sinusoidal scan having the same scan amplitude and scan period. From these considerations, it appears that the sine distorted scan with 65% turn around time would be better choice than the sinusoidal scan. Also from the drive mechanism design consideration, it is very attractive since the torque required for acceleration is constant during active period which results in an efficient drive electronics.

Nevertheless, these advantages are negated by the difficulty of momentum change compensation. Although a good estimate of momentum compensation cannot be obtained without formulating a specific compensation scheme, an analysis of

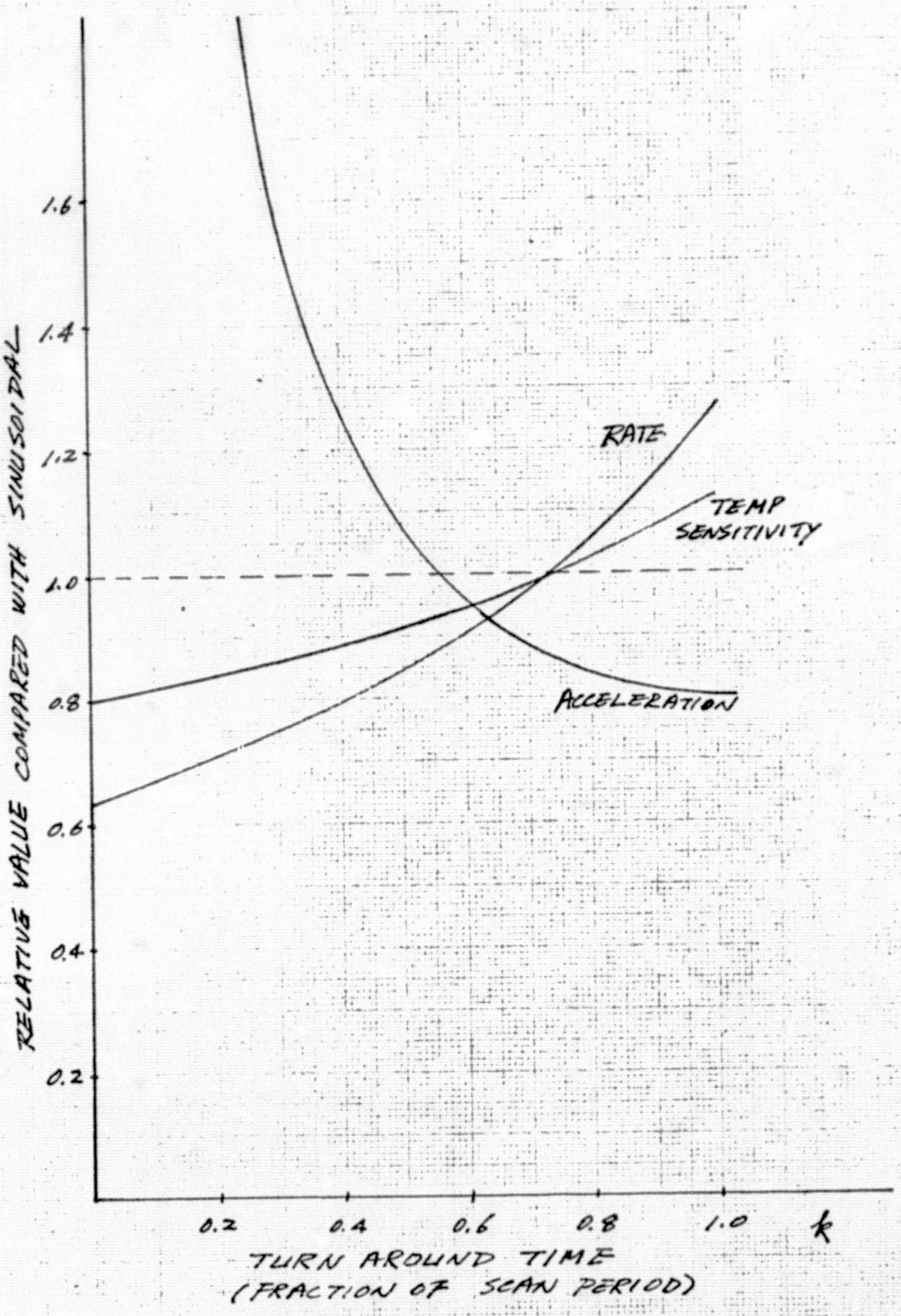

ORIGINAL PAGE IS
OF POOR QUALITY

Figure 2.7 Sine Distorted Scan

harmonic contents in the scan wave form can indicate relative value of residual disturbance momentum. The harmonic contents of sine distorted wave with 65% turn around time is shown in Table 2.1. The angular position pattern has very small amount of harmonics and appears as a sinewave as shown in Figure 2.6 But the angular rate and acceleration patterns have high harmonic contents, especially the fifth harmonic. Since the coupling between the compensation wheel and the scanning antenna would be optimized to compensate the fundamental frequency regardless the type of coupling (mechanical, servo or motor), it can be assumed that the effectiveness of compensation is inversely proportional to the disturbance frequency. (It is noted that, if the coupling is designed to compensate wide band width disturbance, the drive mechanism is more susceptable to noise and more expensive). Then the relative residual disturbing momentum of a sine distorted scan with a compensating wheel is given by

$$\text{(Fundamental Amplitude)} \times \sum \text{(order of harmonics) x (relative harmonic amplitude)}$$

$$= 0.84 \times (1 \times 1 + 3 \times .018 + 5 \times 0.046 + 7 \times 0.016 + \ldots)$$

$$= 1.175$$

Since the rate amplitude of sine distorted scan is 94% of the equivalent sinusoidal scan, the residual disturbing momentum is 10% higher than the sinusoidal scan.

As the momentum is proportional to the moment of inertia, although 10% higher residual momentum for a small antenna might be negligible, it will contribute greatly to the attitude rate error of spacecraft when the diameter of scanning antenna is large. Therefore, the sine distorted scan pattern is not selected for this study.

	AMPLITUDE OF HARMONICS			
	Funda-mental	3rd Harmonic	5th Harmonic	7th Harmonic
Angular Position	REF	0.6%	0.9%	0.2%
Angular Rate	REF	1.8%	4.6%	1.6%
Angular Acceleration	REF	5.1%	23%	11.2%

NOTE: k = 0.65

REF = 0.84 of Original Amplitude

Table 2.1 Harmonic Contents of Sine Distorted Scan

Comparing the continuously rotating scan antenna to a sinusoidally oscillating antenna, a higher scan rate is required if the scan amplitude is less than 1 radian.

For 45 degrees scan amplitude, the scan rate of continuously rotating antenna is 28% higher than maximum rate of equivalent sinusoidally scanning antenna. As the rate does not change, however, there is no momentum disturbance due to the scanning antenna but only a fixed bias momentum. With a counter rotating complementary antenna, this bias can be cancelled and any residual momentum can be easily handled by the spacecraft attitude control system. Even though this scan pattern requires a space for two rotating antennas, it does not require any compensation wheel which is necessary for all oscillating type scan pattern. Hence, the weight penalty can be minimized, although space penalty cannot be easily eliminated. Torque required to drive this scan system is very small compared to any other scan pattern since it is only required to overcome frictions to maintain the constant rate.

For this study, the sinusoidal scan pattern is selected since the peak acceleration torque required at the end of scan travel can be easily supplied from an energy exchange device such as a resonance spring. With the energy exchange device augmentation, torque required to drive sinusoidally oscillating mechanism can be reduced to that necessary to overcome the frictions and that for maintaining the phase synchronism.

2.6 SCAN PERIOD

Although the spatial resolution desired for land observation is as low as 100 m, the antenna diameter required to satisfy such resolution is prohibitively large. Since 5 ~ 100 Km spatial resolution is acceptable by the most of user community, an antenna providing 5 Km resolution at the highest frequency (37 GHz) and 100 Km at the lowest frequency (2 GHz) is considered first. Figure 2.2 shows that the diameter should be 475 and 28 wavelengths respectively for 5 and 100 Km resolution if the orbital altitude is 1000 Km. In other words, the antenna diameter should be at least 4.2m to satisfy the spatial resolution requirement. This is far beyond the range (1 to 2.5m) specified in the work statement. The scan period providing contiguous coverage for a beam with 5 Km footprint size is

$$\tau_s = \frac{5\ km}{6.4\ KM/sec} = 0.78\ sec$$

which is too short to provide satisfactory temperature resolution assuming the same radiometer characteristics as those of Nimbus G SMMR.

If the scan period is increased to 2 seconds, the spatial resolution for the highest frequency is 12.8 Km and the corresponding D/λ is 200. Since the highest frequency is 37 GHz, the antenna diameter becomes 1.6m. The spatial resolution for the lowest frequency (2 GHz) with 1.6m antenna is shown to be 240 Km which results contiguity ratio of 19. Thus, the 2-second scan period is selected as a compromise.

3.0 DRIVE MECHANISM FORMULATION

Two configurations of drive mechanism for a multifrequency microwave radiometer antenna have been formulated during the second phase of this study. The parabolic antenna reflector is to be mechanically rotated to provide RF beams with a sinusoidal scan of 45 degree amplitude and 2 second period. The configurations formulated and discussed in the following paragraphs are:

a) Configuration I - Antenna reflector is mounted on a drive pedestal through a supporting structure and the pedestal wraps around the feed assembly. Hence, the feed assembly and the drive assembly can be mounted on the same base structure.

b) Configuration II - Antenna reflector is attached to a drive shaft in the opposite side of the reflective surface such that the feed assembly is remotely located from the reflector/drive assembly.

Since the drive mechanism and the feed assembly are rigidly coupled through a common structure in Configuration I, the dynamic alignment between the feed and the reflector is dependent on the dynamic characteristics of the reflector supporting structure. In Configuration II, the coupling between the reflector and the drive mechanism can be considered very rigid. Hence, the alignment between the feed assembly and the reflector is dependent on the supporting structure characteristics for the drive assembly and the sensor assembly.

The basic configurations developed are applicable for both 1400mm - and 1000mm - diameter antennas and any sizes in between except that the power spring parameters require optimization for the specified size antenna. If very long run-up time is tolerable (in the order of hours) even a larger size antenna (2.0m or more) can be accommodated.

3.1 DESCRIPTION OF DRIVE SYSTEM

The scanning multifrequency microwave radiometer (SMMR) can be divided into three subsystems; reflector antenna, antenna drive mechanism, and radiometer electronics. The drive mechanism rotates the antenna to cause desired scanning effect. The reflector is an offset parabolic dish illuminated by a feed cluster located at the focal point. The radiometer electronics includes receivers, calibration network and interface electronics.

The reflector is rotated about an axis passing through the focus and parallel to the spacecraft yaw axis while the feed cluster remains fixed on the spacecraft. The scanning pattern selected for this study is sinusoidal with 45^{o} amplitude and 2 second period, as discussed in the previous section. The antenna beam is pointing downward making an nominal angle of 45^{o} from the nadir and the beam footprints sweep across the spacecraft track.

As the reflector antenna is mechanically rotated, a large angular momentum disturbance is generated. If this disturbance is not compensated for, it is transferred to the spacecraft and causes attitude rate errors. Thus, momentum compensation must be built into the drive mechanism as an integral part of SMMR, since the footprint location is referenced to the stabilized spacecraft attitude and location.

The disturbance momentum of SMMR is primarily a function of the antenna scan rate and moment of inertia. In order to provide an ideal compensation, the angular momenta generated by the antenna and the compensating mass of drive mechanism must be equal in magnitude and opposite in polarity, that is, the compensating mass should rotate at an angular velocity equal to the inverse of inertia ratio in opposite direction of the antenna. Although an ideal

compensation may not be achieved for a practical system, it is desired to reduce the residual disturbing momentum imparted on the spacecraft to within a specified acceptable limit for all three axes. The desired limit for the rate error due to disturbing momentum of SMMR is 0.001 degree per second.

The basic functions of drive mechanism are to provide angular rotation for the reflector antenna and to compensate the angular momentum disturbance caused by the scan motion. Since a sinusoidal scan pattern is chosen, a spring coupled oscillatory system with a periodic excitation can be utilized to provide the desired scan motion. The oscillating frequency of such systems might fall in synchronism with the external excitation frequency if the natural frequency of the system resonance and the excitation frequency are not far different. When a resonance spring is coupled to a compensating wheel from the scanning reflector, the tuned oscillatory motion of the wheel provides angular momentum compensation provided there is no friction and no misalignment between rotating axes.

In this resonant drive mechanism, the required acceleration torque is entirely provided by restoring torque of the spring once the oscillation reaches the steady state. Thus, the external torque at steady state is required only to compensate for the friction (Coulomb and viscous) losses and to maintain the system oscillation in synchronism with the external reference. The friction losses causes amplitude and phase errors if they are not compensated. Since the resonant frequency could be tuned to the desired scan frequency before launch of the spacecraft and would remain stable for a long period, the selection of external excitation level is primarily determined by the frictions in the oscillating system.

When the external excitation is applied between the reflector and the compensation wheel, the net angular momentum does not change under an ideal condition since the action and reaction motions produce momenta equal in amplitude and opposite in direction. Hence, the momentum compensation is automatically achieved by the counteraction between the armature and the field of the drive motor. This approach, known as "motor coupled drive", is adopted in the "configuration II" drive mechanism shown in Figures 3.6 through 3.8.

When the external excitation is applied between the drive housing and the reflector, another excitation is necessary to control the motion of compensation wheel. The control of wheel motion can be accomplished by gear-coupling, belt-coupling or through a feedback servo. In this study, "servo-coupled" approach is used in the "configuration I" drive mechanism(Figures 3.1 through 3.3). The selection of the motor-coupled and servo-coupled approaches is based on the results of previous study conducted for the Nimbus G SMMR antenna drive in which the following approaches are considered for momentum compensation:(1)

a. Gear coupled - the compensation wheel is coupled to the antenna shaft through a gear train having a proper ratio.
b. Belt coupled - the compensation wheel is coupled to the antenna shaft through a belt or belts and sprocket wheels having a proper ratio.
c. Motor coupled - the compensation wheel and the antenna shaft is coupled through the electromechanical reaction torque between armature and field of a drive motor.
d. Servo slaved - either the antenna or the compensation wheel is driven by a primary motor and the other is slaved to the primary drive through a servo loop having a closed loop gain equal to the coupling ratio.

e. Hybrid combination - the compensation wheel is coupled to the drive shaft via gear, belt or motor but the drive shaft is displaced from the antenna axis so that it requires an additional gear or belt coupling.

The SMMR drive mechanism for Nimbus G under development at JPL is a belt coupled configuration I type in which the excitation is applied between the wheel and the base structure and the antenna drive shaft is coupled to the wheel through a set of belts.

3.2 DRIVE CONFIGURATION I

3.2.1 MECHANICAL CONFIGURATION

In this configuration, the drive mechanism is placed around the antenna feed, and the reflector is mounted on the top of a hollow drive shaft as shown in Figures 3.1 and 3.2. The drive mechanism and the sensor assembly (feed) are directly mounted on the satellite bus structure. This is basically the same configuration as the one considered in the earlier study. Since the feed must be located at the focus of the parabolic reflector, the large reflector mass is held at a far distance from the main drive shaft bearing by a supporting structure.

In order to provide beam pointing accuracy, the reflector supporting structure requires high stiffness, high strength, minimum thermal distortion and light weight. In a related study, the following three types of support were considered:[2]

a) Truss

b) Continuous Cone

c) Cut-out cone

Although the continuous cone structure showed high stiffness, high strength and weight benefits, it would degrade RF performance of the radiometer due to the thickness of cone required. With the cutout cone, the weight benefits would be lost if the same stiffness and strength as the continuous cone to be maintained. Thus, a truss type support structure was recommended in that study, and is used in this study.

A preliminiary layout of the drive mechanism is shown in Figure 3.3. The torus antenna pedestal is coaxially rotated around the inner housing having an inner diameter of 6 inches (150 mm). It is driven by a dc brushless

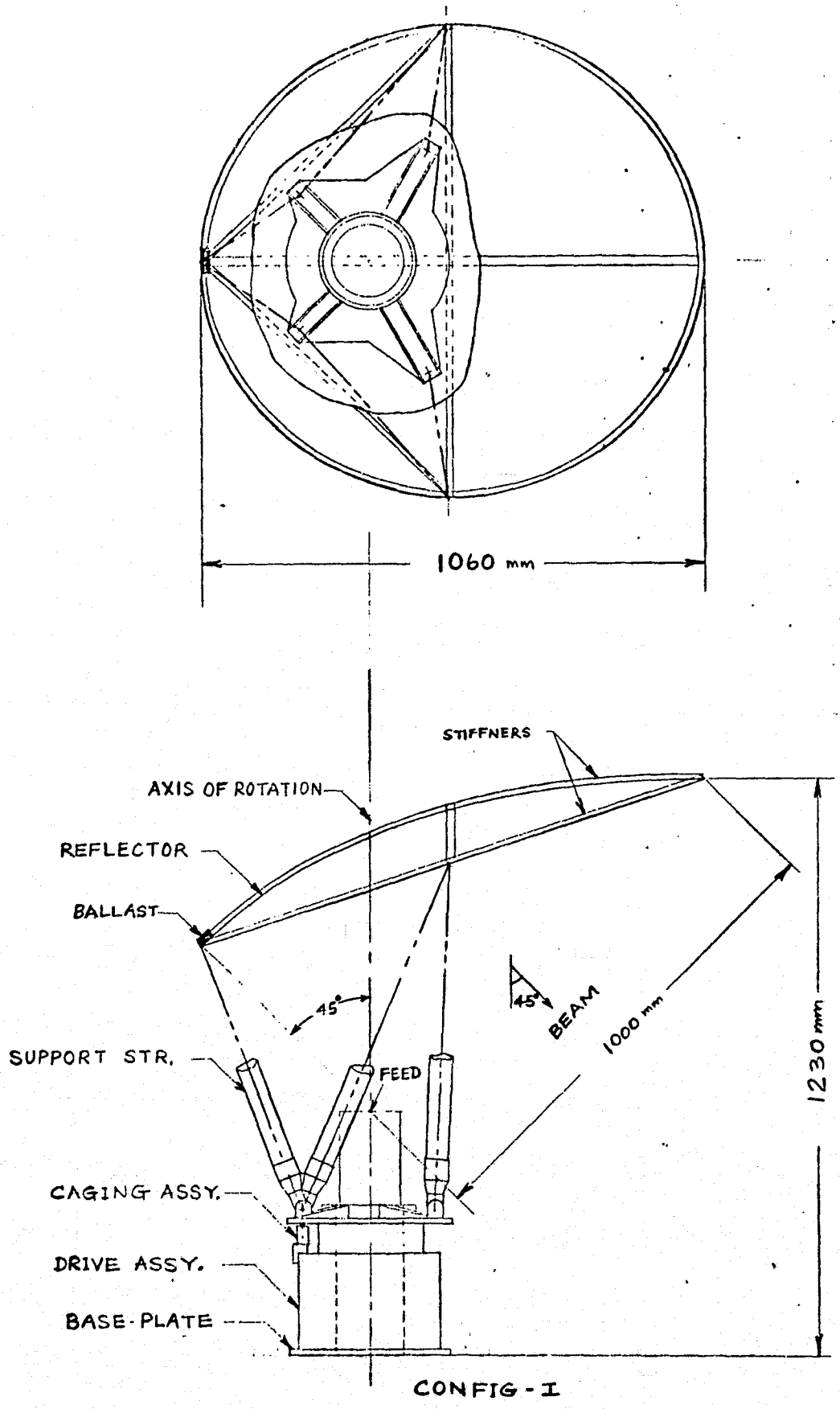

Figure 3.1 System Configuration I - 1.0m Reflector

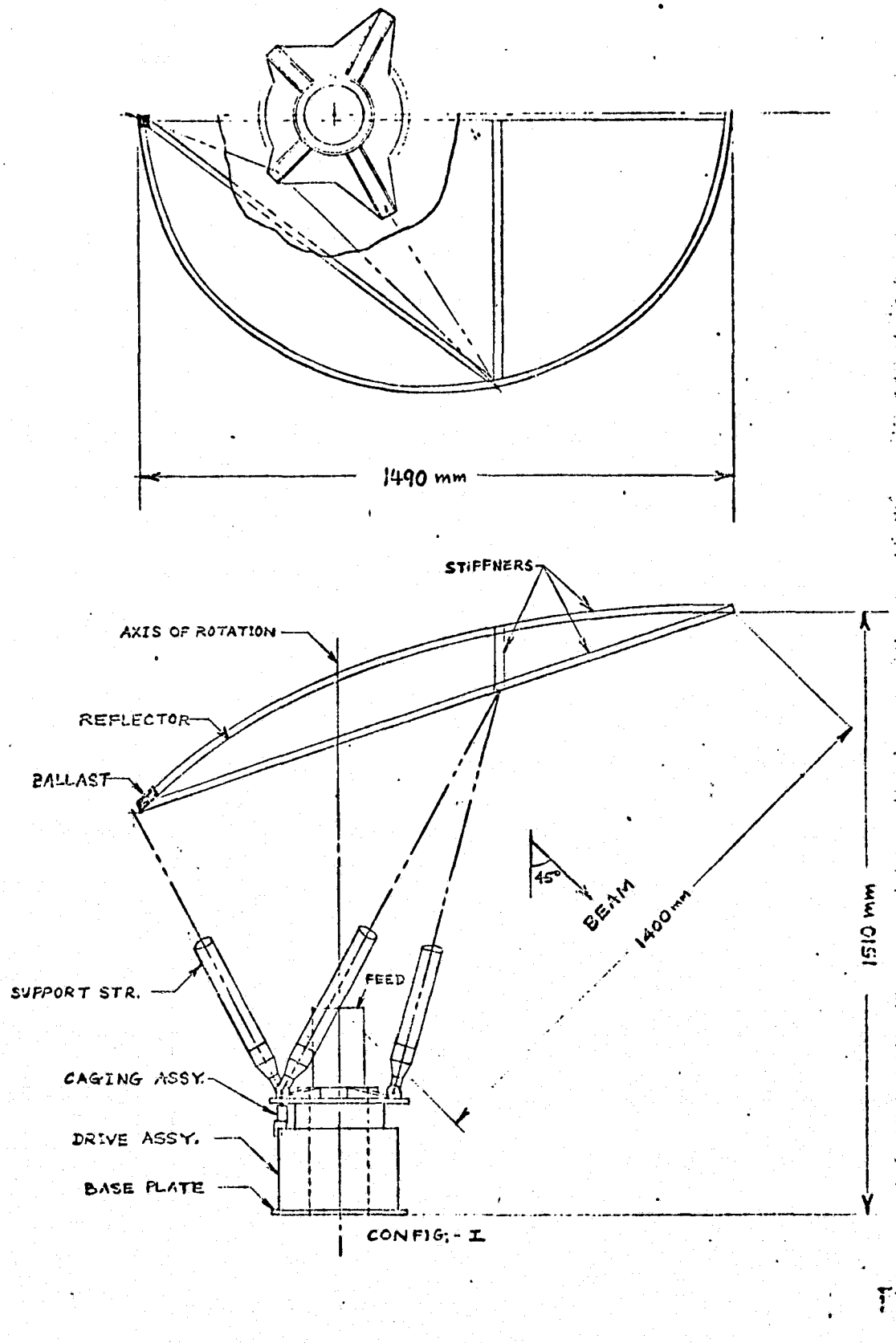

Figure 3.2 System Configuration I - 1.4m Reflector

ORIGINAL PAGE IS
OF POOR QUALITY

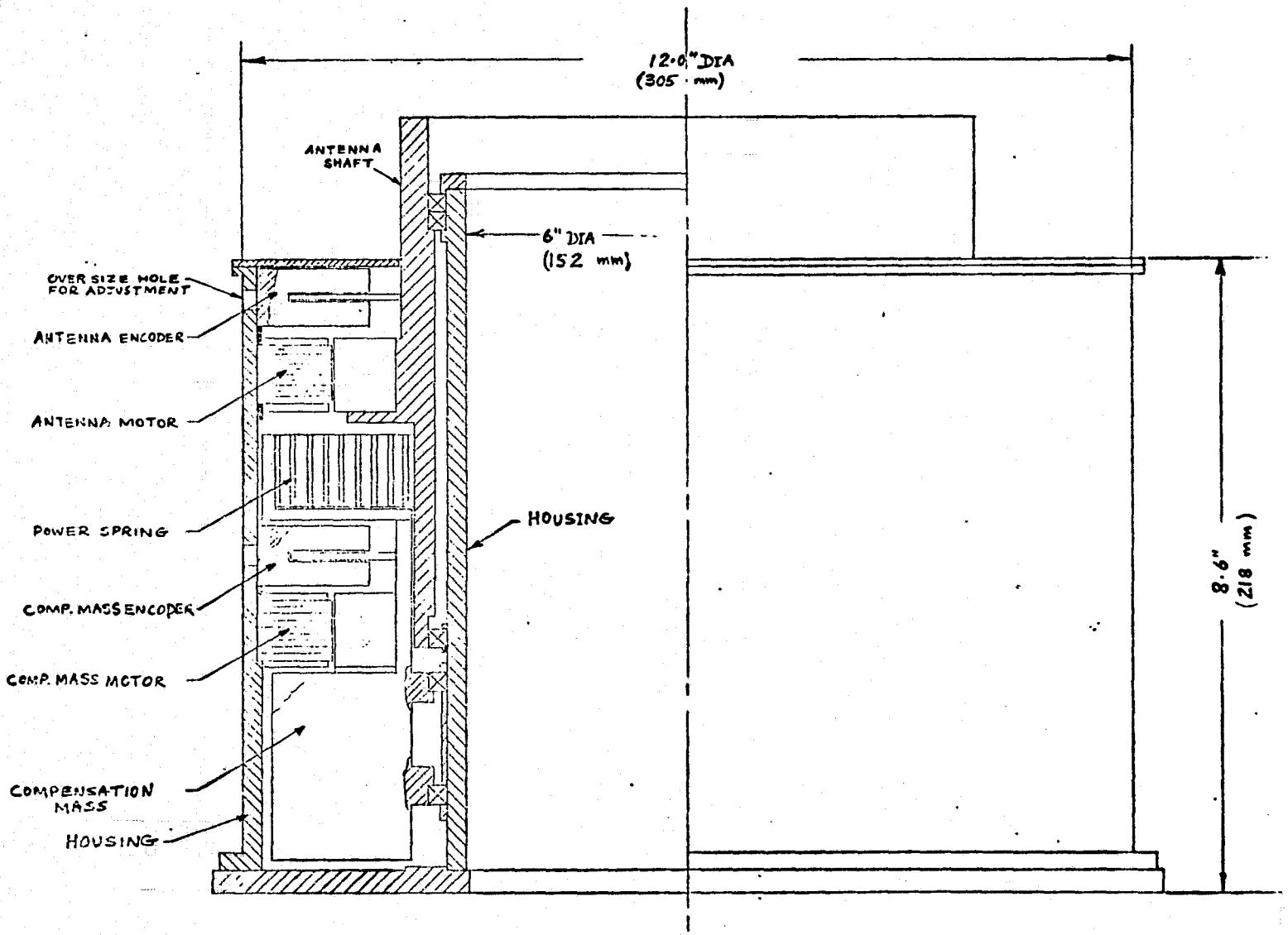

Figure 3.3 Configuration I Drive Mechanism

torque motor mounted on the outer housing. The compensating wheel also coaxially rotated around the inner housing is driven by a second motor mounted on the outer housing. There are two shaft encoders provided to measure angular deflections of antenna pedestal and compensation wheel relative to the housing.

Since the antenna assembly will be statically balanced, the center of mass of the assembly will coincide with the axis of rotation. As the main portion of rotating mass is on the reflector, however, the center of mass is far away from the support bearings and the assembly behaves as a cantilever attached to the inner housing through the bearings. The main bearing in this configuration is a fixed duplex pair located at the top of inner housing and a floating duplex bearing at the bottom provides axial alignment. The antenna assembly will be caged to the outer housing during launch and uncaged by use of pyro-device after the vehicle is placed into the orbit. Because of the chosen bearing arrangement and bearing characteristics, the caging would require only to prevent rotation of shafts as the bearings can sustain the launch load in thrust and radial directions.

The power spring between the pedestial shaft and the compensation wheel will be tuned to synchronize resonant frequency to the desired scan frequency. Since this spring provides the acceleration torque, the torque motors can be sized from the consideration of bearing frictions only.

3.2.2 MOTOR SELECTION AND POWER REQUIREMENTS

In the earlier study, it is shown that the static friction in a ball bearing is related to the static equivalent load, the thrust load and the ball pitch diameter.

If it is assumed that the static and thrust loads are proportional to the antenna mass and the mass is proportional to the reflector surface area, it can be shown that the static friction is proportional to the (8/3) power of the antenna diameter and directly proportional to the ball pitch diameter. Therefore, using the friction value obtained in the previous study for 0.8m antenna diameter, scaled static friction values for various antenna sizes and bearing sizes can be obtained as shown in Figure 3.4. The viscous friction can be also scaled in similar manner. It can be shown that the viscous friction is proportional to (2/3) power of shaft rotating velocity and directly proportional to the bearing pitch diameter while it is independent of the antenna sizes.

With 6-inch bearings for 1.4m reflector the static friction is 0.16 ft-lb from the Figure 3.4. The peak torque of antenna drive should be 1.6 ft-lb (308 oz-in) if 10 to 1 safety factor is used to insure sufficient torque margin for run-up acceleration and synchronization. From a survey of commercial catalogs, it is found that a Magnetic-Technology motor model 11490-100 has dimensions compatible with the feed size and torque capacity required. The characteristics of the motor are given in Table 3.1.

The maximum angular velocity for the antenna assembly which is sinusoidally oscillating at 1/2 Hz with 45-degree amplitude is under 2.5 radian per second. In order to develop a peak torque of 308 oz-in at a motor terminal voltage of 20 volts (nominal 24 volt power source is assumed), the armature resistance should be 27 ohms. The peak armature current is then 0.74 ampere and the torque sensitivity is 415 oz-in/amp. The no load angular velocity with 20 volt excitation (motor terminal voltage) is 6.8 rad/sec and the back emf constant is 2.9 volts per rad/sec.

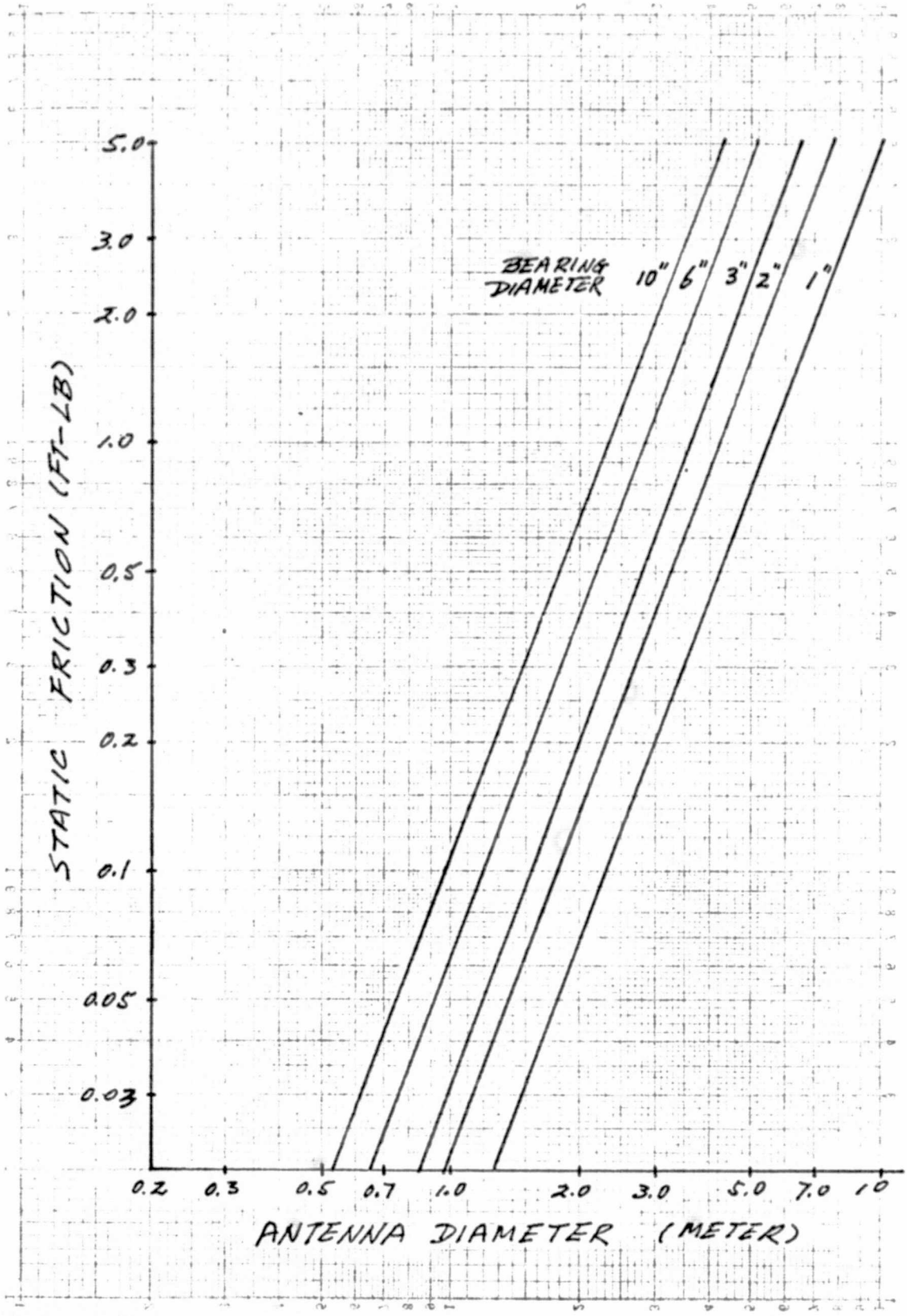

Figure 3.4 Static Friction

Table 3.1 MOTOR PARAMETERS

MAG-TECH MODEL #	6000-090	7000-065	11490-100	11968-093
PEAK TORQUE (oz-in)	300	300	1150	2000
NO LOAD SPEED (rad/sec)	22	31	24	163
MOTOR CONST K_M (oz-in/$\sqrt{\text{watt}}$)	42.4	36	80	130
ROTATING MEMBER	INNER	OUTER	INNER	OUTER
OD (inch)	6.000	7.000	11.488	11.968
ID (inch)	4.000	5.380	7.875	10.250
THICKNESS (inch)	0.900	0.650	1.00	0.920
WEIGHT (lb)	2.8	1.5	6.0	5.3
MOTOR FRICTION TORQUE (oz-in)	5	8.5	25	43

At steady state the torque required to drive the antenna is to overcome the various frictions. The static friction has a constant level of 31 oz-in (except possible random variation) and in phase with the angular rate. As the viscous friction level is proportional to the 2/3 power of angular rate amplitude, its variation is approximately sinusoidal with peak value of 24 oz-in (from scaling law) and in phase with the rate. There is also a friction torque contributed by the motor itself (see Table 3.1). This torque is the sum of the brush-commutator friction (brush type motor only) and the magnetic retarding torques such as hysteresis drag and slot effect drag. For the motor sizes considered in this study, the motor friction is generally about 2 percent of maximum peak torque, between one third to two thirds of which is contributed by the brush-commutator friction. Since the motor selected is a brushless type, it is assumed that the motor friction of this antenna motor is 15 oz-in from the value given in Table 3.1. Hence, the peak torque required at the steady state is 70 oz-in and the rms torque is 63 oz-in. The corresponding input currents are 0.17 ampere and 0.15 ampere respectively.

If the compensation wheel is counter-rotated at 10 times the rate of the reflector, the moment of inertia required is one-tenth of the reflector assembly. Since the required wheel mass will be comparable with the reflector due to smaller radius of gyration, however, the same static friction level as the reflector is used to size the motor driving the compensation wheel. The no load angular velocity required is 25 radian per second, and the armature resistance should be 2 ohms. The torque sensitivity is 114 oz-in/amp and the peak current corresponding to 1140 oz-in peak torque is 10 amperes. The back emf constant is 0.8 volts per rad/sec.

The peak value of viscous friction for the wheel is 110 oz-in due to the higher angular rate while the static friction and the motor friction are 31 oz-in and 15 oz-in respectively as in the case of the antenna drive. Hence, the peak torque at steady state is 156 oz-in and the rms torque is 124 oz-in. The corresponding input currents are 1.37 amperes and 1.09 amperes respectively.

Combining peak current requirements for the antenna and wheel drives and assuming 10% power loss in the drive electronics, the estimated maximum total power input to the drive mechanism at steady state is 41 watts (24 volt nominal input voltage is used). For 1.0m reflector antenna, the static friction is 0.07 ft-lb (13.5 oz-in) from Figure 3.4. Hence, using the same armature winding parameters as the 1.4m antenna drive motor, the input current values are 0.13 ampere peak and 0.11 ampere rms. The input currents for the wheel drive motor are 1.21 ampere peak and 0.94 amperes rms. The estimated maximum total power input to the drive mechanism is 36 watts.

3.2.3 SERVO LOOP

Three possible servo loop configurations can be considered: (a) both motors are slaved to the reference signal, (b) the antenna motor is referenced to the drive signal while the compensation wheel motor is slaved to the antenna position, and (c) the wheel motor is driven by the references signal while the antenna motor is slaved to the wheel position. Because the antenna drive motor has more torque margin than the wheel drive motor as shown in the preceding paragraph, it is advantageous from the torque consideration to slave antenna drive to the wheel drive rather than slaving the wheel to the antenna. As the antenna is indirectly referenced to the drive signal in this configuration, however, the pointing angle of antenna includes the error due to the wheel servo loop as well as the antenna

ORIGINAL PAGE IS
OF POOR QUALITY

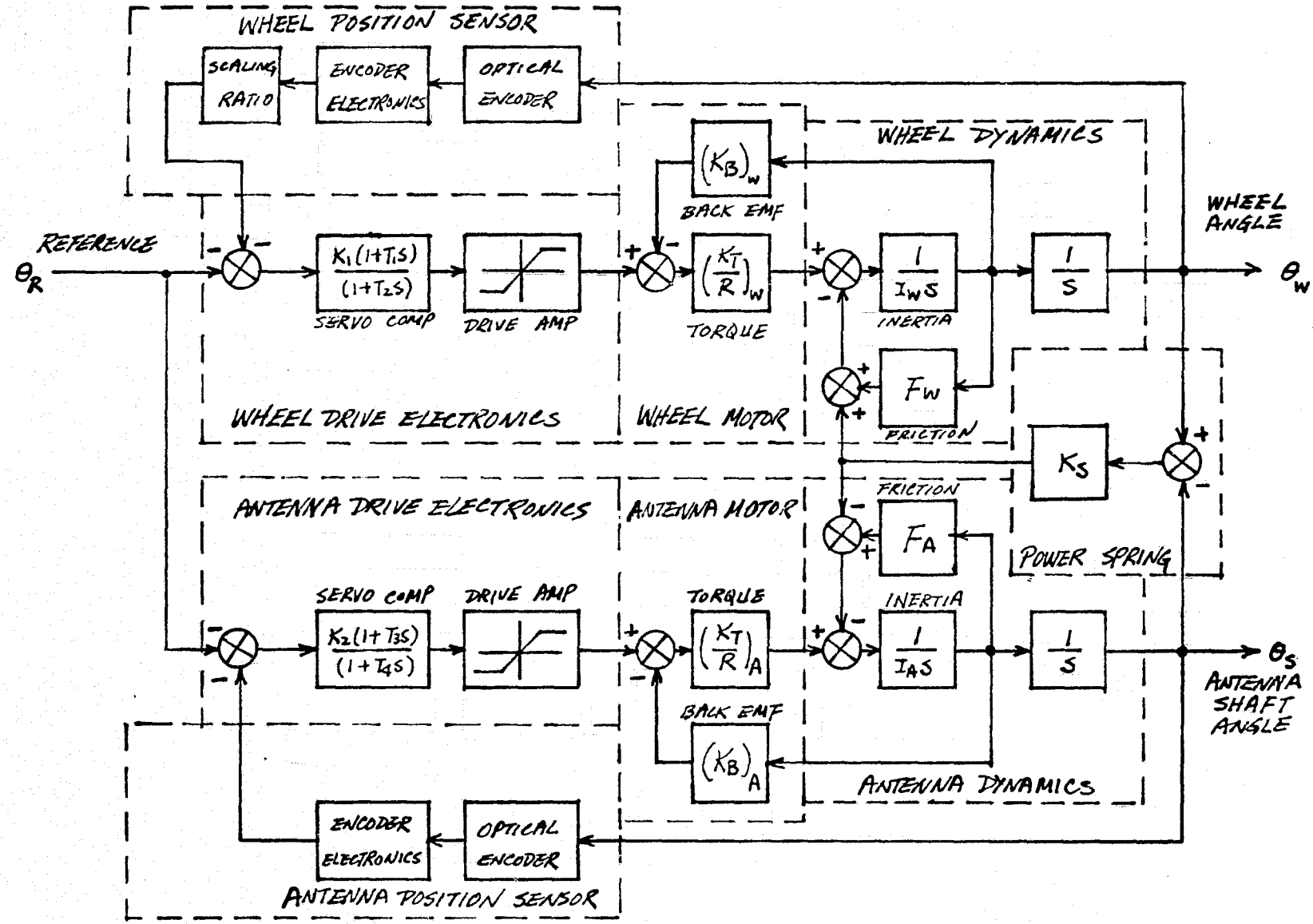

Figure 3.5 Block Diagram - Configuration I

servo loop. If both motors are directly slaved to the reference sinusoidal signal, it is possible to have a large uncompensated disturbance momentum during the starting transient since the motor-load characteristics of the antenna and the wheel are not exactly matched. As the transient disturbance does not affect the steady state operation, this approach is selected for the study.

A block diagram of the servo loop is shown in Figure 3.5. The compensation wheel motor is excited by the error signal derived from the difference between the reference sine wave and the decoded output signal of shaft encoder measuring wheel deflection angle. The wheel angle is scaled by the inertia ratio of the antenna and the wheel such that the error signal becomes zero when the wheel deflection angle is 10 times the reference signal in amplitude and 180 degrees out of phase. When the error signal is zero, no energy is injected by the wheel drive motor into the spring resonance harmonic oscillatory system.

The error signal is passed through a lag-lead compensation network and applied to a power amplifier. As the amplifier characteristics is generally linear, the developed motor torque is also a linear function of the error signal. However, the torque output is limited by the amplifier saturation and the motor winding characteristics when the error signal is large (for example, during the starting transient). The input torque causes the wheel to accelerate and the additional energy to the wheel modifies the oscillation amplitude and phase of the resonance system.

The antenna drive motor is excited by the error signal derived from the sum of the reference signal and the antenna deflection angle measured by a shaft encoder. Hence, when the antenna rotates the angle commanded by the reference signal, the error signal becomes zero. The error signal is passed through a lag-lead

compensation network and a power amplifier as in the case of the wheel drive. Even though the antenna drive output torque is also limited, the operation would be in linear region except during the starting transient. As the servo loop may become unstable due to amplifier saturation during this starting period, the reference signal amplitude should be increased gradually.

3.3 DRIVE CONFIGURATION II

3.3.1 MECHANICAL CONFIGURATION

The reflector in this configuration is attached to a drive shaft at the top, as shown in Figures 3.6 and 3.7. Since the shaft does not have to wrap around the feed, its diameter can be smaller and, consequently, smaller diameter bearings can be utilized to minimize frictions in the drive.

As the reflector is located very close to the main drive shaft bearing, the supporting structure between the drive and the reflector can be made very stiff. However, since either the drive mechanism, the sensor assembly (the feed and the radiometer) or both must be mounted at distances from the satellite bus structure, the dynamics of these supporting structures should be included in the performance analysis. It is assumed for this study that both the drive mechanism and the sensor assembly are mounted to a base plate through separate supporting structures and the base plate is attached to the satellite as shown.

As shown in Figure 3.8, a drive shaft of 2-inch (50 mm) nominal diameter is used to rotate the reflector in this configuration. The compensation wheel is mounted on the drive shaft through a pair of bearings and a dc brushless torque motor and a power spring are installed between the wheel and the shaft. Thus, the antenna assembly and the wheel become a part of coupled harmonic oscillator in which the motor supplies the energy to maintain the oscillation.

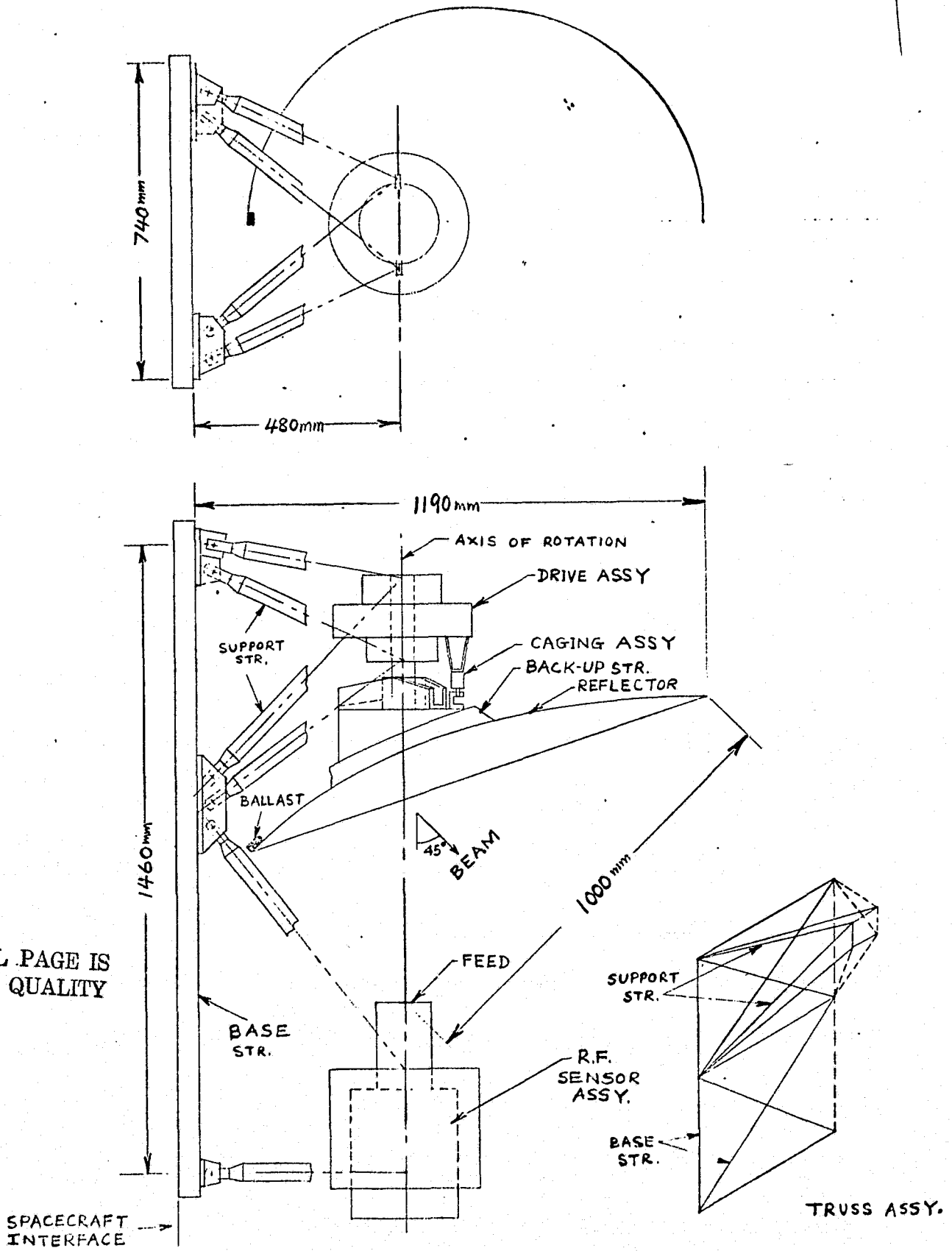

ORIGINAL PAGE IS
OF POOR QUALITY

Figure 3.6 System Configuration II - 1.0m Reflector

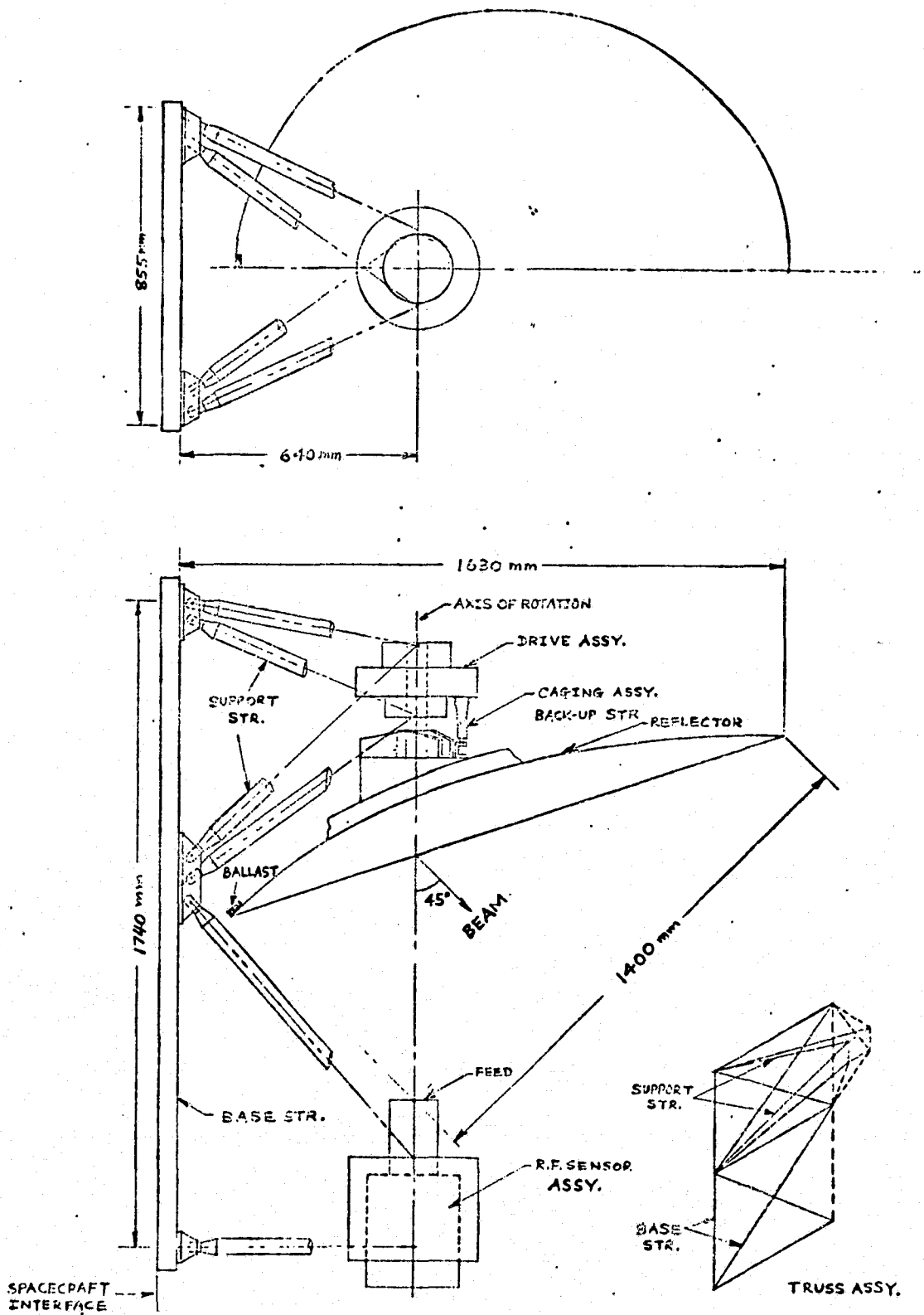

Figure 3.7 System Configuration II - 1.4m Reflector

ORIGINAL PAGE IS
OF POOR QUALITY

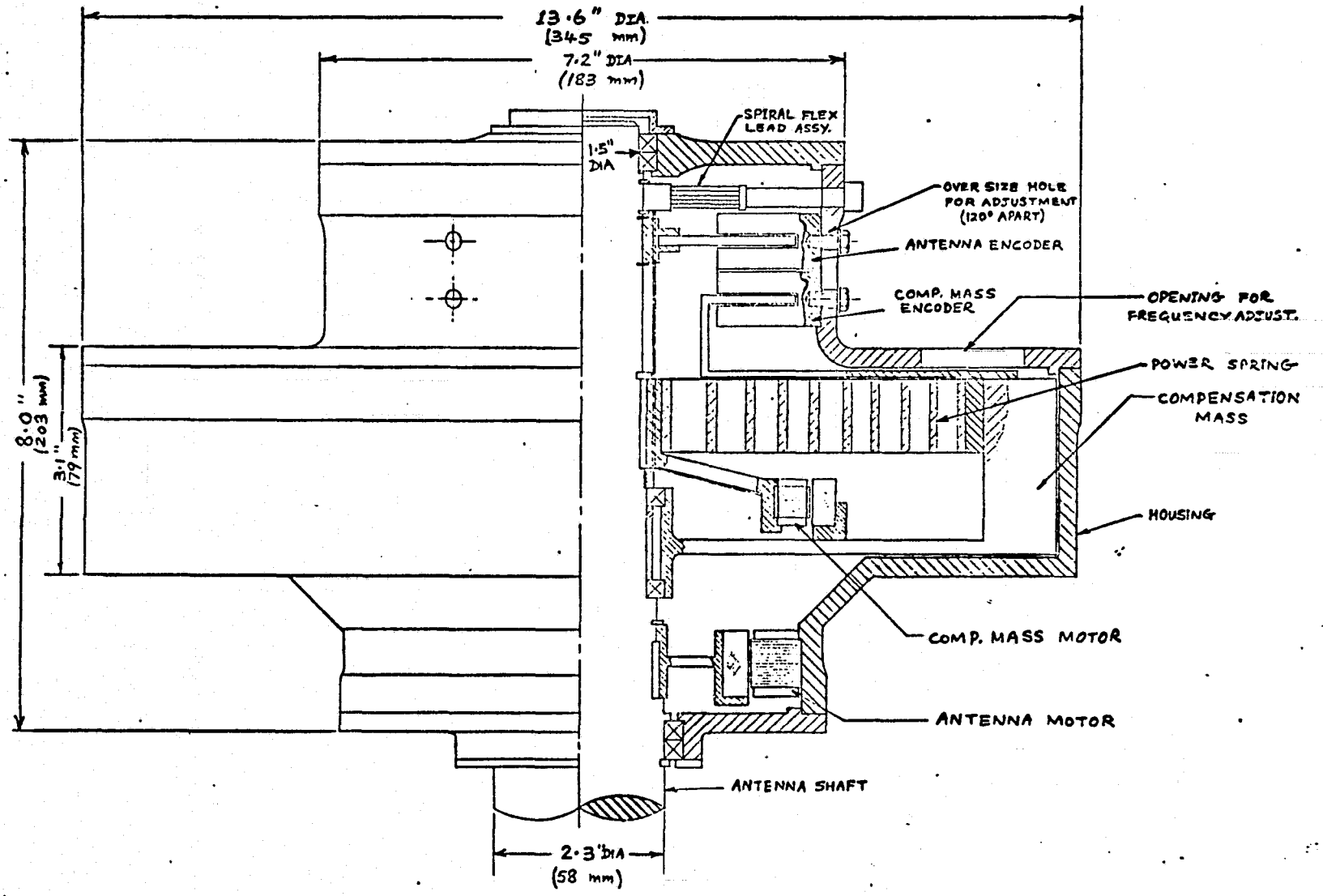

Figure 3.8 Configuration II Drive Mechanism

As the antenna pointing null point might drift due to mismatch of the antenna frictions and the wheel frictions, a second motor is provided between the shaft and the housing to trim the null point. Shaft encoders are provided to measure deflection angles of the antenna shaft and the compensation wheel with respect to the housing. Also included in the drive mechanism is a spiral motor lead wire assembly as shown in Figure 3.9 which is required since the armature of the wheel drive motor (stator) as well as its permanent magnet field rotates with respect to the housing.

The antenna assembly will be statically balanced to have its center of mass coincide with the axis of rotation. The fixed pair of preloaded duplex bearings at the bottom of housing carries the main load of assembly and the floating duplex pair of bearings at the top provides axial alignment. The antenna assembly is caged to the housing to prevent from vibration due to launch disturbances until the satellite is placed into the orbit.

As in the case of Configuration I, the power spring provides acceleration torque for sinusoidal oscillation during the steady state operation and the motors can be sized from friction considerations only.

3.3.2 MOTOR SELECTION AND POWER REQUIREMENT

From Figure 3.4 the static friction for an antenna with 1.4m diameter is less than 0.06 ft-lb (11.5 oz-in) when the bearing diameter is 2 inches. The static friction for the wheel bearings is therefore estimated to be 11.5 oz-in. Since the antenna shaft bearings carry both the antenna reflector and the compensation wheel loads, however, the estimated static friction for the shaft is 23 oz-in. Using 10 to 1 safety factor as before, the peak torque requirement of 1.2 ft-lb (230 oz-in) is obtained. Since the maximum angular velocity of antenna shaft is less than 2.5 radian per second, a motor similar to the Mag-Tech model 6000 - 090 in a commercial catalog (see Table 3.1) can be used. If 230 oz-in peak torque is to be developed at 20 volts, the armature resistance

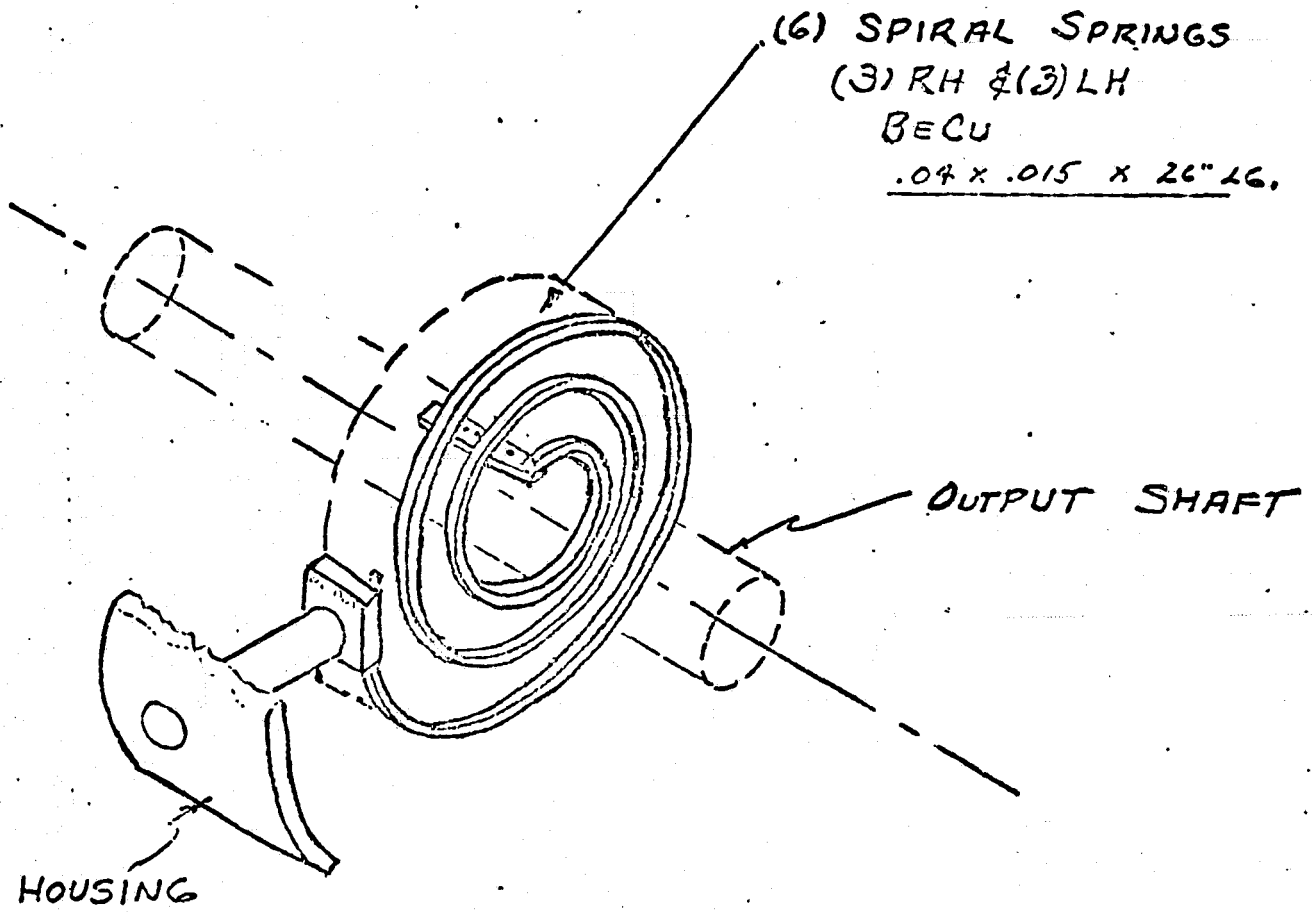

Figure 3.9 Spiral Flex Lead Assembly

should be 13.5 ohms. The peak armature current is then 1.5 amperes and the torque sensitivity is 156 oz-in/amp. The no load angular velocity with 20 volt excitation is 18 rad/sec and the back emf constant is 1.1 volt per rad/sec.

If the antenna shaft is driven against the housing by the antenna motor, at steady state, the constant static friction is 23 oz-in and the peak value of viscous friction (for 2 inch bearings) which approximately varies sinusoidally is 8 oz-in. The motor friction torque due to magnetic retardation is approximately 3 oz-in from Table 3.1. Hence, the peak and rms armature currents required at steady state are 0.22 ampere and 0.20 ampere respectively.

Since the antenna motor is required to correct null drift only, however, the input current required at steady state would be negligible.

When the compensation wheel is counter-rotated at a rate 10 times the antenna shaft rate, the relative angular velocity between the rotor and the stator of the wheel motor is 11 times the antenna rate or approximately 28 radian per second maximum. For the wheel drive, an inverted dc brushless torque motor (Mag-Tech Model 7000-065 in Table 3.1) is considered. If a no load angular velocity of 30 radian per second is to be developed with 20 volts excitation, the required armature resistance is 6.8 ohms. The torque sensitivity is 94 oz-in/amp and the peak current corresponding to 273 oz-in is 2.9 amperes. The back emf constant is 0.67 volts per rad/sec.

At steady state, it is expected that the torque input from the wheel motor compensates friction loss of both the wheel and the antenna shaft since the motor torque work against both bodies. Then, the static friction torque is the sum of 11.5 oz-in for the wheel bearings and 23 oz-in for the shaft bearings while the peak value of quasi-sinusoidally varying viscous friction torque is the sum of 43 oz-in for the wheel bearings and 8 oz-in for the shaft bearings. The estimated motor friction due to magnetic retardation is 5 oz-in. Hence the peak and rms armature currents required are 0.96 ampere and 0.80 ampere respectively.

Assuming ten percent power loss in the drive electronics, the estimated maximum total power input at steady state is 26 watts (24 volt nominal input voltage is used) because only the wheel drive motor would be excited.

For a 1.0m reflector with 2 inch bearings, the static friction from Figure 3.4 is 0.022 ft-lb (4.2 oz-in). Using the same winding parameters as derived for the 1.4m reflector drive, the input current values for the wheel motor are 0.64 ampere peak and 0.48 ampere rms. With the assumption of ten percent power loss in the drive electronics, the input power requirement after reaching steady state is 17 watts maximum.

3.3.3 SERVO LOOP

A block diagram representation of the servo loop for the Configuration II is shown in Figure 3.10. As in the case of Configuration I, the compensation wheel motor is excited by the error signal between the reference sine wave and the scaled shaft encoder output of the wheel angle. The scaling is equal to the ratio of antenna and wheel moments of inertia. Since the motor drives both the wheel and the antenna shaft away from the null in opposite direction, a closed loop is formed by the wheel motor, encoder measuring the wheel rotation angle with respect to the housing, and the drive amplifier. While the closed servo loop tries to have the scaled wheel rotation follow the reference signal, the antenna shaft is counter-rotated by an angle approximately equal to the reference signal by the reaction torque. If there is no friction torque, the ratio of angular rotations exactly matches the inverse ratio of moments of inertia (10 in this design) and no angular momentum disturbance is generated. With the antenna shaft and the compensation wheel being coupled by a power spring, the ideal drive mechanism becomes a harmonic oscillatory system and maintains a sinusoidal scan motion without energy injection once it reaches desired amplitude and the phase.

ORIGINAL PAGE IS
OF POOR QUALITY

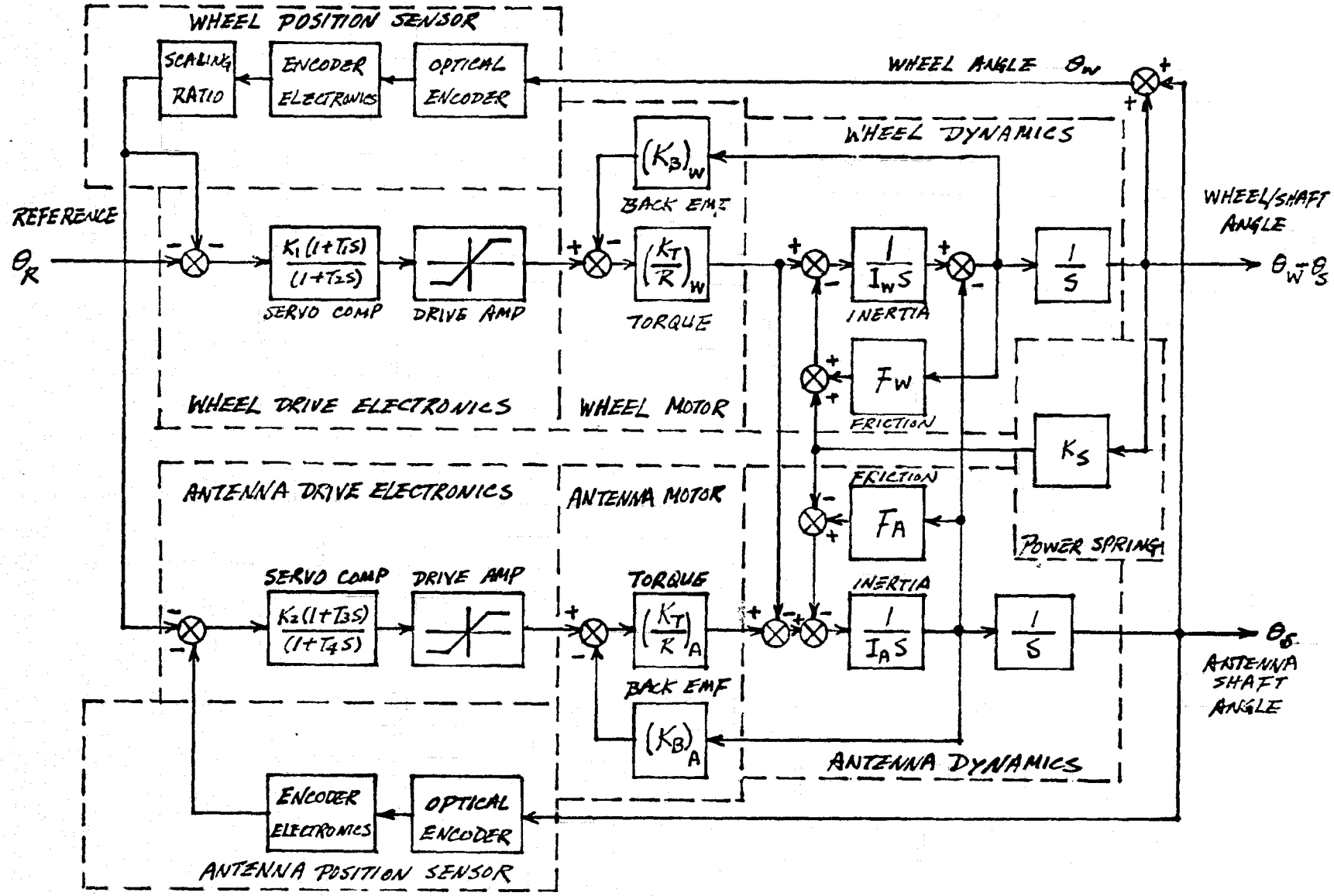

Figure 3.10 Block Diagram - Configuration II

Because of the frictions in any practical bearings, however, a correctional torque has to be injected into the drive. If there is an error between the reference signal and the scaled wheel angle, the error signal is modified by a lag-lead compensation network and amplified by a power amplifier. The developed torque output is generally a linear function of the error signal except when the output torque is limited for a large error (such as during the starting transient). The torque accelerates the antenna shaft and the wheel to null the error.

If the opposing friction torques, of the antenna bearings and the wheel bearings, are not matched, angular rotations of the shaft and the wheel with respect to the housing are not exactly proportional to the inverse of their respective moments of inertia and a drift of the null of harmonic oscillation results. This null drift causes a residual disturbance of angular momentum as well as the shift of antenna pointing null. In order to correct the null drift, the angular rotation angle of the wheel with respect to the housing is divided by the inertia ratio of the antenna and the wheel (10 in this design) and compared with the shaft rotation angle. The resultant error angle is the amount of null drift or null error. The null error signal is passed through a lead-lage compensation network and a power amplifier, and excites the antenna trim motor to drive the shaft. Thus, the antenna rotation angle is modified by the null error signal to correct the drift.

3.4 COUNTER-ROTATION ANTENNAS

Both configurations considered in preceding sections use a power spring as an energy storage device to provide acceleration torque required for oscillatory scanning.

As the energy for harmonic oscillation is conserved, the drive motors are only required to inject the energy to compensate frictional losses to maintain the scan motion once it attains the desired amplitude and the phase. It is noted that in these configurations, heavy counter-rotating compensation wheels are necessary to cancel the angular momentum disturbance caused by oscillating antenna.

Since the weight of the compensation wheel would be comparable with that of the scanning antenna assembly, another scanning antenna in lieu of the wheel can be employed to compensate the disturbance with little weight penalty. If the oscillatory motion is replaced by a continuous rotation with a constant velocity, the spring is no longer needed as the acceleration for turn-around is not required. Hence, a scanning antenna system with momentum disturbance compensation requiring a low input power can be obtained by use of two continuously counter-rotating antennas. Figure 3.11 shows some of the possible configurations obtainable from the basic drives formulated as Configuration I and II.

Each drive element contains only one motor and no compensation wheel. The angular rate of one element drive is controlled by a reference signal and the other is slaved to the former through a coupling servo. Once the drive mechanism reaches steady state (proper angular rates and relative phasing of two antennas) the motors are required to deliver only the energy losses due to frictions.

Disadvantages of this configuration include:

a) A large volume of space is required to install and operate as indicated by the dimensions shown in Figure 3.11.

b) Unless both fore and aft scan swaths can be utilized, the duty cycle is low and it might require higher scan rate to achieve contiguous coverage.

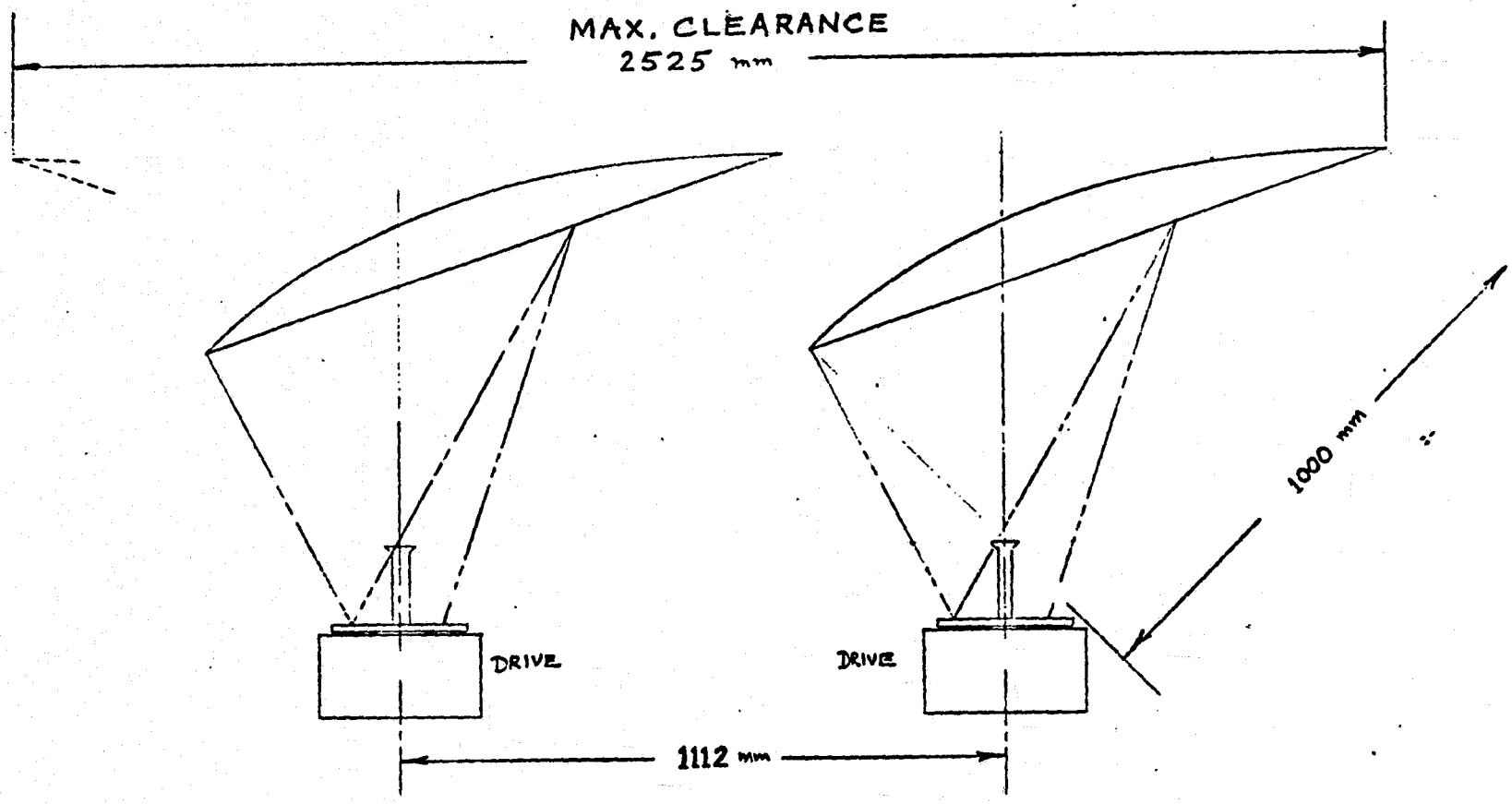

Figure 3.11A Counter-Rotating Configuration I-I

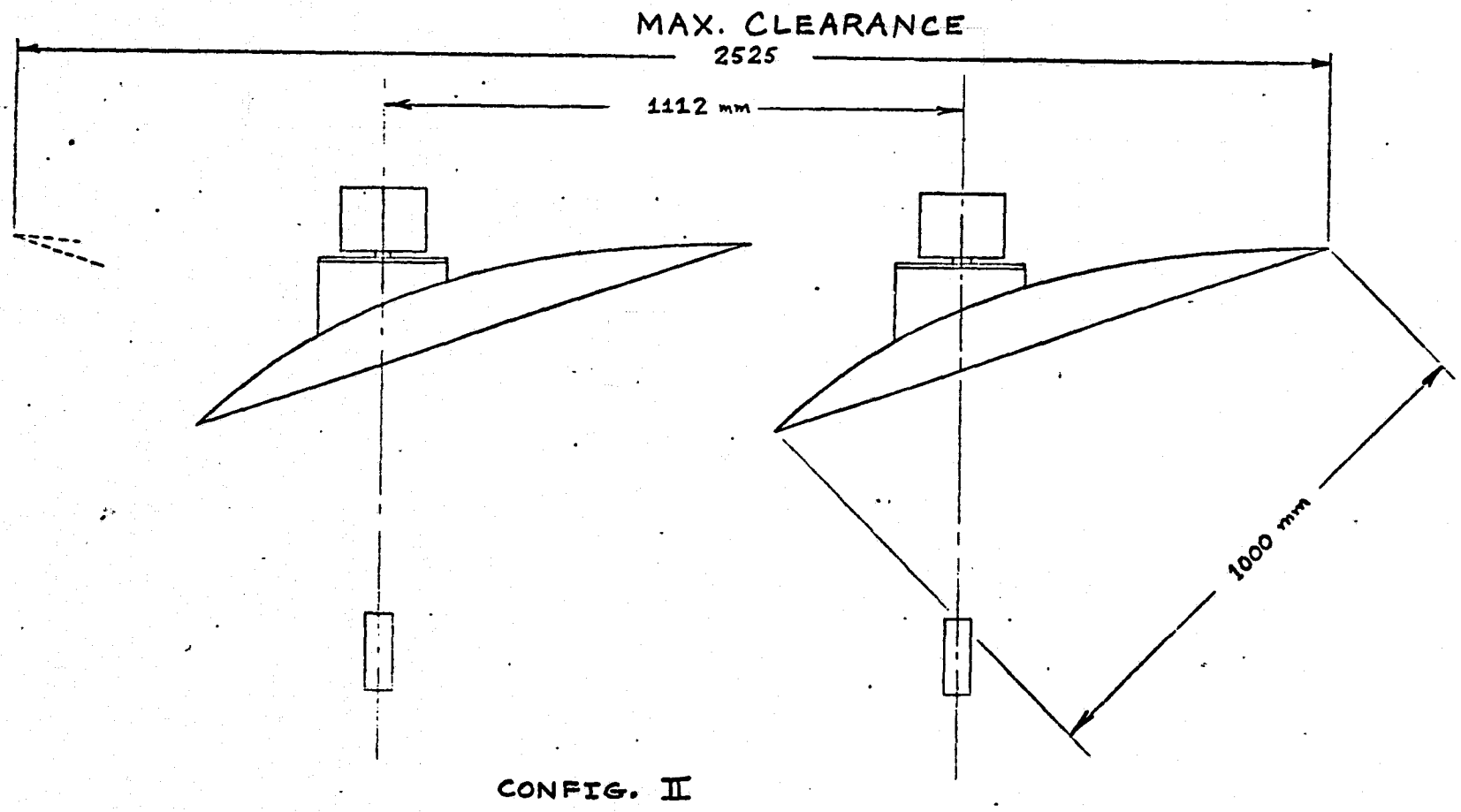

Figure 3.11B Counter-Rotating Configuration II-II

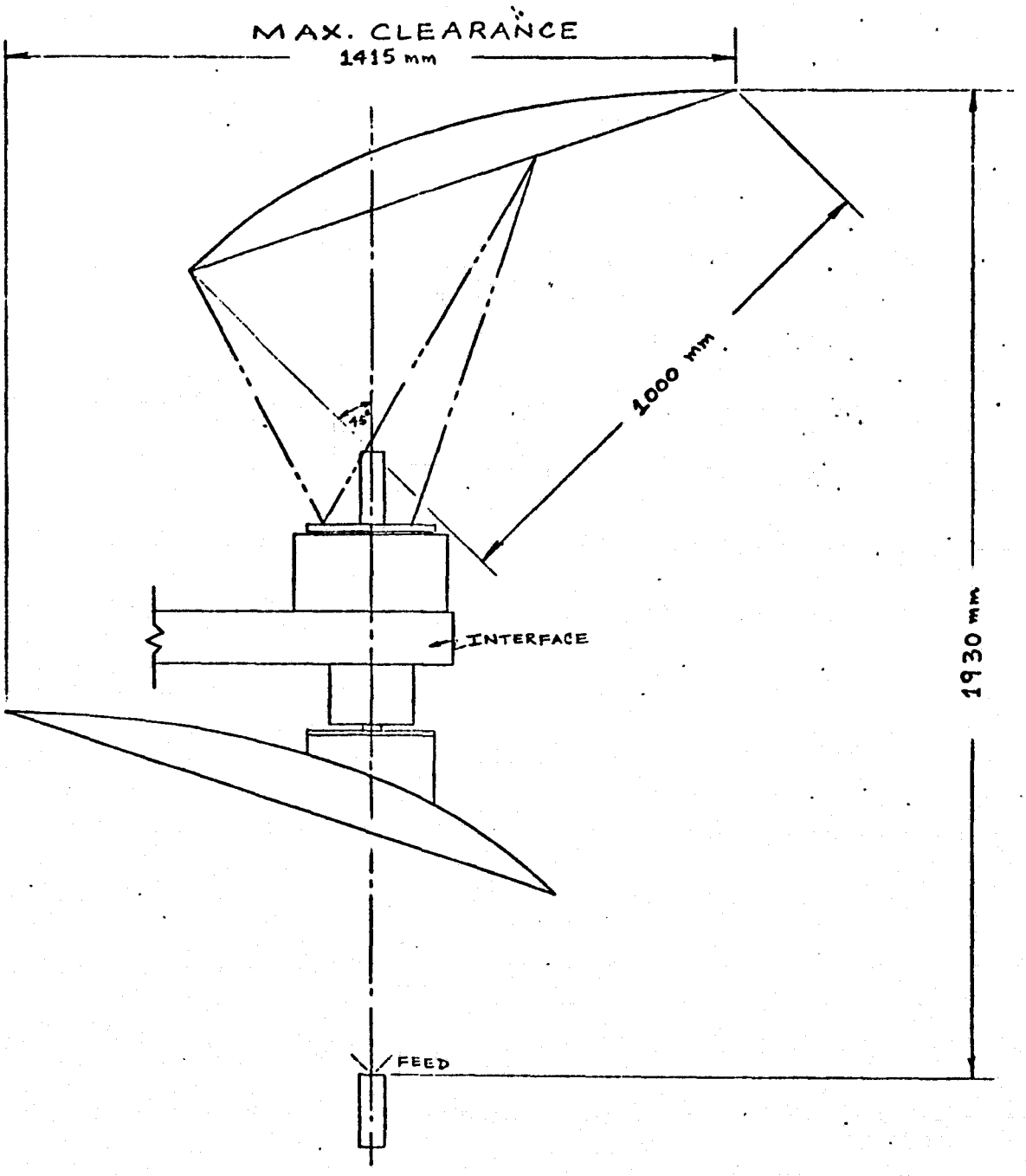

Figure 3.11C Counter-Rotating Configuration I-II

c) It contains structural disadvantages of both Configurations I and II if a stacked version is used to minimize the size.

Therefore, this configuration is not recommended except a case for which a dedicated spacecraft is available.

4.0 COMPONENT SELECTION

The components for the drive mechanisms formulated and analyzed in this study are mostly derived from those available in commercial catalogs. Some of the components may require custom modification while others may be available as "off-the-shelf" items.

4.1 DRIVE MOTORS

Brushless dc torque motors are selected for the two motors required to initiate and control the sinusoidal rotary scanning motion of the antenna and the momentum compensation motion of the wheel. Freedom from brushes decreases the friction load and enhances the reliability by eliminating all mechanical sliding contacts. The motors selected are based on available motors which have been previously manufactured for similar applications.

Basic characteristic parameters of the selected motor are given in Table 3.1 and the winding parameters derived in the previous section are summarized in Table 4.1. Preliminary specifications for these motors are included in Appendix A.

4.2 BEARINGS

The loads which must be accommodated by the mechanical scan drive mechanism are determined from the weight and inertia of the scanning antenna reflector. The following characteristics for 1.4 M reflector are used in the calculations of the load levels.

Mass Rotating with Antenna (Configuration II)

Weight:	21 Kg (46.2 lbs.)
Inertia	2.92 Kg-m^2 (2.5 slug ft^2)
Scan Frequency	0.5 Hz
Scan Amplitude	$\pm$45 degrees

Table 4.1 Motor Winding Parameters

Motor	Configuration I		Configuration II	
	Antenna	Wheel	Antenna	Wheel
Mag-Tech Model #	11490-100	11490-100	6000-090	7000-065
Resistance, R_a ohm	27	2	13.5	6.8
Peak Torque, T_P oz-in	308	1140	230	273
Current @ T_P, I_P ampere	0.74	10	1.5	2.9
Power @ T_P, P_P watt	15	200	30	58
No Load Speed, ω_o rad/sec	6.8	25	18	30
Torque Constant, K_T oz-in/amp	415	114	156	94
Back EMF, K_V volts/rad/sec	2.9	0.8	1.1	0.7

Compensating Mass (Configuration II)

Weight:	16.5 Kg (36.3 lbs.)
Inertia	.29 Kg-m^2 (.22 slug ft^2)
Frequency	0.5 Hz
Amplitude	±450 degrees

Since the motion of the antenna is sinusoidal, the torque required is maximum at the reversal point (neglecting frictions). The maximum reversal torque (to be applied simultaneously on both antenna and compensating mass) is 16.66 ft-lbs at the reversal point.

The maximum bearing loads will occur during launch. Assuming maximum sinusoidal acceleration of 3 G (from Shuttle environment), the maximum radial load will be 248 lbs. at the inboard bearing pair with a corresponding axial load of 124 lbs. Bearing loads due to spacecraft attitude oscillations are extremely small (10^{-5} lbs.) and can be neglected. The level of bearing loads for the configuration I is about the same as the configuration II.

Ball bearings are selected for the drive mechanism assembly since it provides the lowest friction torque values among the conventional bearings. It is desirable to keep the bearing running torques as low as possible in order to maintain a low level of make up power required of the torque motors.

Minimum bearing sizes are dictated by the shaft size needed to support the parabolic reflector with acceptable rigidity characteristics. This requirement results in bearing size of 6½ inch bore diameter for the configuration I as the shaft wraps around the feed horn having an outside diameter of over 5 inches. The requirement for the configuration II results in bearing sizes of approximately 2¼ inch bore diameter at the outboard end of the shaft and 1½ inch diameter at the inboard end.

Duplex pairs are recommended in order to eliminate radial play within the bearing and to stabilize the axis of rotation both radially and axially. Angular contact bearings are chosen because of their adaptability to preloading and their ease of disassembly for thorough inspection, cleaning, and lubrications for space applications.

The inboard bearings for the configurations I and II have static (thrust) load ratings of 7200 lbs. and 1290 lbs. respectively. Hence, the expected launch loads will be less than 10% of the bearing capability. The dimensional characteristics of the bearings utilized for the formulation of drives are summarized in Table 4.2.

For lubrication, either a low viscosity low vapor pressure oil or some form of dry lubricant such as a polyamide retainer containing MoS_2 with MoS_2 burnished raceways would be acceptable. The liquid lubricant impregnated into a porous retainer is preferred if low temperature effects and long life requirements are not limiting.

Among wet lubricants a silicone oil such as GE F-50 appears to meet the requirements of this application. Even at $-40^{\circ}C$ temperature the viscosity of oil is only 500 centistokes. The calculated total torque at this temperature from the bearings with silicon oil lubrication is approximately 15 oz-in for the configuration II drive. For the worst case condition of starting at $-40^{\circ}C$, the motor torque of 300 oz-in provides a 20:1 safety factor in drive torque over expected bearing friction torques. However, silicone oils are subject to crystalization under certain conditions and do not have the best lubricating qualities. Krytox oil would be a possible candidate except for its high viscosity gradient.

Table 4.2 Bearings

CONFIGURATION I:

MFR	Bearing Number	Number Required	ID (inch)	OD (inch)	Width (inch)
Kaydon	KA 65 -AR	5	6.500	7.000	0.25

CONFIGURATION II:

MFR	Bearing Number	Number Required	ID (inch)	OD (inch)	Width (inch)
SSB	TAR 37-46	2	2.3125	2.8750	0.250
SSB	TAR 29-36	2	1.8125	2.2500	0.250
SSB	TAR 25-32	2	1.5625	2.0000	0.250

The viscosity of Krytox 143AA is 35,000 centistokes at -40°C. This condition would be prohibitive unless heaters were incorporated for low temperature operations.

The use of a dry lubricant is attractive since the low temperature problem is essentially eliminated. Lubrication with a polyimide plastic filled with MoS_2 as the bearing retainer material along with burnishing of the raceways with MoS_2 powder is considered to be a good candidate. This approach is preferred over that of coating the raceways with a bonded film of dry lubricant. Bonded films, although completely adequate in many low speed applications, degrade the bearing precision and require considerable run-in. The filled retainer and burnished raceways were used in space by General Electric on the "skylab" scatterometer/altimeter antenna gimbals.

Lubrication of bearings should be reviewed further in the detail design phase. Because of the somewhat unusual mode of oscillatory motion of the bearings in this application, some form of endurance or life test is recommended in the development effort.

4.3 POWER SPRING

The spring which couples the compensating mass to the antenna is a spiral spring tuned to generate the specified frequency of 0.5 HZ under the influence of the combined inertia effects of the antenna and compensation wheel. Once the amplitude of the oscillation has been "built-up" to the required amount, the motors need only supply enough torque to overcome bearing friction.

In the design of this spring, three major parameters must be considered, namely, (1) maximum operating stress, (2) torque gradients, and (3) physical configuration.

The stress in spiral springs is given by:

$$S = \frac{6\,M}{bt^2} \quad \text{psi}$$

where

M = torque in in-lbs.

b = cross section width

t = cross section thickness

The torque gradient (spring constant) of a spiral spring can be expressed as;

$$K_s = \frac{\pi\, E\, bt^3}{6\, L} \quad \text{in.lb/rev}$$

where E = modulus of elasticity

L = effective length in inches

For a given spring constant K_s the resonant frequency f_s is related to the moments of inertia I_A (antenna) and I_W (wheel) by

$$fs = \frac{1}{2\pi} \sqrt{\frac{K_s\,(I_A + I_W)}{I_A\, I_W}}$$

The space available in which to mount the spring is used to establish the basic configuration. The width and thickness of the spring cross section is then varied to provide the necessary characteristics. For configuration II, with a 1.4 meter dish;

K_s = 1.93 ft. lbs/rad. (0.267 Kg-m/rad)

S = 60,000 psi maximum

The resultant spring design must be checked for adequate space between turns to provide "breathing room" during operation. In the preliminary specification included in Appendix A, spring A applies to a 1.4 meter disk in configuration II.

The requirements for spring B apply to a configuration I drive supporting a 1.0 meter disk. The spring has a width of 1 inch (25 m m) and is made of heat treated high carbon steel.

4.4 SPIRAL FLEX LEADS

The stator portion of the wheel drive motor in configuration II rotates with the antenna shaft. Therefore, a power transfer device from the housing to the shaft is needed to accommodate the ±45 degrees of relative rotary motion.

In order to avoid the undesirable friction and wear characteristics of brushes, a low gradient conductive spiral spring is selected. A spring of beryllium copper alloy, heat treated to spring temper, will provide long life when properly sized for stress and current carrying capacity. Since the relative conductivity of BeCu is 21% of that of copper, a rectangular cross sectional area of .005 in^2 is needed to provide a standard conductor resistance for a 1.5 ampere current level. Using the same equations as used for the power spring above, it can be shown that a 0.05 inch (1.3 mm) thick spring with a width of 0.10 inch (2.5 mm) and an effective length of 60 inches (152.4 mm) would exhibit a maximum torque of 3.5 oz-in (0.0028 Kg-m). In the mechanism, the spring would comprise approximately six turns in each lead. It is proposed that the flex assembly consist of six springs, three of which are redundant conductors parallel to the other three, creating a total maximum torque of approximately 20 oz-in or about 6% of the power spring torque level. The corresponding maximum stress level of 6000 psi is low compared to an utlimate strength of 120,000 psi, and theoretically results an infinite fatigue life. A summary of preliminary requirements for this spring are shown on the spiral spring specification sheet included in Appendix A under spring C.

4.5 SHAFT ENCODERS

The shaft encoders considered in the formulation are "naked" type consisting encoder disc, light sources and detectors. All the processing electronics are to be contained in the drive electronics box. The encoder disc provides 2^{16} cycles per revolution shaft angular information and also contains a track for the brushless motor commutation signal. The light source and the pickup sensor are respectively a light emitting diode (LED) and a photo transistor, and provide a quasi-sinusoidal output signal. A pair of read out station for each encoder are to be provided.

For configuration II drive, as mentioned in the next paragraph an aluminum housing and a stainless steel shaft are assumed. The relative axial expansion of the aluminum housing vs stainless steel shaft amounts to .0008"/inch over the length of the drive from room temperature down to -40°C. The antenna shaft is positioned axially by the preloaded bearing pair at the bottom of the drive. The upper shaft bearings are mounted with a slide fit on the shaft to allow for the relative expansion of about .0064".

The encoder air gaps are the factors most susceptible to this thermal expansion condition. The discs and heads must be designed such that they will operate with an air gap in excess of the .0054" of relative contraction that will occur at the low temperature extreme.

4.6 MATERIAL CONSIDERATION

In the formulation of drives it is assumed that the following materials are used for the indicated elements:

Reflector:	Graphite/epoxy
Truss:	Graphite/Epoxy tubes 1.5" O.D., 0.05" wall thickness

Housing:	Aluminum
Shaft for Configuration I:	Aluminum
Shaft for Configuration II:	Stainless Steel
Compensation Wheel:	Inconel

The SMMR antenna will require a low coefficient of thermal expansion material in order to minimize thermal distortions during the different orbit phases of varying sun angles in the sunlight periods and in the earth shadowing periods. Distortions can be caused by the absolute temperature magnitudes of the total configuration, the transient temperatures and the differences in temperature across the configuration. These thermal conditions can cause pointing errors and performance degradation, if the antenna and reflector support materials are not selected carefully. Properties of some material considered are shown in Table 4.3.

The use of composites, such as graphite/epoxy, boron epoxy and Kevlar/epoxy, were considered as acceptable from a thermal standpoint. Although the recommendation at this point is graphite/epoxy material, the choice between these at designlevel of study must be made for other reasons, such as fabricability and background experience.

General Electric Space Division selected the Kevlar/epoxy system for the BSE (Japanese Broadcasting Satellite Experiment) reflector assembly particularly to eliminate the need for a high temperature cure. The Kevlar, 90% Epon 815/10% TETA can be cured at room temperature. As the reflector will be laid up and cured on a mandrel, the room temperature cure eliminates the need to compensate for contour changes in the mandrel due to temperature rise and the need for heating and temperature control of the mandrel.

Therefore, the reflector process is simplified and repeatable, providing consistent results.

An additional consideration for the selection of Kevlar/Epoxy vs. Graphite/Epoxy was the environmental extremes with respect to the bonding temperatures.

The Graphite/Epoxy material is received in a "B" stage condition and bonded at a temperature of 350°F. The Kevlar/Epoxy is bonded at a room temperature of 70-80°F. The operating temperature for the antenna are closer to the room temperature range, therefore, does not induce as high a thermal stress pattern in the Kevlar/Epoxy as in the Graphite/Epoxy. There have been cases reported of Graphite/Epoxy structure that has delaminated due to low temperature exposure. GE-SD has applied LN_2 to built-up Kevlar structural elements and no failures have occurred.

ORIGINAL PAGE IS
OF POOR QUALITY

Table 4.3

TYPICAL MATERIAL PROPERTIES

Material	Ultimate Tensile Strength TU (KSI)	Modulus of Elasticity E (10^3 KSI)	Density W (Lbs/In^3)	Coefficient of Thermal Exp. (10^{-6} in/in/°F)	Thermal Conductivity K (BTU/ [HR.FT.^{2} F/FT])
Aluminum (2024-T4)	68	10.6	0.100	12.6	840
Titanium (GAL 4V Annealed)	135	16.5	0.160	5.7	52
Magnesium AZ31B	37	6.5	0.064	14.5	540
Kevlar/Epoxy *	73	4.5	0.048	0.8	1
Quartz/Epoxy *	24	2.1	0.055	1.7	
Boron/Epoxy *	188	30.0	0.072	1.3	13
Graphite/Epoxy *	187	25.0	0.054	0.2	10
Glass/Epoxy *	37	3.5	0.073	10.0	0.25

* Uniaxial Properties

5.0 ANALYSIS OF MECHANICAL DESIGN

5.1 WEIGHT AND MASS PROPERTIES

Weights of the various elements of the drive mechanism have been estimated based on the design formulation presented in the earlier section. Allowances for miscellaneous items that are needed to assemble the mechanism are also included so that the weight estimate realistically represents the system formulated. The Table 5.1 presents the weights of the configurations I and II with 1.0m and 1.4m reflectors. The mass properties of the rotating members were calculated using a computer mass properties model and the results are shown in Table 5.2. The model is consisted of approximately 30 separate weight elements in order to obtain an accurate assessment of centers of mass, moments of inertia, and products of inertia. Ballasts were added to the reflector to move the center of mass to the axis of rotation (static balance) which gave a favorable effect on the products of inertia.

Although it is highly desirable to have the rotating members dynamically balanced, it is not adopted due to weight penalties. For example, the weight of configuration I drive with 1.4m antenna becomes 61.9 Kg when the antenna mass is dynamically balanced compared to 47.7 Kg for the statically balanced drive.

5.2 STRUCTURAL RESONANT FREQUENCIES

Dynamic analysis of the scanning microwave radiometer system formulated in the preceding section was performed to predict structural frequencies and evaluate the dynamic coupling of the structural mode of the drive mechanism on its supporting structure and the structural interaction with the control system.

Table 5.1 Weight Summary

(weight in Kg)

	Configuration I		Configuration II	
	1.0m Reflector	1.4m Reflector	1.0m Reflector	1.4m Reflector
Reflector	3.3	6.5	3.3	6.5
Ballast	1.8	2.9	1.4	2.8
Other mass rotating with reflector	5.5	5.8	11.7	11.7
Sub Total	10.6	15.2	16.4	21.0
Compensation Wheel	3.9	19.0	1.2	12.6
Other mass rotating with wheel	2.6	2.6	3.9	3.9
Sub Total	6.5	21.6	5.1	16.5
Housing and base plate	6.4	6.4	7.5	7.5
Other fixed mass	4.5	4.5	3.2	3.2
Sub Total	10.9	10.9	10.7	10.7
Total	28.0	47.7	32.2	48.2

ORIGINAL PAGE IS OF POOR QUALITY

Table 5.2 Mass Property Summary

	Configuration I		Configuration II	
	1.0m Reflector	1.4m Reflector	1.0m Reflector	1.4m Reflector
Antenna				
Moments of inertia ($K_g - m^2$)				
I_{ox}	1.98	4.58	0.77	1.86
I_{oy}	2.26	5.58	1.05	2.97
I_{oz}	0.94	3.12	0.90	2.92
Products of inertia ($K_g - m^2$)				
P_{oxz}	+0.16	+0.72	-0.19	-0.75
P_{oxy}	0	0	0	0
P_{ozy}	0	0	0	0
Compensation Wheel				
Moments of inertia ($K_g - m^2$)				
I_{ox}	0.05	0.17	0.05	0.15
I_{oy}	0.05	0.17	0.05	0.15
I_{oz}	0.09	0.31	0.09	0.29
Products of inertia ($K_g - m^2$)				
P_{oxz}	0	0	0	0
P_{oxy}	0	0	0	0
P_{ozy}	0	0	0	0

The analysis was accomplished by a digital computer simulation of mathematical dynamic models illustrated in Figures 5.1 and 5.2 for configurations I and II respectively. Antenna sizes of 1.0 m and 1.4 m are considered for both configurations.

The configuration I model consists of 14 mass points while the configuration II is represented by 24 mass points. The reflectors are represented by a lumped mass having the proper weight and inertia properties. All the mass points are allowed six degrees of freedom each, thereby producing a fully coupled dynamic model. The total weight used for analysis for each configuration is given in Table 5.1.

In the computer program the structural members connecting the mass stations are regarded as beam elements as shown in the models. The supporting structure for both configurations was represented by 1.5" O.D. x .050" graphite epoxy truss tubes ($E = 30 \times 16^6$). Configuration II also included a representation of the primary structure which was represented by structural elements having stiffness characteristics approximately three time higher than the truss assembly. The feed assembly for configuration II was also supported by a truss, having the same tube sizes, cantilevered off the primary structure. For configuration I the feed assembly was considered to be part of the drive assembly and was not modeled separately. The drive assembly for both configurations was modeled in detail. The housing and shaft were modeled as beam elements and the bearings were represented by spring elements providing radial reactions. Only one of the bearings was allowed to react the longitudinal loading.

The dynamic equations for the system of lumped mass points and connecting flexible elements as defined above are formulated by the computer program routines.

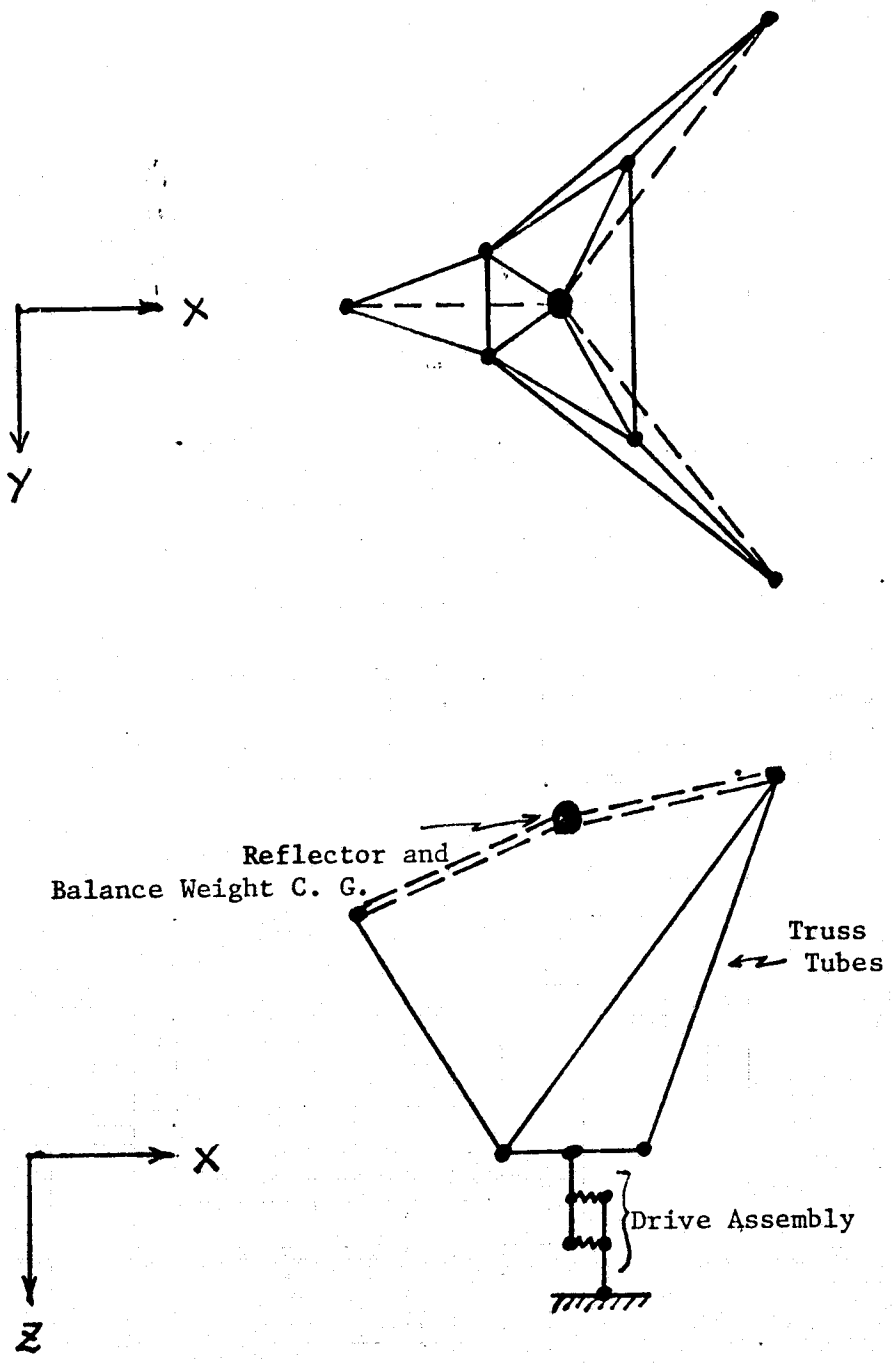

Figure 5.1

Configuration I, Mathematical Dynamic Model of the SMMR Assembly

ORIGINAL PAGE IS
OF POOR QUALITY

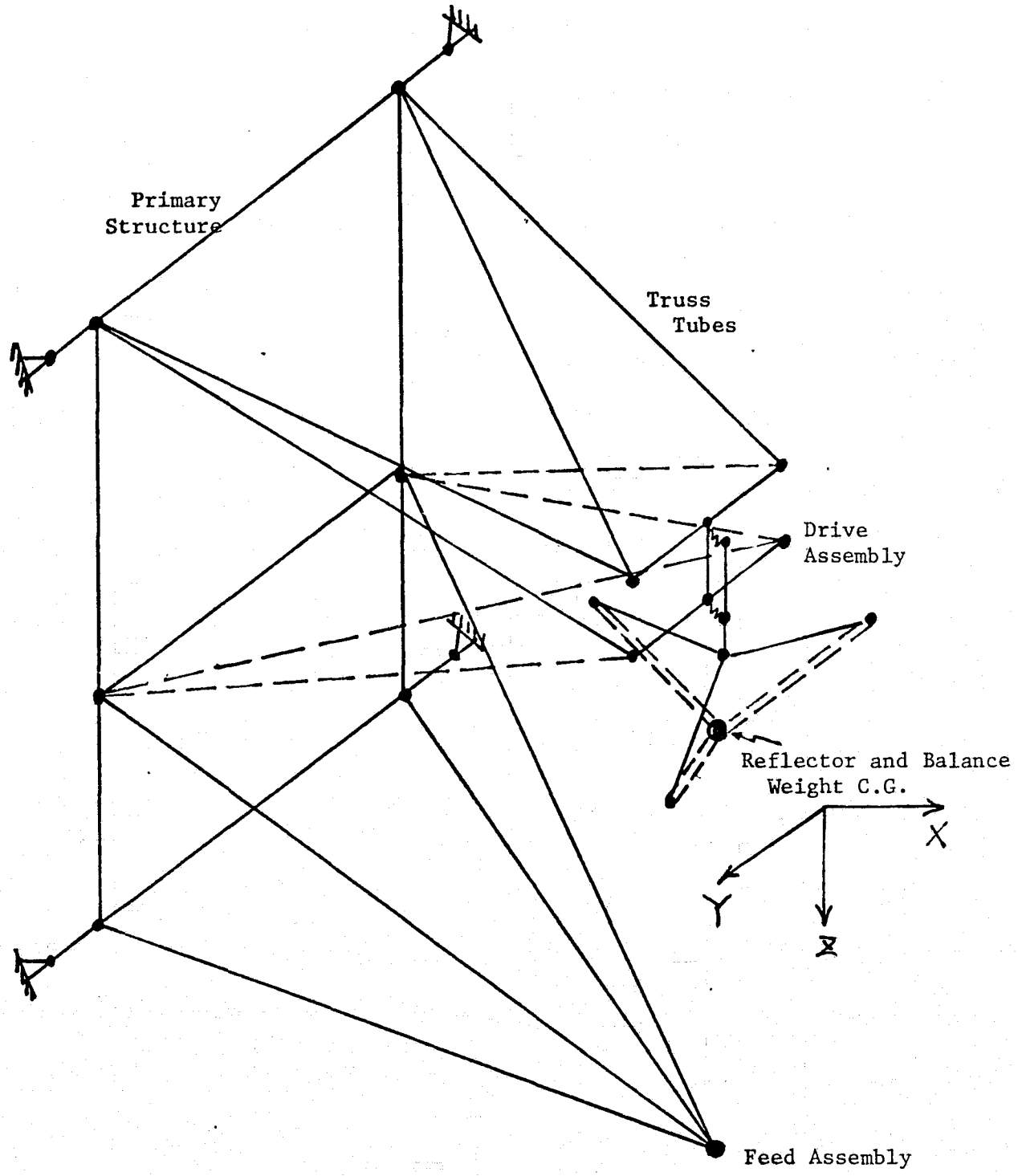

Figure 5.2

Configuration II, Mathematical Dynamic Model of

the SMMR Assembly

The equations are then solved successively for structural modes and frequencies. The cantilevered frequencies from the computer models are presented in Table 5.3.

TABLE 5.3 STRUCTURAL FREQUENCIES

CONFIGURATION		I		II		
ANTENNA DIAMETER		1.0 M	1.4 M	1.0 M	1.4 M	
Reflector/ Shaft	X axis	54 Hz	22 Hz	113 Hz	80 Hz	Bending-Y direction
	Y axis	119	55	107	65	Bending-X direction
	Z axis	193	97	161	90	Torsional
Shaft/ Housing	X axis	256	206	236	139	Bending-Y direction
	Y axis	481	420	262	206	Bending-X direction
	Z axis	-	-	236	139	Bending-Y direction
Feed Assy	X axis	-	-	240	240	Bending-Y direction
	Y axis	-	-	388	388	Bending-X direction
	Z axis	-	-	240	240	Bneding-Y direction
Longitudinal		-	-	145	145	Translation Z direction

NOTE: Reflector/shaft frequencies are obtained by constraining the shaft to the housing in torsion, while shaft/housing frequencies are obtained without constraints.

6.0 PERFORMANCE ANALYSIS

The performance of the formulated scan drive system has been analyzed by use of an analog simulation model. Equations of motion are developed from 3-axes models for configurations I and II, incorporating the characteristics of the components and the structural modes discussed in previous sections.

6.1 EQUATIONS OF MOTION

By use of generalized coordinates the equations of motion are derived from the Lagranges equation:

$$\frac{d}{dT}\left(\frac{\partial T}{\partial \dot{\theta}}\right) - \frac{\partial T}{\partial \theta} + \frac{\partial P}{\partial \theta} = Q$$

where:

T: Kinetic energy

P: Potential energy

Q: Nonconservative force

$\theta, \dot{\theta}$: Generalized coordinate and its time derivative

Since the momentum h for the coordinate θ is

$$h = \frac{\partial T}{\partial \dot{\theta}}$$

$$h = \int_0^t \left(Q - \frac{\partial P}{\partial \theta} + \frac{\partial T}{\partial \theta}\right) dt + h(0)$$

If the coordinates as shown in Figures 6.1 and 6.2 are adopted for configurations I and II respectively and all translational motions are assumed to be negligible,

$$[h_A] = [h_A(0)] + \int_0^t \left\{ -[I_A \lambda_A^2 \theta_A] - [2\zeta \lambda_A \dot{\theta}_A] \right\} dt$$

for the antenna reflector,

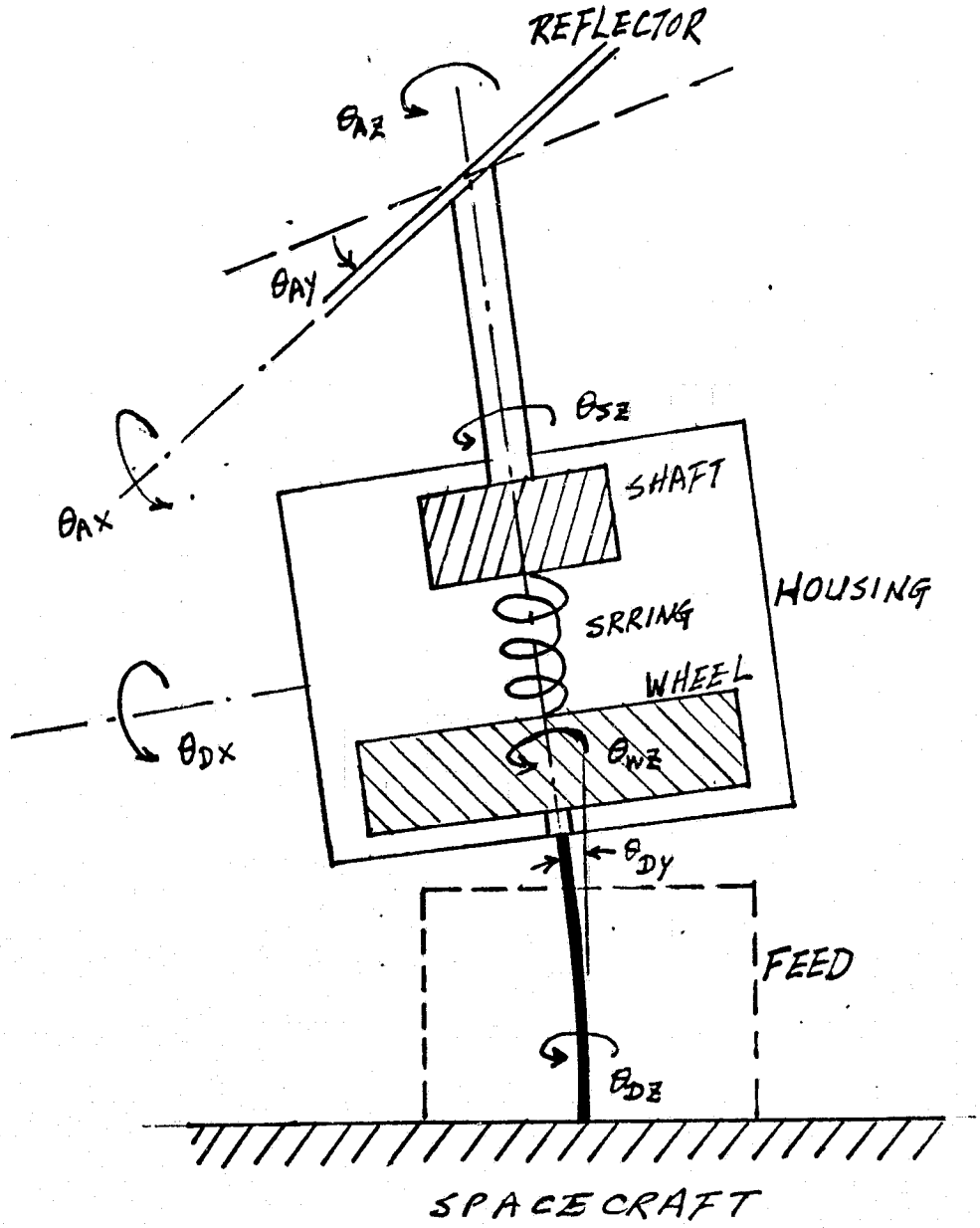

Figure 6.1 Simulation Model of Configuration I Drive

ORIGINAL PAGE IS
OF POOR QUALITY

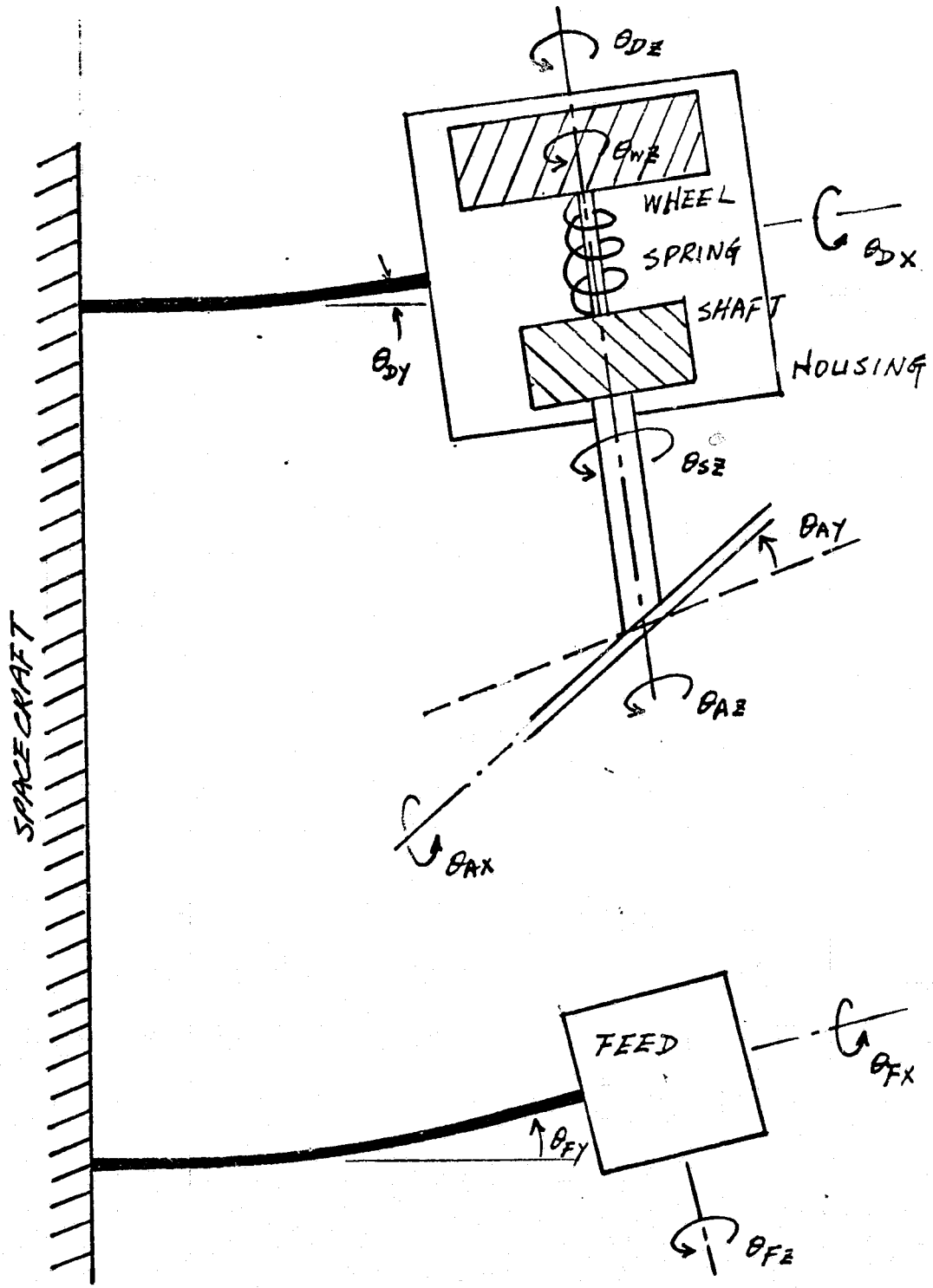

Figure 6.2 Simulation Model of Configuration II Drive

$$\left[A^T\right]\left[h_A\right] + \left[h_D\right] + \left[h_s\right] + \left[h_W\right]$$

$$= \left[A^T\right]\left[h_A(0)\right] + \left[h_D(0)\right] + \left[h_s(0)\right] + \left[h_W(0)\right]$$

$$+ \int_0^t \left\{ -\left[I_D \lambda_D^2 \theta_D\right] - \left[2\zeta_D \lambda_D \dot{\theta}_D\right] - F_{Dz} \right\} dt$$

for the drive housing,

$$\left[h_F\right] = \left[h_F(0)\right] + \int_0^t \left\{ -\left[I_F \lambda_F^2 \theta_F\right] - \left[2\zeta_F \lambda_F \dot{\theta}_F\right] \right\} dt$$

for the feed,

$$h_{WZ} = h_{WZ}(0) + \int_0^t \left\{ T_W - K_s \theta_{WZ} - F_W \right\} dt$$

for the compensation wheel and

$$h_{sz} = H_{sz}(0) + \int_0^t \left\{ T_M - F_s \right\} dt$$

for the antenna shaft, where

I: moment of inertia

λ: structural frequency

ζ: structural damping coefficient

F: Friction (static and viscous)

T: Torque input

K_s: Torque gradient of the power spring

A: Coordinate transformation matrix

A^T: Transpose of A

Complete equations of motion for three axes are rearranged for computer solution and presented in Appendix B with corresponding computational schematics.

For a preliminary analytical assessment of the system performance the equations of motion are simplified by disregarding the structural modes and energy dissipations, and by considering only the yaw axis motions of the antenna shaft and the compensation wheel:

For configuration I,

$$(I_A S^2 + I_W \lambda^2)\,\theta_s - I_W \lambda^2 \theta_w = T_M$$

$$-I_w \lambda^2 \theta_s + I_w (S^2 + \lambda^2)\,\theta_w = T_w$$

and

$$\theta_s = \frac{1}{I_A} \quad \frac{S^2 T_M + \lambda^2 (T_M + T_w)}{S^2 (S^2 + \lambda_s^2)}$$

$$\theta_w = \frac{1}{I_w} \quad \frac{S^2 T_w + \frac{I_w}{I_A^2} \lambda^2 (T_w + T_M)}{S^2 (S^2 + \lambda S^2)}$$

where $\lambda^2 = K_s/I_w$ and $\lambda_s^2 = K_s/(I_A + I_W)$

The residual momentum H is given by

$$H(S) = I_A S \theta_s + I_W S \theta_w = -\frac{1}{S} (T_M + T_w)$$

which is zero only when $T_W = -T_M$

Therefore, if $T_M(S) = -T_W(S) = \lambda_s A$,

$$\theta_s(S) = \frac{A}{I_A} \quad \frac{\lambda_s}{S^2 + \lambda S^2}$$

$$\theta_w(S) = -\frac{A}{I_w} \quad \frac{\lambda_s}{S^2 + \lambda_s^2}$$

or

$$\theta_s(T) = \frac{A}{I_A} \sin \lambda_s t$$

$$\theta_w(T) = -\frac{A}{I_w} \sin \lambda_s t$$

and $H(t) = I_A \dot{\theta}_s + I_W \dot{\theta}_W = 0$

It shows that under the ideal condition this system provides fully momentum compensated sinusoidal scanning with initial pulse excitations by the antenna drive and the wheel drive motors only. The initial excitation torque pulses should be same in magnitude and opposite in polarity. Once the oscillation starts, all acceleration torque is supplied from the energy stored in the power spring.

For configuration II

$$(I_A + I_W)\, s^2\theta_s + I_W\, s^2\theta_w = T_M$$

$$I_W\, s^2\theta_s + I_W\,(s^2 + \lambda^2)\,\theta_w = T_W$$

and

$$\theta_s = \frac{1}{I_A}\ \frac{s^2\,(T_M - T_W) + \lambda^2\, T_M}{s^2\,(s^2 + \lambda_s^2)}$$

$$\theta_w = \frac{1}{I_A}\ \frac{s^2\,(T_W - T_M) + \frac{I_A}{I_W}\, s^2 T_W}{s^2\,(s^2 + \lambda_s^2)}$$

Since the wheel angle θ_w is referenced to the shaft, the wheel angle θ'_w with respect to the housing is

$$\theta'_w = \theta_s + \theta_s = \frac{1}{I_W}\ \frac{s^2\, T_W + \frac{Iw}{I_A}\lambda^2\, T_M}{s^2\,(s^2 + \lambda_s^2)}$$

and the residual momentum is given by

$$H(s) = \frac{1}{s}\, T_M$$

which is zero whenever $T_M = 0$

ORIGINAL PAGE IS
OF POOR QUALITY

Therefore, if $T_M(S) = 0$ and $T_W(S) = -\lambda_s B$

$$\theta_s(S) = \frac{B}{I_A} \frac{\lambda s}{s^2+\lambda s^2}$$

$$\theta_w(S) = -\frac{B}{I_W} \frac{\lambda s}{s^2+\lambda s^2}$$

or

$$\theta_s(T) = \frac{B}{I_A} \sin \lambda_s t$$

$$\theta_s(T) = \frac{B}{I_w} \sin \lambda_s t$$

and $$H(t) = I_A \dot{\theta}_s + I_W \dot{\theta}_W = 0$$

It shows that the angular momentum is always compensated for provided that the antenna drive motor is not excited. An initial pulse starts a sinusoidal oscillation for the scan antenna and the oscillation is maintained by energy stored in the power spring without any more energy input under the ideal condition. The scan amplitude is determined by the pulse amplitude.

6.2 SERVO CONTROL SIGNAL

As discussed in the preceding paragraphs, the drive mechanism under an ideal condition can maintain the oscillations without any additional energy input after attaining the desired amplitude and phase. Since there are dissipations, parameter variations and external disturbances in a practical drive system, however, the drive motors have to provide control torques to maintain the desired oscillation. The motors also should provide starting torques to build up the amplitude and synchronize the phase to the desired oscillation. As the motor torque capacities are selected on the basis of requirements of control torque at normal operating conditions, the starting transient would require a relatively long period.

Although a pulse type control signal can be effectively employed to control the oscillation, a proportional analog control is assumed for this study. Then, there are three different ways to control the drive motors:

(a) Both antenna and wheel drives are slaved to the reference signal

(b) The antenna drive is slaved to the reference and the wheel drive is in turn slaved to the antenna angle

(c) The antenna drive is controlled by the wheel angle while the wheel drive is slaved to the reference.

It is easily shown from the simplified equations of motion that the first scheme of deriving control signal provides the best momentum compensation for the configuration I.

If the transfer functions of antenna and the wheel drives including the torque characteristics of their motor are G_A and G_W respectively, the torque inputs T_M and T_W from the motors are

$$T_M = G_A (\theta_R - \theta_S)$$

$$T_W = -G_W (\theta_R + \frac{1}{N}\theta_W)$$

Hence the antenna and the wheel angles are given by

$$\theta_s (S) = \frac{I_W S^2 G_A + I_W \lambda^2 (G_A - G_W) + \frac{1}{N} G_A G_W}{D (S)} \theta_R (S)$$

$$-\theta_w (S) = \frac{I_A S^2 G_W + I_W \lambda^2 (G_W - G_A) + G_A G_W}{D (S)} \theta_R (S)$$

where

$$D (S) = I_W I_A S^2 (S^2 + \lambda_s^2) + I_W (S^2 + \lambda^2) G_A$$

$$+ (I_A S^2 + I_W \lambda^2) \frac{G_W}{N} + \frac{1}{N} G_A G_W$$

The residual momentum is

$$H(S) = I_A \dot{\theta}_S(S) + I_W \dot{\theta}_W(S)$$

$$= \frac{S}{D} \left[I_A I_W S^2 (G_A - G_W) + (I_A + I_W) I_W \lambda^2 (G_A - G_W) + G_A G_W \left(\frac{I_A}{N} - I_W \right) \right] \theta_R(S)$$

$$= \frac{I_A I_W S}{D} (S^2 + \lambda_s^2)(G_A - G_W) \theta_R(S)$$

since $I_A = NI_W$ and $(I_A + I_W)\lambda^2 = I_A \lambda_s^2$. It indicates that the residual momentum is always zero provided $G_A = G_W$. The dissipation effects, parameter changes and cross coupling between the axes are neglected.

For the configuration II, the last scheme provides the best momentum compensation. The torque inputs are

$$T_W = - G_W \left(\theta_R + \frac{\theta'_W}{N} \right)$$

$$T_M = - G_A \left(\frac{\theta'_W}{N} + \theta_S \right)$$

where $\theta'_W = \theta_W + \theta_S$

The antenna and the wheel angles are

$$\theta_S(S) = \frac{\left(I_W S^2 + \frac{1}{N} G_A\right) G_W}{D(S)} \theta_R(s)$$

$$\theta'_W(S) = \theta_W(S) + \theta_S(S)$$

$$= - \frac{(I_A S^2 + G_A) G_W}{D(S)} \theta_R(S)$$

where $D(S) = I_W I_A S^2 (S^2 + \lambda S^2) + I_W (S^2 + \lambda S^2) G_A + I_A S^2 G_W + \frac{1}{N} G_A G_W$

the residual momentum is

$$H(S) = I_A \dot{\theta}_A(S) + I_W \dot{\theta}'_W(S)$$

$$= \frac{S}{D}\left(\frac{I_A}{N} - I_W\right) G_A G_W \theta_R(S) = 0$$

Hence the residual momentum is always zero under the ideal condition independent of the transfer characteristics of the scan compensation networks.

6.3 PERFORMANCE SIMULATION

Equations of motion of the drive system have been simulated on an analog computer (Beckman 2200) to assess the system performance. The simulation models include 3 axes dynamics of the antenna, 3 axes dynamics of the housing/support structure and single axis motion of the compensating wheel. The bearing friction is modeled by a static coulomb type (constant amplitude), and the torque motor output limit is modeled by limits on the terminal voltage applied. The control servo loop is modeled by a gain and a simple lead/lag filter circuit, while the motor characteristics are represented by a linear model with constant parameters.

Performances of the formulated drive system in configurations I and II are simulated for both 1M and 1.4M diameter antenna sizes. The simulation results for various operating modes are presented in Appendix C.

Figure 6.3 shows a typical result - 1.4M antenna in configuration II operating in a normal mode. It shows that the starting transient last more than 6 cycles (or 12 seconds). Although the amplitude of antenna rotation angle (Θ_{ZA}) matches that of the reference signal (Θ_R) the error between them ($\Theta_R - \Theta_S$) can be as large as 5 degrees because of a phase error at the maximum deflection points.

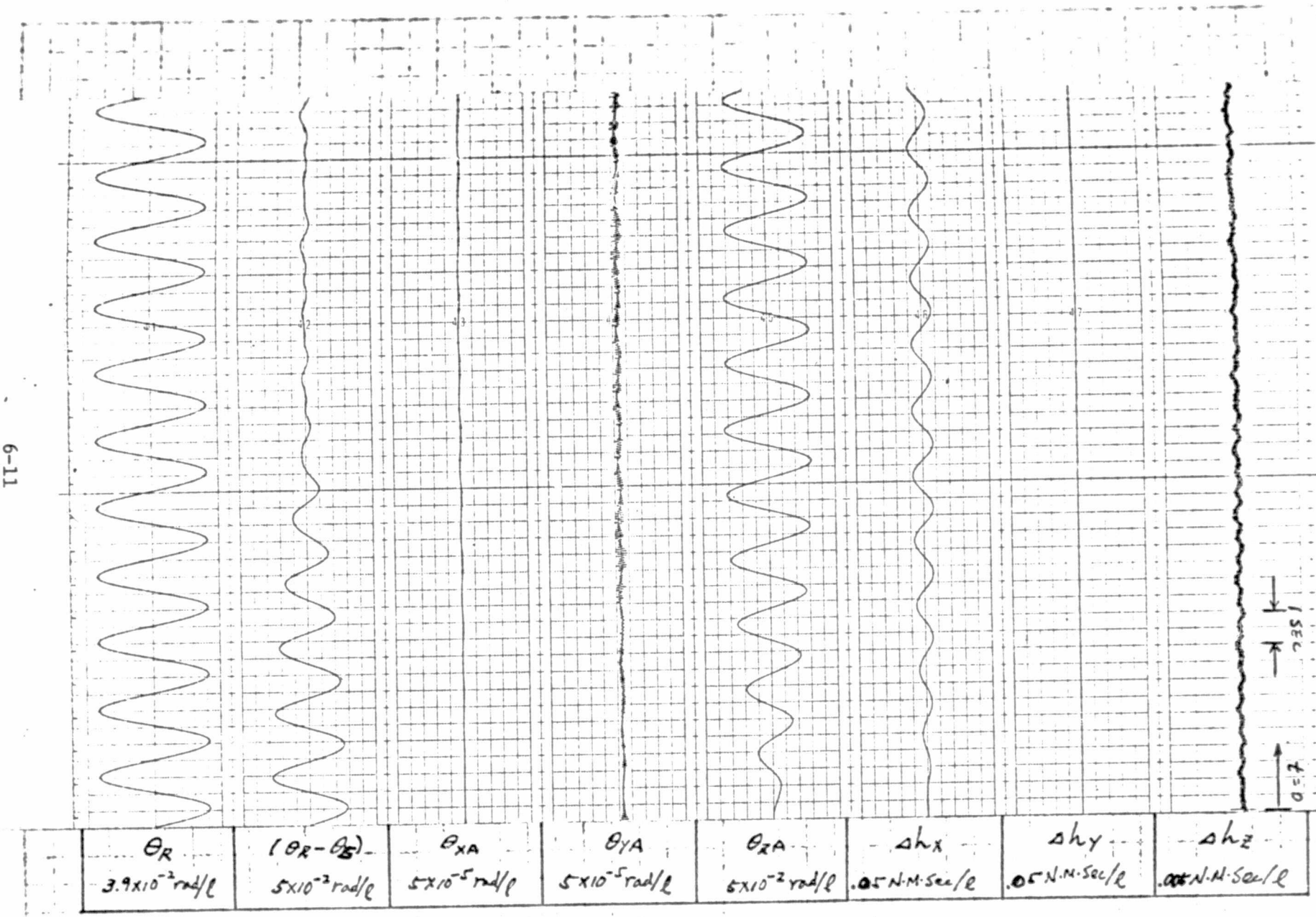

Figure 6.3 (a) Drive Mechanism Performance Configuration II, 1.4M Antenna, Normal Mode

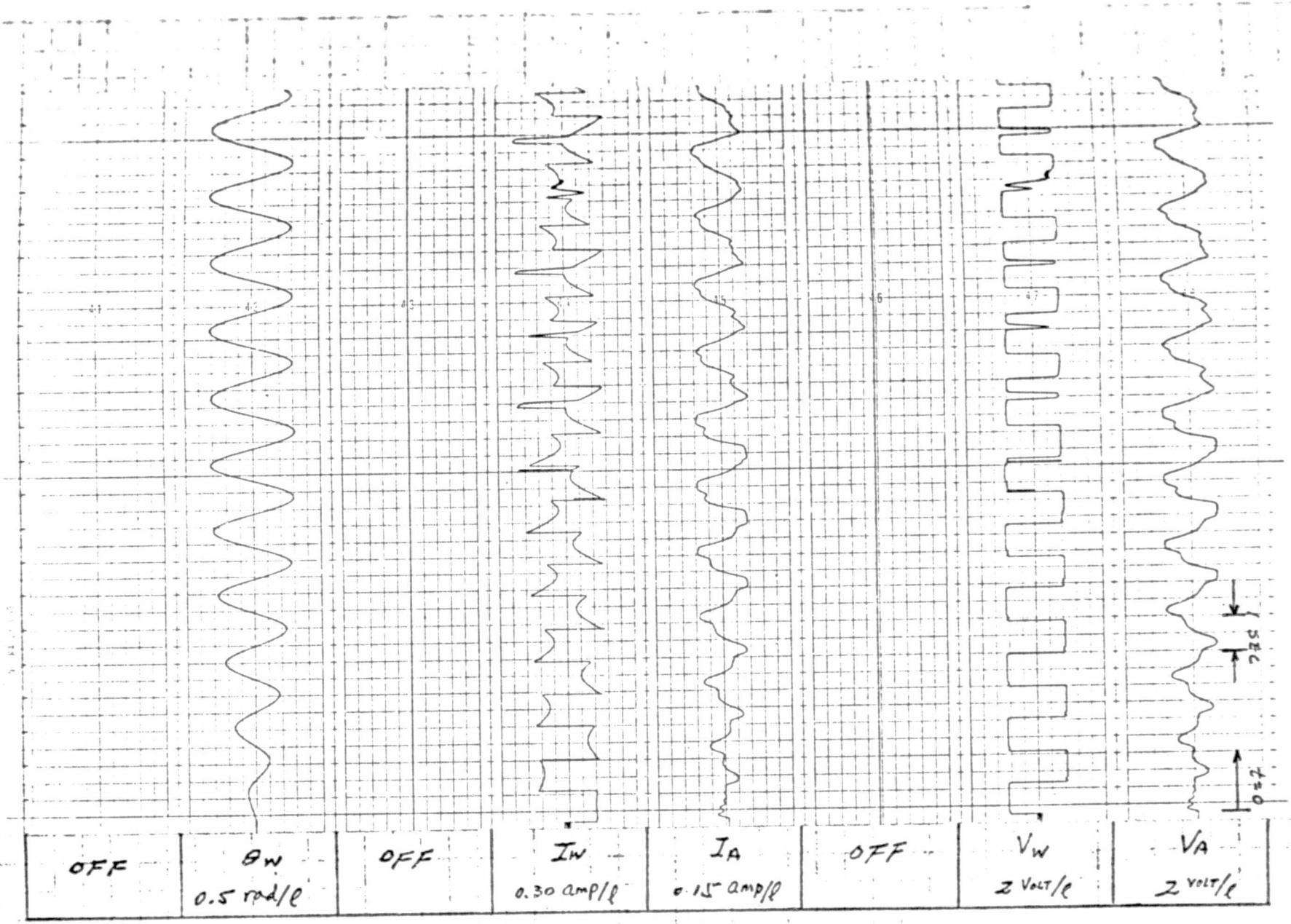

Figure 6.3 (b) Drive Mechanism Performance configuration II, 1.4M Antenna, Normal Mode

The phase error is due to the fact that the antenna drive is slaved to the reference signal through the wheel drive servo. When the antenna is directly referenced to the reference signal while the wheel drive is slaved to the antenna angle, the angular error is reduced to 1 degree. The angular error for 1 M diameter antenna for both configurations I and II is less than 1 degree even when the antenna is slaved to the wheel angle.

The residual angular momentum in yaw (scan) axis is less than 0.01N-M-sec (0.008 ft-lb-sec) throughout the transient and steady state periods. Because of the product of inertia, however, the residual momentum in x-axis reaches 0.2 N-M-sec (0.15 ft-lb-sec) during steady state. No residual momentum is present in y-axis. The power input to the compensation wheel drive motor at steady state is about 20 watts rms while that for the antenna drive motor is about 13 watts rms. The calculated value from the design data ware 18 watts rms and 4.3 watts rms respectively. The discrepancy in power input for the antenna drive motor is caused by a slight error in the tuned frequency of power spring. The input power requirement is very sensitive to mismatch between the drive frequency and the tuned frequency. When the motors are exicted by pulse type drive, the power requirement is less sensitive to the frequency mismatch while the angular error is increased.

When the excitation of both motor fails, the antenna scan amplitude decays gradually with a degradation in momentum compensation. When the motor terminals are shorted, the amplitude diminishes very rapidly since the motor winding acts as a damper. When the motor windings are open the oscillation lasted for a long time (more than 50 cycles in simulation). The residual angular momentum is increased to 0.05 N-M-sec (0.04 ft-lb-sec).

As the antenna drive is slaved to the compensation wheel angle, the antenna scan stops immediately when the wheel is stopped due to a failure. Hence there is no increase in disturbing angular momentum for this type of failure. When only the antenna drive motor fails, a large angular momentum disturbance results as the compensation wheel does not stop. The disturbing momentum during a period immediately following the failure is about the same as the case of both motor failure since the antenna continues the scanning motion with a gradually diminishing amplitude due to interactions with the power spring.

Even though there is a sizable amount of disturbing angular momentum due to the cross coupling, the angular deflection of antenna with respect to the vehicle in roll (x) axis, θ_{XA}, is negligible because of stiff structure. For pitch (y) axis, however, there is a angular deflection of less than 10^{-4} radian (0.005 degree) amplitude having a frequency corresponding to the supporting structure resonance. Although this structural oscillation is excited by the rotating antenna, the scan frequency component is neglible. For 1M diameter antenna the deflections in both axes are neglible.

With configuration I structure the deflection in pitch (y) axis is negligible, while there is deflection in roll (x) axis having scan frequency component as well as structural resonance frequency. For 1.4M antenna system, both frequency components have amplitudes of 10^{-4} radian (0.005 degrees). The deflection amplitude for 1M antenna system in configuration I is also neglible.

6.4 TELEMETRY NEED

In order to monitor the performance of the scanning mechanism it is necessary to have an adequate data link to a monitoring station. In case of a unmanned vehicle it will be a telemetry link to a ground station. The desired data to be monitored are:

1. Antenna motor current
2. Antenna motor temperature
3. Compensation wheel motor current
4. Compensation wheel motor temperature
5. Antenna shaft angle
6. Compensation wheel angle.

The motor temperature and current monitorings do not require high data rate: The temperature may be updated for every 10 scan cycles while the rms current can be updated every cycle. The number of data bit required for each measurement can be as low as 2 bits.

In order to correlate the microwave measurement data with the target position, however, the antenna pointing angle should be updated at a higher rate. It would require at least 4 measurements (two extremum points and two null points) per scan cycle assuming an interpolation between the measurement is sufficient for the data reduction. Since the sampling point for the measurement is to be based on a clock time rather than the angle, however, the number of measurement per scan cycle should be increased. Since 16-bit encoders are selected for the drive mechanism, it is desired to make 16 measurements per cycle.

Since the scan amplitude is ± 45 degrees, the antenna shaft encoder requires only 15-bit information to be transmitted. The compensation wheel encoder, however, requires all 16-bit information if it is desired to monitor the wheel angle. The total number of encoder bits to be transmitted through the telemetry per second is given by

$$(15 + 16) \text{ bit} \times 16 \text{ measurement} \div 2 \text{ sec} = 248 \text{ bit/sec.}$$

Hence, including the requirements for currents and temperature as well as a margin, 0.5K bit per second telemetry channel is sufficient for the drive mechanism.

6.5 SUMMARY OF DRIVE CHARACTERISTICS

The major characteristic parameters are summarized in Table 6.1

Table 6.1 Characteristic Parameters

Configuration	I		II		
Antenna Diameter	1.0 M	1.4 M	1.0 M	1.4 M	
. Weight (Kg)	28.0	47.7	32.2	48.2	
. Electrical Power rms/peak (w)	28/36	33/41	13/17	22/26	Steady State
. Residual Momentum rms/peak (N-M-sec)					Steady State
X-Axis	0.02/0.05	0.1/0.2	0.02/0.05	0.1/0.2	roll-axis
Y-Axis	-	0.005/0.01	-	0.005/0.01	pitch-axis
Z-Axis	0.001/0.003	0.01/0.03	0.003/0.005	0.005/0.01	yaw (scan)-axis
. Scan Angle Tracking Error rms/peak (deg)	0.3/2	0.5/3	0.2/1	1/5	steady state
. Transverse Axis Pointing Error Peak (radians)					steady state
X-axis	-	10^{-4}	-	10^{-5}	roll axis
Y-axis	-	-	-	$5x10^{-4}$	pitch axis
. Time to acquire (sec)	2	6	6	12	

7.0 CONCLUSION

In this study it is shown that a scan mechanism capable of driving a large diameter antenna can be developed with components currently available. The weight (48.2 Kg) and the input power requirements (33 watts rms at steady state) are comparable to the smaller antenna (0.8 M diameter) drive currently being developed.

The scanning mechanism is for multi-frequency microwave radiometers. A scan mode having the following parameters is selected for this study from a tradeoff between the scientific needs and the engineering:

1. Scan pattern - sinusoidal
2. Scan period - 2 seconds (0.5 Hz)
3. Scan amplitude - $\pm$45 degrees
4. Scan cone angle - 45 degrees

Two scanning mechanism configurations providing the scan mode with angular momentum compensation are formulated and their performances are simulated.

The simulation results show that both configurations can provide adequate angular momentum compensation for antennas having up to 1.4M diameter in the scanning axis. Due to the cross coupling, however, there are large disturbing angular momentum in roll axis when the antenna diameter is large. For the 1.4M antenna in configuration II this coupled disturbance is almost 20 times the residual disturbance in the scan axis and can cause large attitude error. To keep the attitude errors in all three axes below a preset required level, therefore, the coupled momentum disturbance should be compensated. As it is not practical to dynamically balance the offset paraboloid reflector for passive compensation, it is necessary to compensate the disturbance by an active device. Since the disturbance is directly related to the scan motion, a small wheel slaved to the antenna scan motion through a servo loop can be utilized to cancel the disturbing momentum.

Since the an infinitely large inertia spacecraft is assumed, pointing errors in transverse directions (x- and y-axis) are results of structural deflections in the antenna system. For the configuration II the structure formulated is rigid enough to maintain the pointing accuracy within 0.005 degrees for the large antenna while the configuration I provided 0.01 degree pointing accuracy for the large antenna as the truss structure supporting the antenna is deflected in roll axis under cross coupling torque.

With the antenna drive slaved to the reference through wheel drive servo loop, the pointing angle of the antenna lags as much as 5 degrees at reflection points although it provides a favorable momentum compensation in case of the antenna drive failure. When the antenna is directly slaved to the reference signal the error is less than 1 degree. Since the antenna pointing angle is measured 16 times per scan cycle. Five degree lag at the maximum deflection point can be tolerated.

For 1M antenna the performance of mechanisms in two different configurations are comparable. However, the simulation shows that for 1.4M antenna the configuration II provides better performance thant the configuration I. As the configuration II drive can be easily scaled to a larger antenna, it is recommended for future development.

As the feasibility of development is analytically shown, it is recommended to design, fabricate and test an engineering feasibility model capable of driving a large diameter antenna (preferably over 2M) in the next phase of this program. The configuration II mechanism formulated in this study can be easily interfaced with the space shuttle for which an experiment involving large diameter antenna microwave radiometer is being considered.

APPENDIX A

PRELIMINARY SPECIFICATIONS

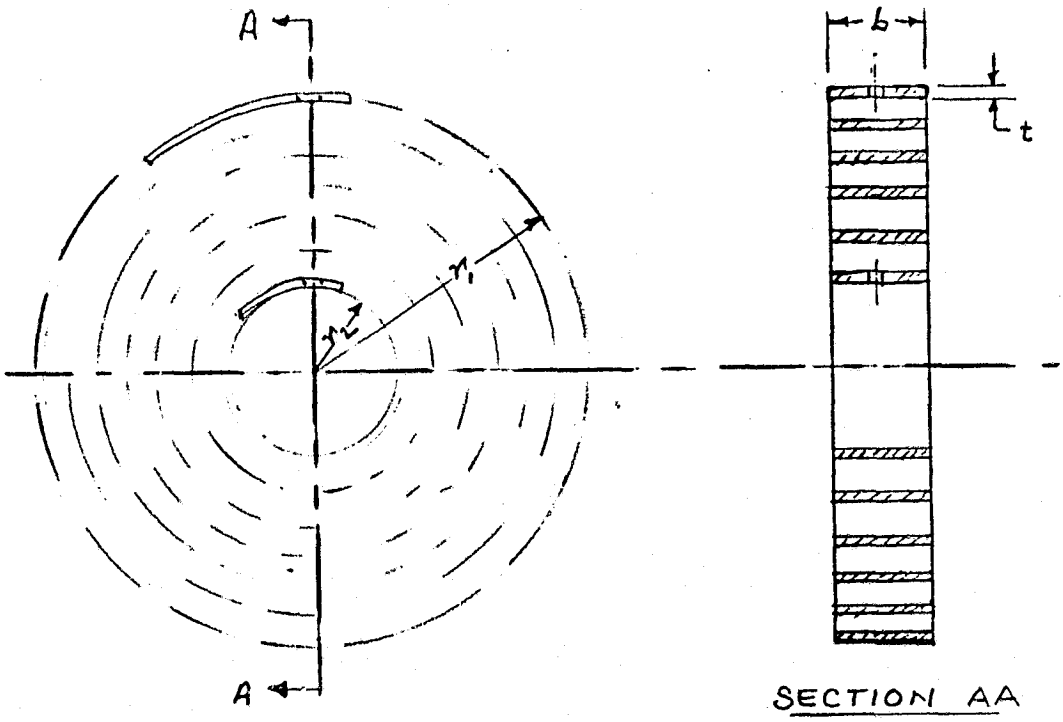

SECTION AA

	UNITS	SPRING A	SPRING B	SPRING C
Minimum Radius (r_2)	Inches	1.5	3.7	1.25
Maximum Radius (r_1)	Inches	5.5	5.8	2.25
Thickness (t)	Inches	0.143	0.086	0.05
Width (b)	Inches	1.0	1.0	0.10
Effective Length (Ref)	Inches	314	225	60
Number of Turns (Approx.)	-	14	7.7	6
Gradient	Ft.Lbs/Rad.	1.93	0.592	.023
Angular Range	Degrees	±500	±500	±45
Material	-	AISI 1095	AISI 1095	BeCu

Material ------ AISI 1095 High Carbon Steel

Edge Contour ------ #1 Round

PRELIMINARY SPECIFICATION

SPIRAL SPRINGS

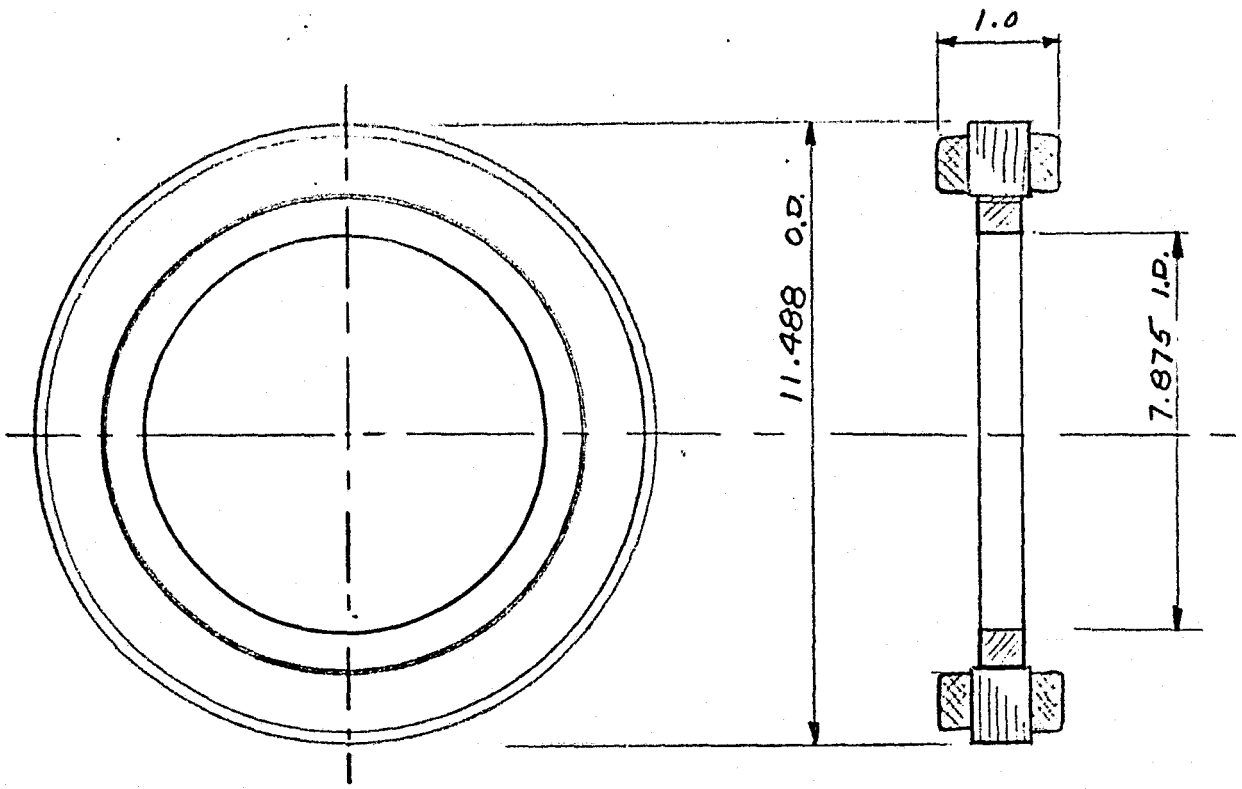

	ANTENNA	COMP. MASS
Type	Brushless	Brushless
Model (Typical), Mag-Tech	11490-100	11490-100
Resistance (R_M), Ohms	27	1
Peak Torque (T_p), Oz-IN	308	1600
Current @ Peak Torque, Amps	0.76	20
Peak Power, Watts	15	400
No Load Speed, Rad/Sec	6.8	35
Torque Constant (K_T), Oz.-In./Amp	415	80
Back EMF (K_B) Volts/Rad/Sec	2.9	0.6

PRELIMINARY SPECIFICATION

DRIVE MOTORS

CONFIGURATION I

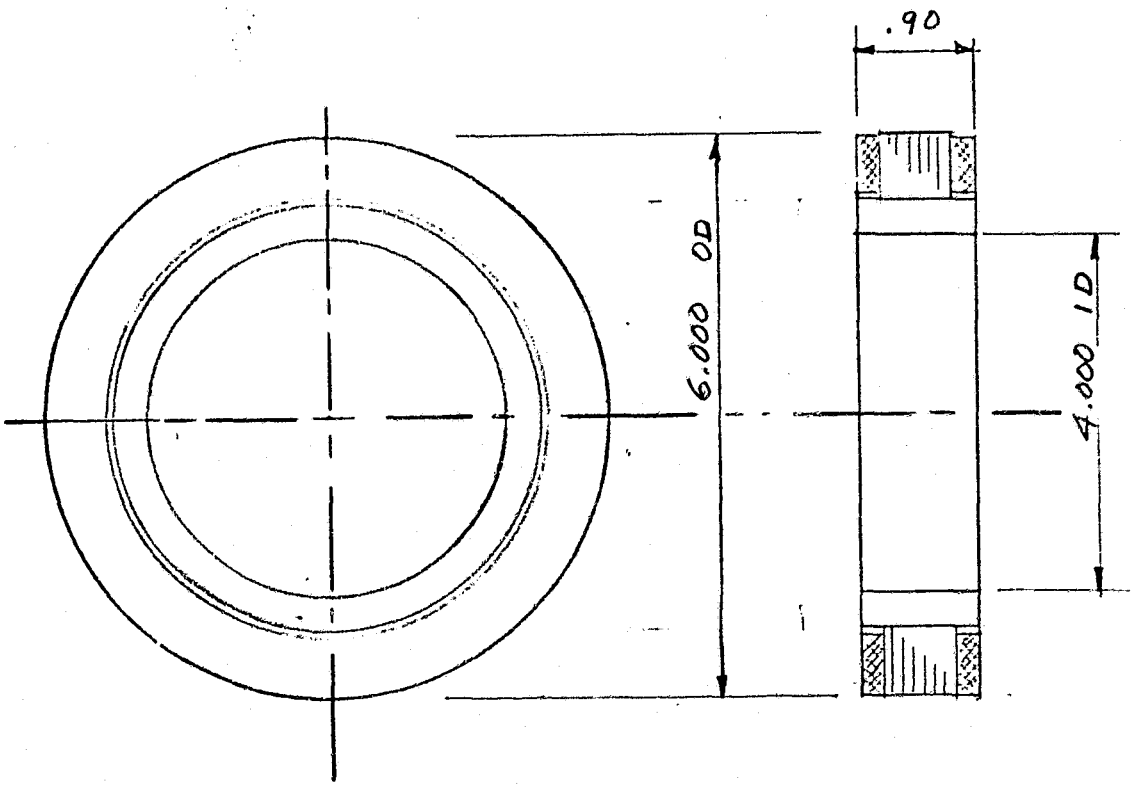

Type	Brushless DC, 3 Ø	
Model (Typical),	Mag - Tech	6000-090
Resistance (R_M), Ohms		13.5
Peak Torque (T_P) Oz.In.		230
Current @ T_P, Amps		1.5
Peak Power, Watts		30
No Load Speed, Rad/Sec		18
Torque Constant (K_T), Oz.In/Amp		156
Back EMF (K_B), Volts/Rad/Sec		1.1

PRELIMINARY SPECIFICATION

ANTENNA MOTOR

CONFIGURATION II

PRECEDING PAGE BLANK NOT FILMED

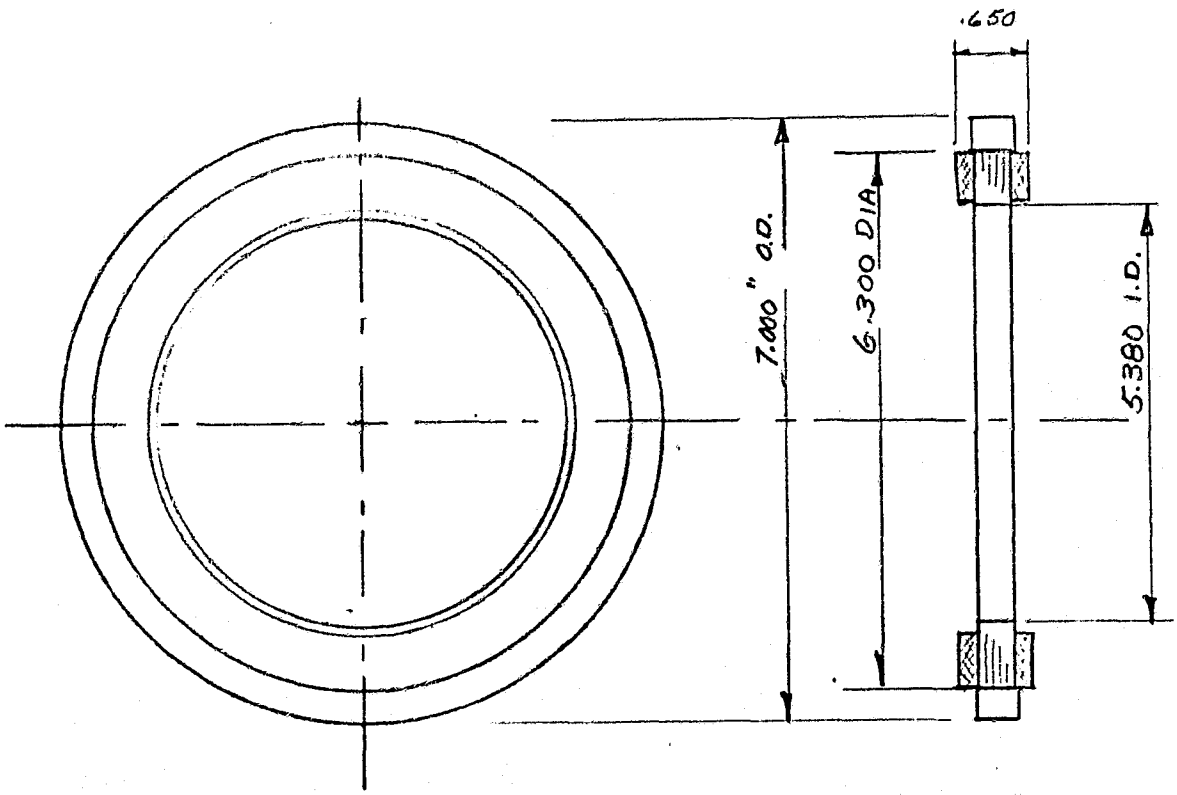

Type	Brushless DC, 3 Ø	
Model (Typical),	Mag-Tech	7000-065
Resistance (R_M),	Ohms	3.8
Peak Torque (T_P),	Oz.In.	374
Current @ Peak Torque (Amps)		5.3
Peak Power (Watts)		106
No Load Speed (Rad./Sec)		40
Torque Constant (K_T), Oz.In/Amp		71
Back EMF (K_B) Volts / Rad/Sec		0.5

PRELIMINARY SPECIFICATION

COMPENSATION MASS MOTOR

CONFIGURATION II

APPENDIX B

EQUATIONS OF MOTION

1. Equations of Motion for Antenna

$$\dot{\theta}_{AX} = \frac{1}{I_{xx}^{A}} h_{AX}(0) - w_{SX}^{A} + \frac{I_{xy}^{A}}{I_{xx}^{A}} w_{AY} + \frac{I_{xz}^{A}}{I_{xx}^{A}} w_{AZ} - \lambda_{AX}^{2} \int_{0}^{t} \theta_{AX}\, dt - 2 \} \lambda_{AX} \theta_{AX}$$

$$\dot{\theta}_{AY} = \frac{1}{I_{yy}^{A}} h_{AY}(0) - w_{SY}^{A} + \frac{I_{xy}^{A}}{I_{yy}^{A}} w_{AX} + \frac{I_{yz}^{A}}{I_{yy}^{A}} w_{AZ} - \lambda_{AY}^{2} \int_{0}^{t} \theta_{AY}\, dt - 2 \} \lambda_{AY} \theta_{AY}$$

$$\dot{\theta}_{AZ} = \frac{1}{I_{zz}^{A}} h_{AZ}(0) - w_{SZ}^{A} + \frac{I_{xz}^{A}}{I_{zz}^{A}} w_{AX} + \frac{I_{yz}^{A}}{I_{zz}^{A}} w_{AZ} - \lambda_{AZ}^{2} \int_{0}^{t} \theta_{AZ}\, dt - 2 \} \lambda_{AZ} \theta_{AZ}$$

Where

$$W_{SX}^{A} = W_{DX} \cos \theta_{SZ} + N_{DY} \sin \theta_{SZ}$$

$$W_{SY}^{A} = - W_{DX} \sin \theta_{SZ} + W_{DY} \cos \theta_{SZ}$$

$$W_{SZ}^{A} = W_{DZ} + \dot{\theta}_{SZ}$$

$$W_{AX} = W_{SX}^{A} + \dot{\theta}_{AX}$$

$$W_{AY} = W_{SY}^{A} + \dot{\theta}_{AY}$$

$$W_{AZ} = W_{SZ}^{A} + \dot{\theta}_{AZ}$$

2. Equations of Motion for Drive Housing

$$\dot{\theta}_{DX} = \frac{1}{I_{XX}^{D}}\left[h_{AX}^{D}(0) + h_{DX}(0) - h_{AX}^{D}\right] - \omega_{BX}$$

$$+ \frac{I_{XY}^{D}}{I_{XX}^{D}}\omega_{DY} + \frac{I_{XZ}^{D}}{I_{XX}^{D}}\omega_{DZ} - \lambda_{DX}^{2}\int_{0}^{t}\theta_{DX}\,dt - 2\left\{\lambda_{DX}\theta_{DX}\right.$$

$$\dot{\theta}_{DY} = \frac{1}{I_{YY}^{D}}\left[h_{AY}^{D}(0) + h_{DY}(0) - h_{AY}^{D}\right] - \omega_{BY}$$

$$+ \frac{I_{XY}^{D}}{I_{YY}^{D}}\omega_{DX} + \frac{I_{YZ}^{D}}{I_{YY}^{D}}\omega_{DZ} - \lambda_{DY}^{2}\int_{0}^{t}\theta_{DY}\,dt - 2\left\{\lambda_{DY}\theta_{DY}\right.$$

$$\dot{\theta}_{DZ} = \frac{1}{I_{ZZ}^{D}}\left[h_{AZ}^{D}(0) + h_{DZ}(0) + h_{WZ}(0) - h_{AZ}^{D} - h_{WZ}\right] - \omega_{BZ}$$

$$+ F_{D} + \frac{I_{XZ}^{D}}{I_{ZZ}^{D}}\omega_{DX} + \frac{I_{YZ}^{D}}{I_{ZZ}^{D}}\omega_{DY} - \lambda_{DZ}^{2}\int_{0}^{t}\theta_{DZ}\,dt - 2\left\{\lambda_{DZ}\theta_{DZ}\right.$$

Where

$$W_{DX} = W_{BX} + \theta_{DX}$$

$$W_{DY} = W_{BY} + \theta_{DY}$$

$$W_{DZ} = W_{BZ} + \theta_{DZ}$$

$$h_{A}^{D} = A^{T} h_{A}$$

$$A^{T} = \begin{bmatrix} \cos\theta_{SZ} & \sin\theta_{SZ} & 0 \\ -\sin\theta_{SZ} & \cos\theta_{SZ} & 0 \\ 0 & 0 & 1 \end{bmatrix}$$

3. Equations of Motion for Feed

$$\dot{\theta}_{FX} = \frac{1}{I_{XX}^{F}} \mathcal{M}_{FX}(o) - \omega_{BX} + \frac{I_{XY}^{F}}{I_{XX}^{F}} \omega_{FY} + \frac{I_{XZ}^{F}}{I_{XX}^{F}} \omega_{FZ}$$

$$- \lambda_{FX}^{2} \int_{o}^{t} \theta_{FX}\, dt - 2\zeta \lambda_{FX} \theta_{Fx}$$

$$\dot{\theta}_{FY} = \frac{1}{I_{YY}^{F}} \mathcal{M}_{FY}(o) - \omega_{BY} + \frac{I_{XY}^{F}}{I_{YY}^{F}} \omega_{FX} + \frac{I_{YZ}^{F}}{I_{YY}^{F}} \omega_{FZ}$$

$$- \lambda_{FY}^{2} \int_{o}^{t} \theta_{FY} dt - 2\zeta \lambda_{FY} \theta_{FY}$$

$$\dot{\theta}_{FZ} = \frac{1}{I_{ZZ}^{F}} \mathcal{M}_{FZ}(o) - \omega_{BZ} + \frac{I_{XZ}^{F}}{I_{ZZ}^{F}} \omega_{FX} + \frac{I_{YZ}^{F}}{I_{ZZ}^{F}} \omega_{FY}$$

$$- \lambda_{FZ}^{2} \int_{o}^{t} \theta_{FZ}\, dt - 2\zeta \lambda_{FZ} \theta_{FZ}$$

Where

$$W_{FX} = W_{BX} + \dot{\theta}_{FX}$$

$$W_{FY} = W_{BY} + \dot{\theta}_{FY}$$

$$W_{FZ} = W_{BZ} + \dot{\theta}_{FZ}$$

4. Equations of Motion for Wheel and Shaft

(a) Configuration I

$$\dot{\theta}_{wz} = \frac{1}{I_{zz}^{w}} \mathcal{L}_{wz}(0) - \omega_{Dz} + \frac{1}{I_{zz}^{w}} \int_0^t T_w \, dt + F_w(\dot{\theta}_{wz}) - \frac{K_s}{I_{zz}^{w}} \int_0^t (\theta_{wz} - \theta_{sz}) \, dt$$

$$\dot{\theta}_{sz} = \frac{1}{I_{zz}^{A}} \left[\mathcal{L}_{Az}(0) - I_{zz}^{A} \dot{\theta}_{Az} \right] - \omega_{Dz} + \frac{1}{I_{zz}^{A}} \int_0^t T_m \, dt + F_s(\dot{\theta}_{sz}) - \frac{K_s}{I_{zz}^{A}} \int_0^t (\theta_{sz} - \theta_{wz}) \, dt$$

Where

$$\omega_{wz} = \omega_{Dz} + \dot{\theta}_{wz}$$

(b) Configuration II

$$\dot{\theta}_{wz} = \frac{1}{I_{zz}^{w}} \mathcal{L}_{wz}(0) - \omega_{sz} + \frac{1}{I_{zz}^{w}} \int_0^t T_w \, dt + F_w(\dot{\theta}_{wz} \; \dot{\theta}_{sz}) - \frac{K_s}{I_{zz}^{w}} \int_0^t \theta_{wz} \, dt$$

$$\dot{\theta}_{sz} = \frac{1}{I_{zz}^{T}} \left[\mathcal{L}_{Az}^{D}(0) + \mathcal{L}_{wz}(0) - I_{zz}^{A} \dot{\theta}_{Az} - I_{zz}^{w} \dot{\theta}_{wz} \right] - \omega_{Dz} + \frac{1}{I_{zz}^{T}} \int_0^t T_m \, dt + F_s(\dot{\theta}_{sz}, \dot{\theta}_{wz})$$

Where

$$I_{zz}^{T} = I_{zz}^{A} + I_{zz}^{w}$$

$$\omega_{wz} = \omega_{sz} + \dot{\theta}_{wz}$$

5. Equations for Momentum

$$h_{AX} = I_{XX}^{A} W_{AX}$$

$$h_{AY} = I_{yy}^{A} W_{AY}$$

$$h_{AZ} = I_{ZZ}^{A} W_{AZ}$$

$$h_{DX} = I_{XX}^{D} W_{DX}$$

$$h_{DY} = I_{yy}^{D} W_{DY}$$

$$h_{DZ} = I_{ZZ}^{D} W_{DZ}$$

$$h_{WZ} = I_{ZZ}^{W} W_{WZ}$$

$$h_{FX} = I_{XX}^{F} W_{FX}$$

$$h_{FY} = I_{YY}^{F} W_{FY}$$

$$h_{FZ} = I_{ZZ}^{F} W_{FZ}$$

ANTENNA ROLL

1/26/76

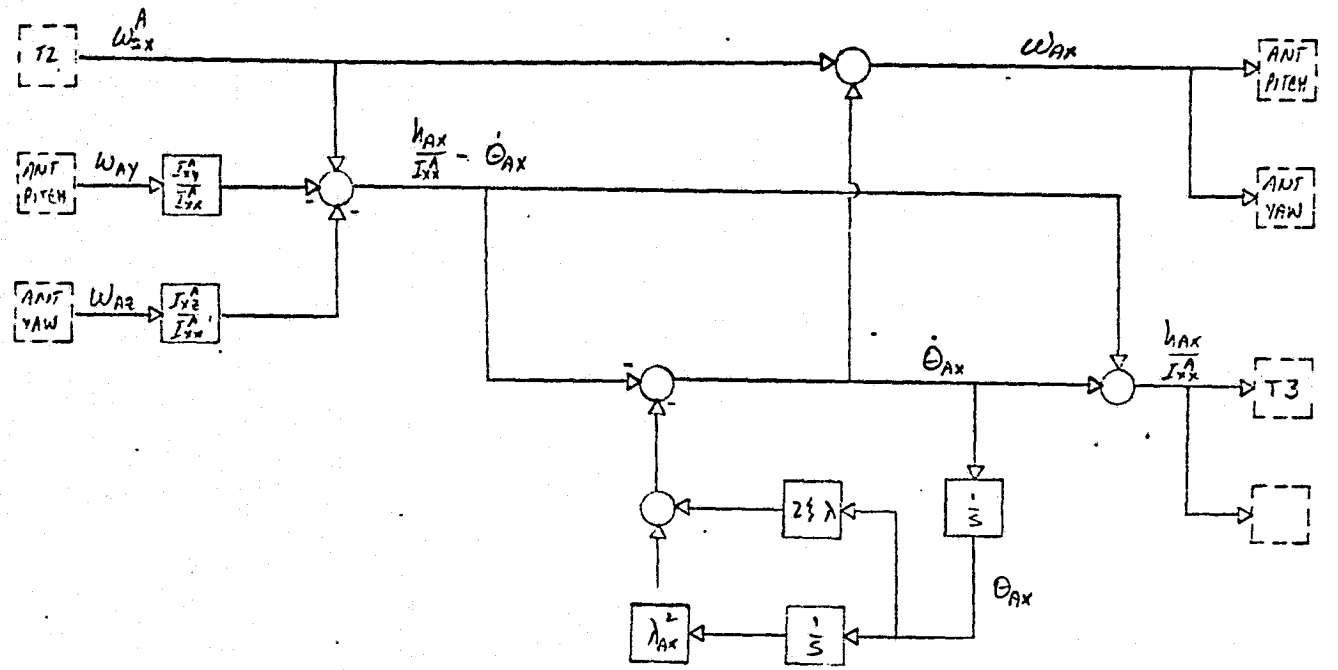

$$\dot{\theta}_{Ax} = -\omega_{sx}^A + \frac{I_{xy}^A}{I_{xx}^A}\omega_{Ay} + \frac{I_{yz}^A}{I_{xx}^A}\omega_{Az} - \lambda_{Ax}^2 \int_0^t \theta_{Ax}\,dt - 2\zeta\lambda_{Ax}\theta_{Ax}$$

Variables		Maximum
ω_{Ax}	ANTENNA ROLL RATE $(0.1 \cdot 2\pi \cdot 79.7)$	* 50. RAD/sec
ω_{Ay}	ANTENNA PITCH RATE $(0.1 \cdot 2\pi \cdot 15.)$	9.42 RAD/sec
ω_{Az}	ANTENNA YAW RATE $(0.1 \cdot 2\pi \cdot 89.8 \cdot \frac{2\pi^2}{10})$	59.4 RAD/sec
ω_{sx}^A	SHAFT RATE ALONG ANTENNA ROLL (ω_{Dx})	87.33 RAD/sec
h_{Ax}	ANTENNA ROLL MOMENTUM $(I_{xx}^A \omega_{Ax})$	
θ_{Ax}	ANTENNA ROLL DEFLECTION/HOUSING	0.1 RAD

Parameters		Nominal
I_{xx}^A	ANTENNA ROLL INERTIA	1.9 NT-M-SEC^2
I_{xy}^A	ANTENNA ROLL/PITCH INERTIA PRODUCT	0.0 "
I_{yz}^A	ANTENNA ROLL/YAW INERTIA	-0.15 "
ζ	DAMPING RATIO	0.05
λ_{Ax}	RESONANCE	500 RAD/S
ω_{sx}	MAXIMUM SHAFT ROLL RATE	100 RAD/S
ω_{Ax}	MAXIMUM ANTENNA ROLL RATE	100 RAD/S

*SCALING BASED ON MAXIMUM DEFLECTION OF 0.1 RADIAN

ORIGINAL PAGE IS
OF POOR QUALITY

ORIGINAL PAGE IS
OF POOR QUALITY

(A2) ANTENNA PITCH

1/26/76

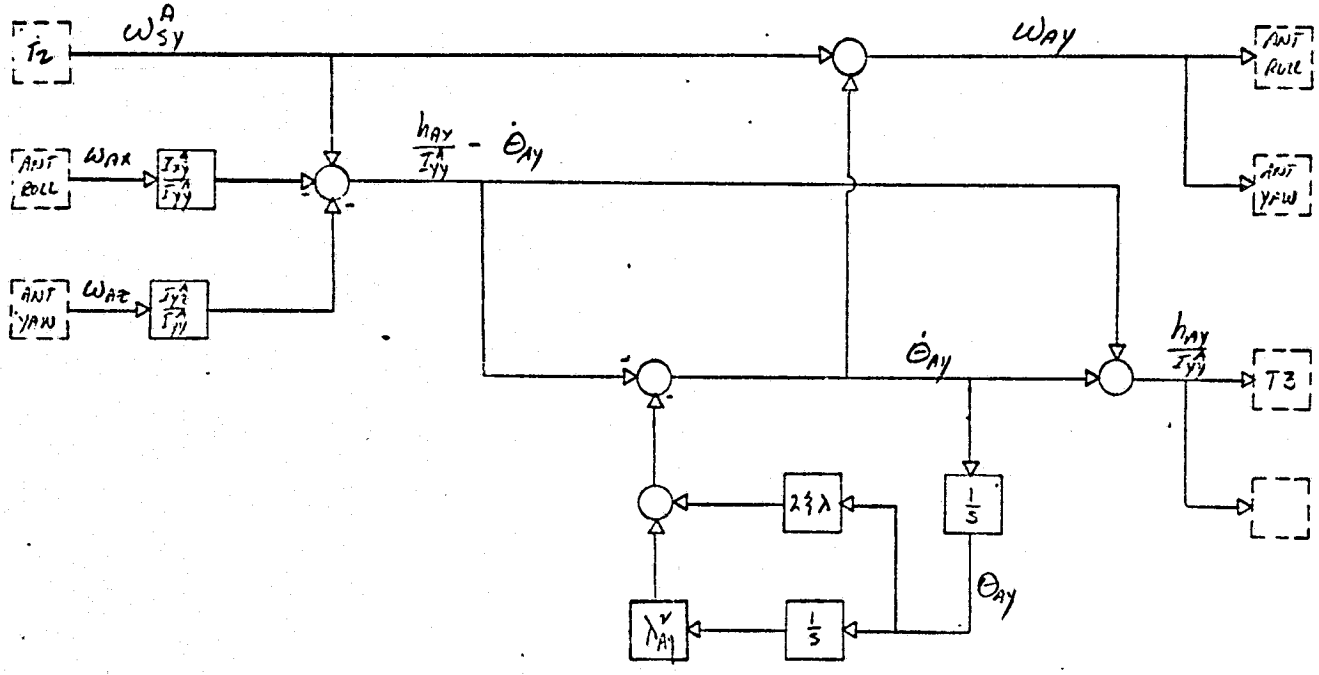

$$\dot\theta_{AY} = -\omega^A_{sy} + \frac{I^A_{xy}}{I^A_{yy}}\omega_{AX} + \frac{I^A_{yz}}{I^A_{yy}}\omega_{AZ} - \lambda^V_{AY}\int_0^t \theta_{AY}\,dt - 2\zeta\lambda_{AY}\theta_{AY}$$

Variables		Maximum
ω_{AX}	ANTENNA ROLL RATE	50 RAD/sec
ω_{AY}	ANTENNA PITCH RATE	9.42 RAD/sec
ω_{AZ}	ANTENNA YAW RATE	59.4 RAD/sec
ω^A_{sy}	SHAFT RATE ALONG ANTENNA PITCH (ω_{by})	129 RAD/sec
h_{AY}	ANTENNA PITCH MOMENTUM ($I_{yy}\omega_{AY}$)	
θ_{AY}	ANTENNA PITCH DEFLECTION/HOUSING	0.1 RAD

Parameters		Nominal
I_{xy}	ANTENNA ROLL/PITCH INERTIA PRODUCT	0.0 NT-m-sec^2
I_{yz}	ANTENNA PITCH/YAW INERTIA PRODUCT	0.0 "
I_{yy}	ANTENNA PITCH INERTIA	3.0 "
ζ	DAMPING RATIO	0.05
λ_{AY}	RESONANCE K_{AY}/I^A_{yy}	99.25 R/s
ω_{MS}	MAXIMUM SHAFT PITCH RATE	100. R/s
ω_{MA}	MAXIMUM SHAFT PITCH RATE	100. R/s

(A3) ANTENNA YAW

1/26/76

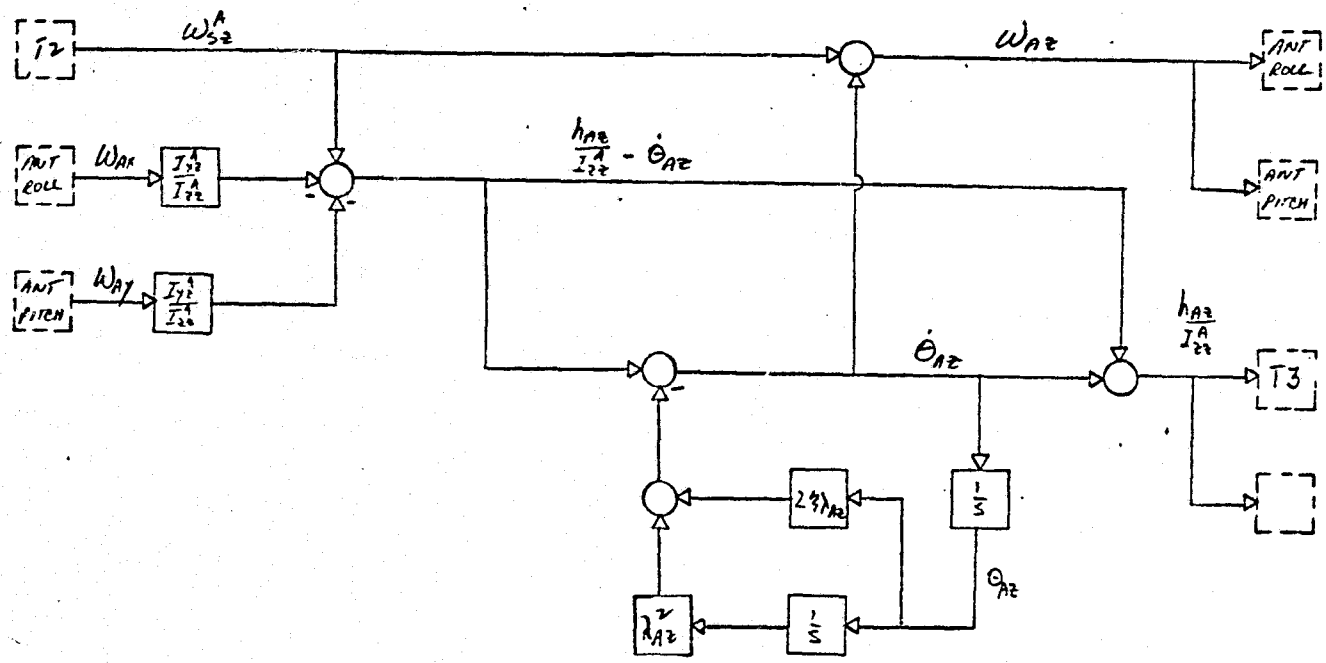

$$\dot{\theta}_{Az} = -\omega_{sz}^A + \frac{I_{xz}^A}{I_{zz}^A}\omega_{Ax} + \frac{I_{yz}^A}{I_{zz}^A}\omega_{Ay} - \lambda_{Az}^2\int_0^t \theta_{Az}\,dt - 2\zeta\lambda_{Az}\theta_{Az}$$

Variables	Maximum
ω_{Ax} ANTENNA ROLL RATE	50 RAD/SEC
ω_{Ay} ANTENNA PITCH RATE	9.42 RAD/SEC
ω_{Az} ANTENNA YAW RATE	39.9 RAD/SEC
ω_{sz}^A SHAFT RATE ALONG ANTENNA YAW	90.0 RAD/SEC
h_{Az} ANTENNA YAW MOMENTUM ($I_{zz}\omega_{Az}$)	
θ_{Az} ANTENNA DEFLECTION/SHAFT	0.1 RAD

Parameters	Nominal
I_{xz}^A ANTENNA ROLL/YAW INERTIA PRODUCT	-0.75 NT-M-SEC^2
I_{yz}^A ANTENNA PITCH/YAW INERTIA PRODUCT	0.0 "
I_{zz}^A ANTENNA YAW INERTIA	2.92 "
ζ DAMPING RATIO	0.05
λ_{Az} FREQUENCY K_{Az}/I_{zz}^A	564.2 R/S
ω_{As} MAXIMUM SHAFT YAW RATE	100. R/S
ω_{Am} MAXIMUM ANTENNA YAW RATE	100. R/S

ORIGINAL PAGE IS
OF POOR QUALITY

Ⓓi DRIVE HOUSING ROLL.

12/16/75

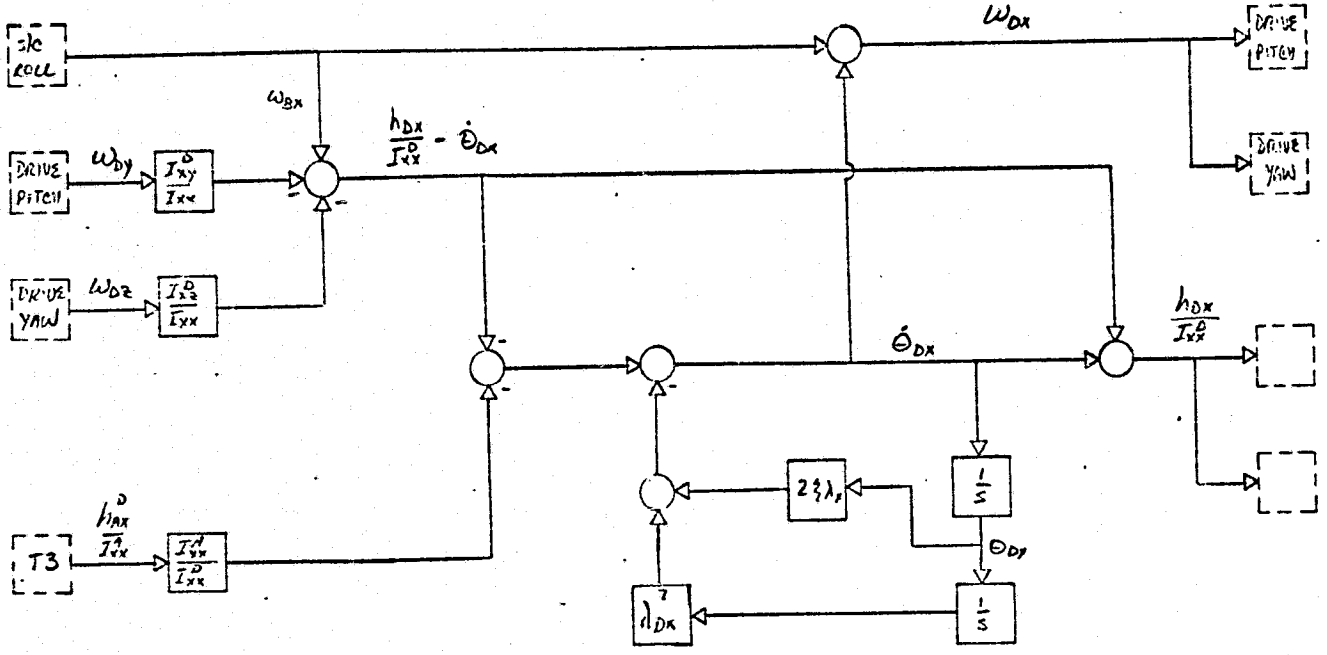

$$\dot\theta_{Dx} = -\frac{1}{I^D_{xx}} h_{Ax} - \left(\omega_{Bx} - \frac{I^D_{xy}}{I^D_{xx}}\omega_{Dy} - \frac{I^D_{xz}}{I^D_{xx}}\omega_{Dz}\right) - \lambda^2_{Dx}\int_0^t \theta_{Dx}\,dt - 2\zeta\lambda_{Dx}\theta_{Dx}$$

Variables		Minimum
ω_{Bx}	SPACECRAFT ROLL RATE (0.01 RHO/sec)	0.01 R/S
ω_{Dx}	DRIVE HOUSING ROLL RATE (0.1·2π·139)	87.33 R/S
ω_{Dy}	DRIVE HOUSING PITCH RATE (0.1·2π·206)	129 R/S
ω_{Dz}	DRIVE HOUSING YAW RATE (0.1·2π·139)	87.33 R/S
h^D_{Ax}	ANTENNA MOMENTUM ALONG HOUSING ROLL	
h_{Dx}	DRIVE HOUSING ROLL MOMENTUM ($I^D_{xx}\omega_{Dx}$)	
θ_{Dx}	DRIVE HOUSING ROLL DEFLECTION/GMSE	0.1 RAD

Parameters		Nominal
I^D_{xx}	DRIVE HOUSING ROLL INERTIA	2.9 NT-M-SEC²
I^D_{xy}	DRIVE HOUSING ROLL/PITCH INERTIA PRODUCT	0.0 "
I^D_{xz}	DRIVE HOUSING ROLL/YAW INERTIA PRODUCT	2.3 "
I^A_{xx}	ANTENNA ROLL INERTIA	1.9 "
I^W_{xx}	COMPENSATING WHEEL ROLL INERTIA	0.15 "
ζ	DAMPING RATIO	0.05
λ_{Dx}	RESONANCE $\lambda_x = \sqrt{K_{Dx}/I^D_{xx}}$	873.4 R/S

ORIGINAL PAGE IS OF POOR QUALITY

(D2) DRIVE HOUSING PITCH 12/16/75

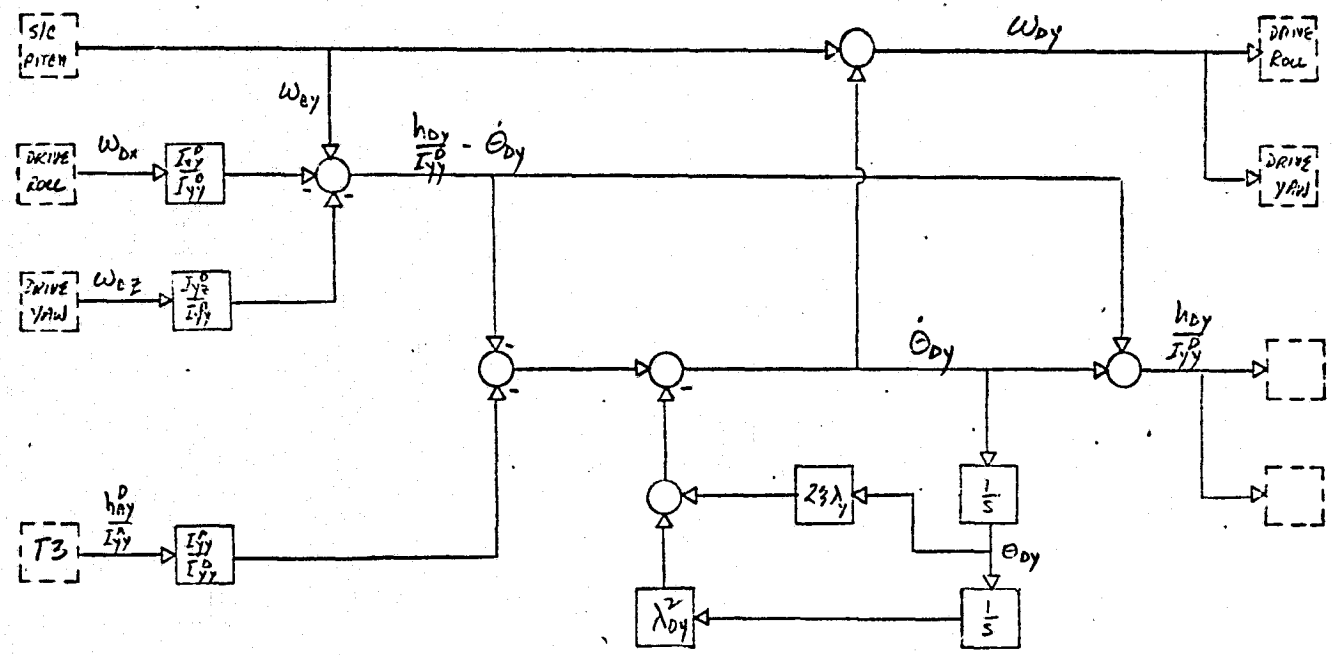

$$\dot{\theta}_{Dy} = -\frac{1}{I_{yy}^D} h_{Ay} - \left(\omega_{By} - \frac{I_{xy}^D}{I_{yy}^D}\omega_{Dx} - \frac{I_{yz}^D}{I_{yy}^D}\omega_{Dz}\right) - \lambda_{Dy}^2 \int_0^t \theta_{Dy}\,dt - 2\zeta\lambda_{Dy}\theta_{Dy}$$

Variables		Maximum	Parameters		Nominal
ω_{By}	SPACECRAFT PITCH RATE	0.01 RAD/SEC	I_{xy}^D	DRIVE HOUSING ROLL/PITCH INERTIA PRODUCT	0.0 KG-M-S^2
ω_{Dx}	DRIVE HOUSING ROLL RATE	17.33 R/S	I_{yz}^D	DRIVE HOUSING PITCH/YAW INERTIA PRODUCT	0.0 "
ω_{Dy}	DRIVE HOUSING PITCH RATE	129 R/S	I_{yy}^D	DRIVE HOUSING PITCH INERTIA	75.9 "
ω_{Dz}	DRIVE HOUSING YAW RATE	87.33 R/S	I_{yy}^A	ANTENNA PITCH INERTIA	3.0 "
			I_{yy}^W	REMANENCIATING WHEEL PITCH INERTIA	0.15 "
h_{AY}^D	ANTENNA MOMENTUM ALONG HOUSING PITCH				
h_{Dy}	DRIVE HOUSING PITCH MOMENTUM		ζ	DAMPING RATIO	0.05
θ_{Dy}	DRIVE HOUSING PITCH DEFLECTION/BASE	0.1 RAD	λ_{Dy}	RESONANCE $\lambda_y = \sqrt{k_{Dy}/I_{yy}^D}$	1214 R/S

(D2) DRIVE HOUSING YAW

1/26/76

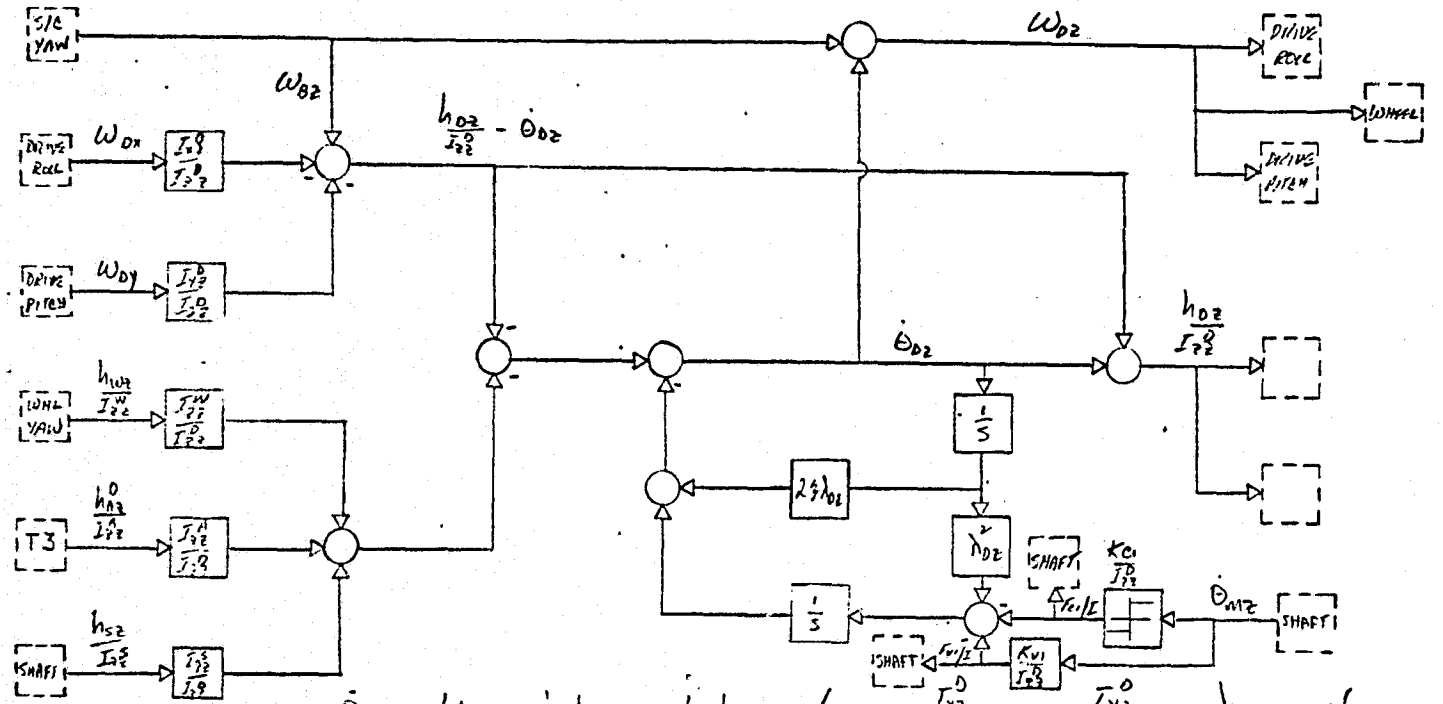

$$\dot{\Theta}_{D2} = -\frac{1}{I_{22}^{D}} h_{S2} - \frac{1}{I_{22}^{D}} h_{A2} - \frac{1}{I_{22}^{D}} h_{W2} - \left(\omega_{B2} - \frac{I_{x2}^{D}}{I_{22}^{D}}\omega_{Dx} - \frac{I_{y2}^{D}}{I_{22}^{D}}\omega_{Dy}\right) - \lambda_{D2}^{V}\int \Theta_{D2}\,dt + \int \frac{K_{C1}}{I_{22}^{D}} \text{SIGN}(\dot{\Theta}_{M2}) \cdot H$$

$$+ \int \frac{F_{C1}}{I}dt + \int \frac{F_{V1}}{I}dt + \int \frac{K_{V1}}{I_{22}^{D}}dt - 2\zeta\lambda_{D2}\Theta_{D2}$$

PARAMETERS

VARIABLES		MAXIMUM
ω_{B2}	SPACECRAFT YAW RATE	0.01 R/S
ω_{Dx}	DRIVE HOUSING	67.33 R/S
ω_{Dy}	DRIVE HOUSING	129 R/S
ω_{D2}	DRIVE HOUSING	67.33 R/S
h_{W2}	COMPENSATING WHEEL YAW MOMENTUM	
h_{A2}^{D}	ANTENNA MOMENTUM ALONG HOUSING YAW	
h_{D2}	DRIVE HOUSING YAW MOMENTUM	
Θ_{D2}	DRIVE HOUSING YAW DEFLECTION/BASE	0.1 RAD
Θ_{M2}	SHAFT POSITION/DRIVE HOUSING	0.785 RAD
h_{M2}	MOMENTUM OF BASE OF ANTENNA SHAFT	

I_{x2}^{D}	DRIVE HOUSING	2.3 NT-M-SEC²
I_{y2}^{D}	DRIVE HOUSING	0.0 "
I_{22}^{D}	DRIVE HOUSING	22.5 "
I_{22}^{A}	ANTENNA	2.9 "
I_{22}^{W}	COMPENSATING WHEEL	0.29 "
I_{22}^{S}	SHAFT INERTIA	0.005 "
ζ	DAMPING RATIO	0.05
λ_{D2}	RESONANCE	873 RAD/SEC
K_{C1}	BEARING FRICTION COEFFICIENT SHAFT/HOUSING	0.1765 NT-M
F_{V1}	VISCOUS FRICTION COEFFICIENT SHAFT/HOUSING	0.00353 NT-M/R/S

(21) FEED ROLL

11/12/75

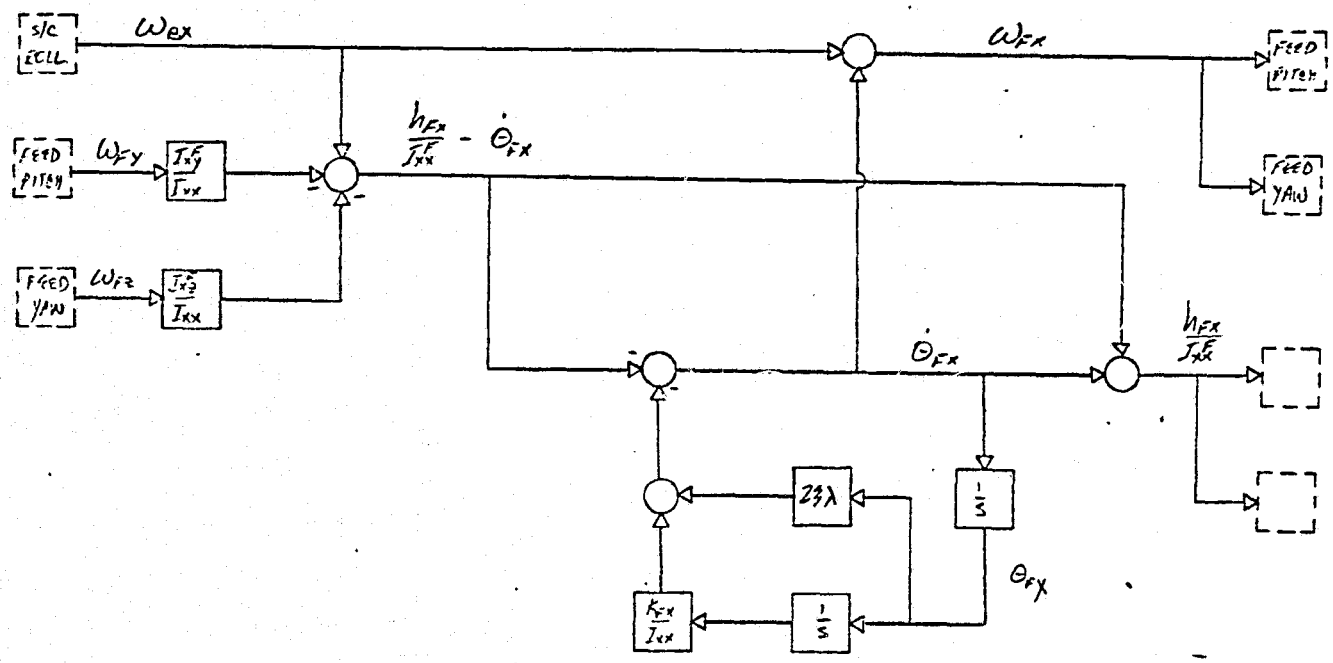

$$\dot{\theta}_{Fx} = -\omega_{ex} + \frac{I^F_{xy}}{I^F_{xx}}\omega_{Fy} + \frac{I^F_{xz}}{I^F_{xx}}\omega_{Fz} - \frac{K_{Fx}}{I^F_{xx}}\int_0^t \theta_{Fx}\,dt$$

VARIABLES		MAXIMUM
ω_{Fx}	FEED ROLL RATE	
ω_{Fy}	FEED PITCH RATE	
ω_{Fz}	FEED YAW RATE	
ω_{ex}	SPACECRAFT ROLL RATE	
I_{xx}	FEED ROLL MOMENTUM	
θ_{Fx}	FEED ROLL DEFLECTION	0.066 RAD

PARAMETER		MAXIMUM	NOMINAL
J^F_{xx}	FEED ROLL INERTIA	100 N/S	0.1 KG-M²
I^F_{xy}	FEED ROLL/PITCH INERTIA PRODUCT	100 N/S	0.0 KG-M²
I^F_{xz}	FEED ROLL/YAW INERTIA PRODUCT	100 N/S	0.0 KG-M²
K_{Fx}	FEED ROLL SPRING RATE	0.01 N/S	
ζ	DAMPING RATIO		
f_{Fx}	RESONANCE $\sqrt{K_{Fx}/I_{xx}}$		240 Hz
ω_{mB}	MAXIMUM BASE RATE, ROLL		
ω_{mF}	MAXIMUM FEED RATE, ROLL		

(F2) FEED PITCH 11/12/75

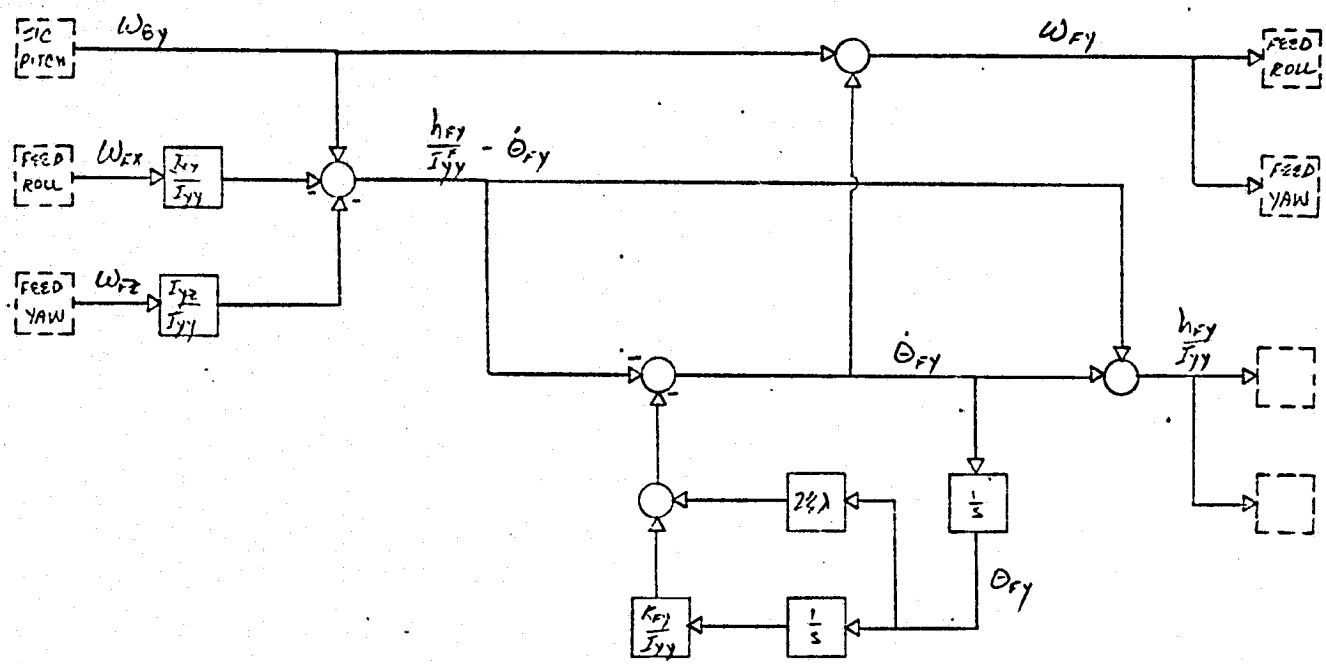

$$\dot{\theta}_{Fy} = -\omega_{By} + \frac{I_{xy}^F}{I_{yy}}\omega_{Fx} + \frac{I_{yz}}{I_{yy}}\omega_{Fz} - \frac{K_{Fy}}{I_{yy}^F}\int_0^t \theta_{Fy}\,dt$$

Variables		Maximum	Parameter		Nominal
ω_{Fx}	FEED ROLL RATE	100 R/S	I_{xy}^F	FEED ROLL/PITCH INERTIA PRODUCT	0.0 KG-M^2
ω_{Fy}	FEED PITCH RATE	100 R/S	I_{yy}^F	FEED PITCH INERTIA	5.3 KG-M^2
ω_{Fz}	FEED YAW RATE	100 R/S	I_{yz}^F	FEED PITCH/YAW INERTIA PRODUCT	0.0 KG-M^2
ω_{By}	SPACECRAFT PITCH RATE	0.01 R/S	K_{Fy}	FEED PITCH SPRING RATE	
h_{Fy}	FEED PITCH MOMENTUM		ζ	DAMPING RATIO	
θ_{Fy}	FEED PITCH DEFLECTION	0.042 RAD	f_{Fy}	RESONANCE $\sqrt{K_{Fy}/I_{yy}}$	388 Hz
			ω_{MB}	MAXIMUM BASE RATE PITCH	
			ω_{MF}	MAXIMUM FEED RATE PITCH	

(F3) FEED YAW

11/12/75

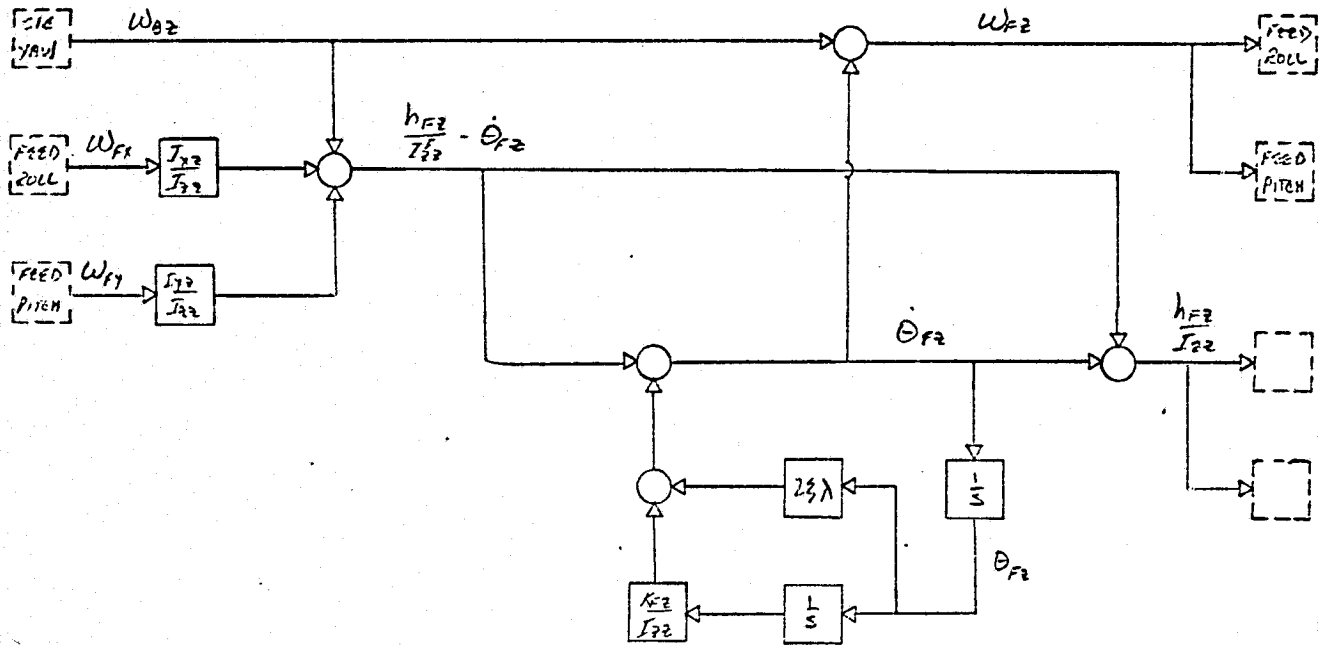

$$\dot{\theta}_{FZ} = -\omega_{BZ} + \frac{I_{XZ}^F}{I_{ZZ}}\omega_{FX} + \frac{I_{YZ}^F}{I_{ZZ}}\omega_{FY} - \frac{K_{FZ}}{I_{ZZ}^F}\int_0^t \theta_{FZ}\,dt$$

Variables		Maximum
ω_{FX}	FEED ROLL RATE	100 R/S
ω_{FY}	FEED PITCH RATE	100 R/S
ω_{FZ}	FEED YAW RATE	100 R/S
ω_{ZZ}	SPACECRAFT YAW RATE	
h_{FZ}	FEED YAW MOMENTUM	
θ_{FZ}	FEED YAW DEFLECTION	0.066 RAD

Parameters		Nominal
I_{XZ}^F	FEED ROLL/YAW INERTIA PRODUCT	0.0 KG-M²
I_{YZ}^F	FEED PITCH/YAW INERTIA PRODUCT	0.0 KG-M²
I_{ZZ}^F	FEED YAW INERTIA	5.3 KG-M²
K_{FZ}	FEED YAW SPRING RATE	
ζ	DAMPING RATIO	
f_{FZ}	RESONANCE $\sqrt{K_{FZ}/I_{ZZ}}$	240 HZ
ω_{MB}	MAXIMUM BASE RATE, YAW	
ω_{MF}	MAXIMUM FEED RATE, YAW	

(31) BASE OF ANTENNA SHAFT

1/26/76

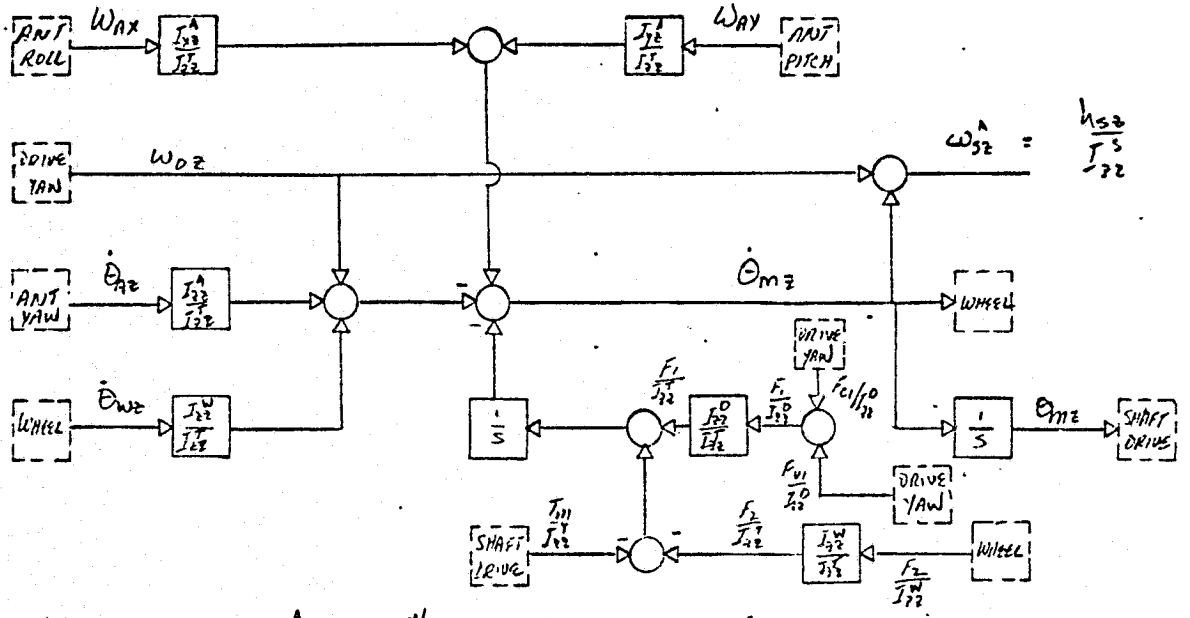

$$\dot\theta_{MZ} = -\omega_{DZ} - \frac{I^A_{ZZ}}{I^T_{ZZ}}\dot\theta_{AZ} - \frac{I^W_{ZZ}}{I^T_{ZZ}}\dot\theta_{WZ} + \int\frac{T_m}{I^T_{ZZ}}dt - \int\frac{F_1}{I^T_{ZZ}}dt + \int\frac{F_2}{I^T_{ZZ}}dt$$

$$F_1 = +K_{C1}\,\text{SIGN}[\dot\theta_{MZ}] + K_{V1}\dot\theta_{MZ} \qquad \omega^A_{SZ} = \omega_{DZ} + \dot\theta_{MZ}$$

VARIABLES		MINIMUM	PARAMETERS		NOMINAL
ω_{DZ}	DRIVE HOUSING YAW RATE	47.33 R/S	I^A_{ZZ}	ANTENNA YAW INERTIA	2.92 NT-M-S^2
			I^W_{ZZ}	WHEEL YAW INERTIA	0.29 "
			I^S_{ZZ}	SHAFT YAW INERTIA	0.005 "
θ_{MZ}	SHAFT DISPLACEMENT/HOUSING	0.785 RAD			
θ_{WZ}	WHEEL DISPLACEMENT/HOUSING	7.85 RAD			
T_m	SHAFT DRIVE TORQUE		I^D_{ZZ}	HOUSING YAW INERTIA	22.5 "
ω^A_{SZ}	TOTAL SHAFT VELOCITY	100 R/S	$I^T_{ZZ} = I^A_{ZZ} + I^W_{ZZ} + I^S_{ZZ}$		3.21 "
F_1	COULOMB/VISCOUS FRICTION SHAFT/HOUSING	(TORQUE)			
F_2	COULOMB/VISCOUS FRICTION SHAFT/WHEEL	(TORQUE)	(ALL COEFFICIENTS REFERENCED IN ANTENNA REFERENCE SYSTEM)		
$\dot\theta_{MZ}$	SHAFT RATE/HOUSING (45°,0)	2.47 RAD/S			

(52) SHAFT DRIVE 1/26/76

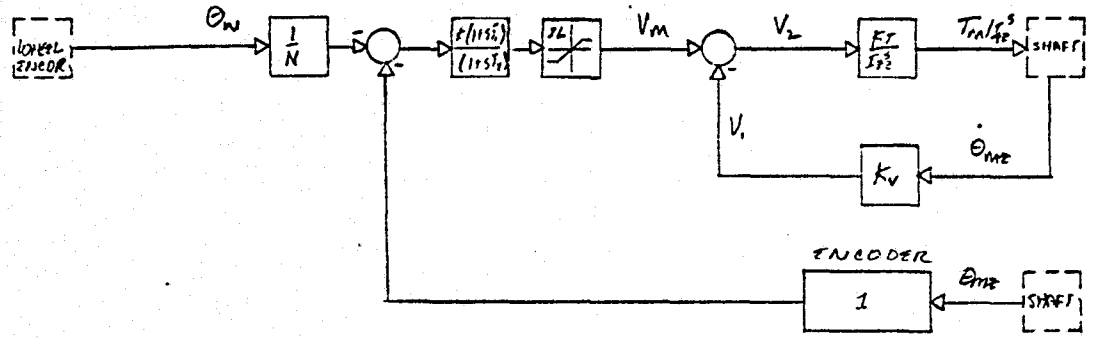

VARIABLES		MINIMUM PARAMETERS		NOMINAL
V_R	REFERENCE SIGNAL	T_1	LEAD TIME CONSTANT	0.1
V_E	ERROR SIGNAL	T_2	LAG TIME CONSTANT	0.01
V_A	COMPENSATED ERROR SIGNAL	K	GAIN	1000.
V_M	MOTOR DRIVE SIGNAL	L	AMPLIFIER SATURATION	
V_1	BACK EMF	K_T	MOTOR TORQUE CONSTANT	0.0816 NT-M/V
V_2	NET MOTOR VOLTAGE	K_V	MOTOR VELOCITY CONSTANT	1.1 V/RAD/S
T_m	MOTOR SHAFT TORQUE	J_{s2}	INERTIA OF SHAFT	0.005 NT-M-SEC^2
$\dot{\theta}_{mr}$	SHAFT RATE/HOUSING	N	$= I_A + I_S/I_W$	10
θ_{mr}	SHAFT DISPLACEMENT/HOUSING	C	CONVERSION FACTOR (NT-M/IN-OZ)	0.00706
θ_s	ENCODER OUTPUT, SHAFT			

K = 272, 13.5Ω

ORIGINAL PAGE IS
OF POOR QUALITY

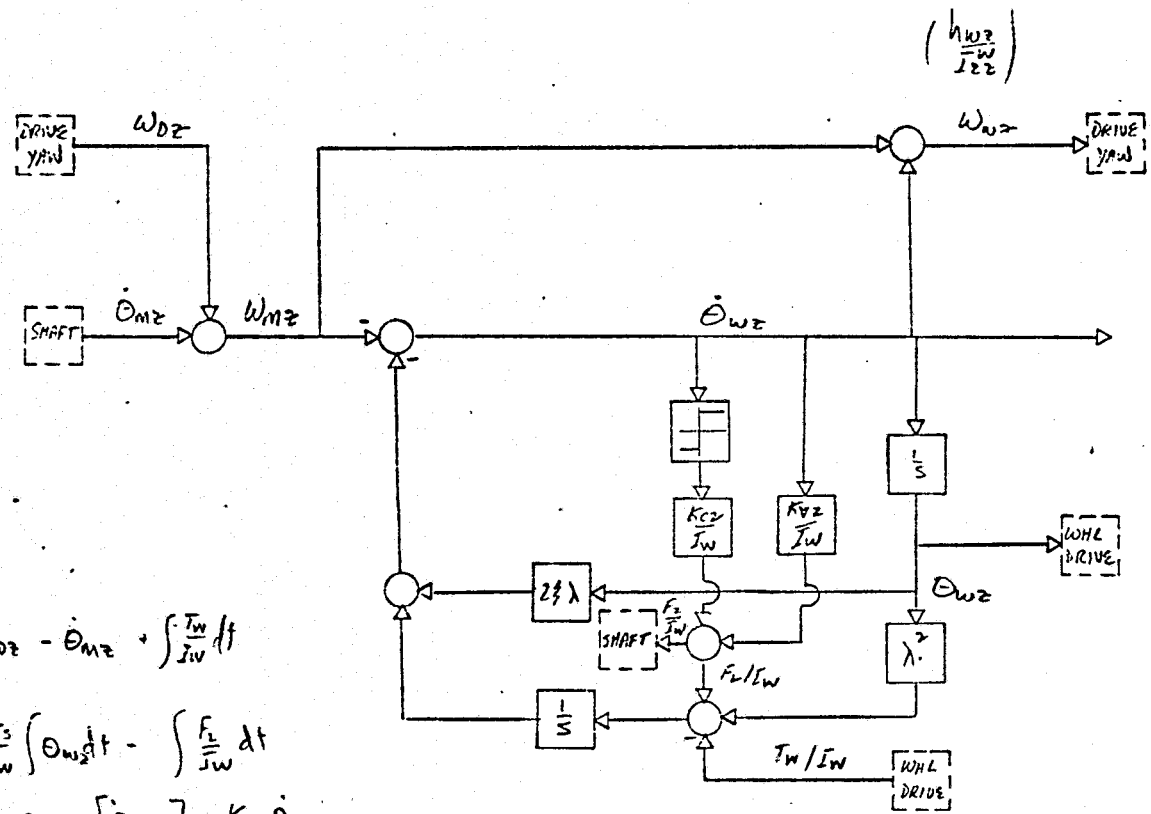

$$\dot\theta_{WZ} = -\omega_{DZ} - \dot\theta_{MZ} + \int \frac{T_W}{I_W}\,dt$$

$$- \frac{K_S}{I_W}\int \theta_{WZ}\,dt - \int \frac{F_Z}{I_W}\,dt$$

$$F_Z = K_{CZ}\,\text{SIGN}\left[\dot\theta_{WZ}\right] + K_{VZ}\,\dot\theta_{WZ}$$

VARIABLES		MINIMUM	PARAMETERS		NOMINAL
ω_{DZ}	DRIVE HOUSING YAW RATE	± 7.33 RAD/S	K_{VZ}	VISCOUS FRICTION COEFFICIENT	0.00353 NT-M/r
ω_{WZ}	TITAN WHEEL RATE		K_{CZ}	COULOMB FRICTION COEFFICIENT	0.0947 NT-M
θ_{MZ}	SHAFT DISPLACEMENT/HOUSING (45 DEG)	0.785 RAD	ζ	DAMPING RATIO	0.0
T_W	WHEEL DRIVE TORQUE		λ_S	BEARING (0.5 HZ)	17 RAD/S
F_Z	COULOMB FRICTION WHEEL/SHAFT		I_W	WHEEL INERTIA	0.29 KG-M-SEC^2
θ_{WZ}	WHEEL DISPLACEMENT/SHAFT (495 DEG)	8.65 RAD	$\lambda^2 = \frac{K_S}{I_W} = \lambda_S^2\left(I_{ZZ}^A / I_{ZZ}^T\right)$		8.97 (RAD/S)^2
$\dot\theta_{WZ}$	WHEEL RATE/SHAFT (495°.11)	24.7 RAD/SEC			

IONGEL DRIVE

1/26/76

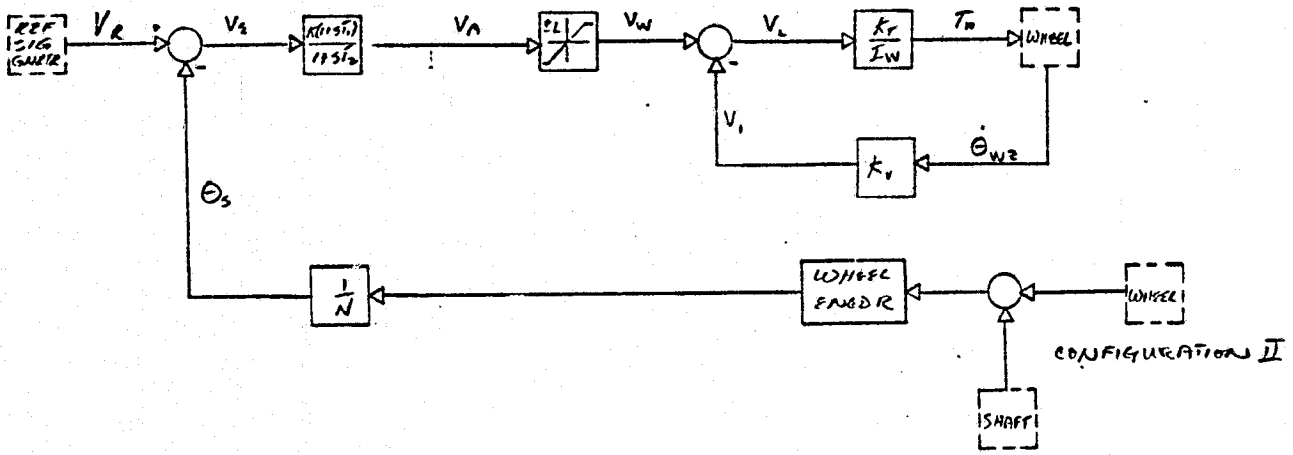

VARIABLES

θ_S	ENCODER OUTPUT, SHAFT
V_E	ERROR SIGNAL
V_A	COMPENSATED ERROR SIGNAL
V_W	WHEEL DRIVE SIGNAL
V_1	BACK EMF
V_L	NET MOTOR VOLTAGE
T_W	WHEEL TORQUE
$\dot{\theta}_{WE}$	WHEEL RATE / SHAFT
θ_{WE}	WHEEL DISPLACEMENT/SHAFT
θ_W	ENCODER OUTPUT, WHEEL
θ_{WE}	SHAFT DISPLACEMENT

MAXIMUM PARAMETERS

		NOMINAL
T_1	LEAD TIME CONSTANT	0.1
T_2	LAG TIME CONSTANT	0.01
L	AMPLIFIER SATURATION	20V
K_T	MOTOR TORQUE CONSTANT	
K_V	MOTOR VELOCITY CONSTANT	
N	WHEEL / SHAFT TURNS RATIO	10
K	COMPENSATION GAIN	252.9

(T1) TRANSFORMATION FROM HOUSING TO ANTENNA REFERENCE

1:1.24.75

$a_{11} = \cos \theta_{mz}$

$a_{12} = \sin \theta_{mz}$

$a_{13} = 0$

$a_{21} = -\sin \theta_{mz}$

$a_{22} = \cos \theta_{mz}$

$a_{23} = 0$

$a_{31} = 0$

$a_{32} = 0$

$a_{33} = 1$

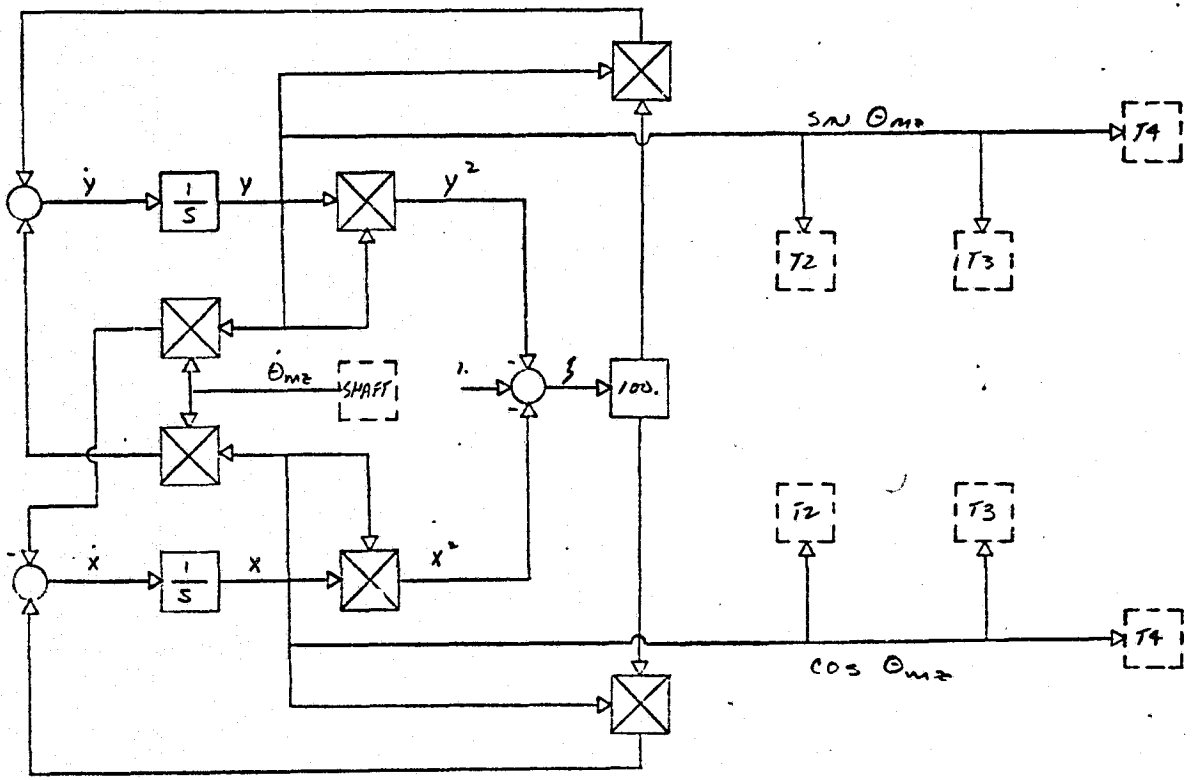

VARIABLE		MAXIMUM
$\dot{\theta}_{mz}$	SHAFT VELOCITY	
x	COS θ_{mz}	1.0
y	SIN θ_{mz}	1.0
a_{ij}	DIRECTION COSINES; HOUSING TO SHAFT REFERENCE	1.0

(12) TRANSFORMATION OF HOUSING VELOCITY TO ANTENNA REFERENCE 12/8/75

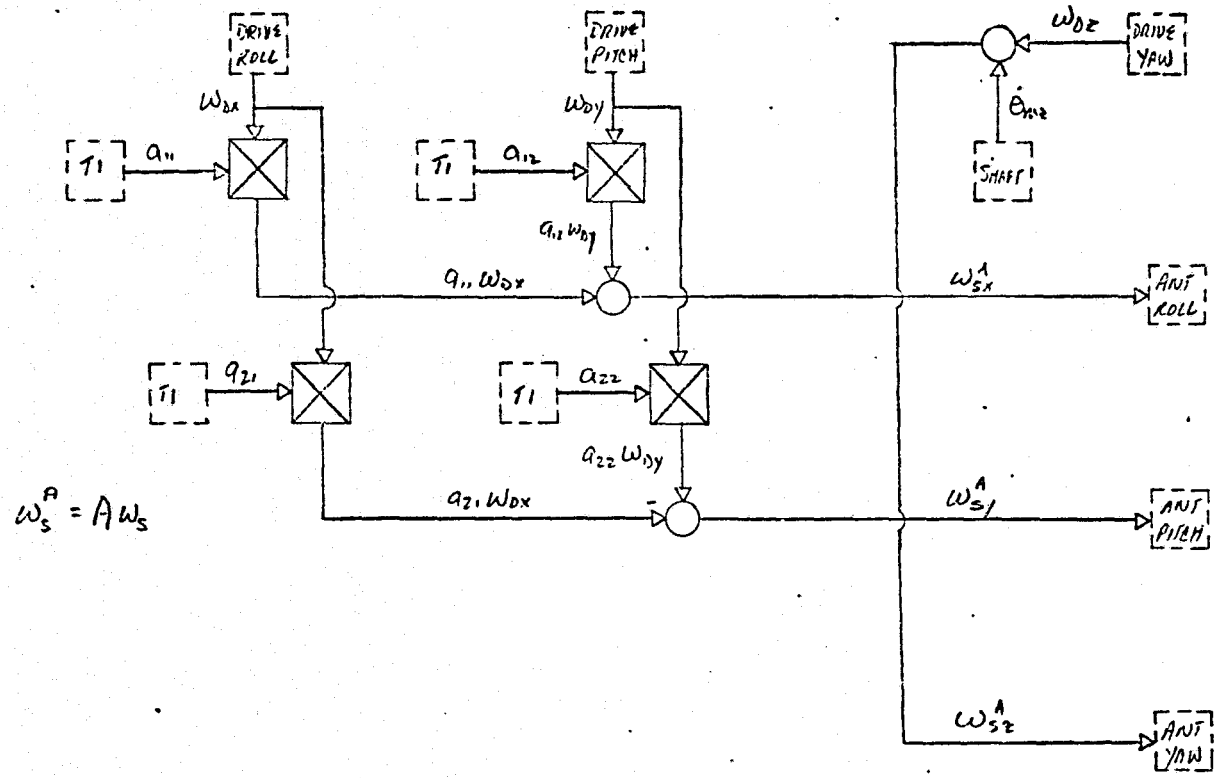

VARIABLES — MINIMUM PARAMETERS — OPTIONAL

ω_{DX}	DRIVE HOUSING ROLL RATE
ω_{DY}	DRIVE HOUSING PITCH RATE
ω_{DZ}	DRIVE HOUSING YAW RATE
$\dot{\theta}_{MZ}$	SHAFT RATE RELATIVE TO HOUSING
ω_{SX}^A	SHAFT RATE ALONG ANTENNA ROLL
ω_{SY}^A	SHAFT RATE ALONG ANTENNA PITCH
ω_{SZ}^A	SHAFT RATE ALONG ANTENNA YAW
a_{ij}	DIRECTION COSINES

1.0

ORIGINAL PAGE IS
OF POOR QUALITY

(T3) TRANSFORMATION OF ANTENNA MOMENTUM TO S/C REFERENCE 12/2/75

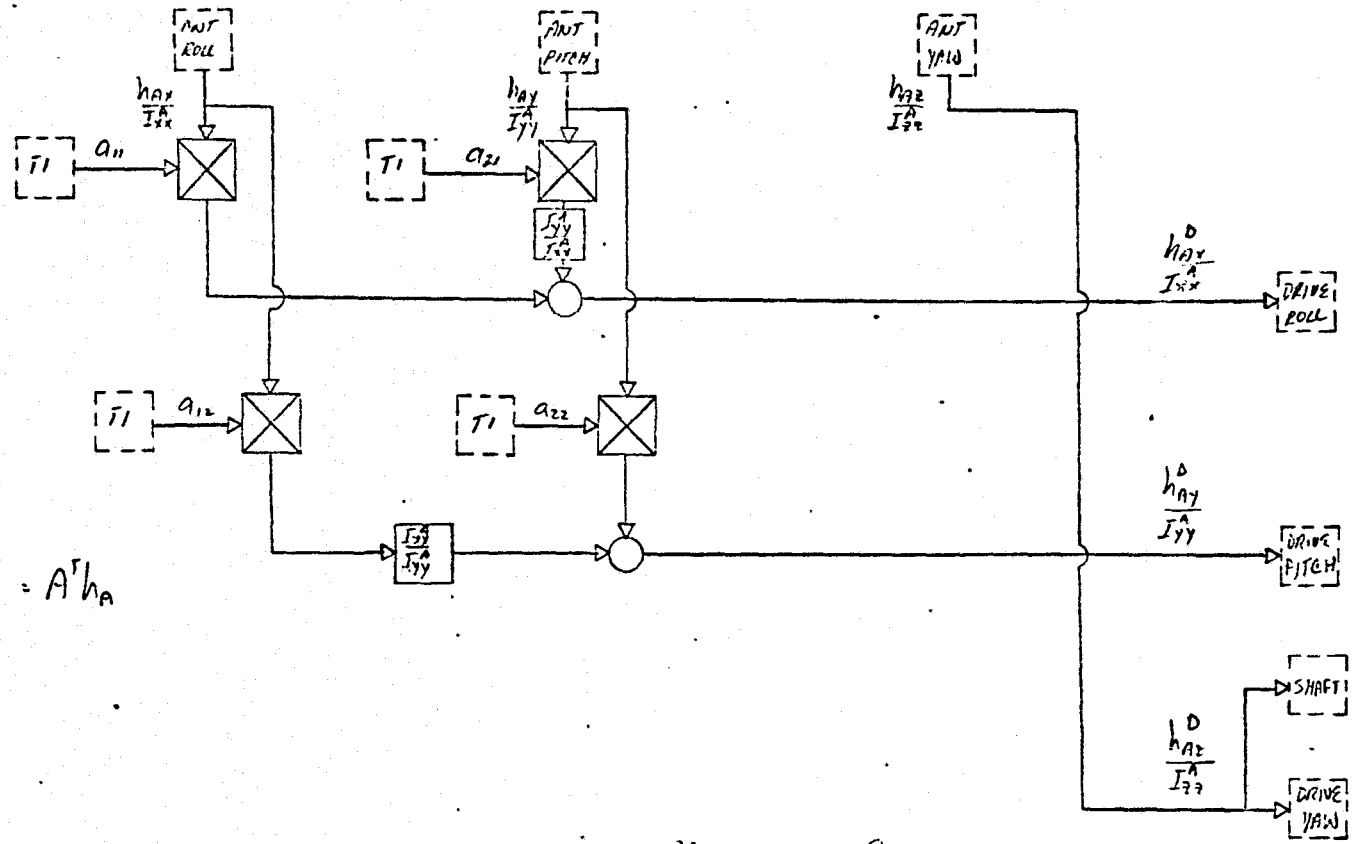

$h_A^D = A^T h_A$

VARIABLES

h_{Ax} ANTENNA ROLL MOMENTUM
h_{Ay} ANTENNA PITCH MOMENTUM
h_{Az} ANTENNA YAW MOMENTUM
h^D_{Ax} ANTENNA MOMENTUM ALONG DRIVE ROLL
h^D_{Ay} ANTENNA MOMENTUM ALONG DRIVE PITCH
h^D_{Az} ANTENNA MOMENTUM ALONG DRIVE YAW
a_{ij} DIRECTION COSINES

MAXIMUM PARAMETERS

I^A_{xx} ANTENNA ROLL INERTIA
I^A_{yy} ANTENNA PITCH INERTIA
I^A_{zz} ANTENNA YAW INERTIA

NOMINAL

(E1) REFERENCE SIGNAL GENERATOR

12/12/75

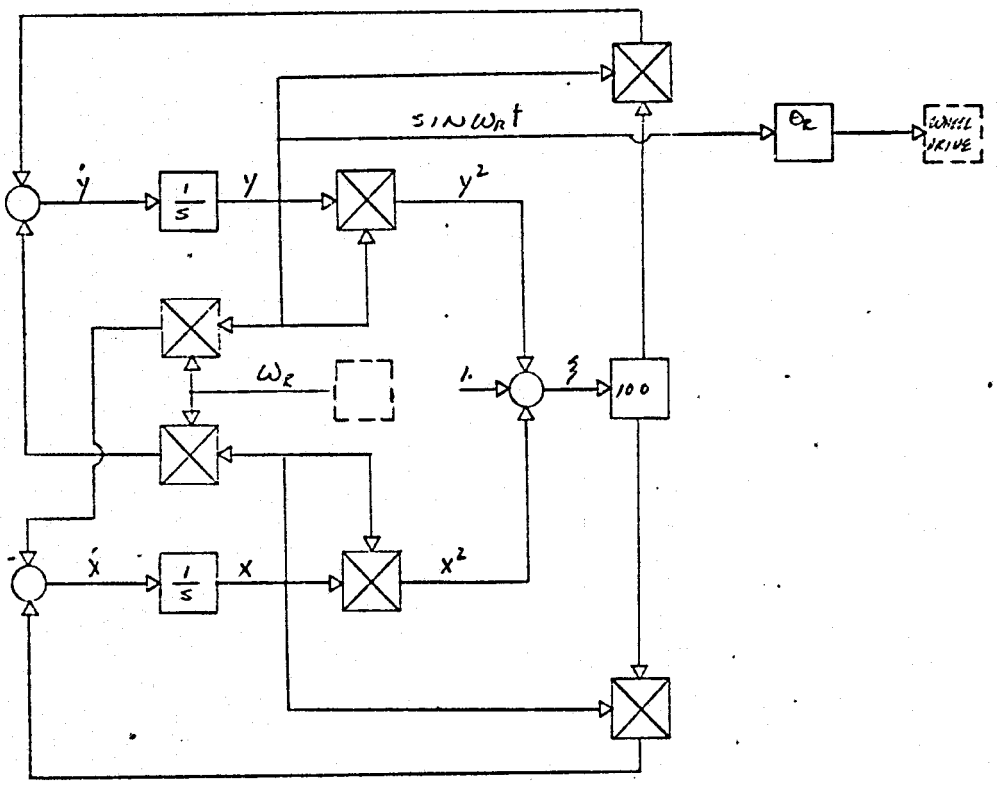

VARIABLES		MAXIMUM PARAMETERS		NOMINAL
x	$\cos \omega_R t$	1.0	ω_R VELOCITY	0.5 HZ
y	$\sin \omega_R t$	1.0	θ_R AMPLITUDE	450°
ζ	$1 - x^2 - y^2$	0.1		

APPENDIX C

SIMULATION RESULTS

Results of analog simulation for various drive configurations are shown in this section. The operational modes simulated for each configuration are tabulated in Table C1 with corresponding figure numbers. Variables shown in the figures are tabulated in Table C2.

Note

In the simulation for configuration I the antenna drive motor was slave to the wheel angle instead of the reference signal.

TABLE C1

SIMULATION MODES

Configuration	Antenna Size	Simulation Mode	Figure Number
I	1M	Normal	C 1
		No Friction	C 2
		5X Friction	C 3
		No Drive Excitation	C 4
		Loss of Antenna Drive	C 5
		Loss of Wheel Drive	C 6
	1.4M	Normal	C 7
		No Friction	C 8
		5X Friction	C 9
		Loss of Antenna Drive	C10
		Loss of Wheel Drive	C11
II	1M	Normal	C12
		No Friction	C13
		5X Friction	C14
		No Drive Excitation	C15
		Loss of Antenna Drive	C16
		Loss of Wheel Drive	C17
	1.4M	Normal	C18
		No Friction	C19
		5X Friction	C20
		No Drive Excitation	C21
		Loss of Antenna Drive	C22
		Loss of Wheel Drive	C23

TABLE C2

VARIABLES

θ_R:	Reference Signal
$\theta_R - \theta_S$:	Antenna Shaft Rotation Error
θ_{XA}:	Antenna Deflection in x-axis (roll)
θ_{YA}:	Antenna Deflection in y-axis (pitch)
θ_{ZA}:	Antenna scan angle (yaw)
Δ hx:	Residual momentum in x-axis
Δ hy:	Residual momentum in y-axis
Δhz:	Residual momentum in scan axis
θ_W:	Compensation wheel rotation angle
I_W:	Wheel drive motor current
I_A:	Antenna drive motor current
V_W:	Wheel motor drive voltage
V_A:	Antenna motor drive voltage

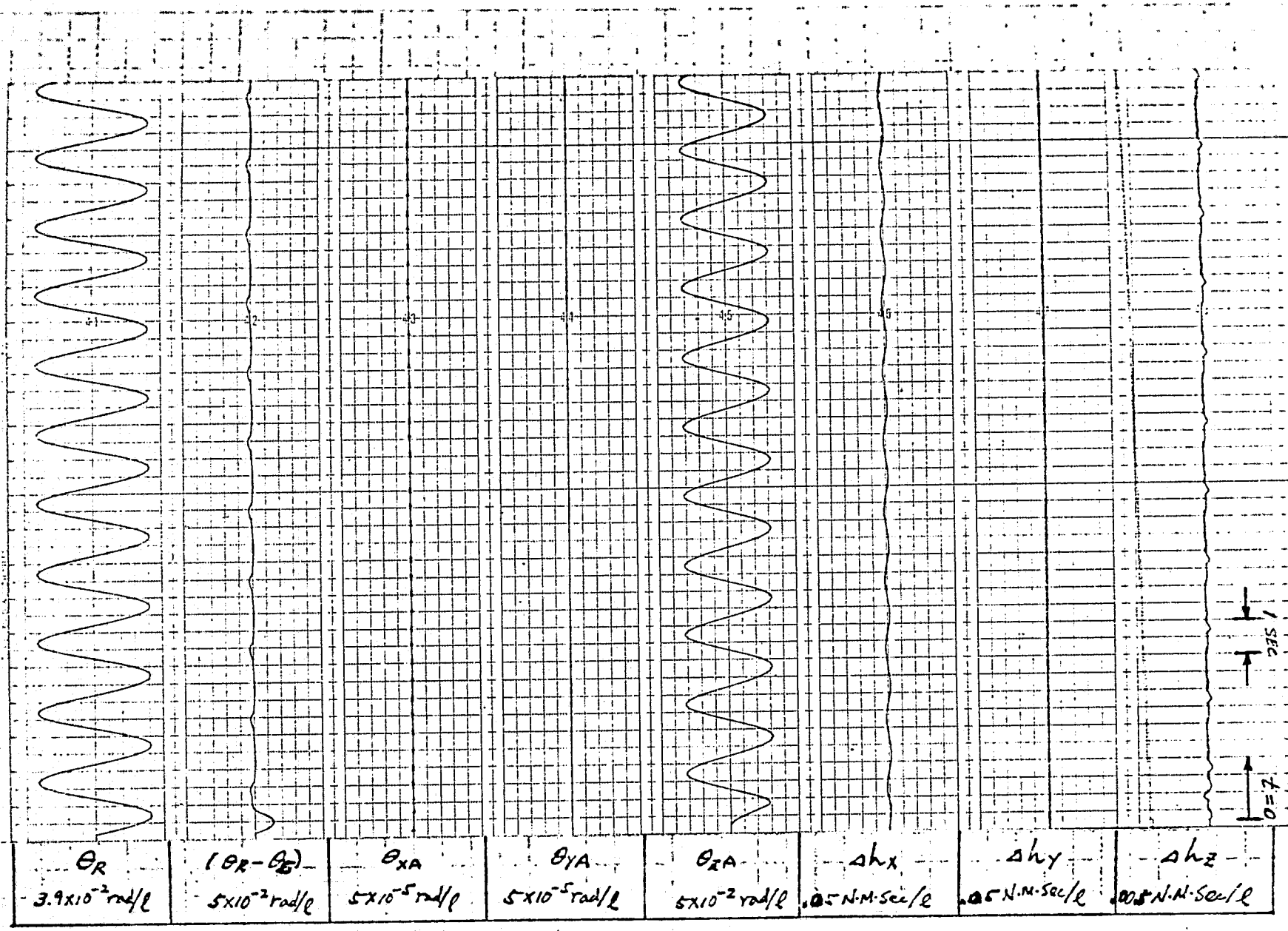

θ_R	$(\theta_R - \theta_E)$	θ_{XA}	θ_{YA}	θ_{ZA}	Δh_X	Δh_Y	Δh_Z
3.9×10^{-2} rad/ℓ	5×10^{-2} rad/ℓ	5×10^{-5} rad/ℓ	5×10^{-5} rad/ℓ	5×10^{-2} rad/ℓ	.05 N.M.Sec/ℓ	.05 N.M.Sec/ℓ	.005 N.M.Sec/ℓ

C1 (a)

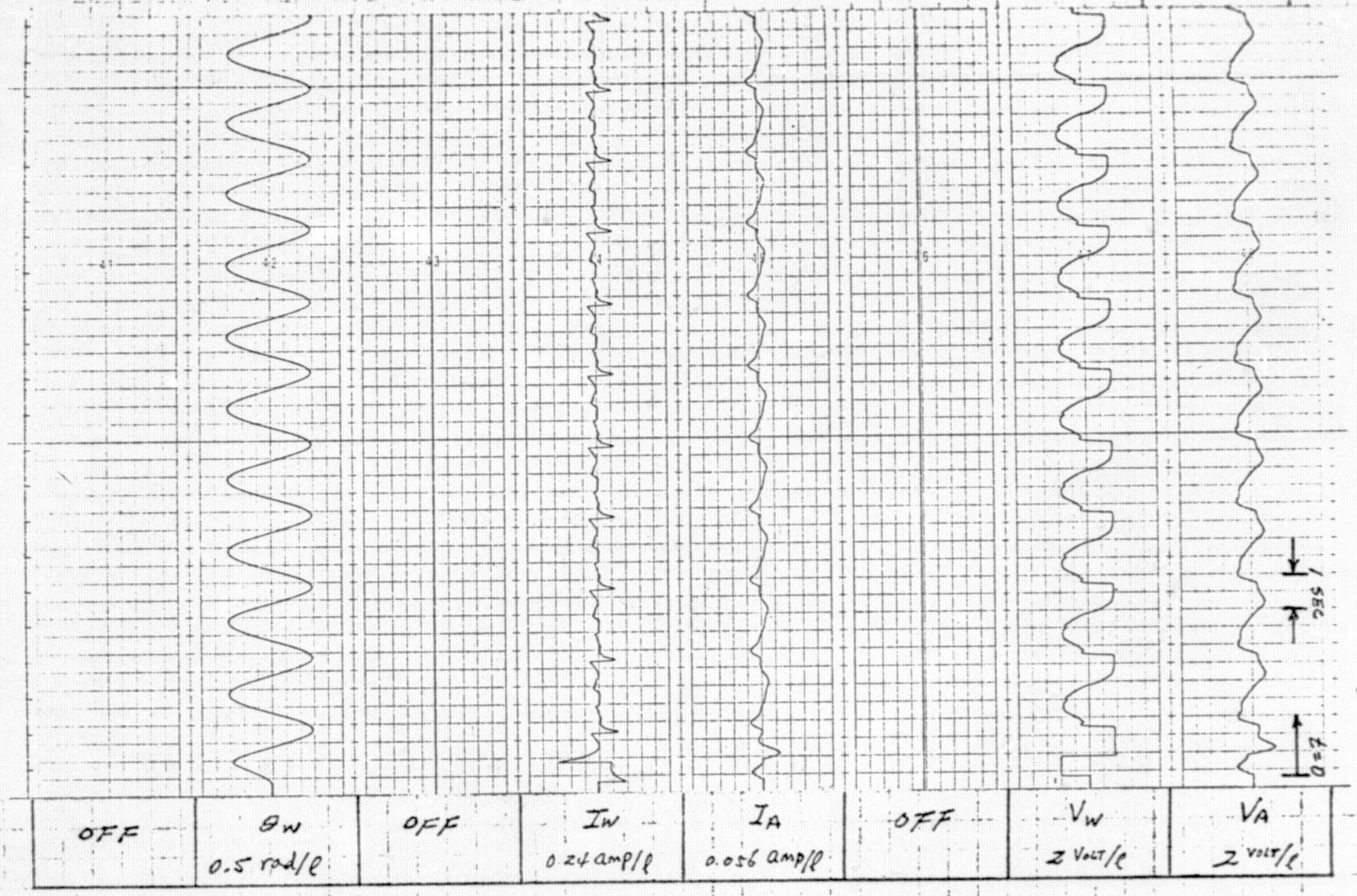
OFF
θ_W
0.5 rad/ℓ
OFF
I_W
0.24 amp/ℓ
I_A
0.056 amp/ℓ
OFF
V_W
2 VOLT/ℓ
V_A
2 VOLT/ℓ
1 SEC
0=7

C1 (b)

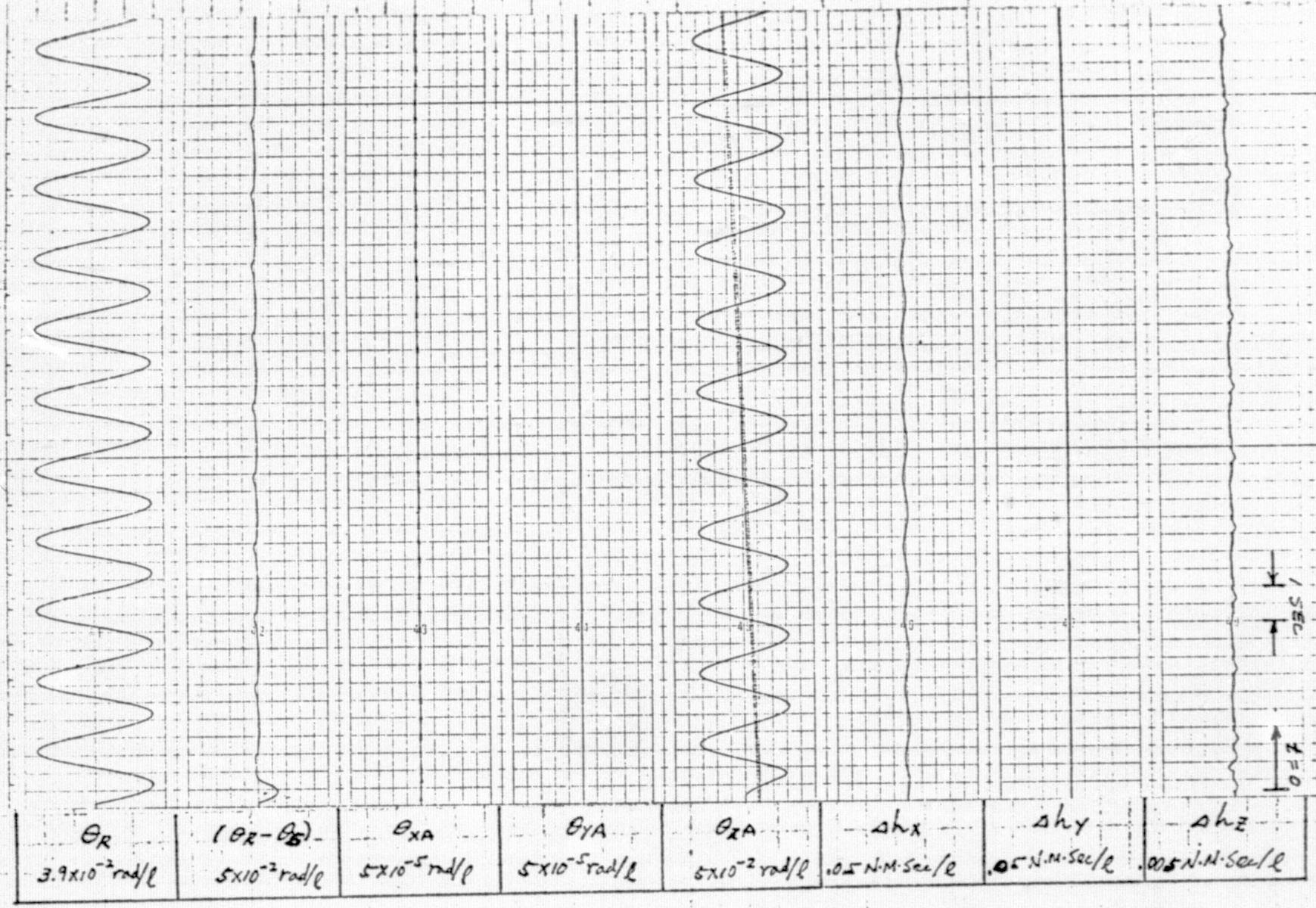
θ_R
3.9×10^{-2} rad/ℓ
$(\theta_R-\theta_B)$
5×10^{-2} rad/ℓ
θ_{XA}
5×10^{-5} rad/ℓ
θ_{YA}
5×10^{-5} rad/ℓ
θ_{ZA}
5×10^{-2} rad/ℓ
Δh_X
.05 N.M.Sec/ℓ
Δh_Y
.05 N.M.Sec/ℓ
Δh_Z
.005 N.M.Sec/ℓ
1 sec
0 = T

C2 (a)

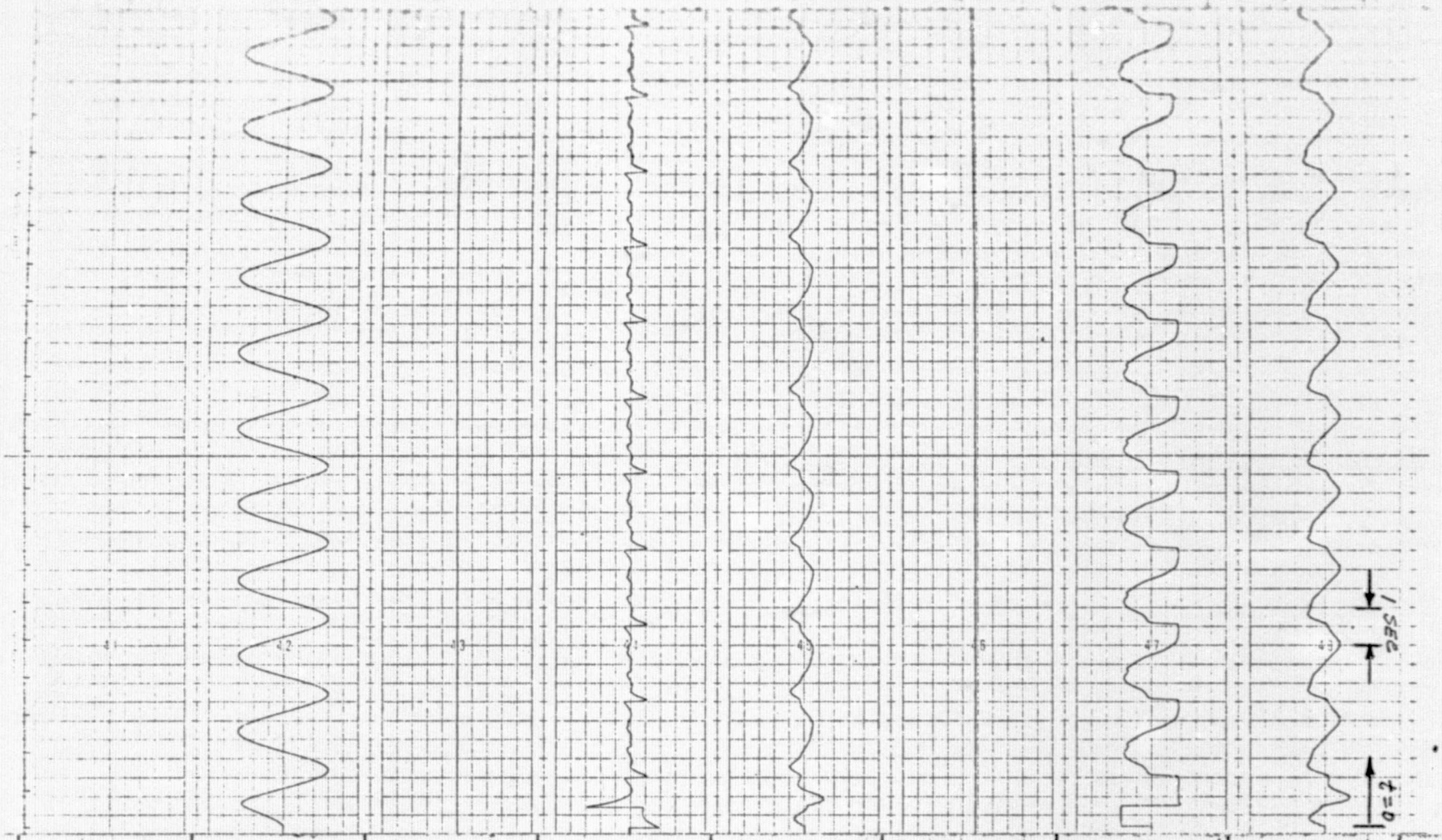

OFF	θ_W 0.5 rad/ℓ	OFF	I_W 0.24 amp/ℓ	I_A 0.056 amp/ℓ	OFF	V_W 2 VOLT/ℓ	V_A 2 VOLT/ℓ

C2 (b)

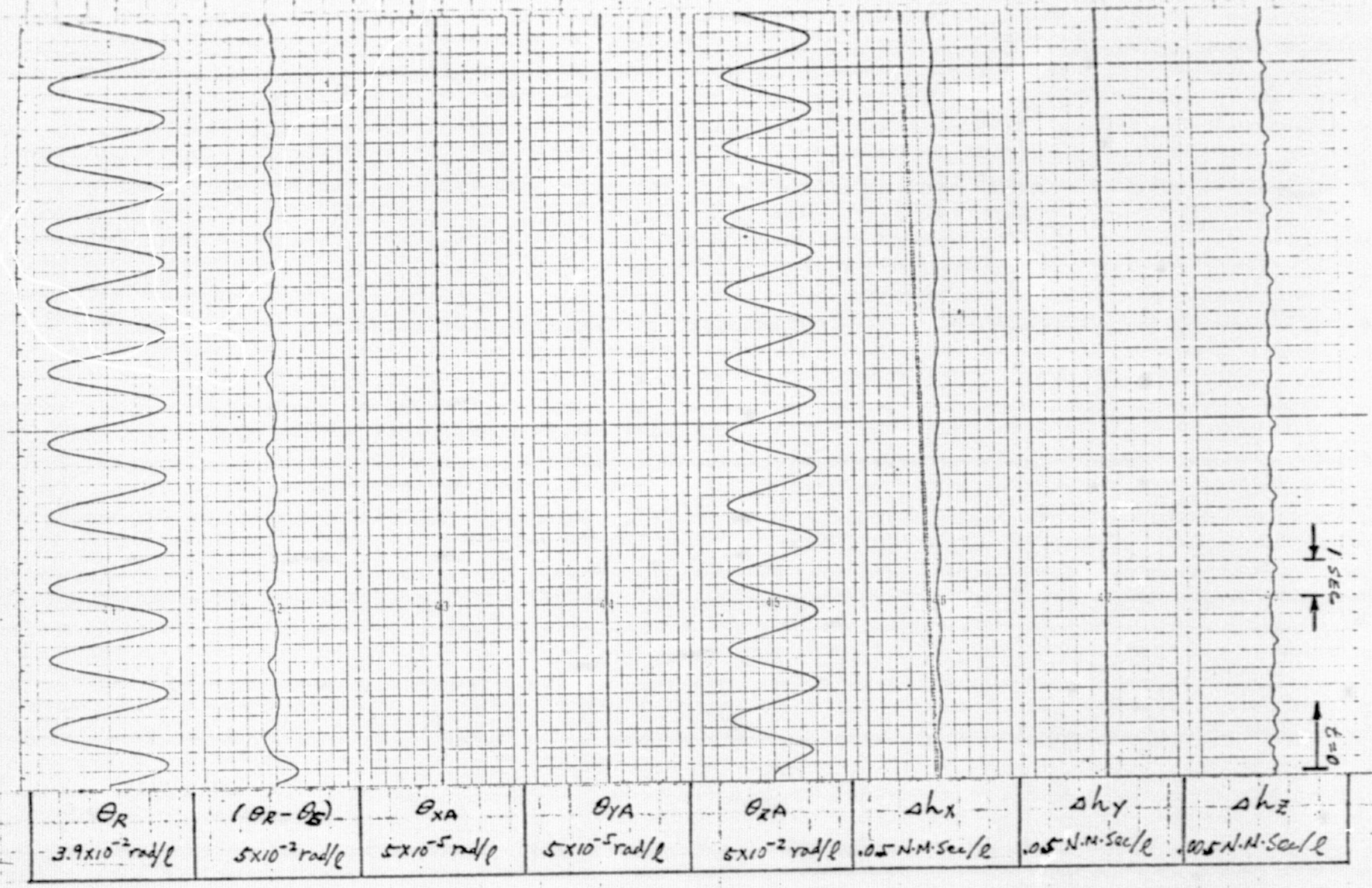

θ_R	$(\theta_R - \theta_S)$	θ_{XA}	θ_{YA}	θ_{ZA}	Δh_X	Δh_Y	Δh_Z
3.9×10^{-2} rad/l	5×10^{-2} rad/l	5×10^{-5} rad/l	5×10^{-5} rad/l	5×10^{-2} rad/l	.05 N·M·Sec/l	.05 N·M·Sec/l	.05 N·M·Sec/l

C3 (a)

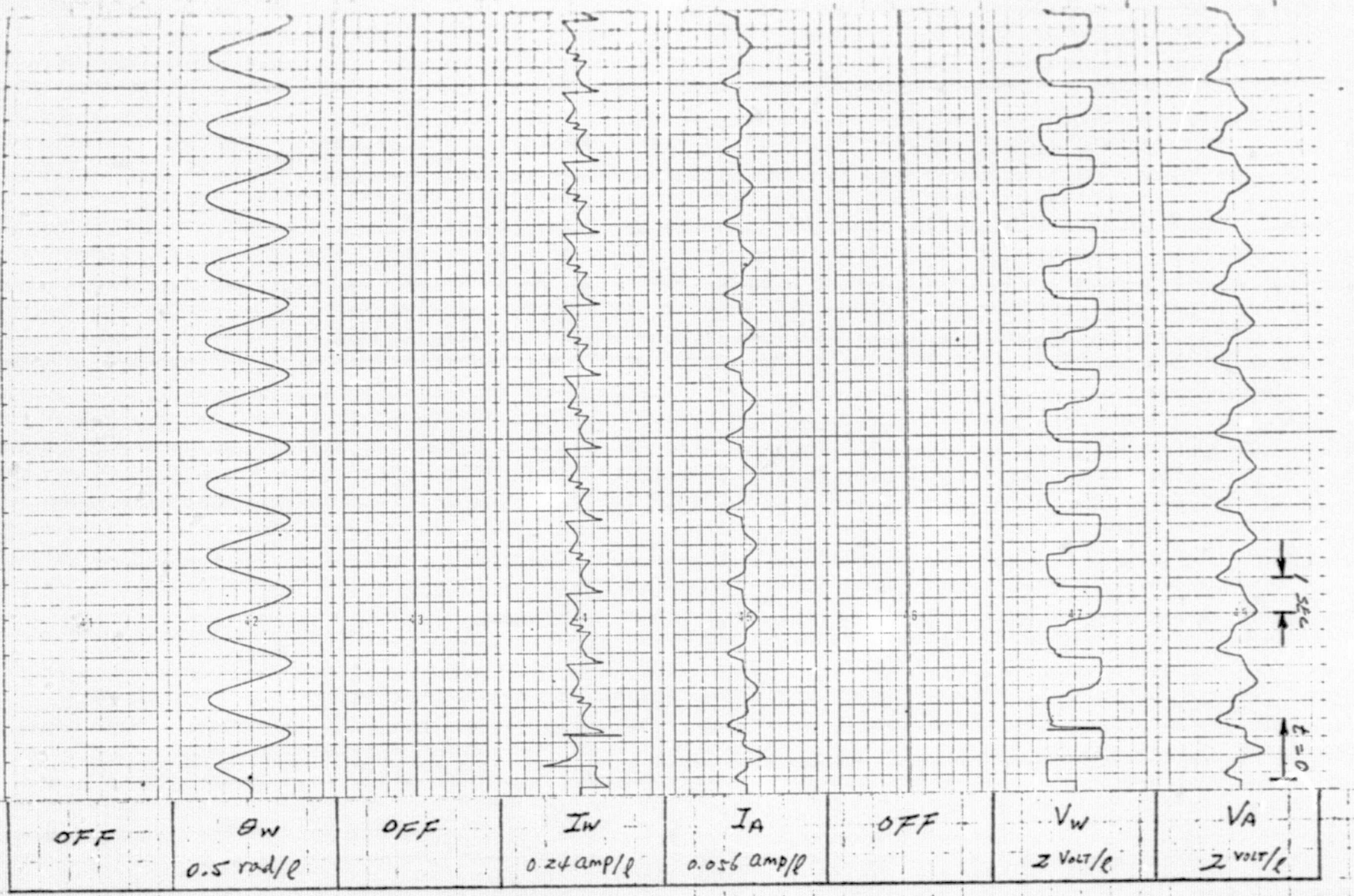

OFF	θ_W 0.5 rad/ℓ	OFF	I_W 0.24 amp/ℓ	I_A 0.056 amp/ℓ	OFF	V_W 2 VOLT/ℓ	V_A 2 VOLT/ℓ

C3 (b)

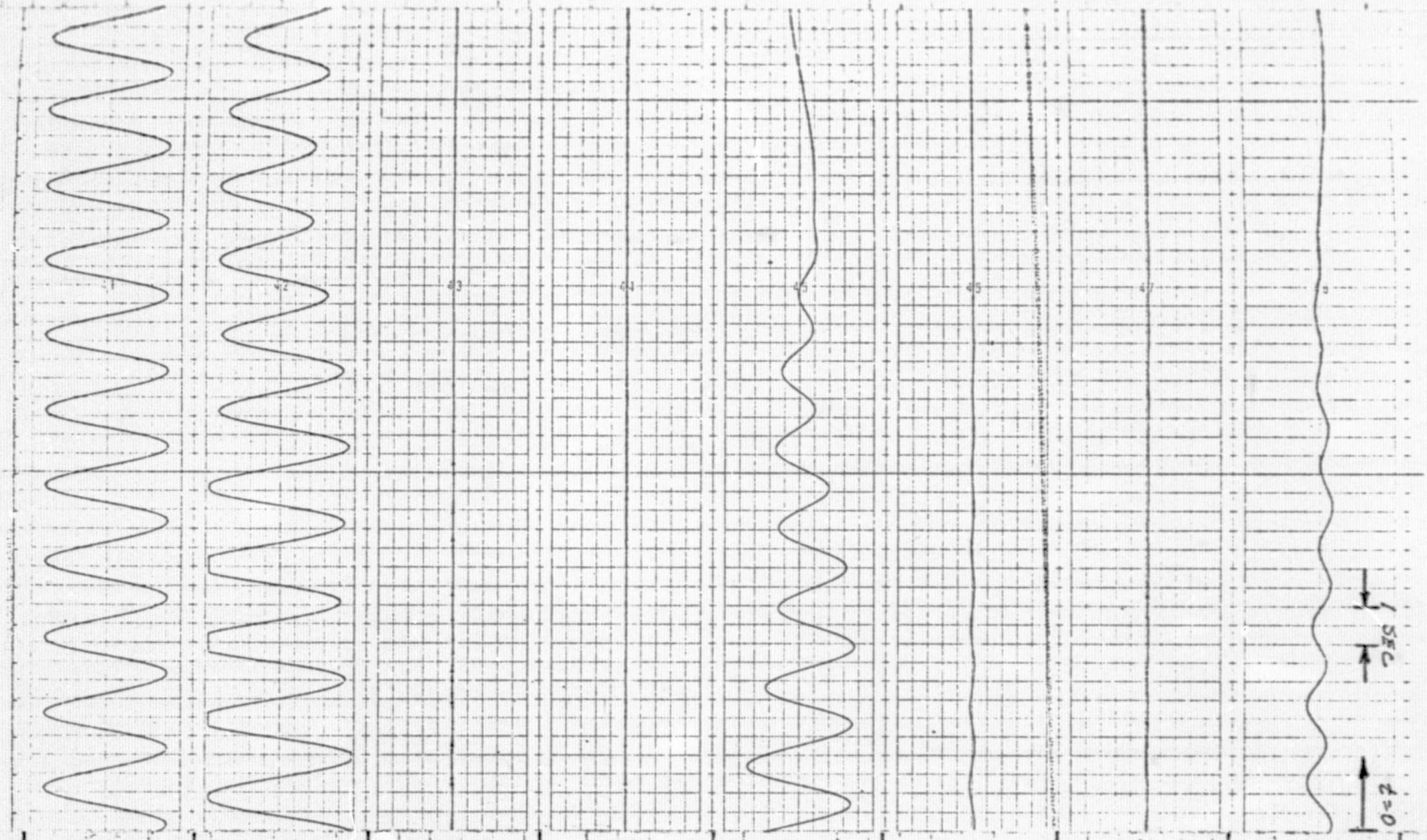
θ_R
3.9×10^{-2} rad/l
$(\theta_R-\theta_B)$
5×10^{-2} rad/l
θ_{xA}
5×10^{-5} rad/l
θ_{yA}
5×10^{-5} rad/l
θ_{zA}
5×10^{-2} rad/l
Δh_x
.05 N·M·Sec/l
Δh_y
.05 N·M·Sec/l
Δh_z
.05 N·M·Sec/l
1 SEC
0 = 2

C4 (a)

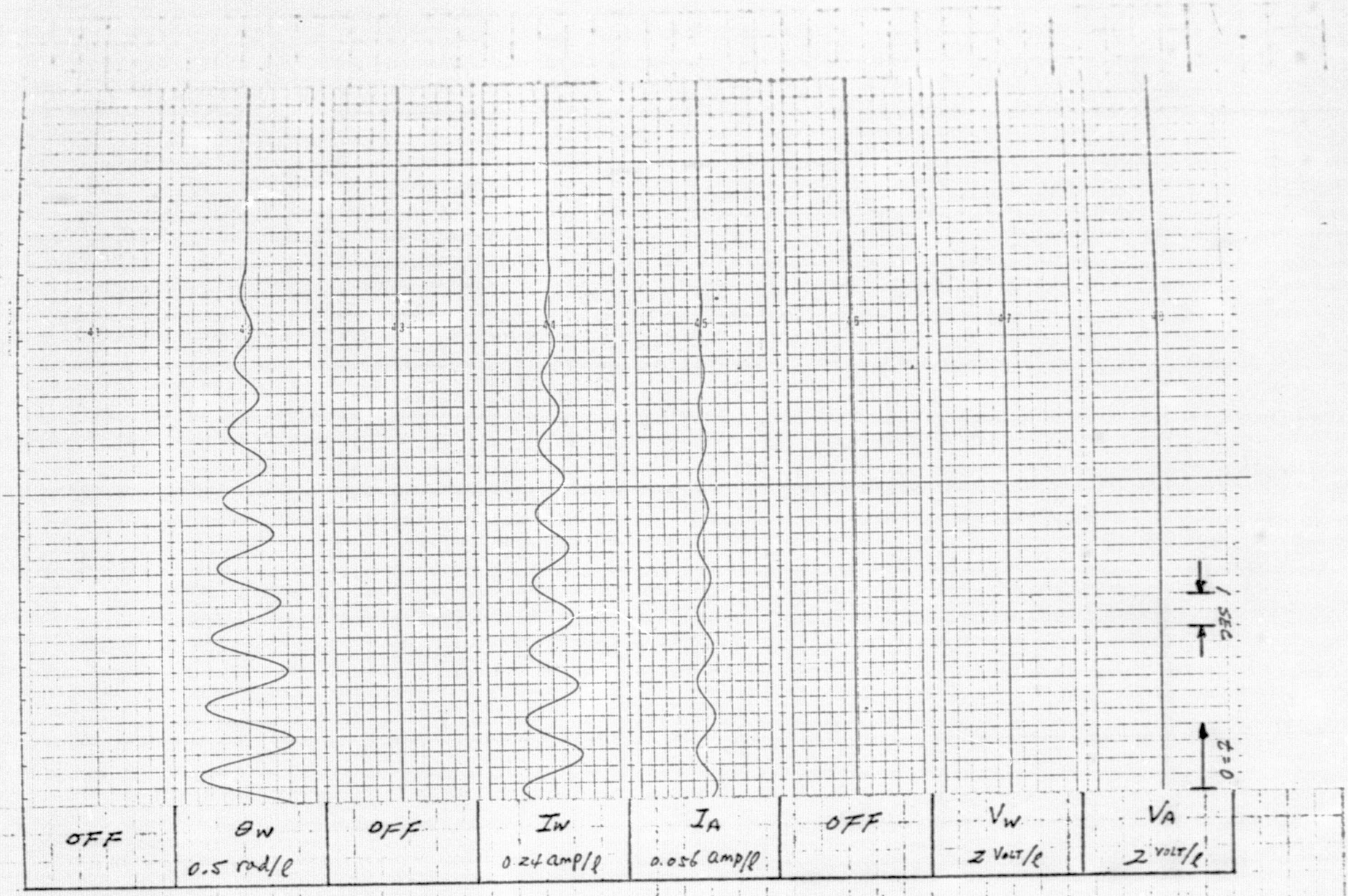
OFF
θW
0.5 rad/ℓ
OFF
IW
0.24 amp/ℓ
IA
0.056 amp/ℓ
OFF
VW
2 VOLT/ℓ
VA
2 VOLT/ℓ
1 SEC
t=0

C4 (b)

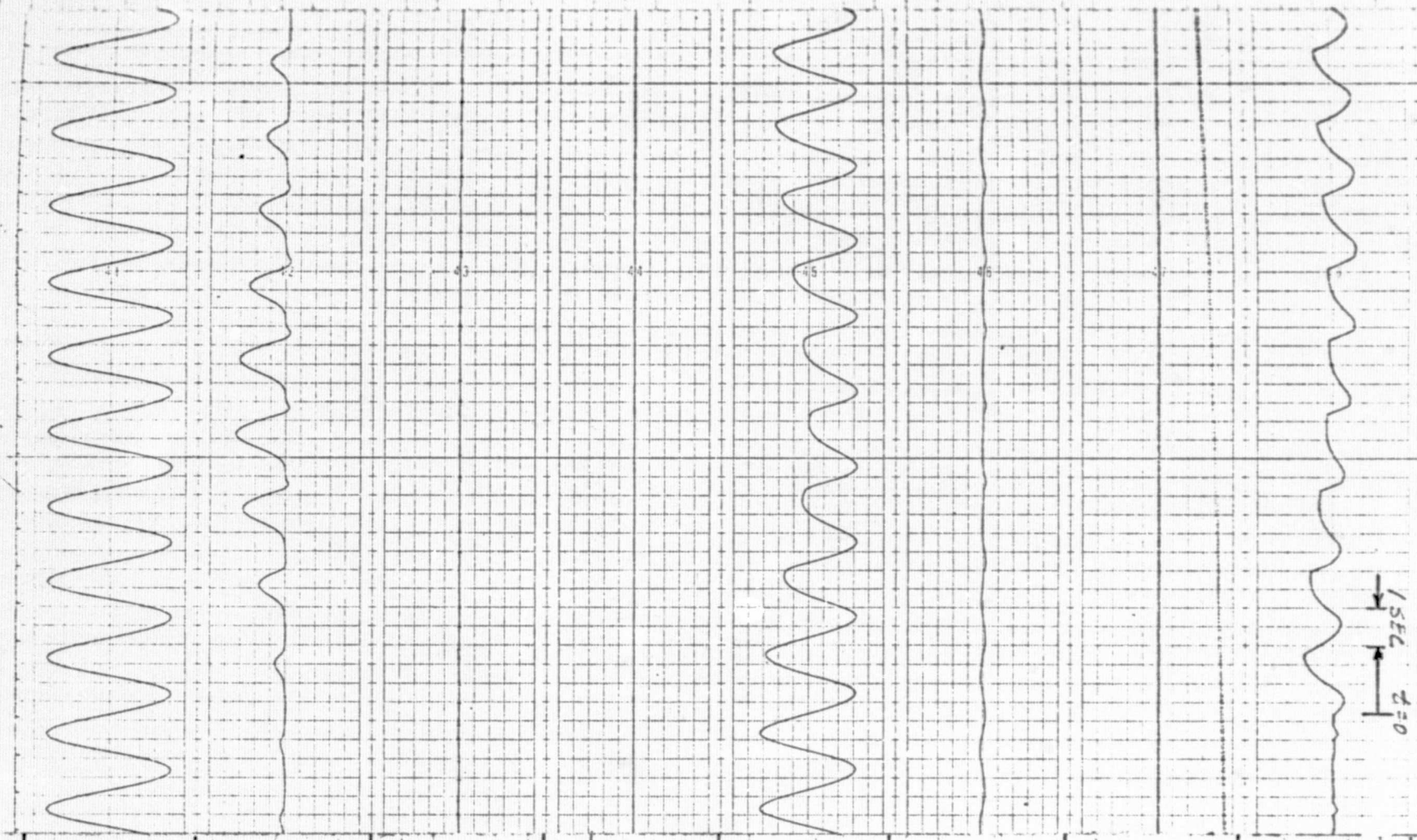

θ_R	$(\theta_Z - \theta_E)$	θ_{XA}	θ_{YA}	θ_{ZA}	Δh_X	Δh_Y	Δh_Z
3.9×10^{-2} rad/ℓ	5×10^{-2} rad/ℓ	5×10^{-5} rad/ℓ	5×10^{-5} rad/ℓ	5×10^{-2} rad/ℓ	.05 N·M·Sec/ℓ	.05 N·M·Sec/ℓ	.005 N·M·Sec/ℓ

C5 (a)

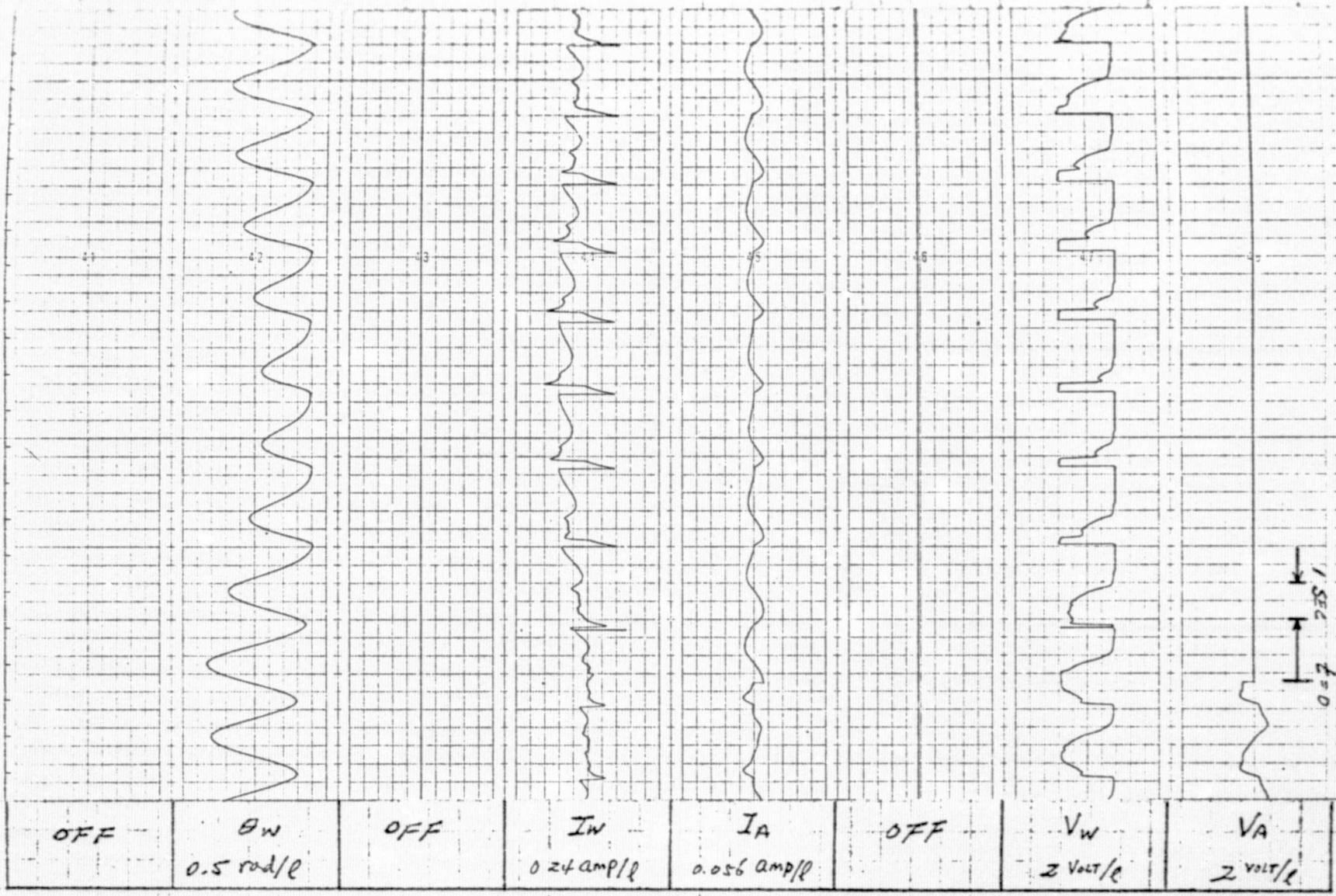
OFF
θ_W
0.5 rad/ℓ
OFF
I_W
0.24 amp/ℓ
I_A
0.056 amp/ℓ
OFF
V_W
2 VOLT/ℓ
V_A
2 VOLT/ℓ
1 SEC
t=0

C5 (b)

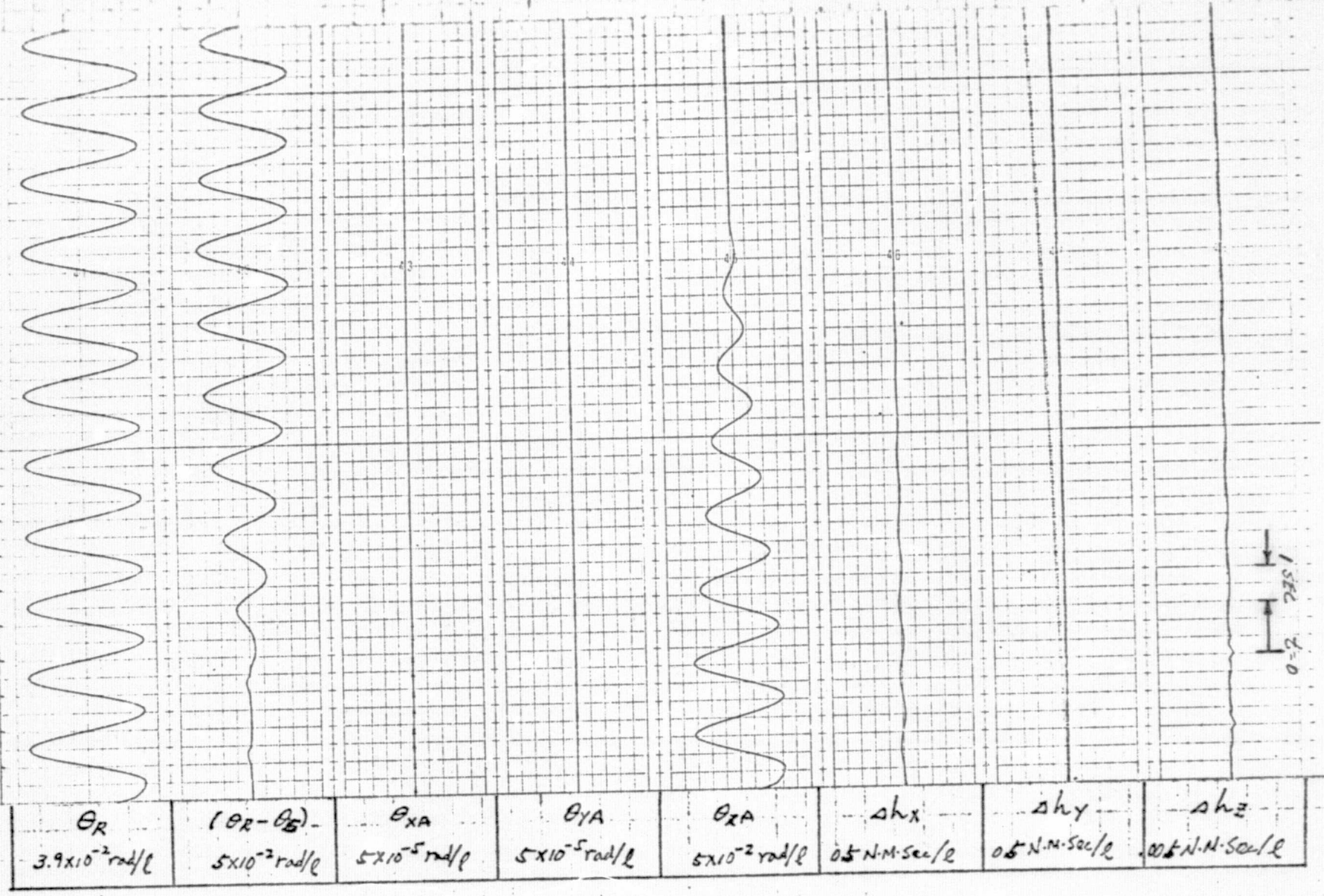
θ_R
3.9×10^{-2} rad/ℓ
$(\theta_R-\theta_B)$
5×10^{-2} rad/ℓ
θ_{XA}
5×10^{-5} rad/ℓ
θ_{YA}
5×10^{-5} rad/ℓ
θ_{ZA}
5×10^{-2} rad/ℓ
Δh_X
.05 N·M·Sec/ℓ
Δh_Y
.05 N·M·Sec/ℓ
Δh_Z
.005 N·M·Sec/ℓ
1 SEC
t=0

C6 (a)

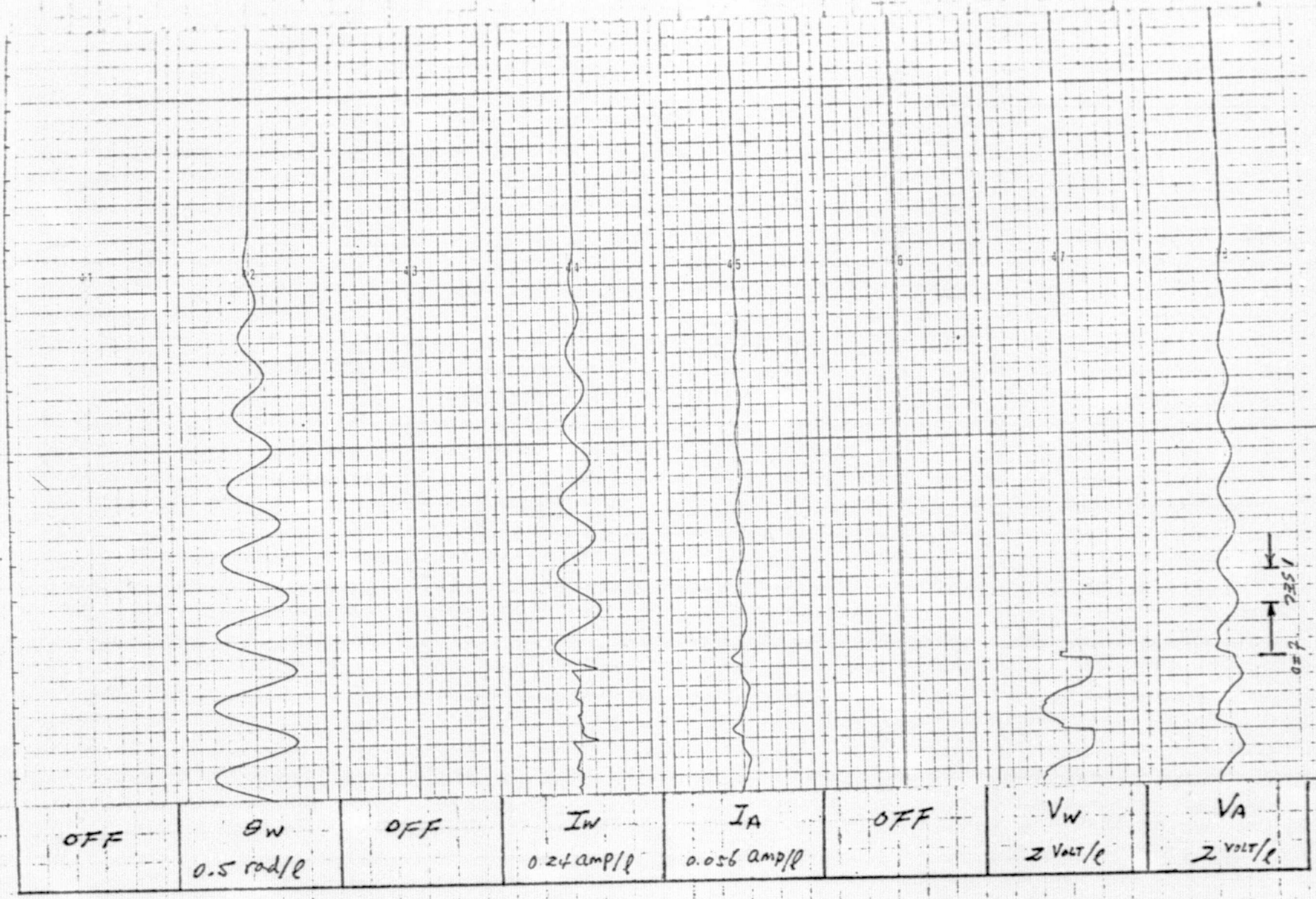
OFF
θw
0.5 rad/ℓ
OFF
Iw
0.24 amp/ℓ
IA
0.056 amp/ℓ
OFF
Vw
2 VOLT/ℓ
VA
2 VOLT/ℓ
0.235 I

C6 (b)

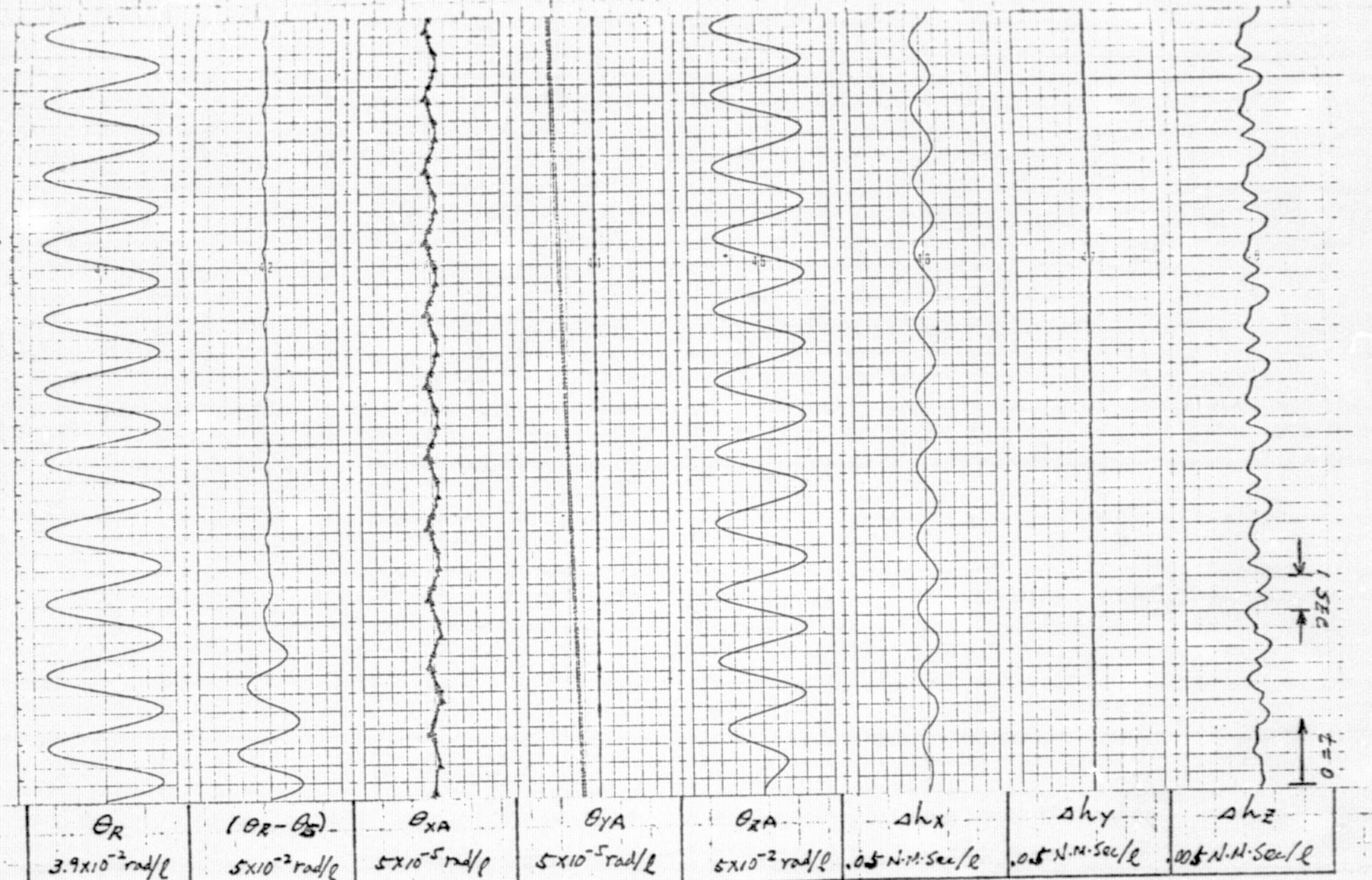

θ_R	$(\theta_R - \theta_{ZA})$	θ_{XA}	θ_{YA}	θ_{ZA}	Δh_X	Δh_Y	Δh_Z
3.9×10^{-2} rad/ℓ	5×10^{-2} rad/ℓ	5×10^{-5} rad/ℓ	5×10^{-5} rad/ℓ	5×10^{-2} rad/ℓ	.05 N·M·Sec/ℓ	.05 N·M·Sec/ℓ	.005 N·M·Sec/ℓ

C-16

C7 (a)

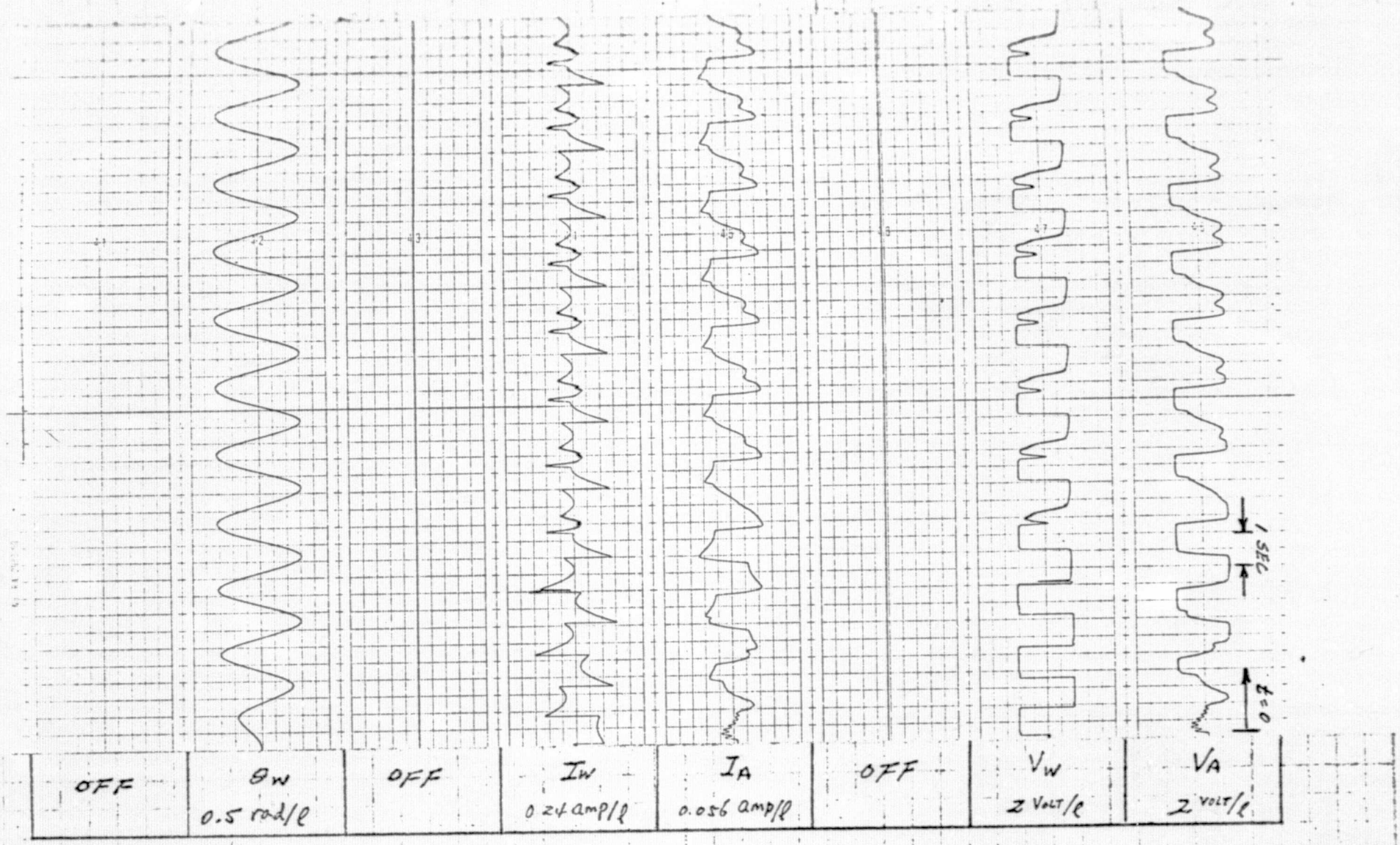
OFF
θ_W
0.5 rad/l
OFF
I_W
0.24 amp/l
I_A
0.056 amp/l
OFF
V_W
2 VOLT/l
V_A
2 VOLT/l
1 SEC
t=0

C7 (b)

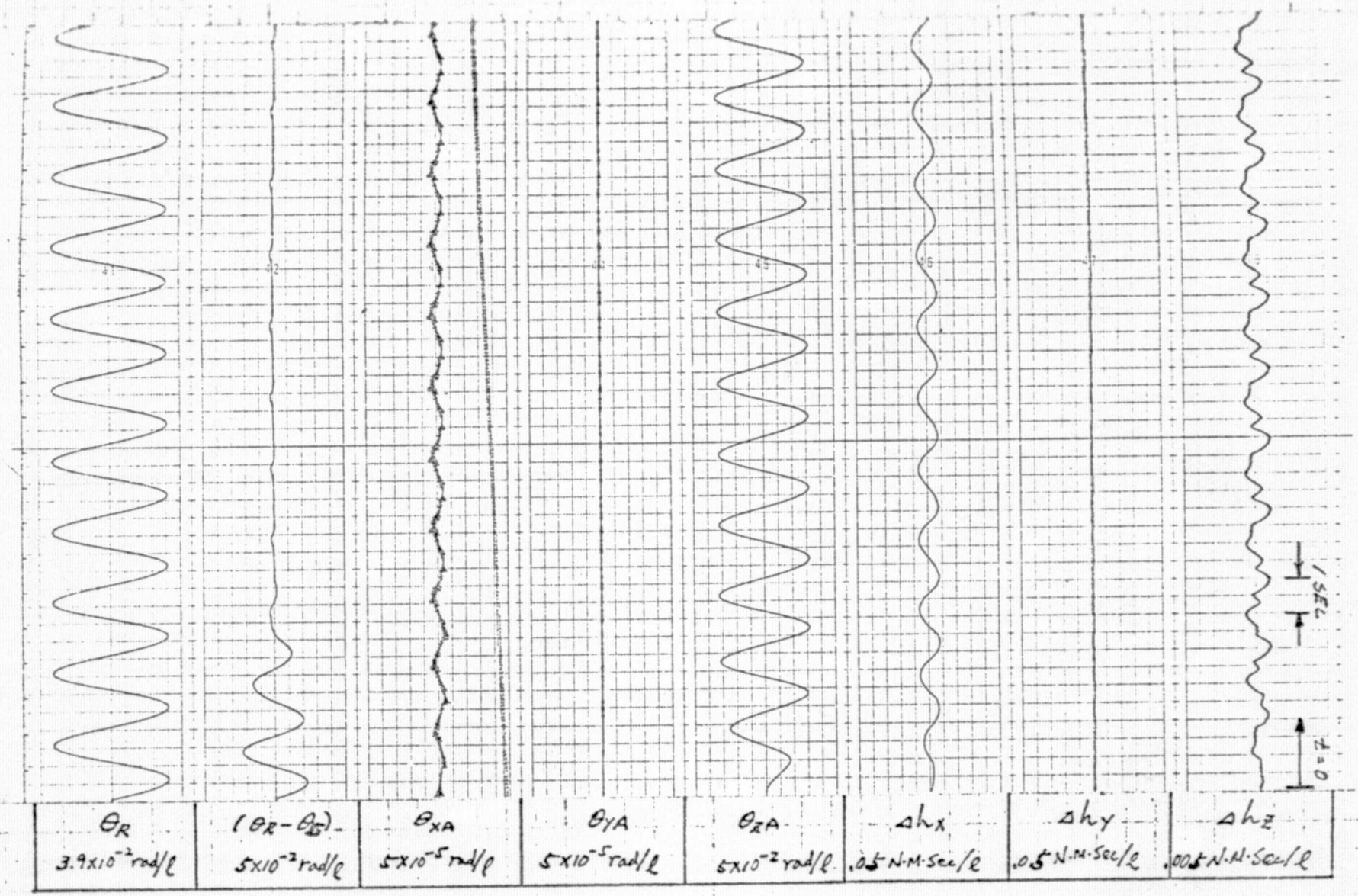
1 SEC
t = 0
θ_R 3.9x10⁻² rad/ℓ
$(\theta_R - \theta_{RS})$ 5x10⁻² rad/ℓ
θ_{XA} 5x10⁻⁵ rad/ℓ
θ_{YA} 5x10⁻⁵ rad/ℓ
θ_{ZA} 5x10⁻² rad/ℓ
Δh_x .05 N·M·Sec/ℓ
Δh_y .05 N·M·Sec/ℓ
Δh_z .005 N·M·Sec/ℓ

C8 (a)

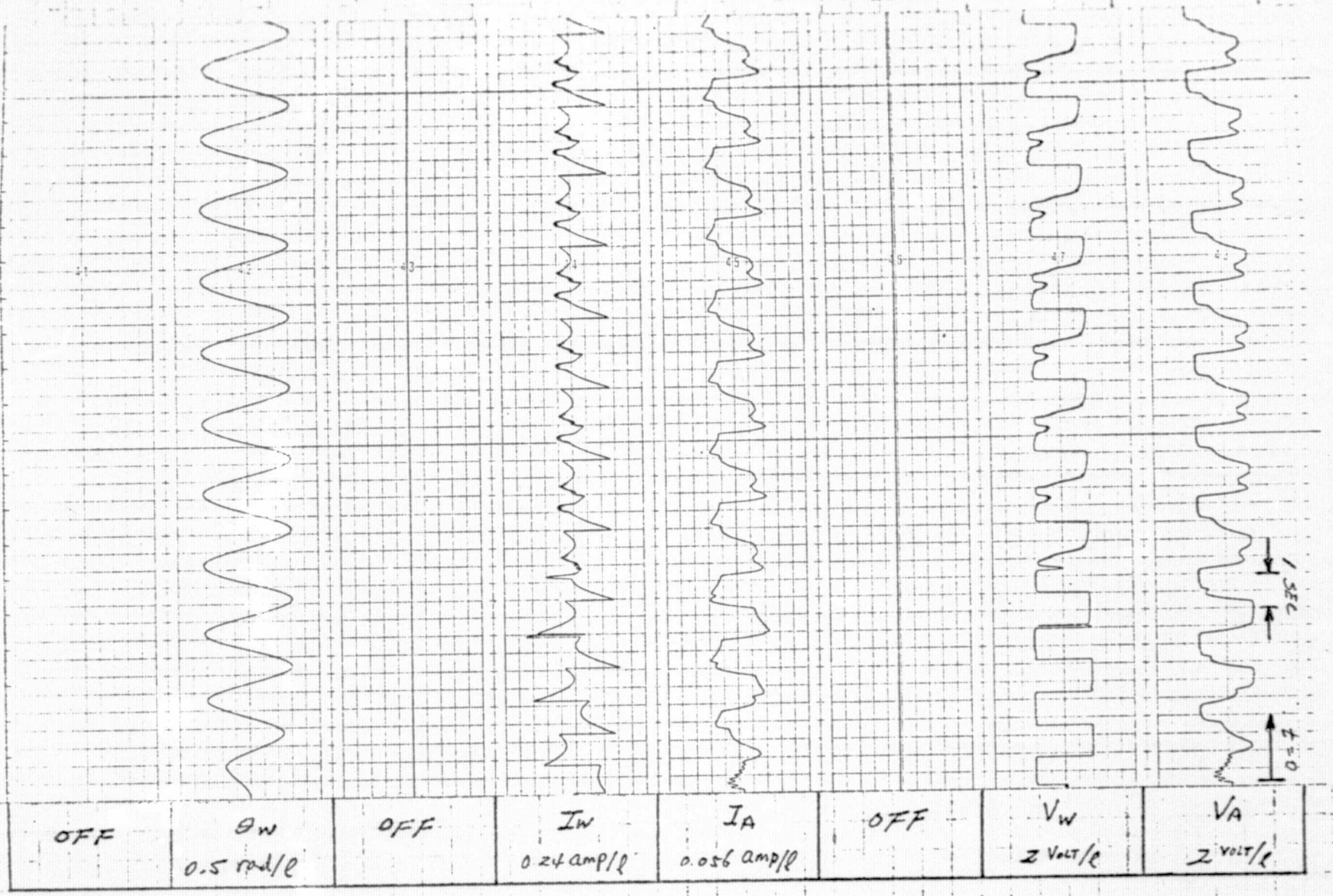
OFF
θ_W
0.5 rad/ℓ
OFF
I_W
0.24 amp/ℓ
I_A
0.056 amp/ℓ
OFF
V_W
2 VOLT/ℓ
V_A
2 VOLT/ℓ
1 SEC
t=0

C8 (b)

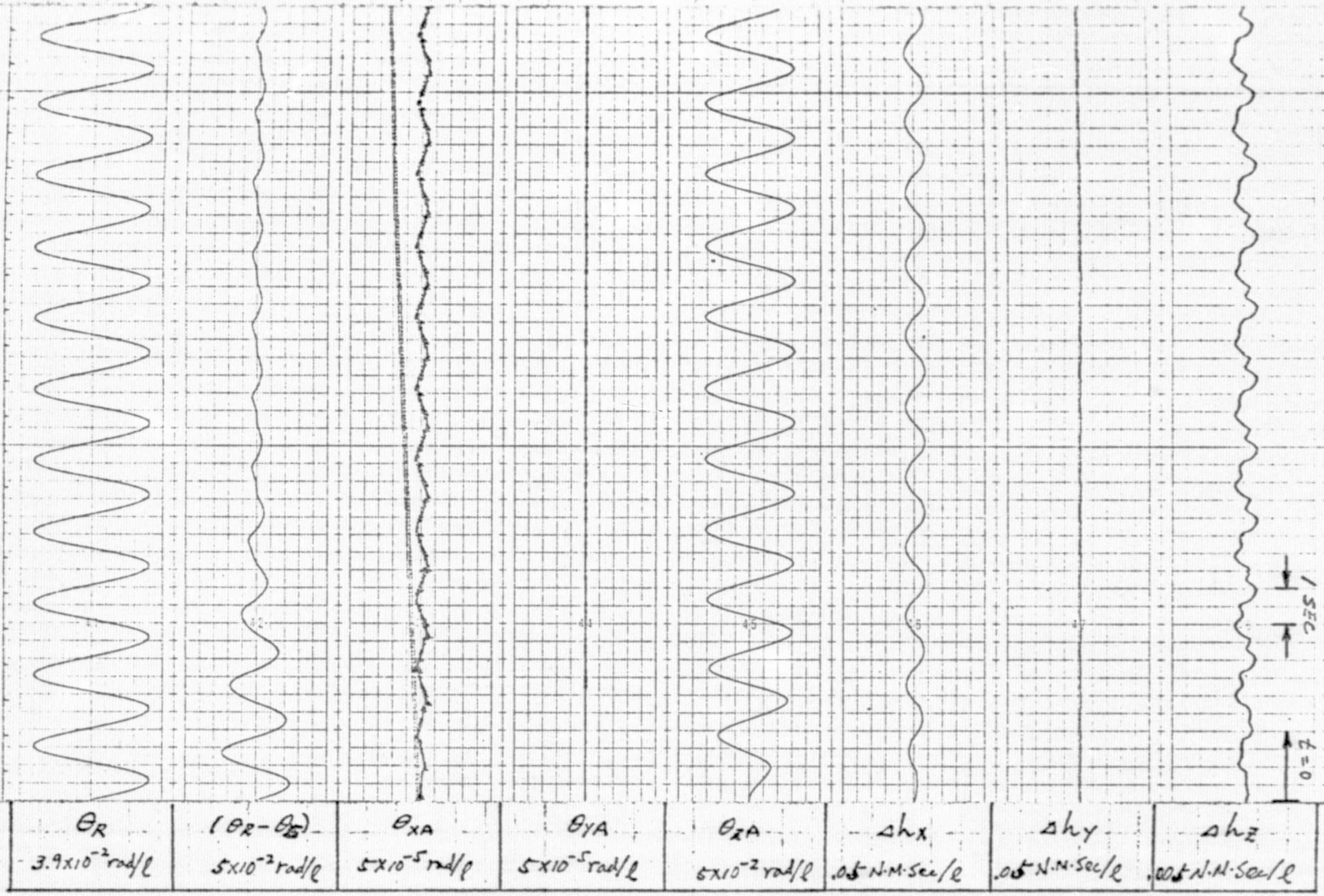
1 SEC
t=0
θ_R
3.9x10^{-2} rad/ℓ
$(\theta_R - \theta_{\overline{R}})$
5x10^{-2} rad/ℓ
θ_{XA}
5x10^{-5} rad/ℓ
θ_{YA}
5x10^{-5} rad/ℓ
θ_{ZA}
5x10^{-2} rad/ℓ
Δh_X
.05 N·M·Sec/ℓ
Δh_Y
.05 N·M·Sec/ℓ
Δh_Z
.05 N·M·Sec/ℓ

C9 (a)

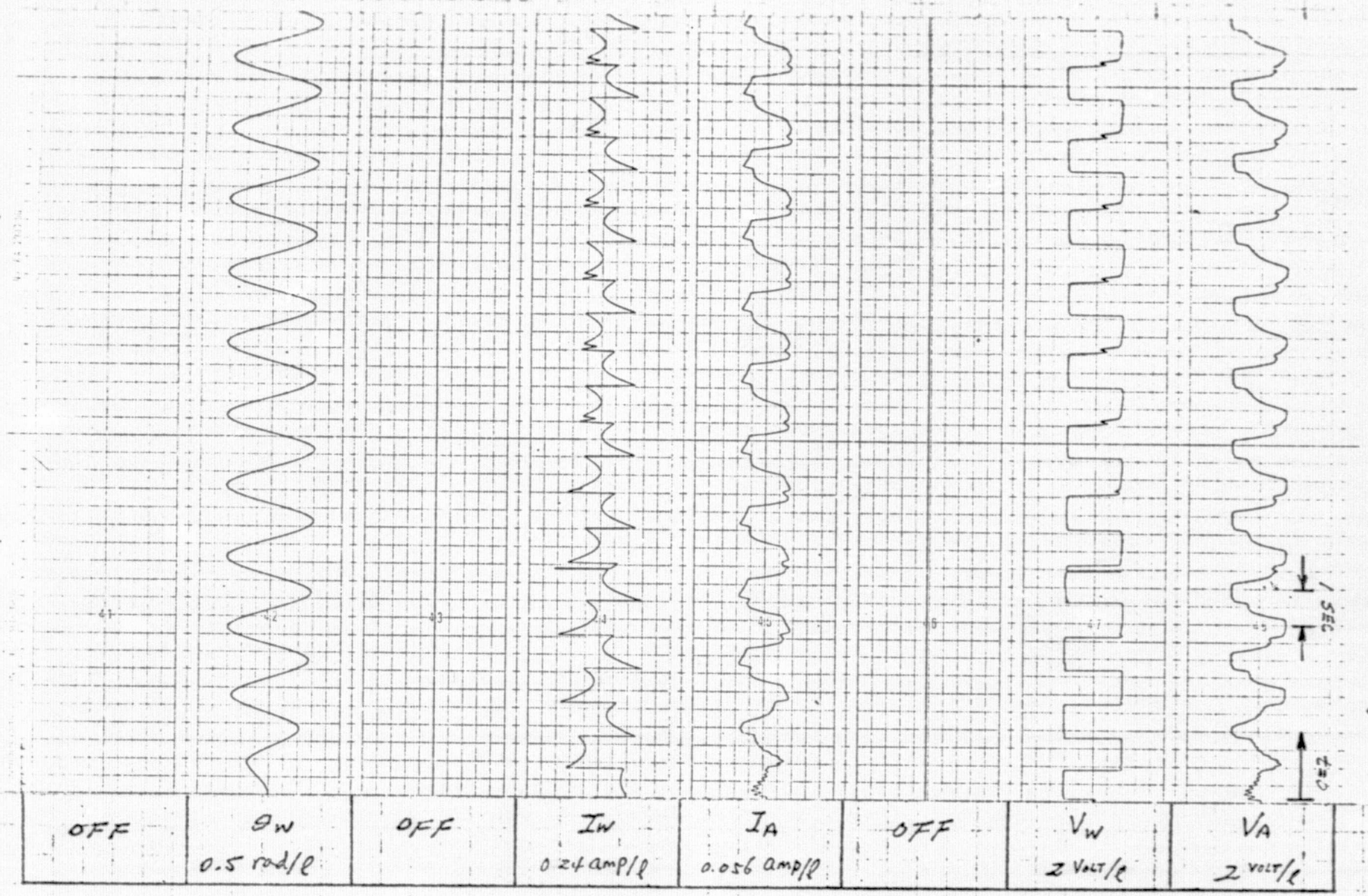
OFF
θ_W
0.5 rad/ℓ
OFF
I_W
0.24 amp/ℓ
I_A
0.056 amp/ℓ
OFF
V_W
2 VOLT/ℓ
V_A
2 VOLT/ℓ
1 SEC

C9 (b)

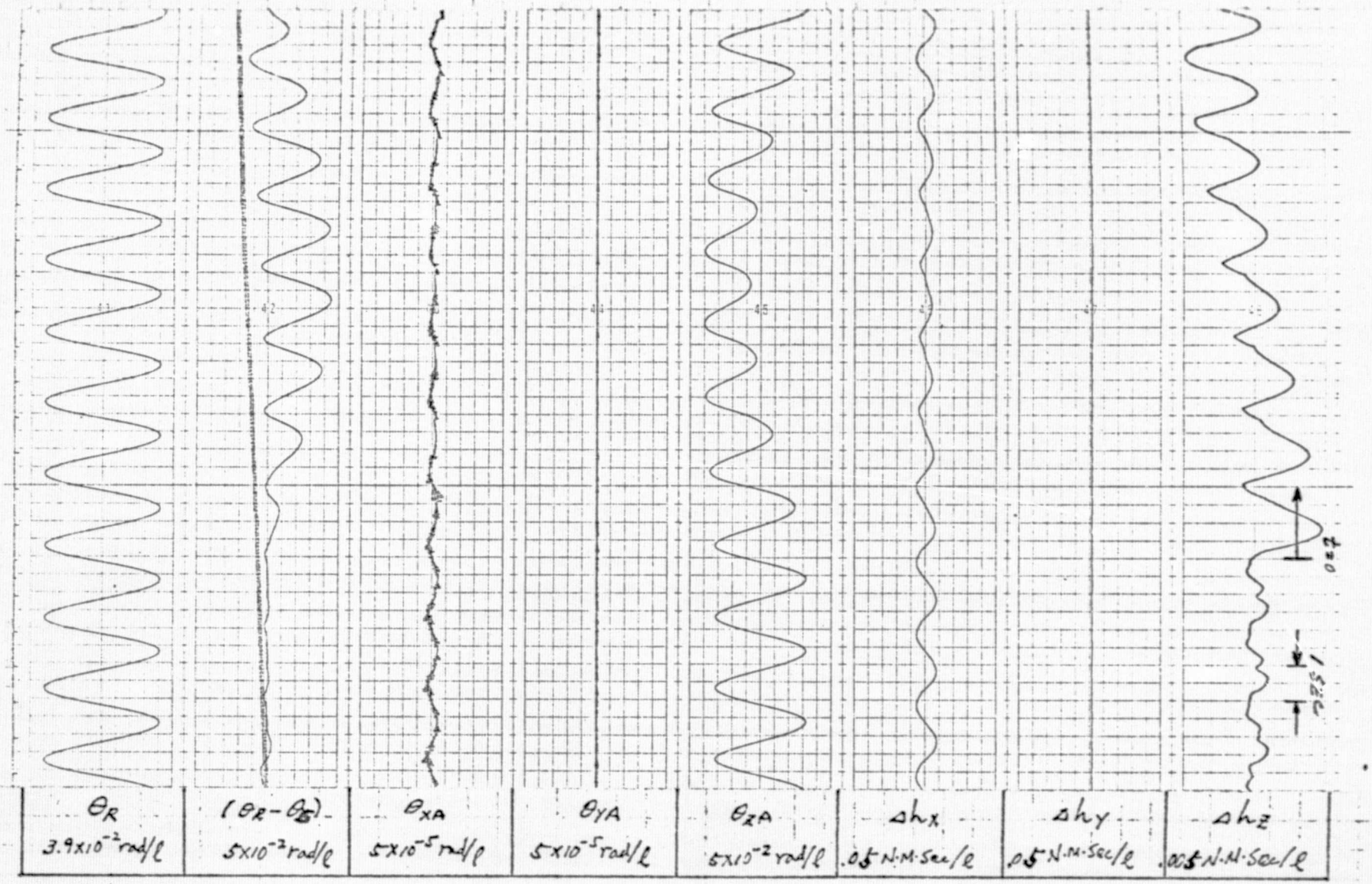
θ_R
3.9×10^{-2} rad/ℓ
$(\theta_R-\theta_S)$
5×10^{-2} rad/ℓ
θ_{XA}
5×10^{-5} rad/ℓ
θ_{YA}
5×10^{-5} rad/ℓ
θ_{ZA}
5×10^{-2} rad/ℓ
Δh_X
.05 N·M·Sec/ℓ
Δh_Y
.05 N·M·Sec/ℓ
Δh_Z
.05 N·M·Sec/ℓ
±20
1 sec

C10 (a)

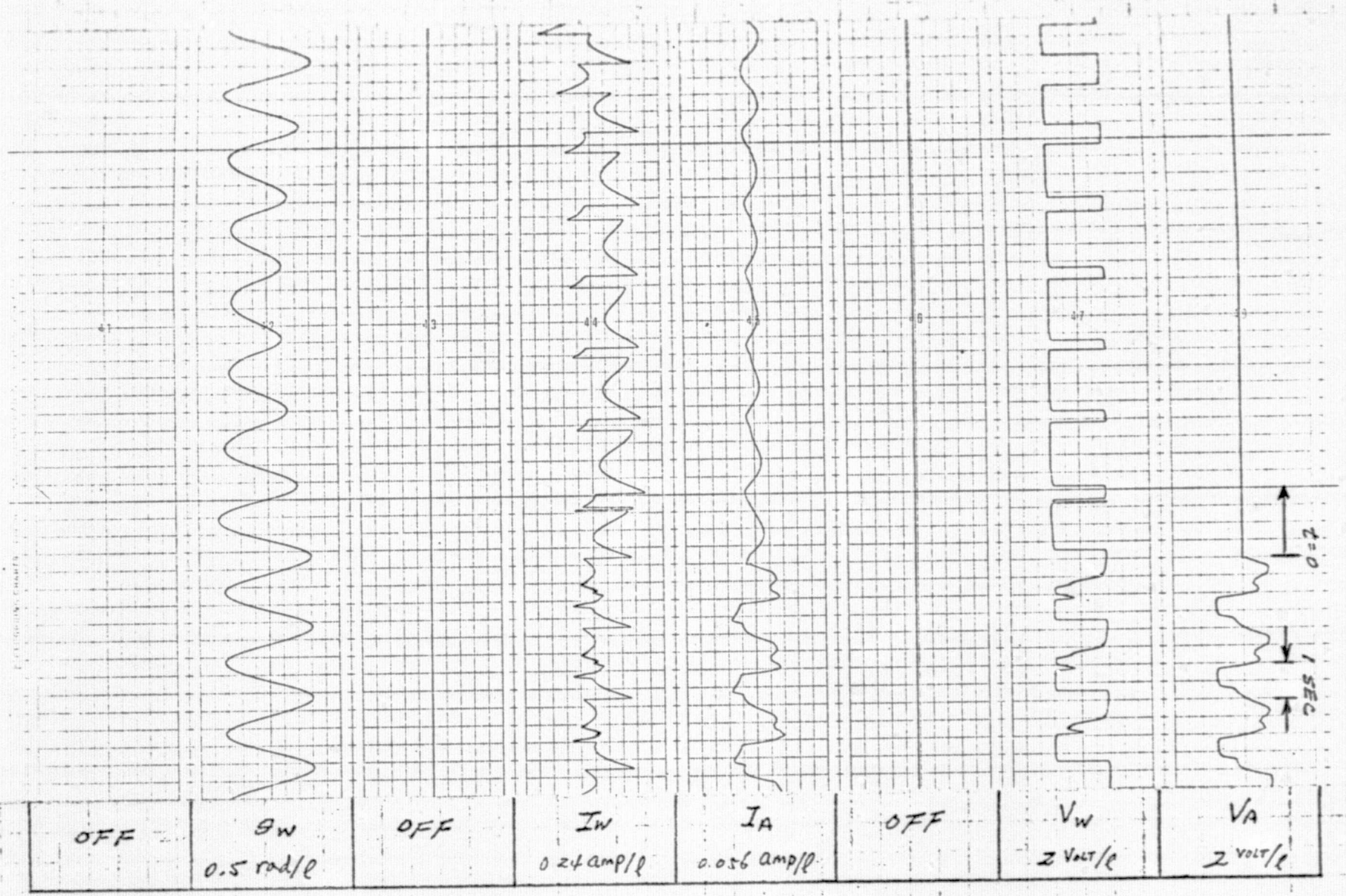
t=0
1 SEC
OFF
θ_W
0.5 rad/ℓ
OFF
I_W
0.24 amp/ℓ
I_A
0.056 amp/ℓ
OFF
V_W
2 VOLT/ℓ
V_A
2 VOLT/ℓ

C10 (b)

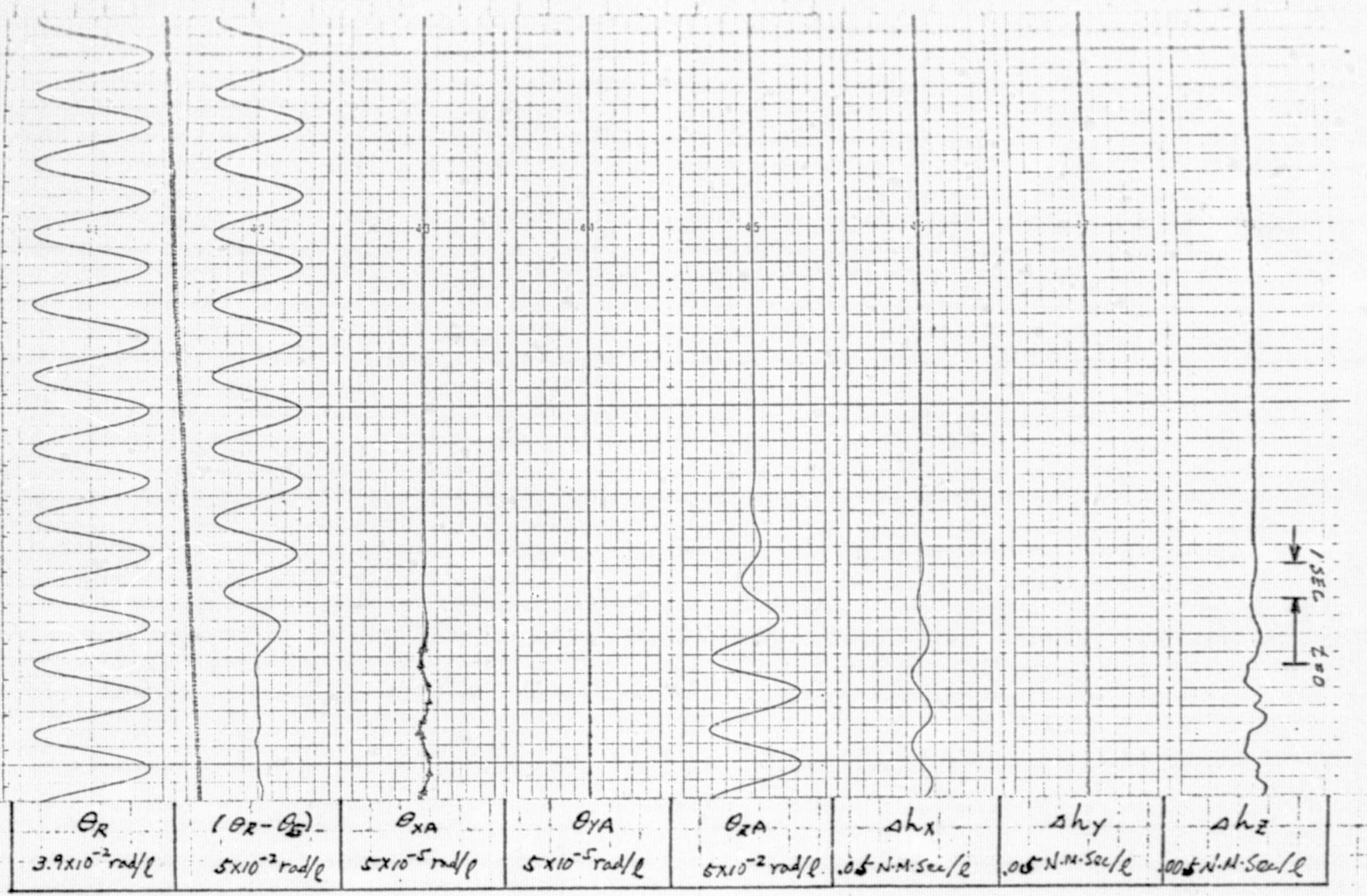

θ_R	$(\theta_R - \theta_G)$	θ_{XA}	θ_{YA}	θ_{ZA}	Δh_X	Δh_Y	Δh_Z
3.9×10^{-2} rad/ℓ	5×10^{-2} rad/ℓ	5×10^{-5} rad/ℓ	5×10^{-5} rad/ℓ	6×10^{-2} rad/ℓ	.05 N·M·Sec/ℓ	.05 N·M·Sec/ℓ	.005 N·M·Sec/ℓ

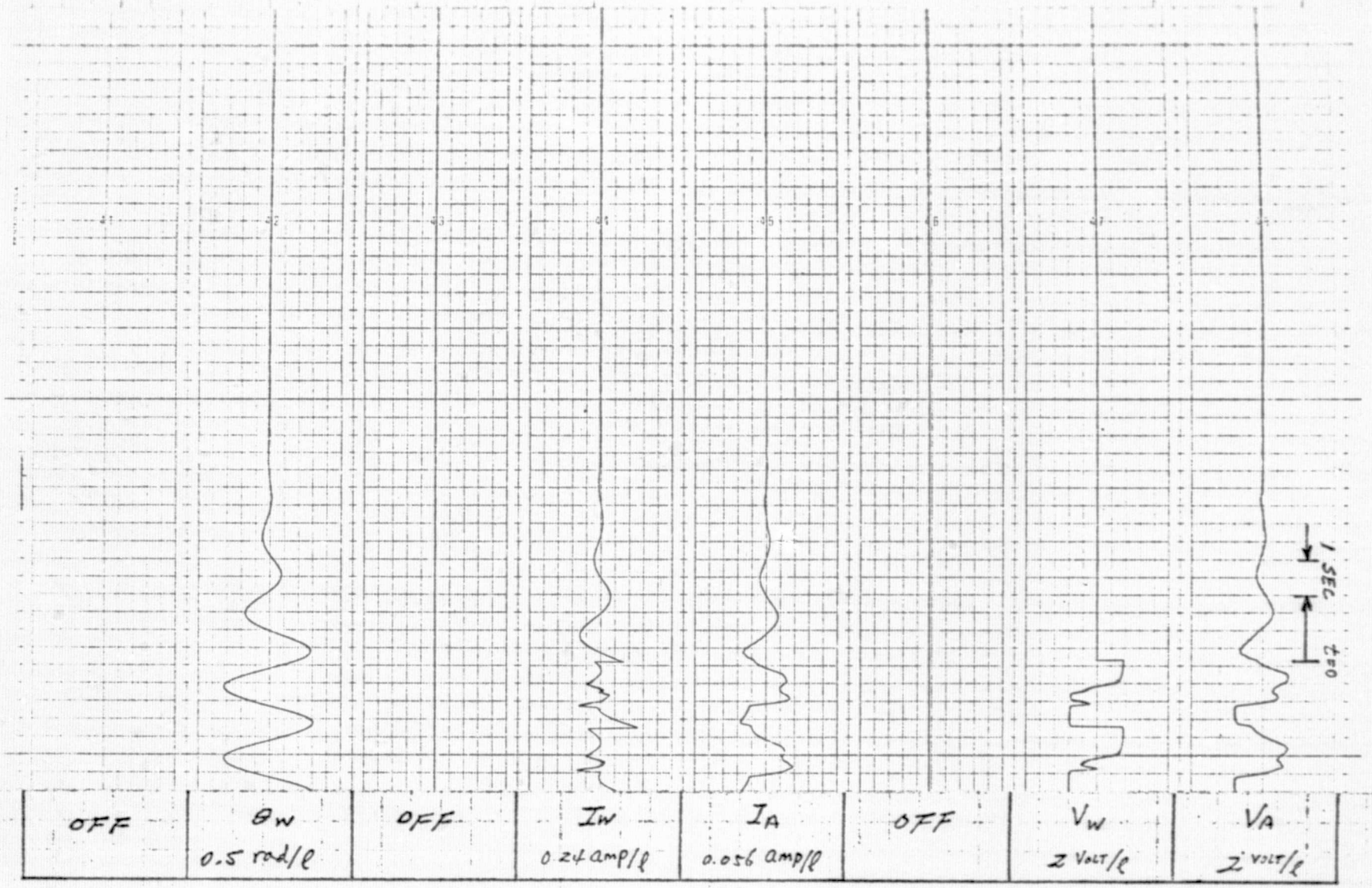
1 SEC
t=0
OFF
θ_W
0.5 rad/ℓ
OFF
I_W
0.24 amp/ℓ
I_A
0.056 amp/ℓ
OFF
V_W
2 VOLT/ℓ
V_A
2 VOLT/ℓ

C11 (b)

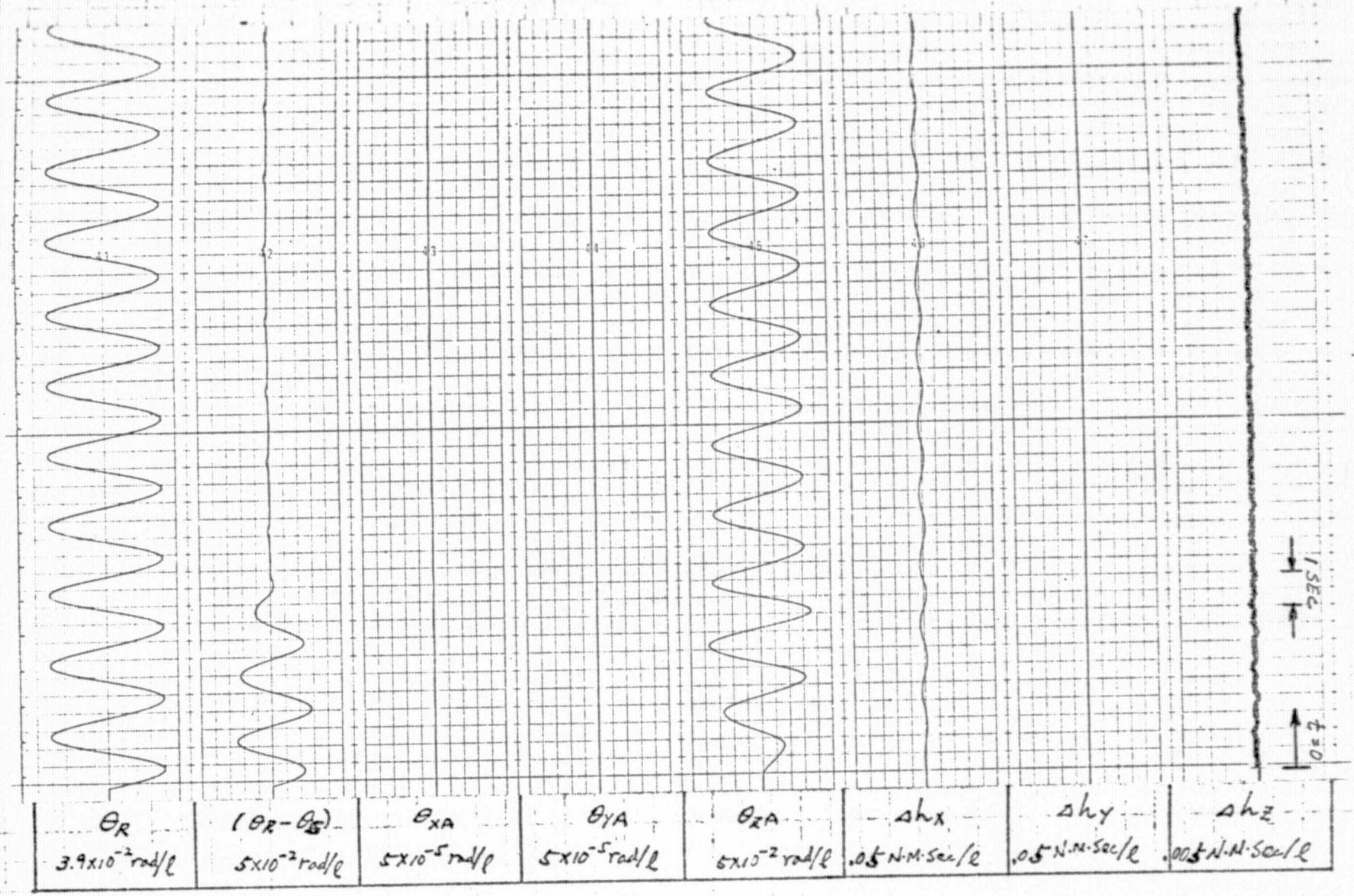
1 SEC.
t=0
θ_R
3.9×10^{-2} rad/l
$(\theta_R-\theta_S)$
5×10^{-2} rad/l
θ_{XA}
5×10^{-5} rad/l
θ_{YA}
5×10^{-5} rad/l
θ_{ZA}
5×10^{-2} rad/l
$-\Delta h_X$
.05 N·M·Sec/l
Δh_Y
.05 N·M·Sec/l
Δh_Z
.005 N·M·Sec/l

C12 (a)

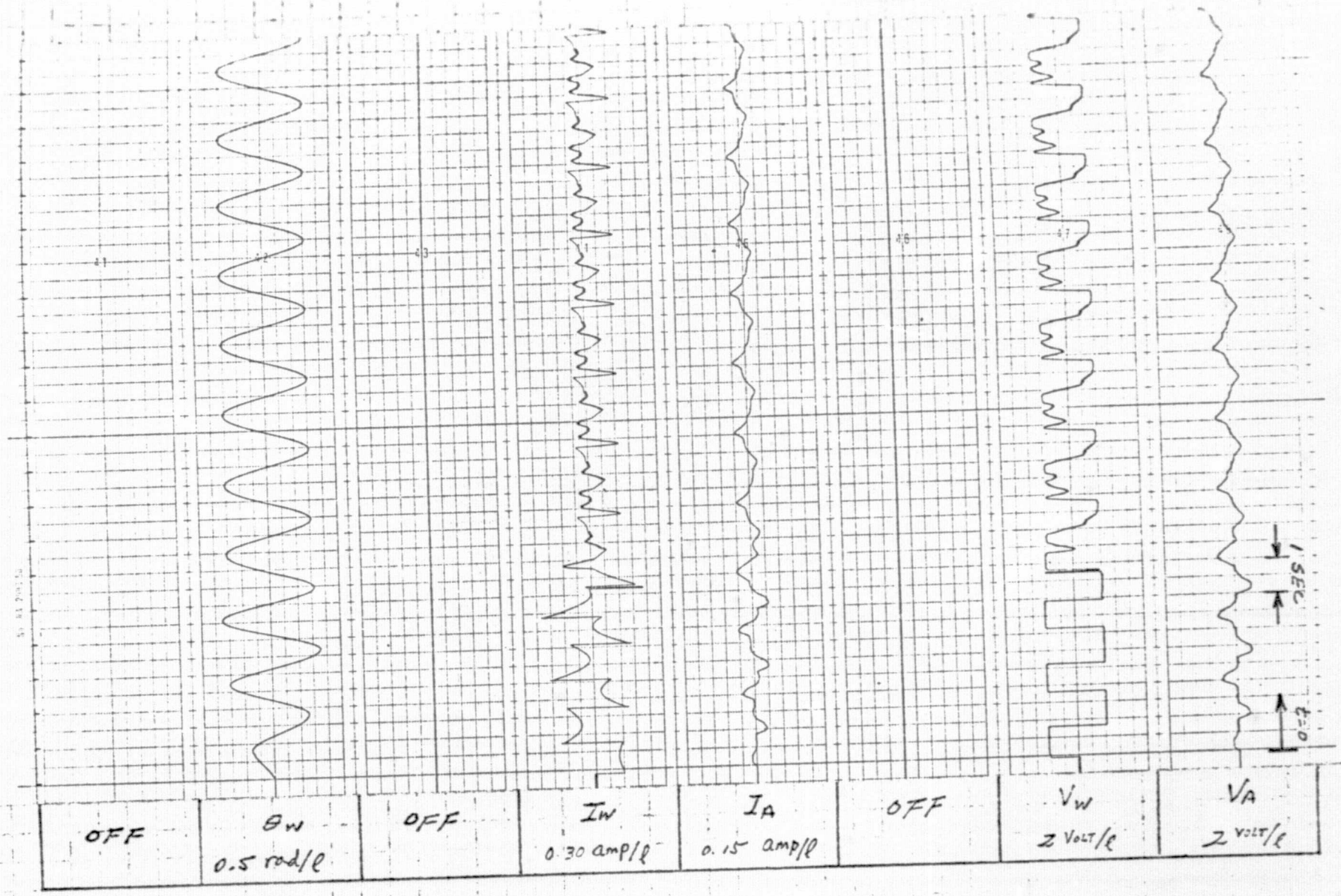
OFF
θ_W
0.5 rad/ℓ
OFF
I_W
0.30 amp/ℓ
I_A
0.15 amp/ℓ
OFF
V_W
2 VOLT/ℓ
V_A
2 VOLT/ℓ
1 SEC
t=0

C12 (b)

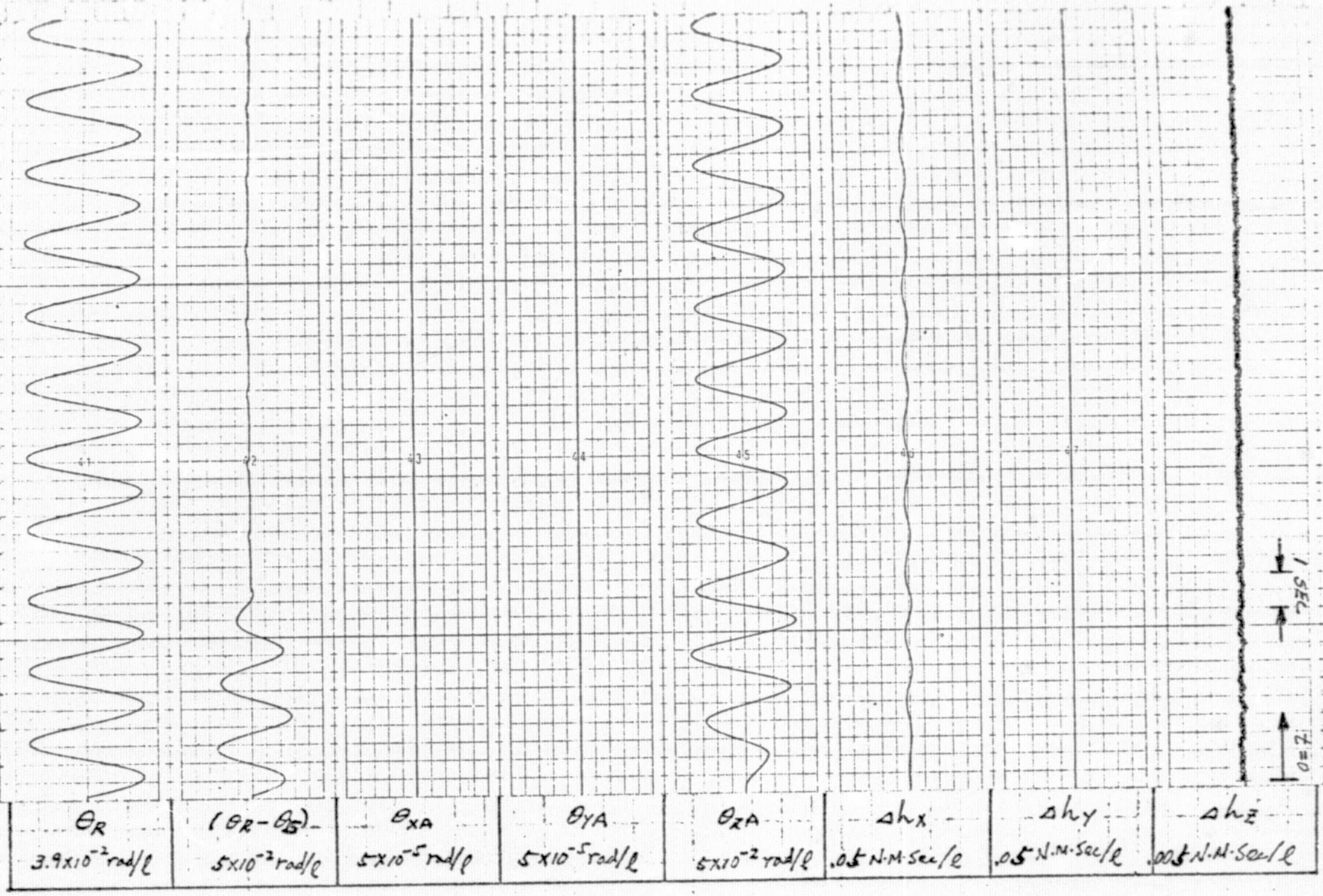
θR
3.9x10⁻² rad/l
(θR-θB)
5x10⁻² rad/l
θXA
5x10⁻⁵ rad/l
θYA
5x10⁻⁵ rad/l
θZA
5x10⁻² rad/l
ΔhX
.05 N.M.Sec/l
ΔhY
.05 N.M.Sec/l
ΔhZ
.005 N.M.Sec/l
1 SEC.
θ=Z

C13 (a)

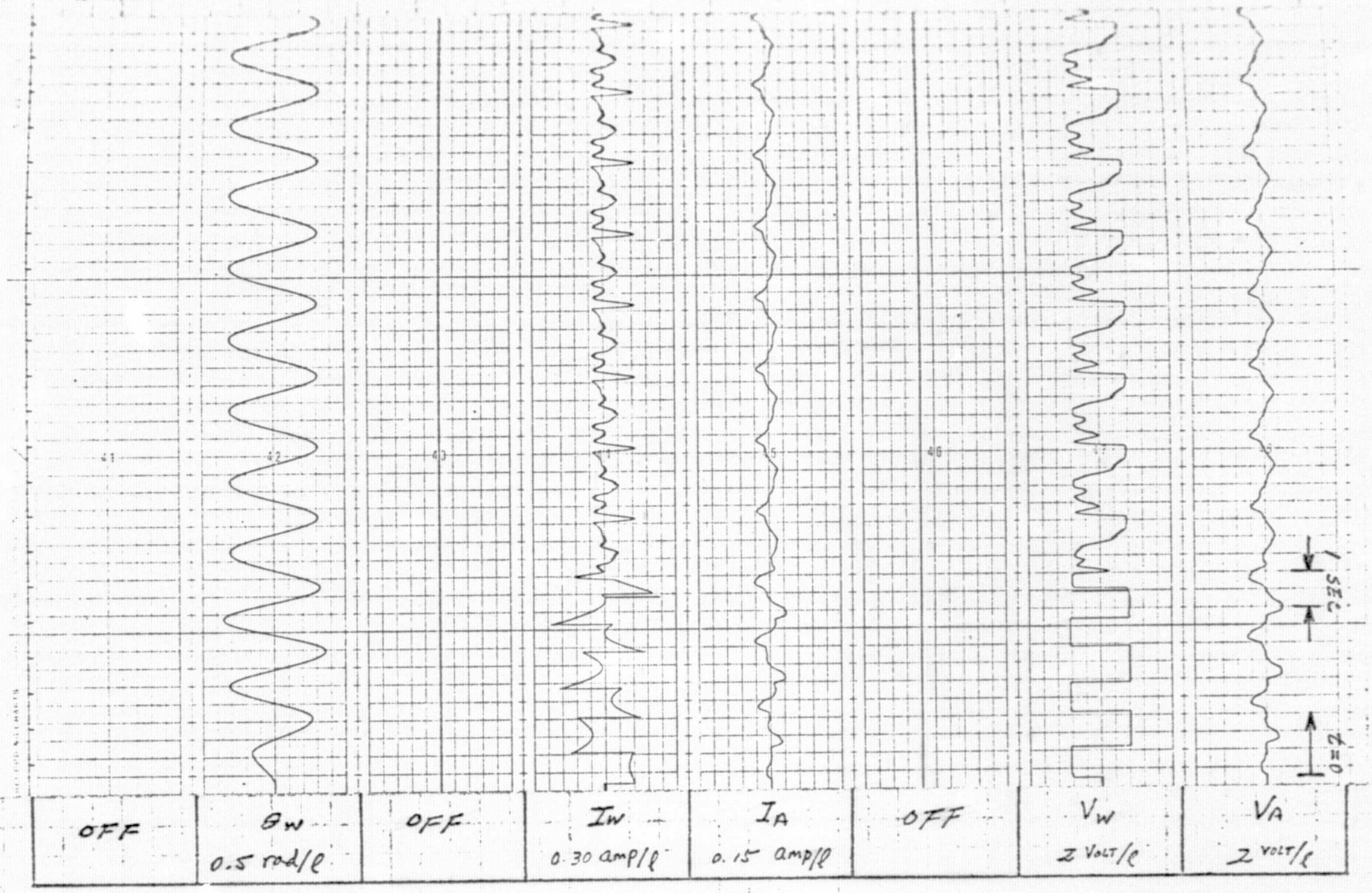
OFF
θw
0.5 rad/ℓ
OFF
Iw
0.30 amp/ℓ
IA
0.15 amp/ℓ
OFF
VW
2 VOLT/ℓ
VA
2 VOLT/ℓ
1 SEC
I=0

C13 (b)

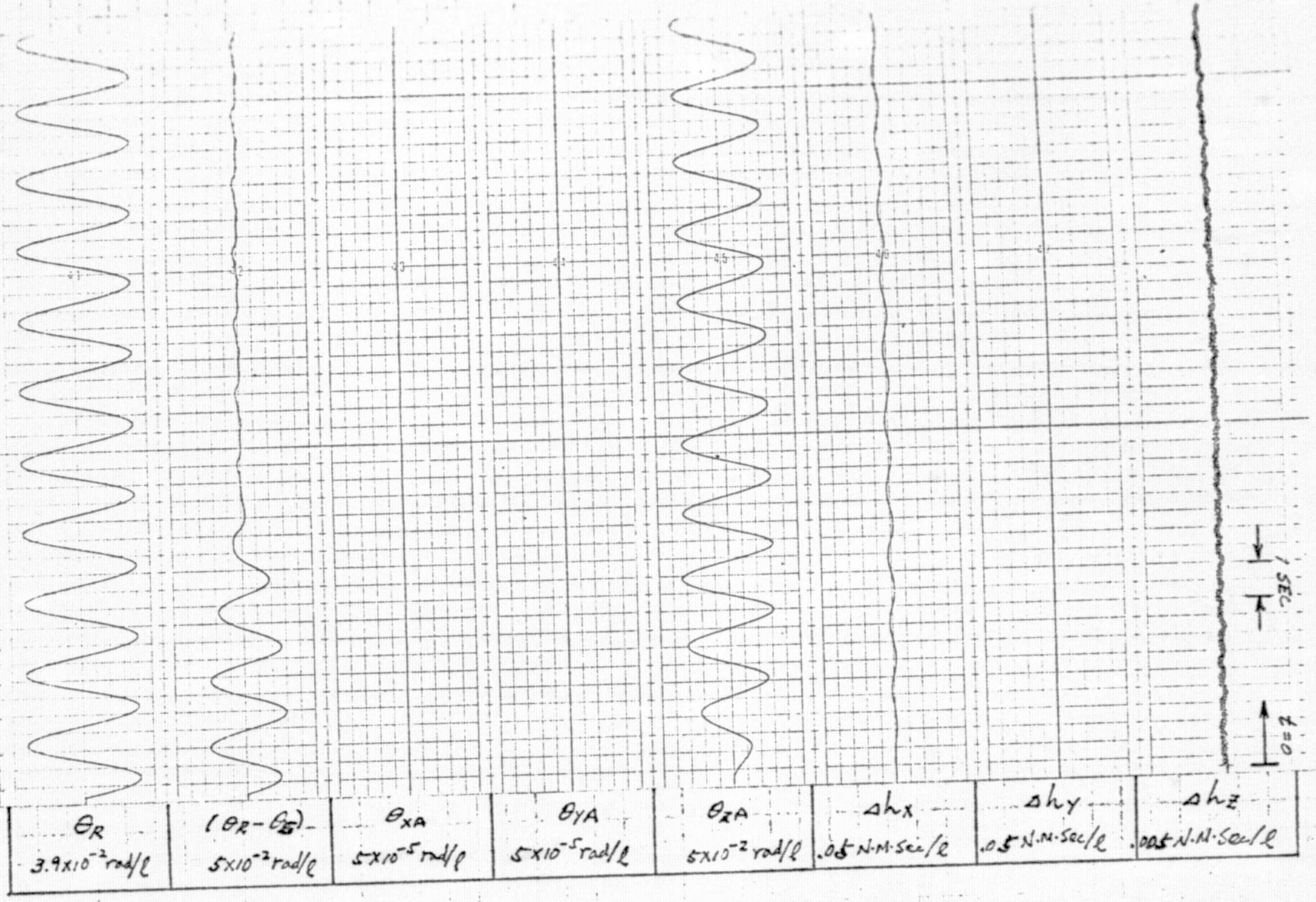
θ_R
3.9×10^{-2} rad/l
$(\theta_R-\theta_E)$
5×10^{-2} rad/l
θ_{XA}
5×10^{-5} rad/l
θ_{YA}
5×10^{-5} rad/l
θ_{ZA}
5×10^{-2} rad/l
Δh_X
.05 N.M.Sec/l
Δh_Y
.05 N.M.Sec/l
Δh_Z
.005 N.M.Sec/l
1 SEC.
t=0

C14 (a)

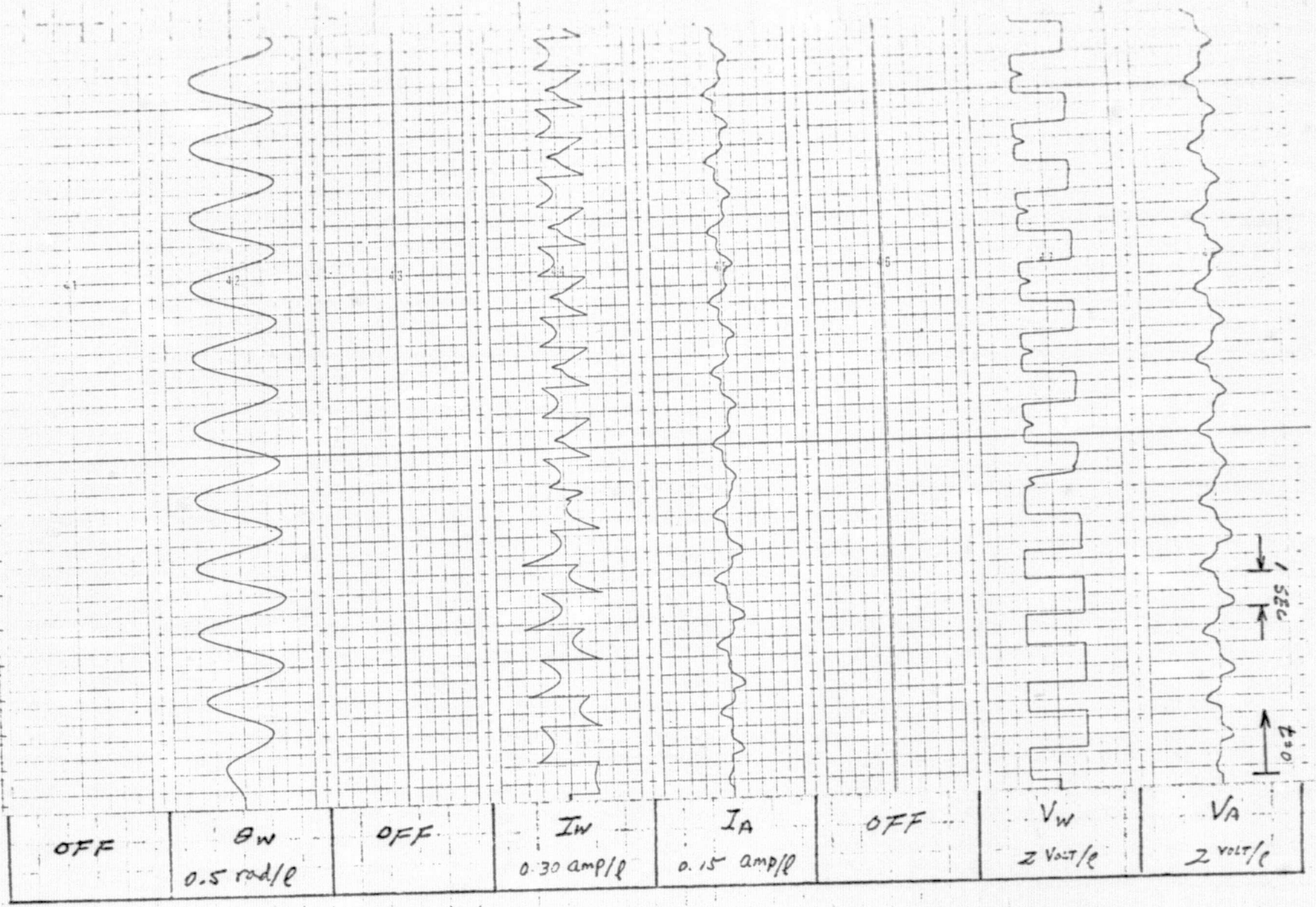
OFF
θ_W
0.5 rad/ℓ
OFF
I_W
0.30 amp/ℓ
I_A
0.15 amp/ℓ
OFF
V_W
2 VOLT/ℓ
V_A
2 VOLT/ℓ
1 SEC
t=0

C14 (b)

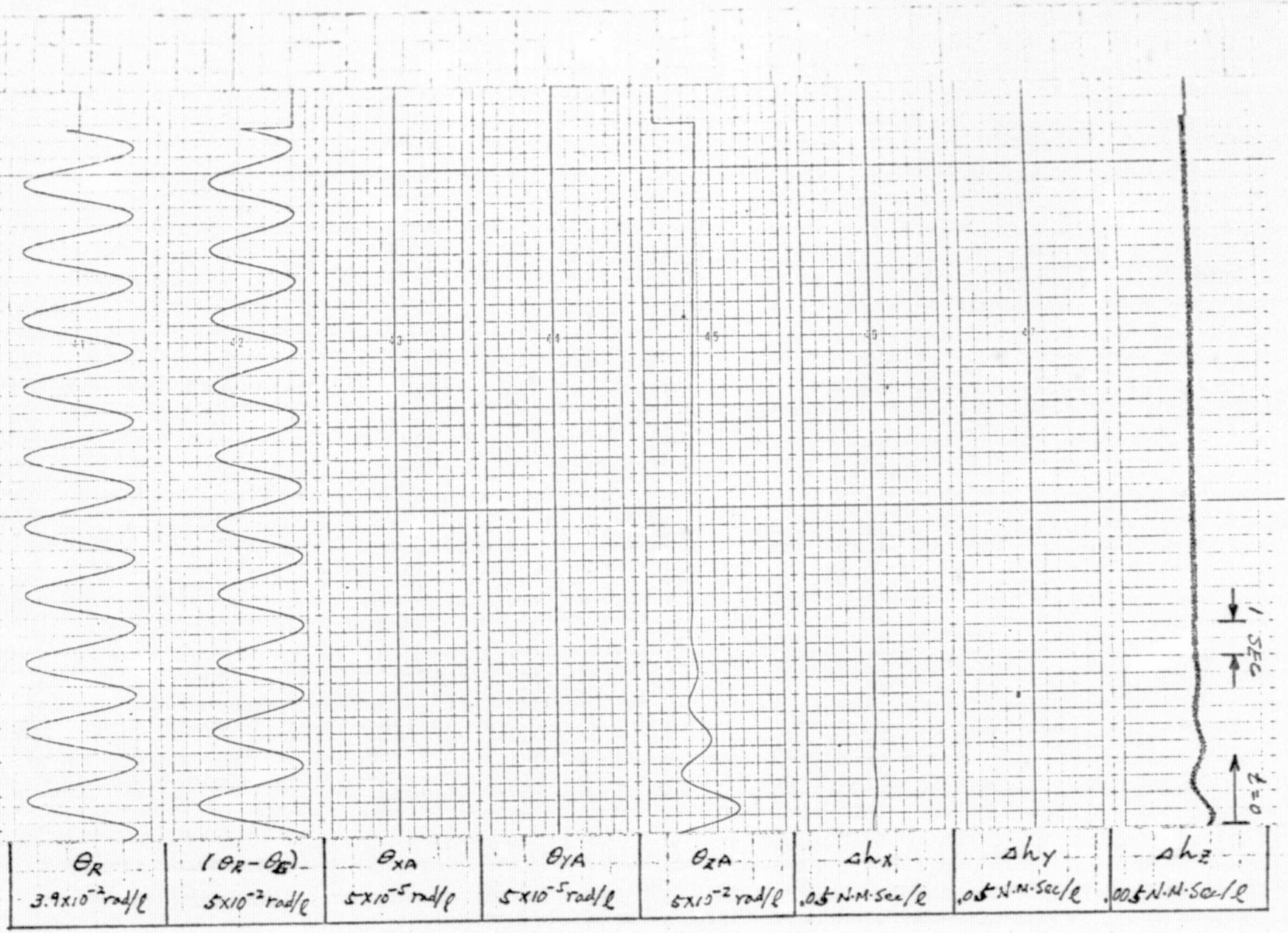
θ_R
3.9×10^{-2} rad/l
$(\theta_R-\theta_E)$
5×10^{-2} rad/l
θ_{XA}
5×10^{-5} rad/l
θ_{YA}
5×10^{-5} rad/l
θ_{ZA}
5×10^{-2} rad/l
Δh_X
.05 N·M·Sec/l
Δh_Y
.05 N·M·Sec/l
Δh_Z
.005 N·M·Sec/l
1 SEC
t=0

C15 (a)

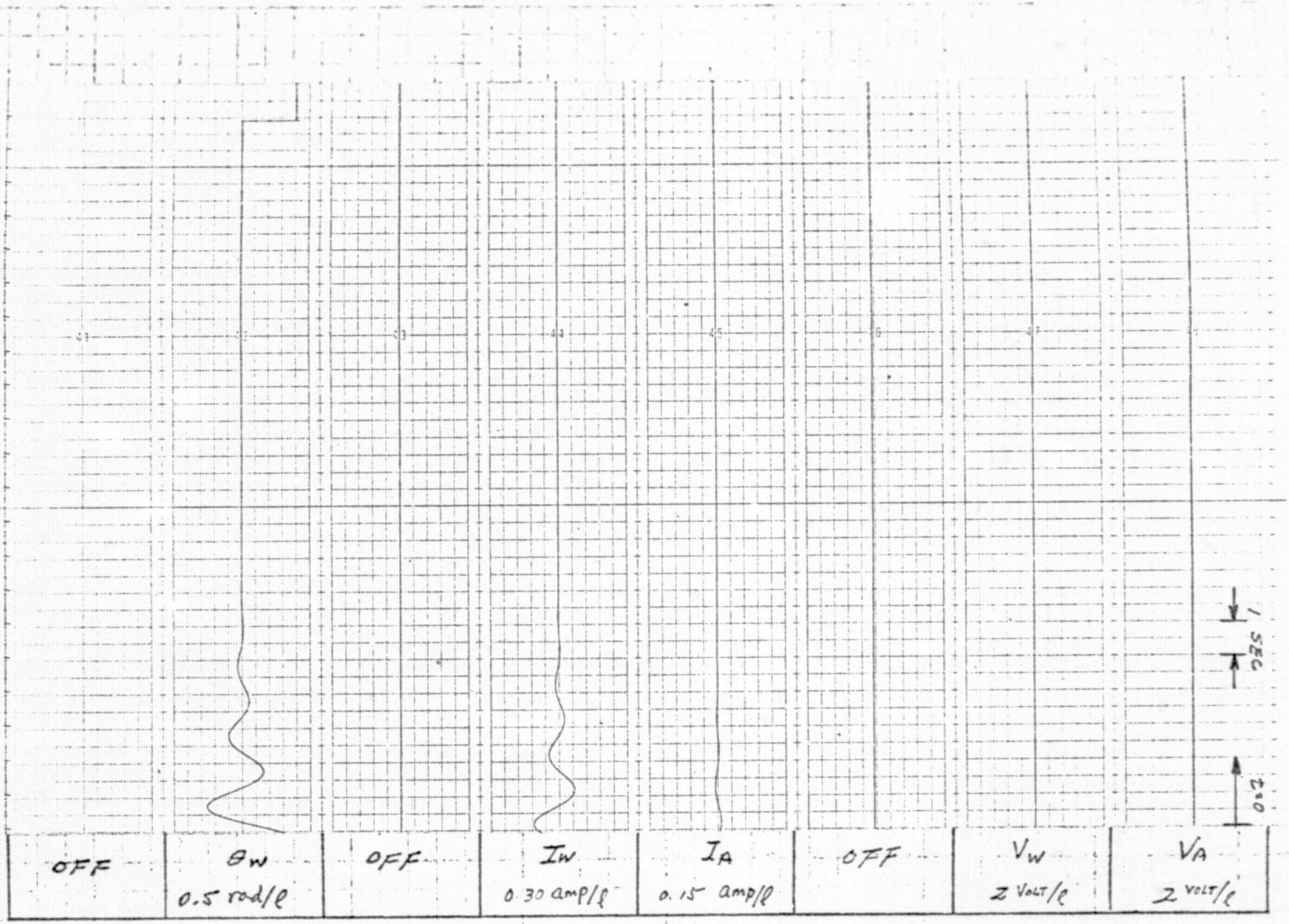
OFF
θ_W
0.5 rad/ℓ
OFF
I_W
0.30 amp/ℓ
I_A
0.15 amp/ℓ
OFF
V_W
2 VOLT/ℓ
V_A
2 VOLT/ℓ
1 SEC
2.0

C15 (b)

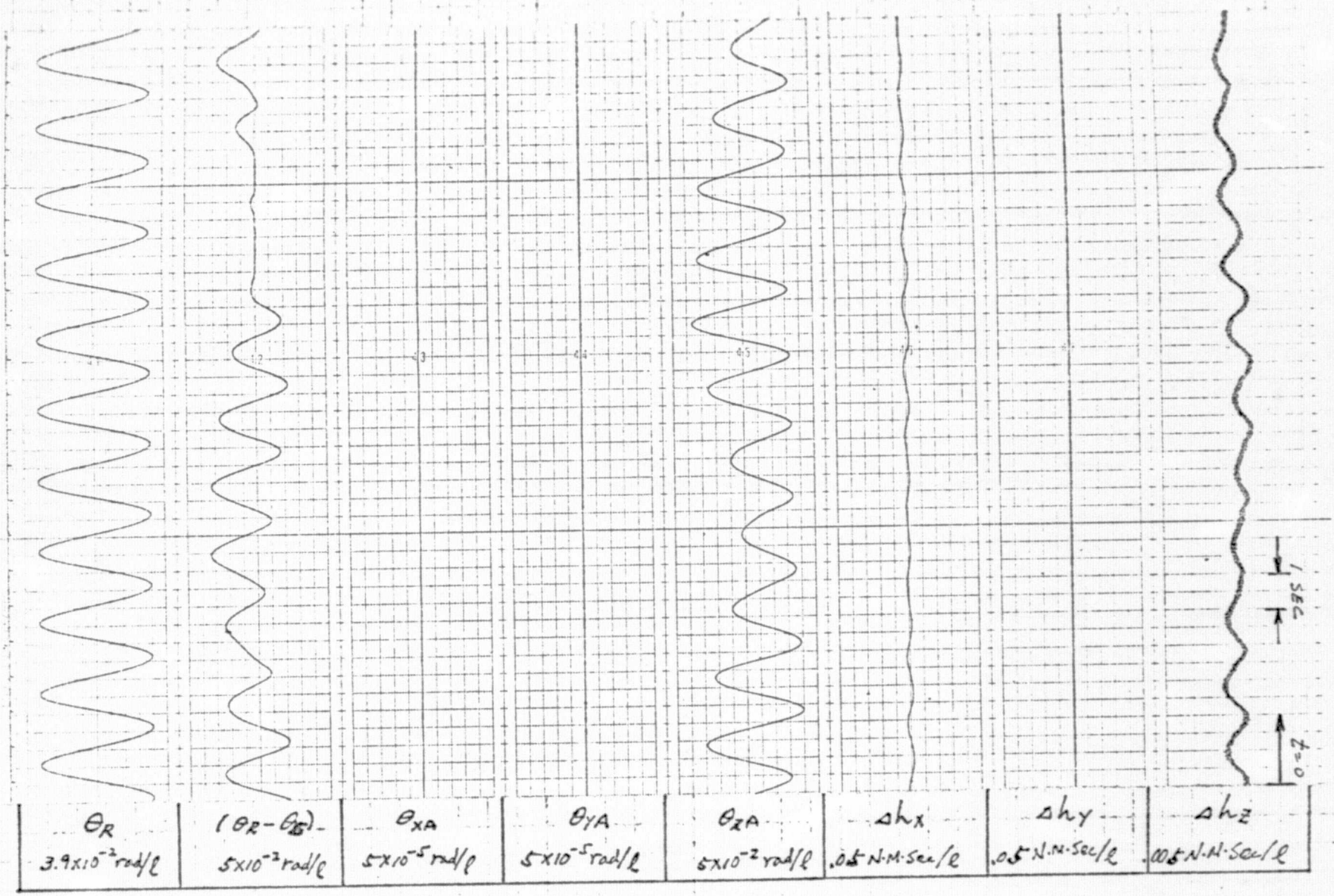
θR
3.9x10⁻² rad/ℓ
(θR-θS)
5x10⁻² rad/ℓ
θXA
5x10⁻⁵ rad/ℓ
θYA
5x10⁻⁵ rad/ℓ
θZA
5x10⁻² rad/ℓ
Δhx
.05 N·M·Sec/ℓ
Δhy
.05 N·M·Sec/ℓ
Δhz
.005 N·M·Sec/ℓ
1 SEC
t=0

C16 (a)

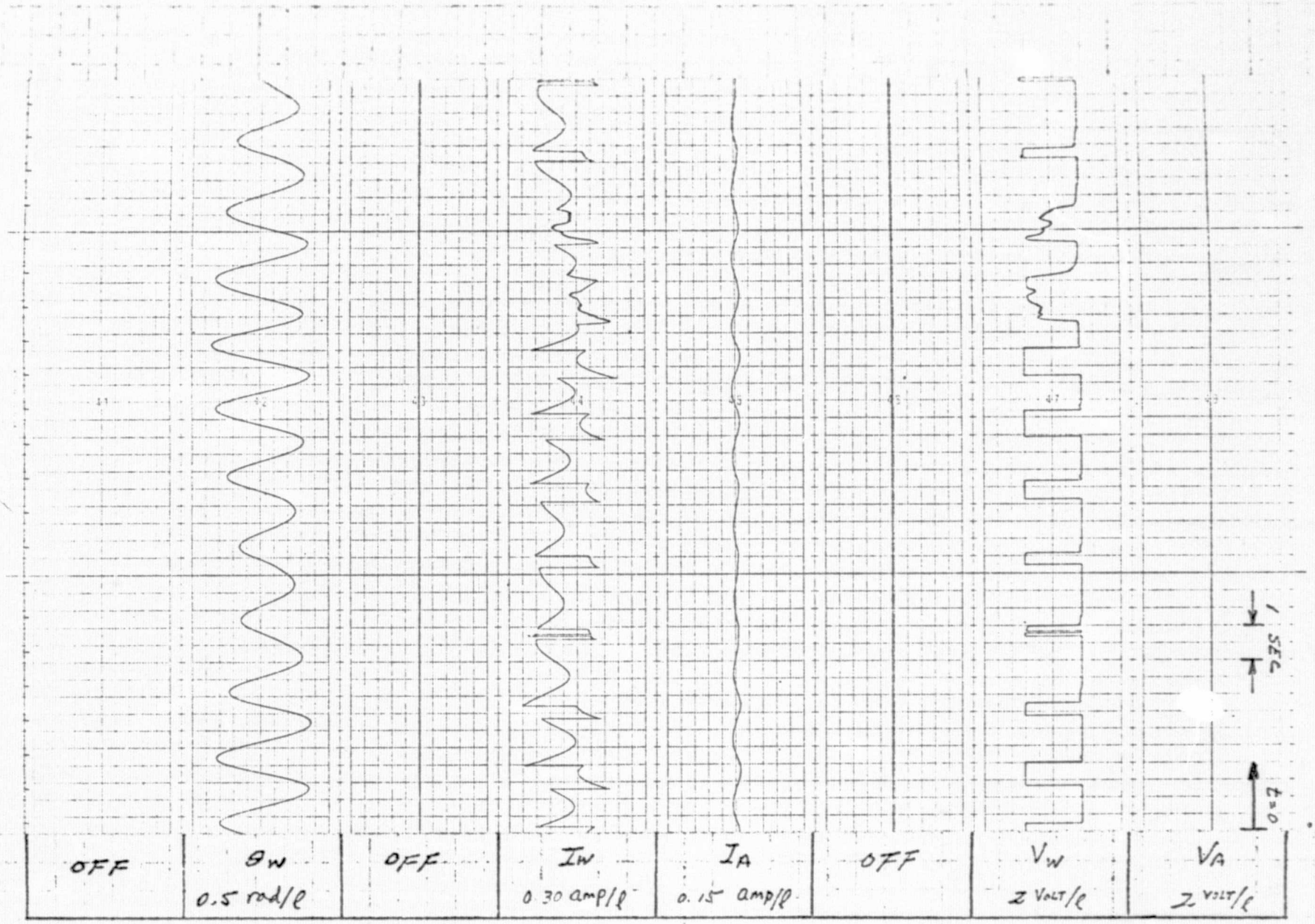
OFF
θ_W
0.5 rad/ℓ
OFF
I_W
0.30 amp/ℓ
I_A
0.15 amp/ℓ
OFF
V_W
2 VOLT/ℓ
V_A
2 VOLT/ℓ
1 SEC
t=0

C16 (b)

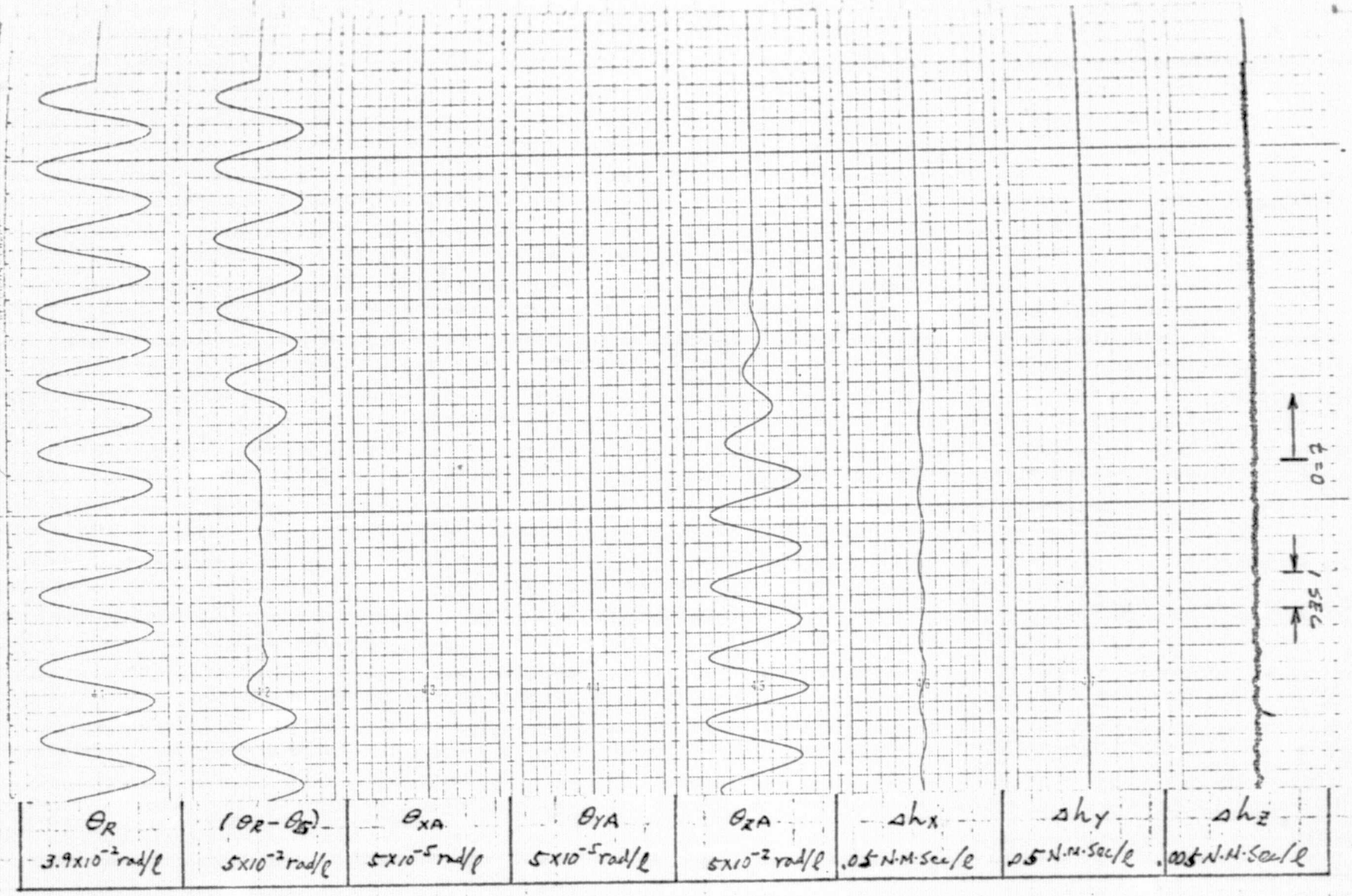
t=0
1 SEC
θ_R
3.9x10^{-2} rad/l
$(\theta_R - \theta_S)$
5x10^{-2} rad/l
θ_{xA}
5x10^{-5} rad/l
θ_{yA}
5x10^{-5} rad/l
θ_{zA}
5x10^{-2} rad/l
Δh_x
.05 N·M·Sec/l
Δh_y
.05 N·M·Sec/l
Δh_z
.005 N·M·Sec/l

C17 (a)

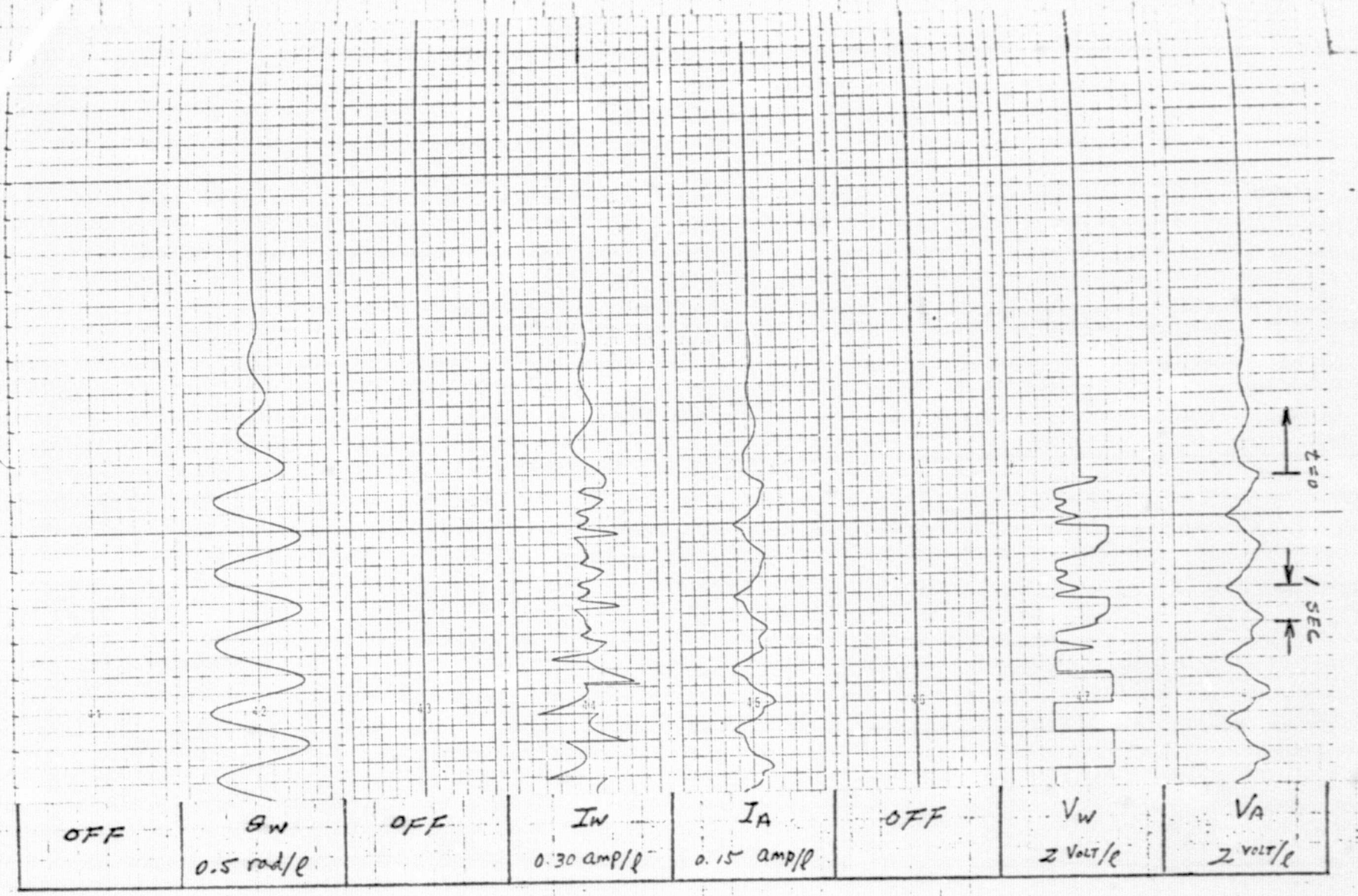
OFF
ϑ_W
0.5 rad/ℓ
OFF
I_W
0.30 amp/ℓ
I_A
0.15 amp/ℓ
OFF
V_W
2 VOLT/ℓ
V_A
2 VOLT/ℓ
t=0
1 SEC

C17 (b)

1 SEC
t = 0
θ_R
3.9×10^{-2} rad/ℓ
$(\theta_R - \theta_S)$
5×10^{-2} rad/ℓ
θ_{XA}
5×10^{-5} rad/ℓ
θ_{YA}
5×10^{-5} rad/ℓ
θ_{ZA}
5×10^{-2} rad/ℓ
Δh_X
.05 N·M·Sec/ℓ
Δh_Y
.05 N·M·Sec/ℓ
Δh_Z
.005 N·M·Sec/ℓ

C18 (a)

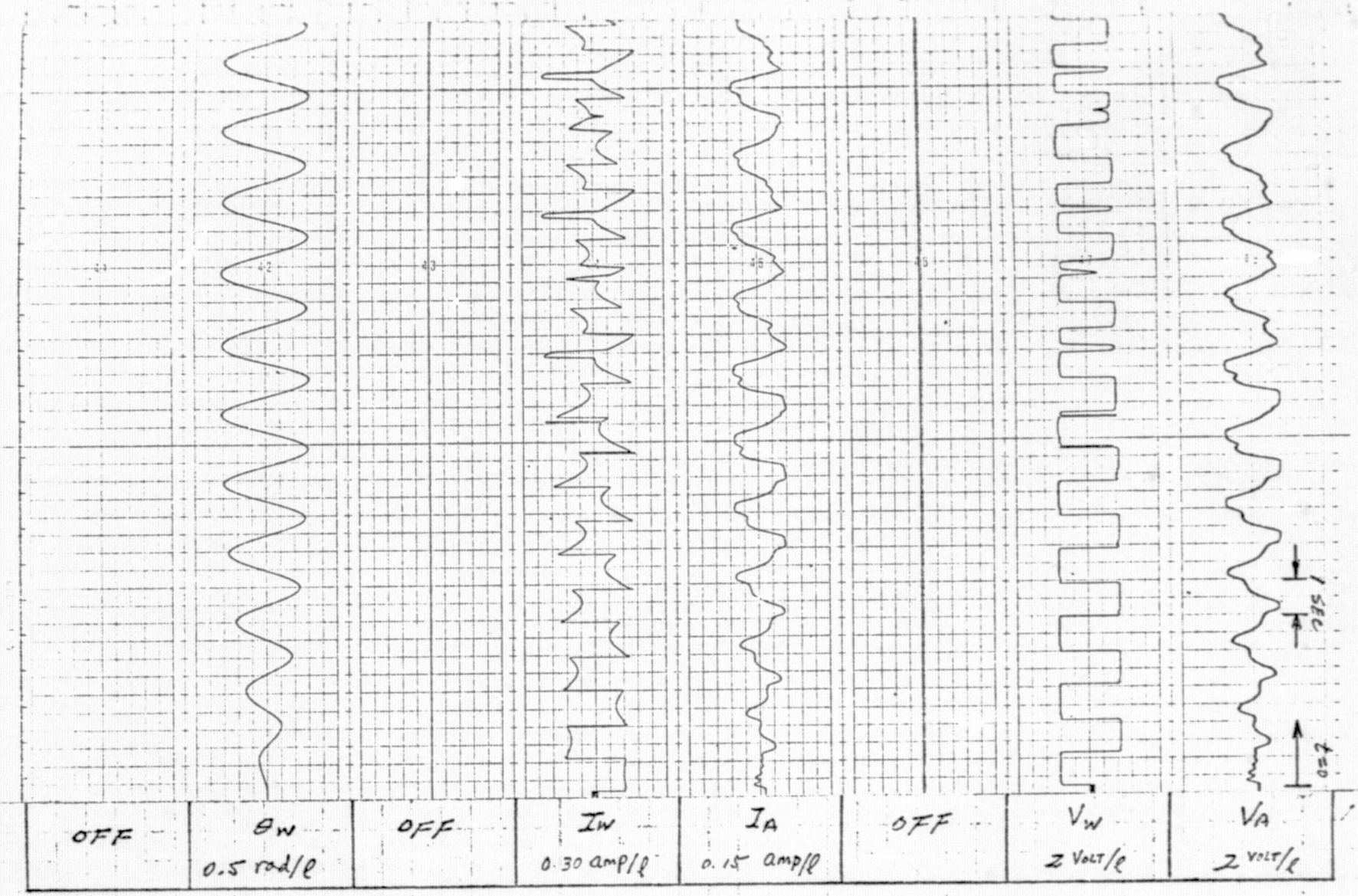
OFF
θ_W
0.5 rad/ℓ
OFF
I_W
0.30 amp/ℓ
I_A
0.15 amp/ℓ
OFF
V_W
2 VOLT/ℓ
V_A
2 VOLT/ℓ
1 SEC
t=0

C18 (b)

θ_R
3.9×10^{-2} rad/ℓ
$(\theta_R-\theta_B)$
5×10^{-2} rad/ℓ
θ_{XA}
5×10^{-5} rad/ℓ
θ_{YA}
5×10^{-5} rad/ℓ
θ_{ZA}
5×10^{-2} rad/ℓ
Δh_X
.05 N·M·Sec/ℓ
Δh_Y
.05 N·M·Sec/ℓ
Δh_Z
.005 N·M·Sec/ℓ
1 SEC
ZERO

OFF
θ_W
0.5 rad/ℓ
OFF
I_W
0.30 amp/ℓ
I_A
0.15 amp/ℓ
OFF
V_W
2 VOLT/ℓ
V_A
2 VOLT/ℓ
1 SEC
t=0

C19 (b)

θ_R
3.9×10^{-2} rad/ℓ
$(\theta_R-\theta_S)$
5×10^{-2} rad/ℓ
θ_{XA}
5×10^{-5} rad/ℓ
θ_{YA}
5×10^{-5} rad/ℓ
θ_{ZA}
5×10^{-2} rad/ℓ
Δh_X
.05 N·M·Sec/ℓ
Δh_Y
.05 N·M·Sec/ℓ
Δh_Z
.005 N·M·Sec/ℓ
1 SEC
t=0

C20 (a)

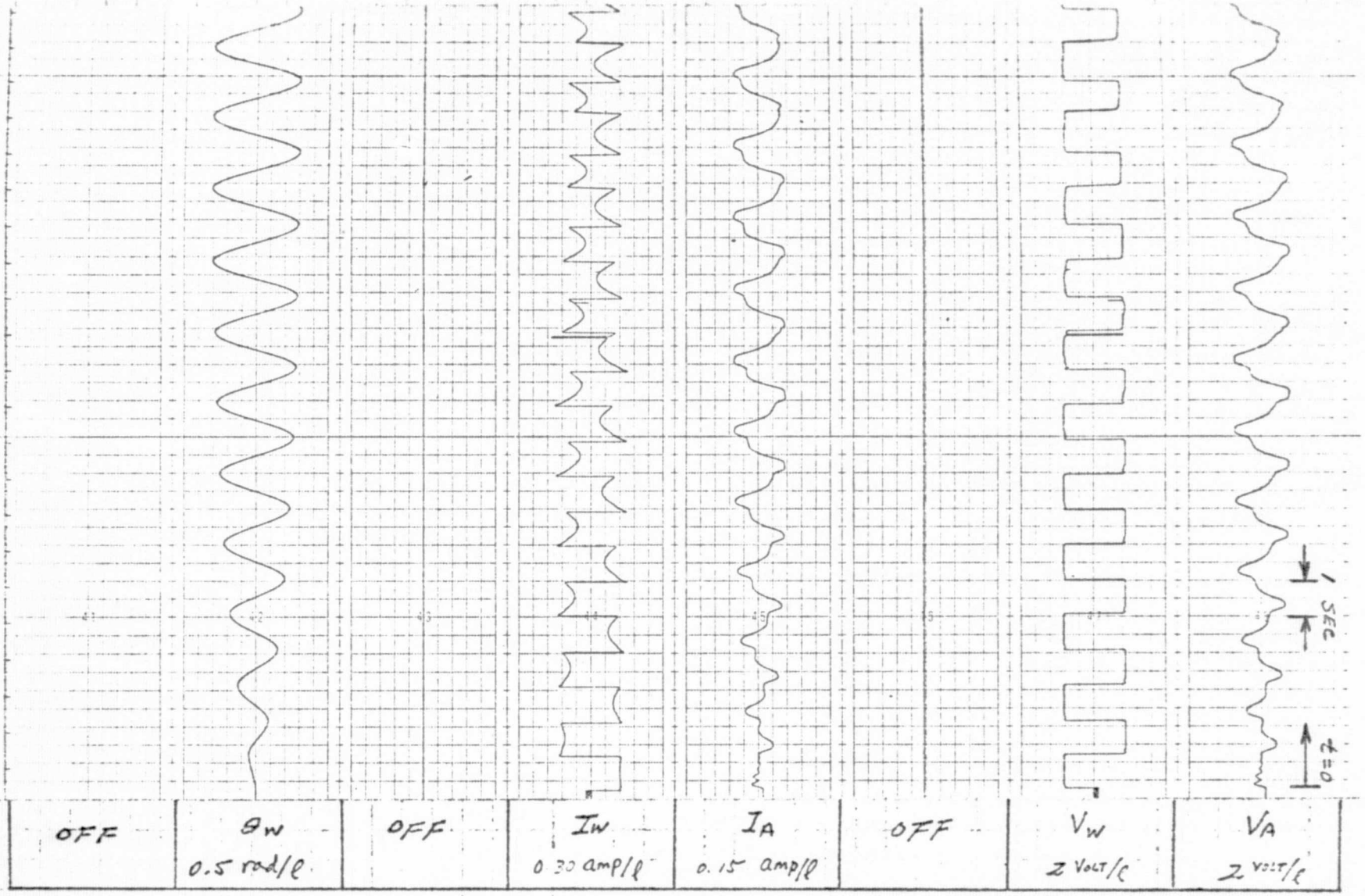
OFF
θ_W
0.5 rad/ℓ
OFF
I_W
0.30 amp/ℓ
I_A
0.15 amp/ℓ
OFF
V_W
2 VOLT/ℓ
V_A
2 VOLT/ℓ
1 SEC
t=0

C20 (b)

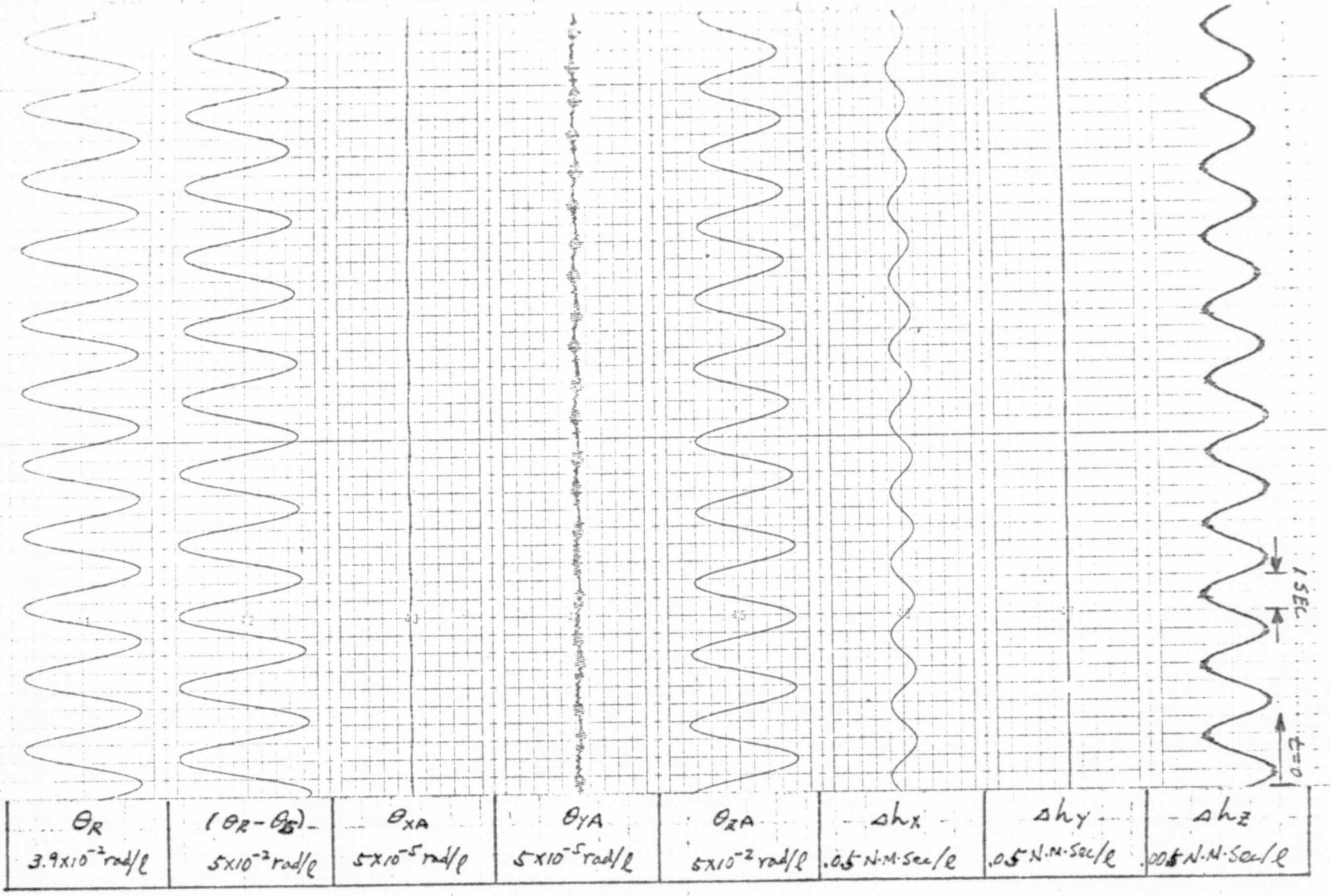
1 SEC.
t=0
θ_R
3.9×10^{-2} rad/ℓ
$(\theta_R-\theta_S)$
5×10^{-2} rad/ℓ
θ_{XA}
5×10^{-5} rad/ℓ
θ_{YA}
5×10^{-5} rad/ℓ
θ_{ZA}
5×10^{-2} rad/ℓ
Δh_x
.05 N·M·Sec/ℓ
Δh_y
.05 N·M·Sec/ℓ
Δh_z
.05 N·M·Sec/ℓ

C21 (a)

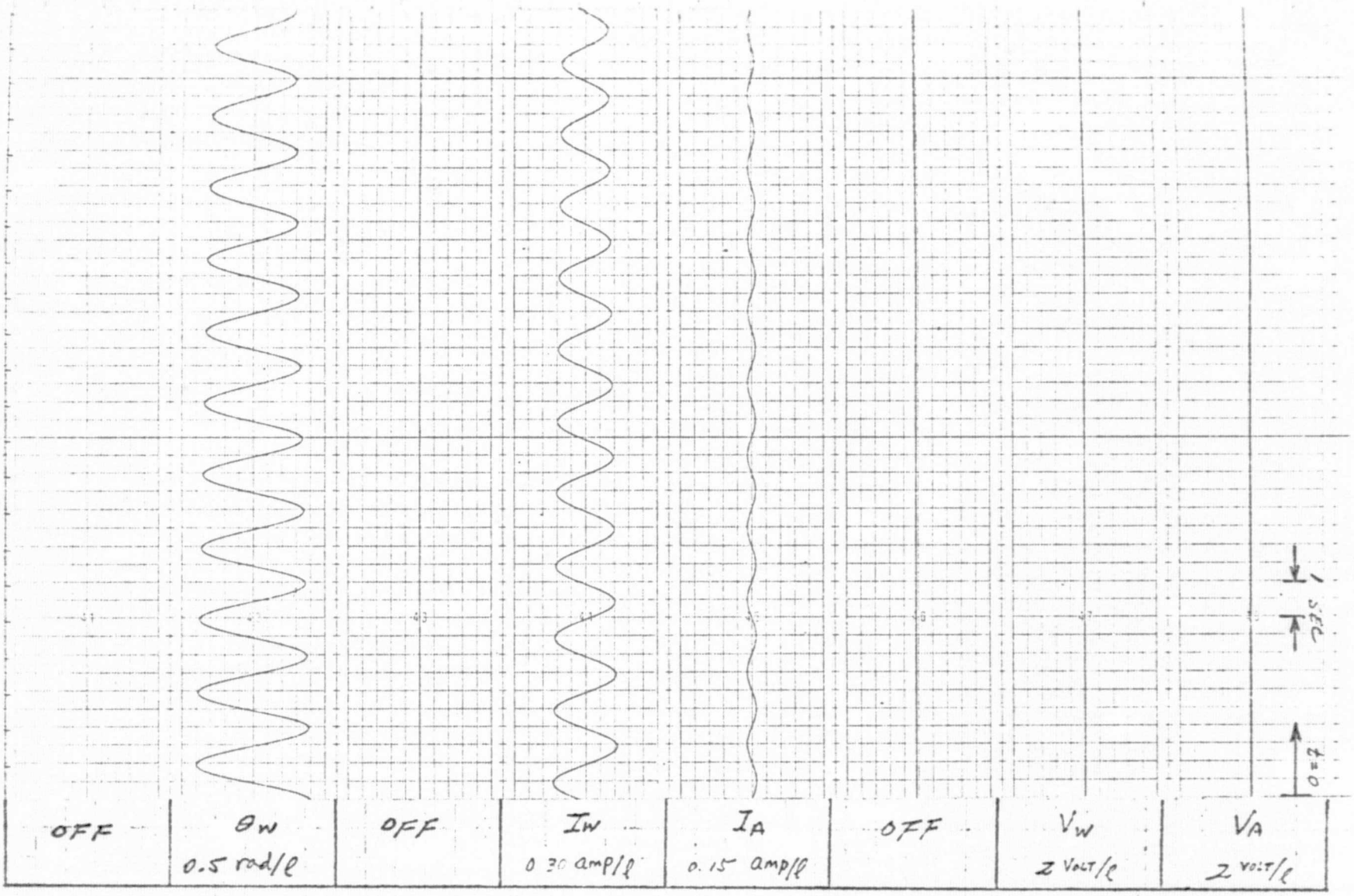
1 SEC
t=0
OFF
θW
0.5 rad/ℓ
OFF
IW
0.30 amp/ℓ
IA
0.15 amp/ℓ
OFF
VW
2 VOLT/ℓ
VA
2 VOLT/ℓ

C21 (b)

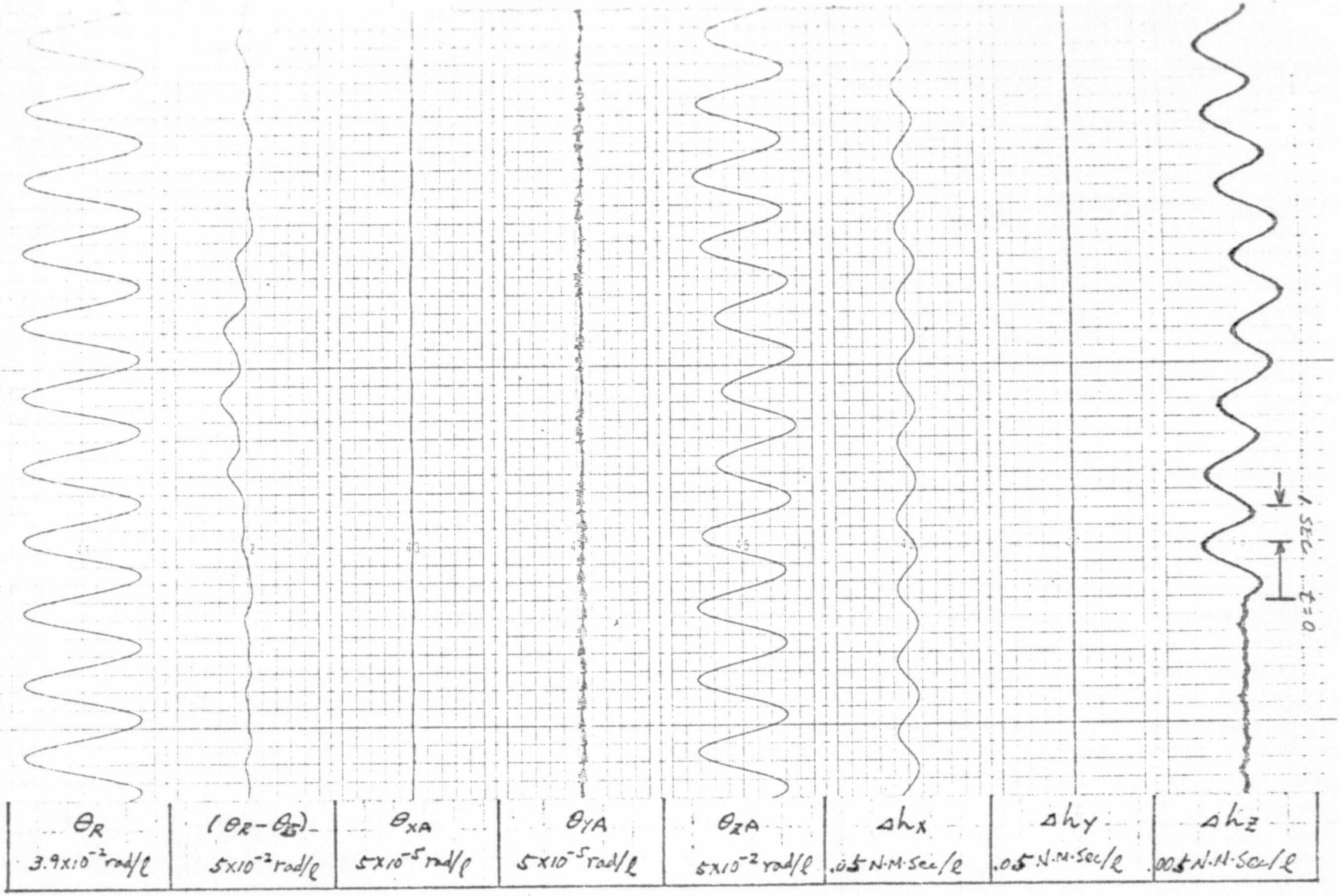
1 SEC.
t=0
θ_R
3.9×10^{-2} rad/ℓ
$(\theta_R-\theta_S)$
5×10^{-2} rad/ℓ
θ_{XA}
5×10^{-5} rad/ℓ
θ_{YA}
5×10^{-5} rad/ℓ
θ_{ZA}
5×10^{-2} rad/ℓ
Δh_X
.05 N·M·Sec/ℓ
Δh_Y
.05 N·M·Sec/ℓ
Δh_Z
.05 N·M·Sec/ℓ

C22 (a)

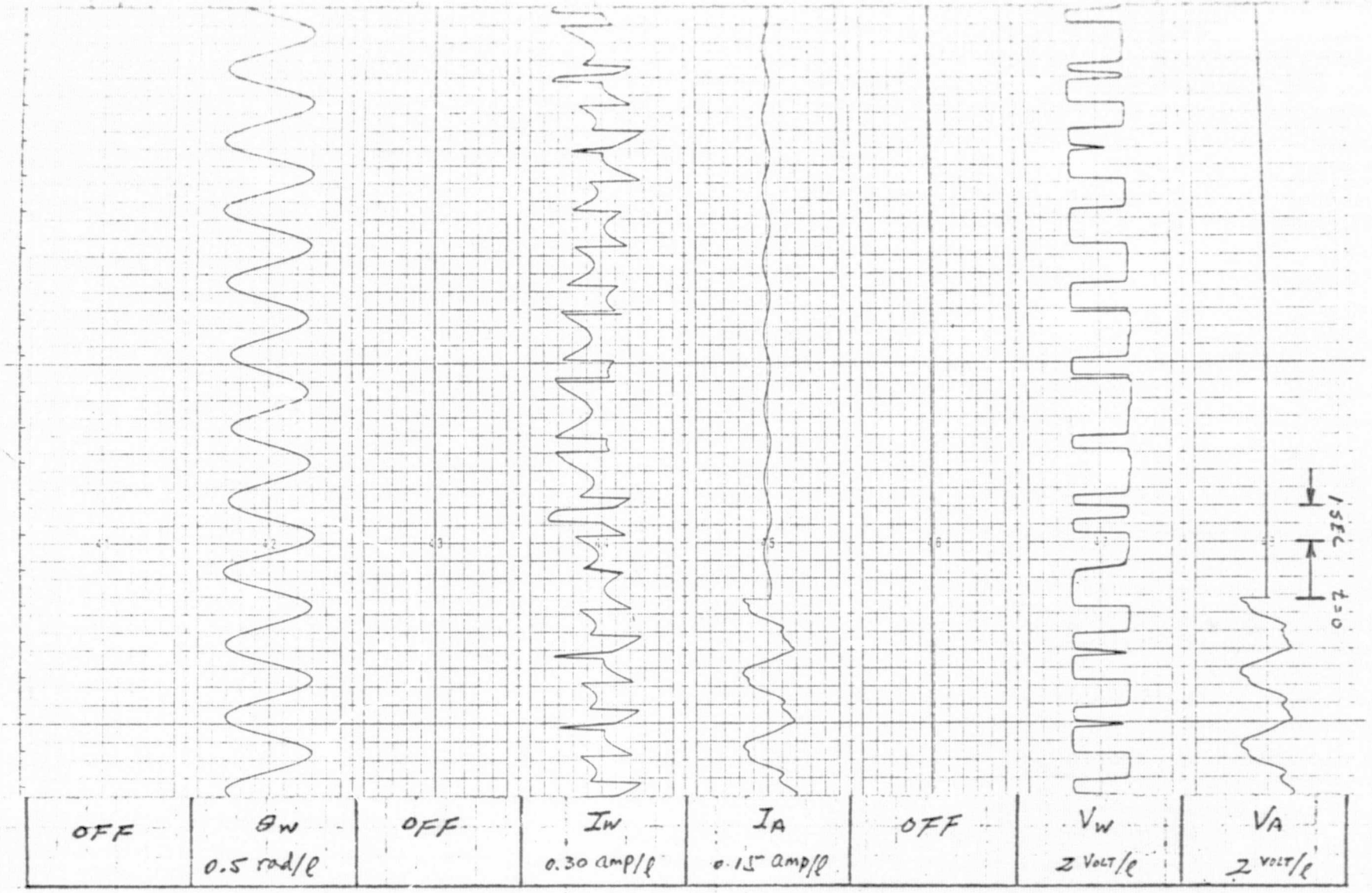
OFF
θ_W
0.5 rad/ℓ
OFF
I_W
0.30 amp/ℓ
I_A
0.15 amp/ℓ
OFF
V_W
2 VOLT/ℓ
V_A
2 VOLT/ℓ
1 SEC
t=0

C22 (b)

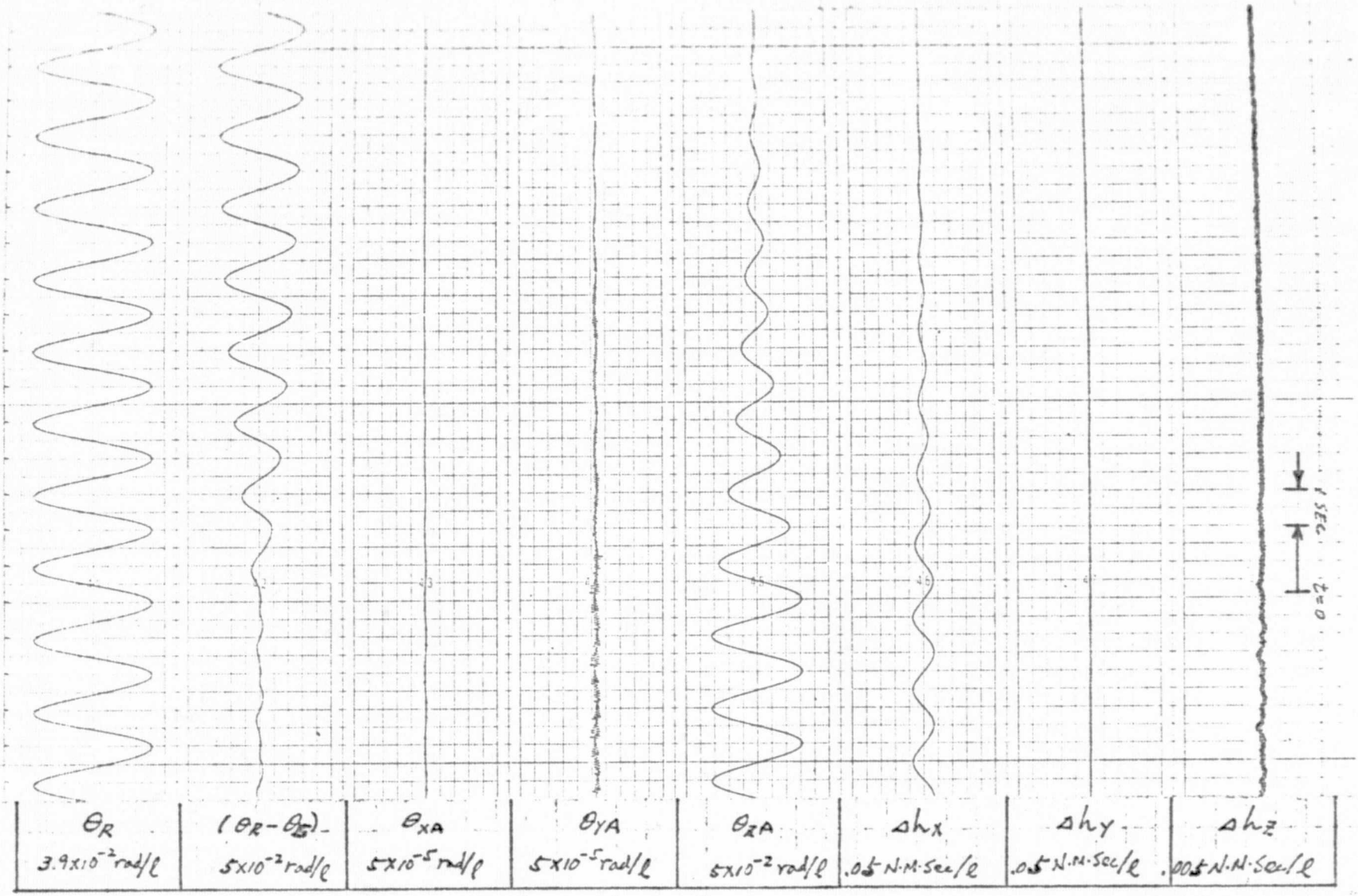
1 SEC.
t=0
θ_R
3.9×10^{-2} rad/l
$(\theta_R-\theta_{\dot{R}})$
5×10^{-2} rad/l
θ_{XA}
5×10^{-5} rad/l
θ_{YA}
5×10^{-5} rad/l
θ_{ZA}
5×10^{-2} rad/l
Δh_X
.05 N·M·Sec/l
Δh_Y
.05 N·M·Sec/l
Δh_Z
.005 N·M·Sec/l

C23 (a)

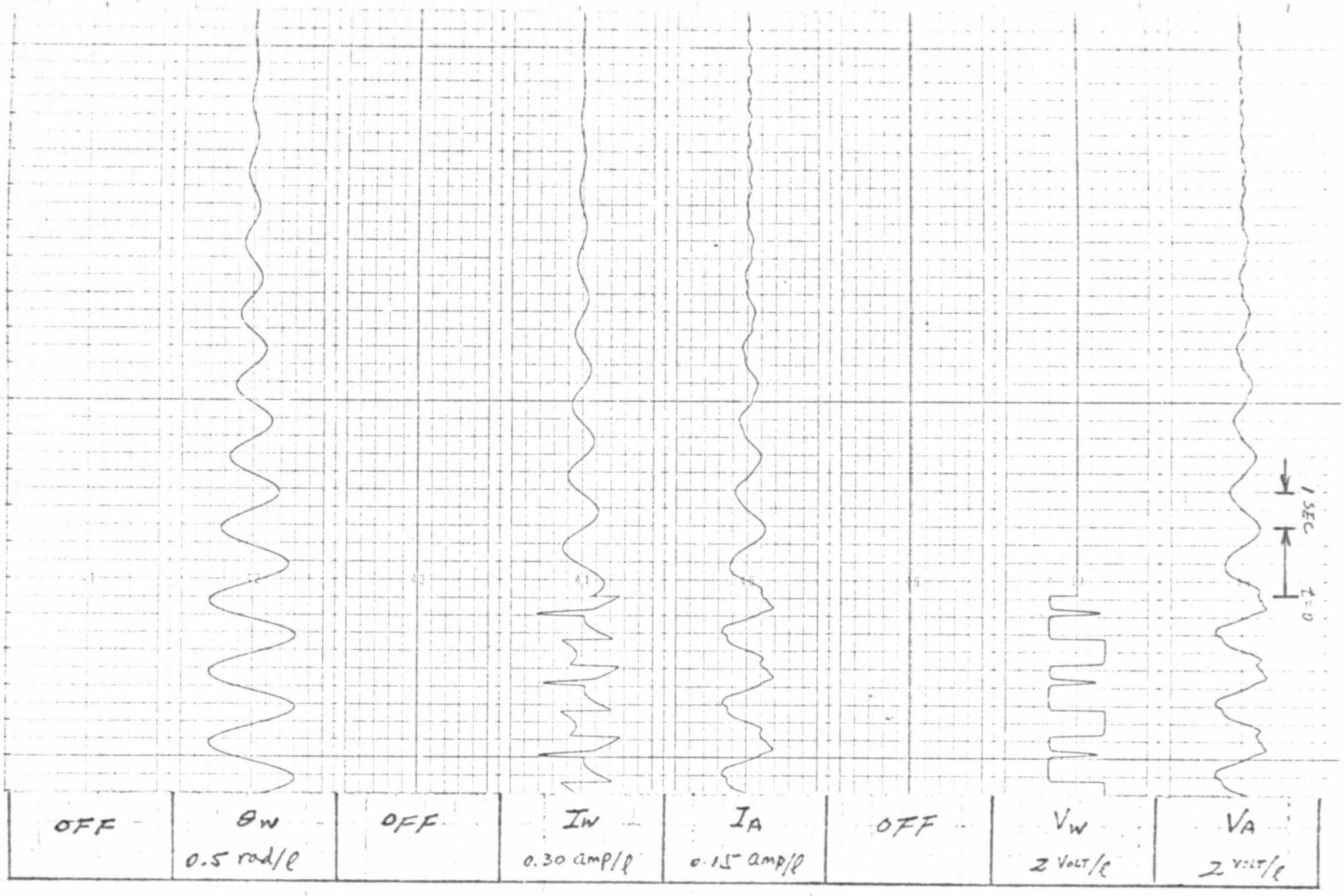
OFF
θ_W
0.5 rad/ℓ
OFF
I_W
0.30 amp/ℓ
I_A
0.15 amp/ℓ
OFF
V_W
2 VOLT/ℓ
V_A
2 VOLT/ℓ
1 SEC
T=0

C23 (b)